bimestrale dell'ENEA
anno 61

Speciale

OCEAN ENERGY: ONGOING RESEARCH IN ITALY

ISSN/1124 - 0016

SPECIALE II - 2015

Energia, Ambiente e Innovazione

Speciale

Ocean energy: Ongoing research in Italy
A cura di Gianmaria Sannino

Registrazione
Tribunale Civile di Roma
Numero 148 del 19 aprile 2010 del Registro Stampa

Direttore Responsabile
Diana Savelli

Coordinamento editoriale
dei fascicoli: Giuliano Ghisu
di questo speciale: Antonino Dattola

Collaboratori
Daniela Bertuzzi, Paola Carrabba, Sergio Cappucci, Orietta Casali, Antonino Dattola, Barbara Di Giovanni, Giovanni Puglisi

Traduzioni e revisione lingua inglese
Carla Costigliola

Progetto grafico
Paola Carabotta, Bruno Giovannetti

Edizione web
Antonella Andreini, Serena Lucibello, Concetta Manto

Promozione
Paola Crocianelli

Per informazioni e contatti: infoeai@enea.it

Impaginazione
Varigrafica Alto Lazio
Via Cassia, km 36,300 (Zona industriale)
01036 Nepi (VT)

Stampa
Laboratorio Tecnografico - Centro Ricerche ENEA Frascati

Disponibile sul sito www.enea.it e
App Store: in https://itunes.apple.com/it/app/energia-ambiente-e-innovazione/id542172540?l=it&ls=1&mt=8

Numero chiuso nel mese di luglio 2015

Prodotto realizzato impiegando carta Symbol Freelife certificata FSC

II-2015

Indice

Foreword/Prefazione

Gianmaria Sannino

Seas and oceans can possibly become important sources of clean energy. They represent a vast and largely untapped source of renewable energy usually known as 'marine energy' or 'ocean energy'.
Ocean energy is available in five basic forms:

- waves produced by the action of wind over the water surface;
- tides, an alternating motion of large masses of ocean water produced by the gravity force exerted by the sun and the moon;
- currents (both surface and submerged) produced by ocean circulation patterns, which in turn are mostly due to the action of trade winds, gravity, water density differences and the rotation of the earth;
- water temperature differences (gradients) between the surface and the ocean depths (below 1,000 m), due to solar radiation;
- salinity differences (gradients) between salty ocean water and fresh water entering the sea from river estuaries.

The different sources of ocean energy are not uniformly distributed in the oceans. The greatest wave energy potential is found in countries bordering large oceans; in Europe most of the pilot plants, either planned or in operation, are located along the Atlantic coast in countries such as Ireland, Portugal, Spain, Norway and the UK. However, high energy potential implies exceptional wave conditions that pose engineering challenges to the design and maintenance of the devices. On the other hand, in calmer and semi-enclosed seas

Mari e oceani hanno il potenziale per diventare importanti fonti di energia pulita. Essi rappresentano una vasta e in gran parte inutilizzata fonte di energia rinnovabile nota come 'energia marina'.
L'energia marina è disponibile in cinque forme principali:

- onde, prodotte dall'azione del vento sulla superficie dell'acqua;
- maree, movimento alternato di grandi masse di acqua dell'oceano, prodotto dalla gravità del Sole e della Luna;
- correnti (sia di superficie che sommerse) prodotte dalla circolazione oceanica, dovuta a sua volta principalmente all'azione degli alisei, della gravità, alle differenze di densità dell'acqua e alla rotazione della terra;
- differenze di temperatura dell'acqua tra la superficie e le profondità oceaniche (sotto 1.000 m) a causa della radiazione solare;
- differenze di salinità tra l'acqua oceanica salata e l'acqua dolce che entra in mare dalle foci dei fiumi.

Le diverse fonti di energia marina non sono distribuite uniformemente negli oceani. Il maggiore potenziale di energia ondosa si trova in paesi che affacciano sui grandi oceani; in Europa, la maggior parte degli impianti pilota, sia in funzione che pianificati, si trova lungo la costa atlantica in paesi come l'Irlanda, il Portogallo, la Spagna, la Norvegia e il Regno Unito. Tuttavia un alto potenziale energetico implica condizioni eccezionali delle onde che pongono sfide ingegneristiche per la progettazione e la manutenzione dei dispositivi. D'altra parte, in mari più calmi e

such as the Mediterranean, where lower amount of wave energy is available, many technical issues related to extreme waves can be more easily overcome by significantly reducing installation and maintenance costs, making wave energy production still economically viable. The Mediterranean Sea is also particularly attracting for the high-energy tidal currents present in the Strait of Gibraltar and Messina.

In Italy there is an increasing interest in the exploitation of wave and tidal technology to produce clean and renewable energy. Moreover, our Government, according to the National Renewable Energy Action Plan (NREAP), expects to meet by 2020 the target of 3 MW of installed capacity. At the current stage, marine renewable energy is a real opportunity for Italy to generate economic growth and jobs, enhance the security of its energy supply and, most importantly, boost competitiveness through technological innovation.

In such a context, this Special Issue "Ocean Energy: ongoing research in Italy" has been conceived. It is intended to be a comprehensive collection of articles describing the ocean energy converter technologies designed for application in the Italian Seas by the major Research and Academic organizations in Italy.

We hope that this collection of reviews and original papers will be a nice treat to our readers, and will contribute to a comprehensive understanding of the current status of development of ocean energy in Italy. It is also our hope that the research and development presented in this Special Issue will boost and contribute to the growth of the ocean energy sector in Italy.

I take this opportunity to express my special thanks to Adriana Carillo and Orietta Casali: without their great skills and commitment, the making of this Special would have been impossible.

semichiusi come il Mediterraneo, dove è disponibile una quantità di energia marina inferiore, molti problemi tecnici legati alle onde estreme possono essere più facilmente superati, riducendo significativamente i costi di installazione e manutenzione e rendendo la produzione di energia dalle onde ancora economicamente sostenibile. Il Mar Mediterraneo è inoltre uno dei pochi mari marginali a possedere anche un elevato potenziale energetico che deriva dalle correnti di marea presenti nello Stretto di Gibilterra e Messina.

In Italia c'è un crescente interesse relativamente alla tecnologia per lo sfruttamento delle onde e delle maree per produrre energia pulita e rinnovabile. Inoltre, il nostro Governo, secondo il piano d'azione nazionale per le energie rinnovabili (NREAP), si aspetta di raggiungere nel 2020 l'obiettivo di 3 MW di potenza installata. Allo stato attuale, l'energia rinnovabile marina rappresenta una reale opportunità per l'Italia di favorire la crescita economica e l'occupazione, migliorare la sicurezza dell'approvvigionamento energetico e, soprattutto, aumentare la competitività attraverso l'innovazione tecnologica.

In questo contesto, è stato ideato lo Speciale "Energia marina: ricerca in corso in Italia" come raccolta di articoli scientifici che descrivono le tecnologie di conversione dell'energia marina progettate per i mari italiani dai principali enti di ricerca e università nazionali. Il nostro auspicio è che questa raccolta di articoli e documenti originali sia per i nostri lettori un trattato di tutto rispetto e contribuisca a far comprendere in maniera esaustiva lo stato attuale dello sviluppo dell'energia marina in Italia. Ci auguriamo inoltre che le ricerche e i progressi presentati in questo Speciale possano incoraggiare fortemente l'energia marina in Italia, contribuendo alla crescita del settore.

Desidero ringraziare Adriana Carillo e Orietta Casali e dare merito alle loro competenze e all'impegno che ha reso possibile la realizzazione di questo Speciale.

Environmental monitoring techniques and equipment related to the installation and operation of Marine Energy Conversion Systems

Results of activities under project Marine Renewables Infrastructure Network for Emerging Energy Technologies (MaRINET) are reported, which led to DEMTE, a database, created on the basis of standardized monitoring of the marine environment during installation, operation and decommissioning of Marine Energy Conversion Systems. Obtained with the consortium partners' available techniques and equipment, the database shows that such instruments cover all identified marine environmental compartments, despite the lack of underwater vehicles and the reduced skills in using satellite technologies. These weaknesses could be overcome by an accurate planning of equipment, techniques and knowledge sharing. The approach here presented also leads to an effective analysis even in non-marine contexts.

DOI: 10.12910/EAI2015-041

S. Scanu, F.M. Carli, M.A. Peviani, V. Piermattei, S. Bonamano, F. Paladini de Mendoza, K. Dampney, J. Norris, M. Marcelli

Introduction

MaRINET (Marine Renewables Infrastructure Network for Emerging Energy Technologies) is an EC-funded (FP7) consortium of 29 partners bringing together a network of 42 specialist marine renewable energy testing facilities. The network conducts coordinated research to improve testing capabilities, implements common testing standards and provides training and networking opportunities in order to enhance expertise in the industrial sector. The aim of the MaRINET initiative is to accelerate the development of marine renewable energy technology.

Contact person: Sergio Scanu
sergioscanu@unitus.it

MaRINET consists of five main areas of focus, or Work Packages: Management & Administration, Standardisation & Best Practice, Transnational Access & Networking, Research and Training & Dissemination. The initiative runs for four years until 2015.

This paper is based on the results of the Database for Environmental Monitoring Techniques and Equipment (DEMTE), which is part of the Task 4.5 "Environmental monitoring related research" of Work Package 4, "Research to innovate and improve infrastructures, technologies and techniques" of the project. The DEMTE presents a list of instrumentation and measurement methods for performing monitoring activities, in the marine environment, related to the installation and operation of Marine Energy Conversion Systems (MECS). It provides a common information source, which the various MaRINET facilities can refer to when selecting new equipment or techniques, or upgrading or replacing

existing equipment or methodologies. The logical approach used to build the DEMTE could be a useful tool to assess marine environmental issues in a broader context, for it could be used as a standard methodology to evaluate the effectiveness of monitoring activities coverage.

Monitoring of the marine environment

Monitoring in the marine environment is a complex topic. Monitoring is often based on a multidisciplinary approach which includes both abiotic and biotic environmental compartments. This variety of subjects involves several research areas which are interconnected via a large set of interdependent processes. In this context the main challenge in environmental monitoring is to select a robust approach, which:

- is compliant with environmental regulations and accepted practices,
- avoids any potential negative effects on the receiving study environment,
- can provide environmental information appropriate for the research needs.

High variability is inherent in the marine environment; therefore the monitoring activity has to be based on high resolution and synoptic observations. The following elements must be considered in monitoring design:

- spatial and temporal scales of marine processes,
- interactions between the different environmental compartments,
- dynamics.

Spatial and temporal scales, interactions and dynamics

The spatial and temporal scales of marine phenomena and processes are characterized by specific ranges of time and space [1]. Figure 1 shows a scheme which summarizes the main processes from micro- to macro-scale.

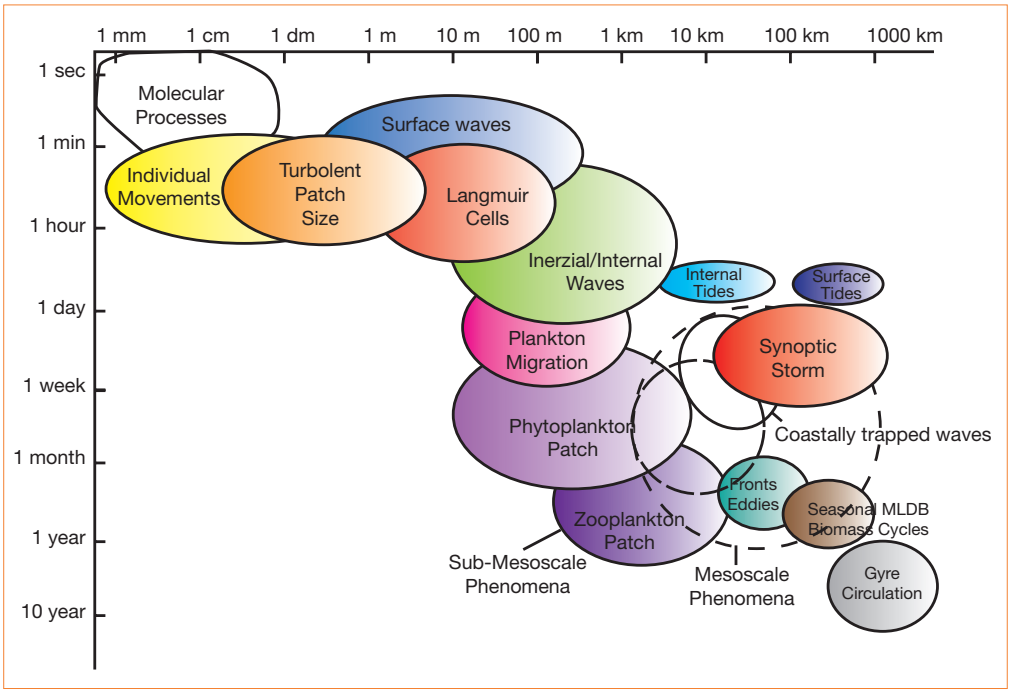

FIGURE 1 Environmental processes: from macro- to micro-scale
Source: [1]

The micro-scale has a spatial limit of 1 m and temporal domain of 1-2 days. Micro-scale processes are dominated by turbulence, including biological and mixed layer as well as vertical structure of coastal water and tidal mixing. The mesoscale has a spatial range between 1 km and 1000 km, with a corresponding temporal range from 1 day to 1 year. Processes belonging to this scale include coastal upwelling, mesoscale eddies and circulation. The macro-scale encompasses everything above 1000 km and has a temporal scale of over 1 year. The basin scale circulation, gyres and vortex all belong to the macro-scale.
All relevant marine environmental compartments should be considered when designing monitoring activities. Some compartments may be deemed of negligible relevance. Other compartments may be relevant but not of a practical scale to monitor. In this situation, existing literature may be consulted to provide the necessary knowledge.

Methodology

The collection of information about the measurement tools and methods used by partners in the MaRINET consortium was preceded by the identification of the main environmental areas of interest. A process was developed to assess the suitability of the measurement instruments used by the project partners of MaRINET to the environmental receptor groups. The findings are presented in tables 2 and 3 in which monitoring equipment and techniques are divided into two main groups:

- measurements of physical parameters,
- measurements of biological parameters.

Each group consists of environmental compartments related to climatic forcing (wind, waves and tidal current) and geomorphological parameters (bathymetry, sediment, mixing) as well as the physico-chemical parameters of the water column, and biological parameters which comprise all ecological and biological structures (plankton, macroalgae, benthic communities, fishes, marine mammals, and birds).

Physical parameters

Physical parameters, generally included in the group of the so-called climatic forcings, are of fundamental importance to the planning of monitoring activities to assess the impacts induced by the installation and operation of marine energy power plants.

Hydrodynamics

Almost all climatic forcings are a form of solar energy, for example wind, waves and marine currents with the exception of tides, which arise due to gravitational forces.
In this section methods and tools for measuring currents, tides, wind, and waves are presented [2]:

- Currents and tides: the main techniques for measuring currents and tides involve the use of acoustic velocimeters, Lagrangian drifters, and satellite observations. Secondary measurement techniques include wave buoys and underwater sonar.
- Waves: the main techniques for measuring wave climate are wave buoys, acoustic velocimeters, radar and satellite observations. In particular the most popular method is based on measurements carried out by surface buoys which are often coupled with the currents via installation of an Acoustic Doppler Profiler (ADP) on the seabed. The difference between the two systems is that in the first case it is possible to have a near-real-time communication and access to data easily, in the second case they are often used for long-term auto-acquisition deployment.
- Wind: the main instrument is the anemometer. Measurements are also possible through satellite observations and radar.

Morphology and sedimentology

Morphology and sedimentology of the marine environment exist in a feedback relationship with both geology and climatic forcing parameters; wind, currents, waves, and tides all shape coastal morphology. The technique of choice for morphological measurements is active acoustics. Techniques such as Single-beam sonar, which measures depth in a single point, Side scan sonar

[3], which is an extension to a sonogram that is function of seabed morphology, and Multi-beam sonar, which allows total, high-resolution coverage of the area.
Sedimentology is closely related to morphology and geology. Climatic forcing, energy extraction and human activities such as dredging can all affect sediment transport. Sediment investigation often requires direct sampling of the seabed. The most used sampling techniques involve grabs, for example Van Veen and Eckman grabs, gravity corers, piston corers, and box corers [4, 5]. The choice of equipment to be used depends on both the sampling depth and the degree of disturbance of the substrate. The best sampling techniques often involve divers, giving the advantages of speed of execution and minimal disturbance of the sample.

Water column
Water column analysis plays a central role in the knowledge of the dynamics and dispersion of chemical, physical and biological parameters and their vertical and horizontal distribution in marine waters. Suspended solids and turbidity can be measured with transmissometers and irradiance techniques, and phytoplankton presence can be measured by fluorimetric sensors.
The main physical properties of water, including depth, conductivity, temperature and the derived variable salinity and density, can be measured by multiparametric probes [4]. Water column parameter measurements can be performed using three main platforms: ships, towed vehicles and buoys. The measurement platform should be chosen according to the spatial and temporal scales of the phenomena to be investigated (Fig. 1).

Biological parameters
The techniques and tools for measuring biological parameters in the marine environment are the basis of study for the processes that generate and regulate the life of marine organisms. Biological parameters are therefore the key elements for assessing the anthropogenic effects, both direct and indirect, on the entire biotics. In the following paragraphs three groups are summarized: plankton and macroalgae, benthos, fish and marine mammals.

Plankton, Macroalgae and Seagrasses
Phytoplankton, the photosynthetic fraction of plankton, usually smaller in dimension than animal one, is studied through the use of samplers and probes. Phytoplankton is sampled with towed nets for the microscopic assessment of species and relative abundance [6, 7]. Bottles are used in the evaluation of pigment concentration, typically chlorophyll a, by sampling of microalgal cells in the water column at selected depths. The collected water, filled with phytoplankton, is filtered; then the filter is analysed through spectrophotometer or liquid chromatography (HPLC).
Additionally, probes can be used for the *in-situ* assessment of phytoplankton populations [8]. The probes must be equipped with fluorometer sensors to exploit the principle of the fluorescence of chlorophyll in photosynthetic cells under a known light impulse. During the immersion of the probe, the absorption-emission behaviour of phytoplankton cells gives information on the abundance and distribution of the populations in the water column, for example the Deep Chlorophyll Maximum (DCM). When water layers with high population are detected, the sampling procedure will allow a better assessment of the abundance. Zooplankton, the animal microorganisms in plankton population, are mainly studied through the use of towed nets that collect animals on a vertical profile or along a fixed bathymetry [8, 9]. Collected water samples are then evaluated at the microscope, allowing the identification of phyla, families and even species of living animals. Information on the abundance of the species is assessed on a statistical basis.
Macroalgae and Seagrasses are sampled using different equipment and techniques involving scientific diving, remote imaging, sonar and laboratory operations [10, 11, 12]. Tools like Remotely Operated Vehicles (ROV) and Side Scan Sonar (SSS) are used not only to assess the presence of species and their distribution, but also to collect information on the density over the

sea bottom substrate. Scientific divers can assess the status and the density by measuring the number of organisms or shoots in a spatial unit. Divers can also collect information on the status and the trend of a typical meadow by observing particular features that characterize a certain species, for example the lower meadow limit in *Posidonia oceanica* or the presence of other target types of algae. If needed, divers can withdraw living samples for further phaenological and genetic analysis at the laboratory.

Benthic communities

Benthic communities are directly dependent on the type of substrate. Physical (particle-size class and depositional gradients) and chemical (total organic matter, total organic carbon and metals) changes of the substrate result in a direct effect on intra-and interspecific distribution of benthic organisms.

Benthos sampling is carried out with Van Veen grabs by capturing sediment samples of comparable volumes [4, 13]. After sampling, sieving is performed in order to separate the organisms from the sediment using a mesh size equal to 1 mm. The biological and non-biological material that remains after sieving is transferred into suitable containers and fixed with a solution of formaldehyde and filtered seawater. Typically, a first phase of the analysis involves identifying priority taxa - polychaetes, molluscs, crustaceans and echinoderms into distinct groups. Subsequent analysis can lead to further identification of the lowest possible taxonomic level. The quantification of priority taxa already provides very important information when compared with the data obtained from the analysis of chemical and sedimentological characteristics of the substrate.

Fish, birds and mammals

Monitoring methodologies and strategies designed to understand the potential impact of offshore renewable energy development on marine fishes are varied and differ according to the aim of the survey and the site characteristics [14, 15]. Methodologies which can be applied to fish monitoring include:

- Desk study
- Commercial techniques (pots, trawls, fixed nets and lines)
- Underwater video and stills photography
- Grabs
- Acoustic Ground Definition System
- 'Scientific' echo-sounder
- Side scan sonar
- Landings data
- Effort data
- Fisheries liaison
- Socio-economic evaluations

For marine mammals, different monitoring approaches have been developed. Techniques vary from desk studies to visual observation and acoustic surveys. In particular, visual assessment is carried out mainly through boat observation. Ad-hoc campaigns can be scheduled but also ships of opportunity are commonly used in the surveys. In presence of capes and headlands, observation from strategic points on the coast can also be an effective method. In case of large marine areas and migratory species, aerial surveys can be employed. Adverse marine condition can inhibit the quality of visual observation. Acoustic surveys are mainly deputed to sonar instrumentation, mainly through passive techniques. Outside shipping routes hydrophones surveys are a resource. Active sonar is currently being trialled and developed to detect and image diving marine mammals.

Seabirds are typically surveyed from a land-based visual observations point, or for larger developments further offshore, boat-based surveys may be used. Active sonar is currently being trialled and developed to detect and image diving seabirds. X-band radar techniques are being developed to image birds in flight above the sea surface, too.

Database for environmental monitoring techniques and equipment

The Database for Environmental Monitoring Techniques and Equipment has been constructed

using information from the tables of monitoring equipment and techniques (Tab. 2 and Tab. 3), in which each technique is ordered in function of the related environmental compound. Methodological approaches have been outlined as a function of both the characteristics of the parameters of interest, both spatial and temporal, and considering the measurement technology available (Fig. 2). The DEMTE (Tab. 3) covers the availability of the instrumentation and of the monitoring techniques present within the consortium, and represents the result of a logical approach that can be used as a standard in different contexts. Considering the high number of partners in the consortium MaRINET, the gaps highlighted in the construction phase of the database can be a framework not really characteristic of the actual difficulty in setting up an effective monitoring plan for the impacts in the marine environment applied to the use of energy from renewable sources. However, the logical approach used can be an effective tool for the rapid assessment of any gaps as it can represent a standard methodology in the planning of this type of monitoring activities. The identification of the gaps also allows a quick estimate of the costs involved since the extension and multidisciplinarity of monitoring activities in the marine environment can result in a significant financial commitment.

Technique	Wind	Tides & Currents	Waves	Geomorphology	Sediments	Mixing	Water Column
Acoustic Backscatter Systems					Primary		Primary
Underwater Sonar		Secondary		Primary			
Acoustic Velocimeter		Primary	Primary		Secondary		
Passive Acoustic							
Optical Backscatter Systems				Secondary	Secondary		Primary
Lagrangian Drifter		Primary					
Sediment Particle Tracking					Primary		
Satellite Obs. and Tracking	Primary	Primary	Primary				Primary
Video		Secondary	Secondary	Secondary	Primary		
Wave Buoys		Secondary	Primary				
Conductivity meter						Primary	Primary
Fluorimeter							Primary
Tagging							Primary
Visual Surveys							Primary
Anemometer	Primary			Primary	Primary		
Non-Acoustic Current Meters		Primary	Secondary			Secondary	
Thermometer						Secondary	Primary
Sampler: Grabs					Primary		
Sampler: Nets					Primary		
Sampler: Vehicles					Primary		Secondary
Sampler: Corers					Primary	Primary	
Radar	Secondary	Primary	Primary	Primary			
Eh Meter					Primary		
Oxygen							Primary
Transmissometer						Secondary	
Water Column Profiler						Secondary	Primary
CTD						Secondary	Primary

Primary Technique
Secondary Technique

TABLE 1 Primary and secondary techniques for physical parameters measurements

Technique	Plankton	Macro-algae	Benthic Communities	Fish	Mammals	Birds	Inter-tidal communities
Acoustic Backscatter Systems							
Underwater Sonar							
Acoustic Velocimeter							
Passive Acoustic							
Optical Backscatter Systems							
Lagrangian Drifter							
Sediment Particle Tracking							
Satellite Obs. and Tracking							
Video							
Wave Buoys							
Conductivity meter							
Fluorimeter							
Tagging							
Visual Surveys							
Anemometer							
Non-Acoustic Current Meters							
Thermometer							
Sampler: Grabs							
Sampler: Nets							
Sampler: Vehicles							
Sampler: Corers							
Radar							
Eh Meter							
Oxygen							
Transmissometer							
Water Column Profiler							
CTD							

Primary Technique
Secondary Technique

TABLE 2 Primary and secondary techniques for biological parameters measurements

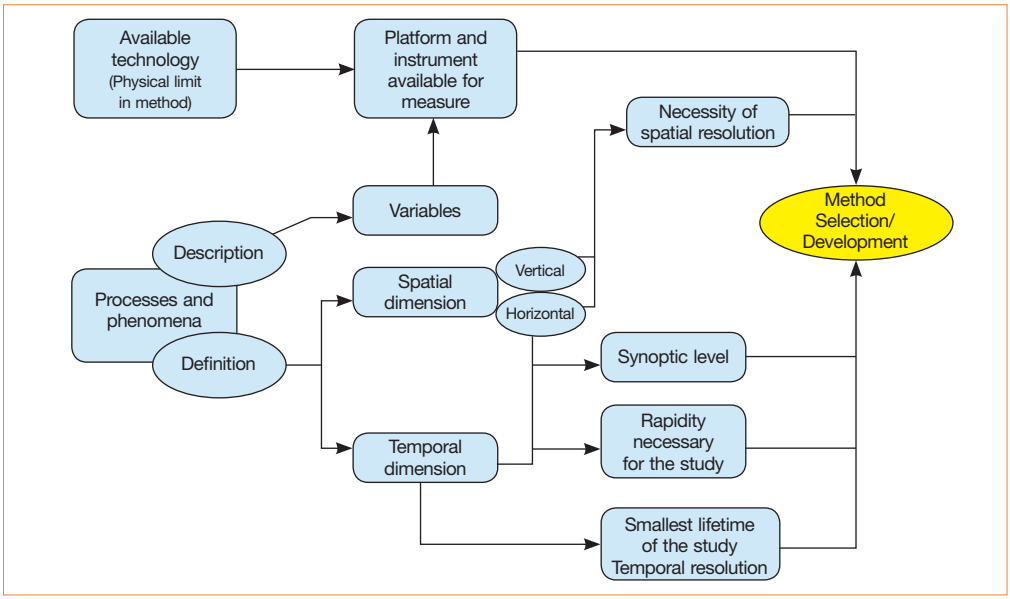

FIGURE 2
Conceptual framework for the implementation of monitoring in the marine and coastal environment

Instrument options	Operating principle	Methodology	Primary parameters	Secondary parameters	Operating range	Sampling frequency	Estimated cost (Euro)
			Acoustic Backscatter Systems				
Aquascat 1000	Record travel time and amplitude of backscattered acoustic signal	Frame mounted, downward facing	Sediment concentration		1 m	128 Hz	>10k
			Underwater Sonar				
Lowrance Structure Scan	Sonar	Fixed to boat	Geomorphology	Mixing benthic communities	Depth dependent	455 kHz and 800 kHz	1-10k
Nortek AWAC wave/current profilers	Doppler effect	Fixed to seabed	Current speed/ direction, wave height	Mixing benthic communities, fish, mammals, birds	Depth dependent	Depth dependent (1 MHz, 600 kHz, 400 kHz)	>10k
Teledyne RDI Sentinel Current Profiler	Doppler effect	Fixed to seabed or boat	Current speed/ direction, wave height	Mixing benthic communities, fish, mammals, birds	Depth dependent	0.05-1 Hz depth dependent, surface trace >1 sec period	>10k
M3i Satellite GPS buoy with echo sounder - Marine Instruments	Satellite GPS buoy with echo sounder	Moored to seabed	Fish	Sea water temperature	From 6-50 m with a 3 m resolution	500W and 50 kHz	1-10k
RESON Sea Bat 7125	High resolution multibeam echosounder	From boat	Sea floor characterization		0.5-500 m	1-50 Hz	>10k
			Acoustic Velocimeter				
Active sonar	Doppler effect	Fixed to seabed or boat	Currents, waves		Depth dependent	4-200 Hz	>10k
			Passive Acoustic				
Drifting Acoustic Recorder and Tracker (DART)	Acoustic recorder	Drifting hydrophone	Underwater noise, marine mammals	GPS location, temperature	5 m depth	4-96 kHz	1-10k
W.A. Inc. SM2M	Autonomous acoustic recorder	Fixed to seabed	Underwater noise, marine mammals	Temperature	150 m max depth	4-96 kHz	1-10k
Cetacean Research C55	Hydrophone	Fixed to seabed or boat	Underwater noise, marine mammals		Depth variable, dependent on attachment options	0.2-44 kHz	<1k
Neptune Sonar d/70	Spherical Hydrophone	Fixed to seabed or boat	Underwater noise, marine mammals		Depth variable, dependent on attachment options	10 Hz-100 kHz	1-10k
Bruel and Kjaer 8104	Hydrophone	Fixed to seabed or boat	Underwater noise, marine mammals		Depth variable, dependent on attachment options	0 Hz-180 kHz	1-10k
High Tech Inc. 99 UHF Broadband Hydrophone	Hydrophone	Fixed to seabed or boat	Underwater noise, marine mammals		Depth variable, dependent on attachment options	Designed for ultrahigh frequency response - Hz to 250 kHz	1-10k
DigitalHyd SR-1	Autonomous acoustic recorder	Fixed to seabed	Underwater noise	Temperature, pressure	35 m max depth	1 Hz - 25 kHz	1-10k
RTSYS EA-SDA14	Autonomous or cabled acoustic recorder	Fixed to seabed or deployed from boat	Underwater noise, marine mammals	Pressure, temperature, attitude	150 m max depth	Variable 39 kHz to 2.5 MHz	>10k
Jasco AMAR G2	Autonomous acoustic recorder	Fixed to seabed	Underwater noise	Temperature		64 kHz - 96 kHz	1-10k
Chelonia Ltd. CPOD	Autonomous acoustic recorder	Fixed to seabed	Cetaceans (whales, dolphin, porpoise), sonar	Temperature	100 mm max depth	20-160 kHz	1-10k
D11 Sonstec sonobuoy	Autonomous acoustic recorder	Fixed to seabed	Underwater noise, marine mammals		300 m max depth	1 Hz - 80 kHz	1-10k
Bruel and Kjaer Hydrophone - type 8105	Autonomous acoustic recorder	Towed	Underwater noise, marine mammals		100 m max depth	0.1 Hz - 160 kHz	1-10k

(continue)

(continue Tab. 3)

Instrument options	Operating principle	Methodology	Primary parameters	Secondary parameters	Operating range	Sampling frequency	Estimated cost (Euro)
			Video				
Baited Remote Underwater Video system	Video	Multiple 1 hour deployments of underwater video cameras	Biodiversity and abundance of mobile marine species	Sediments	100 m max depth	Seasonal to annual dependent on resource available, always at least annual	1-10k
SEAEYE Falcon DR	ROV with underwater camera	From boat	Biodiversity and abundance of mobile marine species	Sediments	1000 m max depth		>10k
Seabotix LBC300-5	ROV with underwater camera	From boat	Biodiversity and abundance of mobile marine species	Sediments	300 m max depth		>10k
Seabotix LBC 200-4	Small Observation class ROV	Visual inspection	Images, depth, temperature	Collection of small samples, fauna and flora identification, other equipment can be attached	200 m max depth		>10k
			Wave buoys				
Fugro Oceanor Seawatch mini II	Surface following accelerometer	Moored to seabed using a clump weight and bungee	Surface motion, waves (height, period and direction)	GPS location	150 m max depth	2 Hz	>10k
Datawell Directional Waverider mk III	Surface following accelerometer	Moored to seabed using a clump weight and a bungee	Waves (height, period and direction)	GPS location	150 m max depth	3.84 Hz	>10k
Fugro Oceanor Seawatch Wave Scan	Sensor for wave direction	Moored to seabed	Waves (height, period and direction)	Wind speed, air pressure, air temperature, solar radiation, currents, water temperature	Unknown		>10k
			Fluorometer				
Seapoint Chlorophyll Fluorometer	Optical	Water column profiler module	Water column quality (chlorophyll a)	Mixing	6000 m max depth	10 Hz	1-10k
Sea Tech Fluorometer	Optical	Water column profiler module	Water column quality (chlorophyll a)	Mixing	3000 m max depth	0.1 - 10 Hz	1-10k
			Visual Surveys				
Scientific divers	Visual survey	Boat-based point-point sample assessment	Seagrass coverage and density			Monthly	<1k per day
Human observers	Visual survey	Shore based wildlife observations	Marine mammals and seabirds	Vessel traffic and weather	4km max	20 hrs per week in 5x4 hr watches	<1k per day
Human observers	Visual survey	Boat-based point-sample assessment	Bird abundance and species diversity			Monthly	<1k per day
			Tagging				
Baited fishing pots	Baited traps	Twice yearly assessment of crabs and lobsters using potting	Species abundance and diversity		100 m max depth	Twice yearly	<1k

(continue)

(continue Tab. 3)

Instrument options	Operating principle	Methodology	Primary parameters	Secondary parameters	Operating range	Sampling frequency	Estimated cost (Euro)
			Meteorological				
1st class Anemometer from Thies, Vector Instruments, Risoe	Cup Anemometer	Help at a position of between 40-100 m above the ground	Wind speed		0-45 m/s wind speed	20 Hz	<1k
WindMaster Ultrasonic Anemometer, Metek, Thies, Lufft	Ultrasonic	Held at a position above ground	Wind speed and direction	Air temperature, humidity, barometric pressure, dew point	0-45 m/s wind speed	3 sec average wind speed, 10 min averages for all other parameters, up to 50 Hz	1-10k
Wind Vane, Thies	Potentiometer	Held at a position of between 40-100 m above the ground	Wind direction	Air temperature, humidity, barometric pressure, dew point	0-360°	1 Hz	<1k
Thies	PT 100, K-Element	Held at a position of between 40-100 m above the ground	Air density determination and correction, thermal effects, stratification		-30°C - +70°C	1 Hz	
GillMet meteorological station	Wind speed/ direction: ultrasonic probe. Air pressure: standard sensor. Temperature, humidity, dewpoint: standard probe	Ground mounter, continuous operation	Wind speed and direction, air temperature, humidity, baro-metric pressure, dew point		0-60 m/s wind speed, -35°C - +70°C air temp, 1-100% relative humidity, 600-1100hPa air pressure	Outputs 10 min average results	1-10k
Vaisala		Held at a position of between 40-100 m above the ground	Air density determination and correction		500-1100hPa	1 Hz	<1k
Lidar (Leosphere, Sgurr Energy, Halo Photonics, Zephir Ltd, Pentalum)	Laser doppler anemometry	Installed on ground: up to 220 m. Installed on nacelle of WTG: wind field in front/ in wake of turbine	Wind speed and direction	Air temperature, humidity, barometric pressure, dewpoint	0-60 m/s wind speed	0.5 Hz	>10k
Lidar (Sgurr Energy, Leosphere)	Laser doppler anemometry	Installed on ground: up to 4000 m	Wind speed and direction	Air temperature, humidity, barometric pressure, dew point	0-70 m/s, 80-4000 m		>10k
			Non-acoustic current meters				
Electromagnetic current meters	Strength of induced magnetic field of moving conductor	Frame mounted	2 components of velocity			Variable 1-32 Hz	>10k
			Sampler - Grabs				
Mini Van Veen Grab	Gravity grab	Small vessels operations	Benthic communities	Sediments	Depth dependent	Sampling area: 0.1 m2	<1k
Van Veen Grab	Gravity grab	Small vessels operations	Benthic communities	Sediments	100 m	Sampling area: 0.1 m2	1-10k
Modified Smith-McIntyre grab	Gravity grab	Medium-big vessels operations	Benthic communities	Sediments	300 m	Sampling area: 0.1 m2	1-10k
Shipeck Grab Sampler	Gravity grab	Small vessels operations	Benthic communities	Sediments	100 m	Sampling area: 0.04 m2	1-10k
			Sampler - Corers				
Uwitec Gravity Core	Gravity corer	Small vessels operations	Sediments	Mixing	Depth dependent		1-10k

(continue)

(continue Tab. 3)

Instrument options	Operating principle	Methodology	Primary parameters	Secondary parameters	Operating range	Sampling frequency	Estimated cost (Euro)
			Radar				
WaMoS	X-band radar	Shore based	Waves and currents	Vessel traffic, flying birds	Variable depending on radar setup	Variable depending on radar setup	>10k
WERA	High frequency radar	Shore based	Waves and currents	Wind speed and direction, vessel traffic	300km max range depending on setup	Currents every 5 mins, waves every 17 mins	>10k
			Transmissometer				
Wetlab C-Star	Optical	Water column profiler module	Water column quality	Mixing	2000 m max depth	8 Hz	1-10k
SeaTech	Optical	Water column profiler module	Water column quality	Mixing	2000 m max depth	10 Hz	1-10k
			Water Column Profiler				
Primprod 1.08 and Primprod 1.11	Multiparametric profiler	Water column profiler	Water column quality (temperature, pression, biomass, photosynthetic activity, underwater irradiance)	Mixing	200 m max depth	1-4 Hz	>10k
Idronaut 316 and Idronaut 317	Multiparametric profiler	Water column profiler	Water column quality (pressure, temperature, conductivity, oxygen, pH)	Mixing	1000 m max depth	20, 30, 40 Hz	>10k
T-FLAP	Multiparametric profiler	Water column profiler	Water column quality (pressure, temperature, conductivity, oxygen, pH)	Mixing	1000 m max depth	5.6 Hz	<1k
			CTD				
SBE 19 Seacat	CTD	Profiler and moored mode	Water column quality (CTD)	Mixing	6800 m max depth	4 Hz	1-10k
Seabird 911	CTD	Water column profiler	Water column quality (CTD)	Mixing	6800 m max depth	24 Hz	>10k
RBR XR 420	CTD	Moored to seabed	Conductivity (salinity), depth, temperature	Mixing		0.05 Hz	>10k
Aanderaa 4120 IW	CTD and salinity	Fixed on the facility buoy	Water column quality (CTD)	Mixing	300 m max depth	0.5 Hz	>10k
Valeport miniCTD	CTD	Water column profiler	Salinity, temperature, depth	Mixing	500 m max depth	4 Hz	<1k
Seabird SBE25	CTD	Water column profiler	Water column quality: conductivity, temperature, pressure, oxygen, irradiance, light transmission, fluorescence (chlorophyll a), pH	Mixing	3000 m max depth depending on senser	8 Hz	>10k

Conclusions

This work shows the Database for Environmental Monitoring Techniques and Equipment which details the instrumentation, equipment and techniques presently in use by MaRINET project partners. The DEMTE database lists all the commonly used techniques, tools and equipment necessary for monitoring the marine environment as related to the installation and operation of marine energy devices. An additional purpose of the work is to present any gaps in the instrumentation and equipment database, especially in view of a proper coverage of all the activities necessary for the implementation of robust environmental impact monitoring plan.
From the analysis of the database it is clear that the number and quality of instruments and the equipment of MaRINET consortium can cover all marine environmental compartments; database gaps pertain mainly to the lack of facilities and laboratories endowed with of underwater vehicles as well as to the reduced skills of the consortium partners in the use of satellite technologies. However, the logical approach adopted can be an effective tool for the rapid assessment of any gaps as it can represent a standard methodology in the planning of this type of monitoring activities. The identification of the gaps also allows a quick estimate of the costs involved since the extension and multidisciplinarity of monitoring activities in the marine environment can result in a significant financial commitment.

Sergio Scanu, Filippo Maria Carli, Viviana Piermattei, Simone Bonamano, Francesco Paladini de Mendoza, Marco Marcelli
University of Tuscia, Department of Environmental and Biological Sciences (DEB) - Laboratory of Experimental Oceanology and Marine Ecology, Civitavecchia, Italy

Peviani Maximo Aurelio
Electric Research System (RSE), Sustainable Development Department, Milano, Italy

Keith Dampney, Jennifer Norris
The European Marine Energy Centre (EMEC) Ltd, Old Academy Business Centre, Stromness, Orkney, Scotland

references

[1] R.R. Bidigare, B.B. Prezelin, R.C. Smith, Bio-optical models and the problems of scaling, in *Primary Productivity and Biogeochemical Cycles in the Sea*, Plenum Press, New York, pp. 175–212, 1992.

[2] M. Marcelli, A. Pannocchi, V. Piermattei, U. Mainardi, New Technological Developments for Oceanographic Observations, in *Oceanography*, pp. 41-78, Edited by Marco Marcelli, Publisher InTech, ISBN: 978-953-51 0301-1, 2012.

[3] U.S. Environmental Protection Agency, Methods for Collection, Storage and Manipulation of Sediment for Chemical and Toxicological Analyses: Technical Manual, EPA-823-B-01-002, 2001.

[4] A.M. Cicero, I. Di Girolamo, ICRAM - Italian Ministry of Environment, Metodologie Analitiche di Riferimento, 2001.

[5] ISO 5667-19:2004 Water quality -- Sampling -- Part 19: Guidance on sampling of marine sediments.

[6] S.W. Jeffrey, R.F.C. Mantoura, S.W. Wright, Phytoplankton Pigments in Oceanography: Guidelines to Modern Methods, Monographs on oceanographic methodology 10, ISBN 92-3-103275-5, UNESCO, 1997.

[7] A. Sournia, Phytoplankton Manual, Monographs on oceanographic methodology 6, ISBN 92-3-101572-9, UNESCO, 1978.

[8] G. Socal, I. Buttino, M. Cabrini, O. Mangoni, A. Penna, C. Totti, Metodologie di Studio del Plancton Marino, ISPRA, Manuali e linee guida 56/2010, ISBN 978-88-448-0427-5, ISPRA, 2010.

[9] D.J. Tranter, J.H. Fraser, Zooplankton Sampling, Monographs on oceanographic methodology 2, ISBN 92-3-101194-4, UNESCO, 1968.

[10] E. Ballesteros, S. Pinedos, M. Garcìa, L. Mangialajo, M. De Torres, A new methodology based on littoral community cartography for the implementation of the European Water Framework Directive, in *Mar. Poll. Bull.*, vol .55, pp. 172-180, 2007.

[11] R.C. Phillips, C.P. McRoy, Seagrass Research Methods, Monographs on oceanographic methodology 9, ISBN 92-3-102660-7, UNESCO, 1990.

[12] F. Borfecchia, C. Micheli, F. Carli, S. Cognetti De Martis, V. Gnisci, V. Piermattei, A. Belmonte, L. De Cecco, S. Martini, M. Mercalli, Mapping spatial pattern of *Posidonia oceanica* meadow by means of Daedalus ATM airborne sensor in the coastal area of Civitavecchia (central Tyrrhenian sea, Italy), in *Remote Sensing*, vol. 5, pp. 4877-4899, doi:10.3390/rs5104877, 2013.

[13] A. Eleftheriou, A. McIntyre, Methods for the Study of Marine Benthos, Blackwell Science Publications, ISBN 0-632-05488-3, 2005.

[14] K. Macleod, C. Lacey, N. Quick, G. Hastie, J. Wilson, Guidance on Survey and Monitoring in Relation to Marine Renewables Deployments in Scotland, Volume 2: Cetaceans and Basking Sharks, unpublished draft report to Scottish Natural Heritage and Marine Scotland, 2011.

[15] C. Sparling, K. Grellier, E. Philpott, K. Macleod, J. Wilson, Guidance on survey and monitoring in relation to marine renewables deployments in Scotland, Volume 3: Seals, unpublished draft report to Scottish Natural Heritage and Marine Scotland, 2011.

Wave energy potential: A forecasting system for the Mediterranean basin

ENEA is performing ocean wave modeling activities with the aim of both characterizing the Italian sea energy resource and providing the information necessary for the experimental at sea and operational phases of energy converters. Therefore a forecast system of sea waves and of the associated energy available has been developed and has been operatively running since June 2013. The forecasts are performed over the entire Mediterranean basin and, at a higher resolution, over ten sub-basins around the Italian coasts. The forecast system is here described along with the validation of the wave heights, performed by comparing them with the measurements from satellite sensors.

DOI: 10.12910/EAI2015-053

A. Carillo, G. Sannino, E. Lombardi

Introduction

Wave energy is a promising renewable resource that is receiving particular attention in countries facing large oceans, where the greatest wave energy potential is found. In Europe, most of the pilot plants either planned or in operation are located along the Atlantic coasts, in countries such as Ireland, Portugal, Spain, Norway, and the UK. The intensity of waves is in fact determined by the winds blowing over the sea and reaches the highest values in the presence of strong winds and long fetches.

The Mediterranean is a semi-enclosed sea and is characterized by lower values of wave energy with respect to the major oceans. Nevertheless, the conversion of wave energy can represent, even under these conditions, an economically profitable resource if ad-hoc designed energy converters are developed. In these lower energy areas, in fact, devices of reduced size can be more suitable to extract energy. This, together with the need of facing lower extreme weather conditions, can significantly reduce installation and maintenance costs.

The first step to perform for the development of wave energy production is the characterization of the resource. Climatology of the energy available in the Mediterranean basin has been performed using a wave model at the horizontal resolution of 1/16°; results are presented in [1]. The most productive areas along the Italian coasts have been identified in western Sardinia and north-western and southern coasts of Sicily.

Actually some wave energy converters developed for the Mediterranean conditions are at the field experimental stage. A wave forecast system has been implemented with the aim of providing a support to field activities. It has to be stressed that high resolution forecast in specific sites will be also necessary in the operational stage, for the management of the energy network in which the

Contact person: Adriana Carillo
adriana.carillo@enea.it

wave resource will be inserted. It will also provide an important support for the planning of marine operations and the device maintenance.
The operational forecast system has been achieved at the spatial resolution of 1/32° for the entire Mediterranean basin. Boundary conditions provided by this model are then used to force laterally ten higher resolution models developed in the most interesting areas around the Italian coasts. The forecast system has been running for more than one year and now a validation against data derived from satellite measurements has been performed.

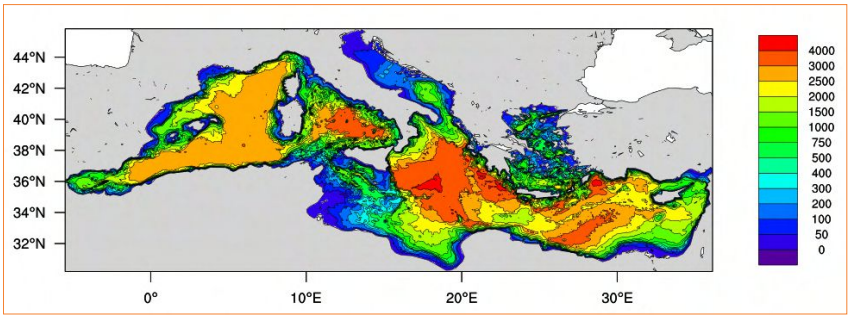

FIGURE 1 Model bathymetry for the Mediterranean basin (in meters)

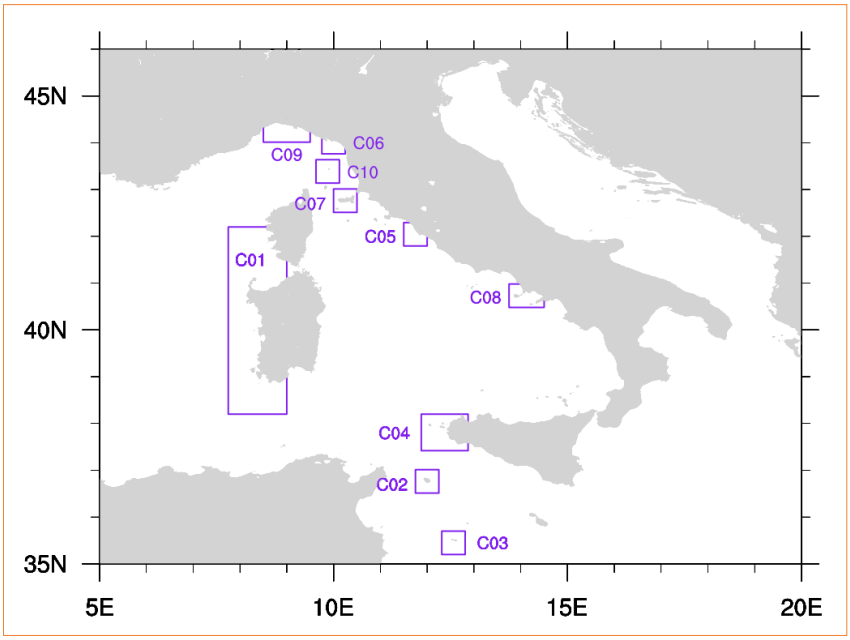

FIGURE 2 Model domains of the ten higher resolution models around the Italian coast

Numerical models

Wave simulations are performed using a parallel version of the WAM wave model Cycle 4.5.3. [2, 3]. WAM is a spectral model that solves the wave transport equation explicitly without any presumptions on the shape of the wave spectrum. The model is widely applied at basin scale and has been developed to simulate wave propagation in deep water. In the forecast system the model domain covers the entire Mediterranean Sea, from 5.50°W to 36.125°E of longitude and from 30.2°N to 45.825°N of latitude. The domain is discretized in spherical coordinates with a uniform resolution of 1/32° in each direction, corresponding to a linear mesh size of about 3.5 km. Model bathymetry has been calculated from the General Bathymetric Chart of the Oceans (GEBCO) 30 arc-second gridded data set [4] by averaging the depths of data points falling in each computational cell. Figure 1 shows the computational domain and the model bathymetry.
The directional wave energy density spectrum is discretized using 36 directional bins, corresponding to an angular resolution of 10°, and 32 frequency bins starting from 0.06 Hz with relative size increments of 0.1 between one frequency bin and the next one.

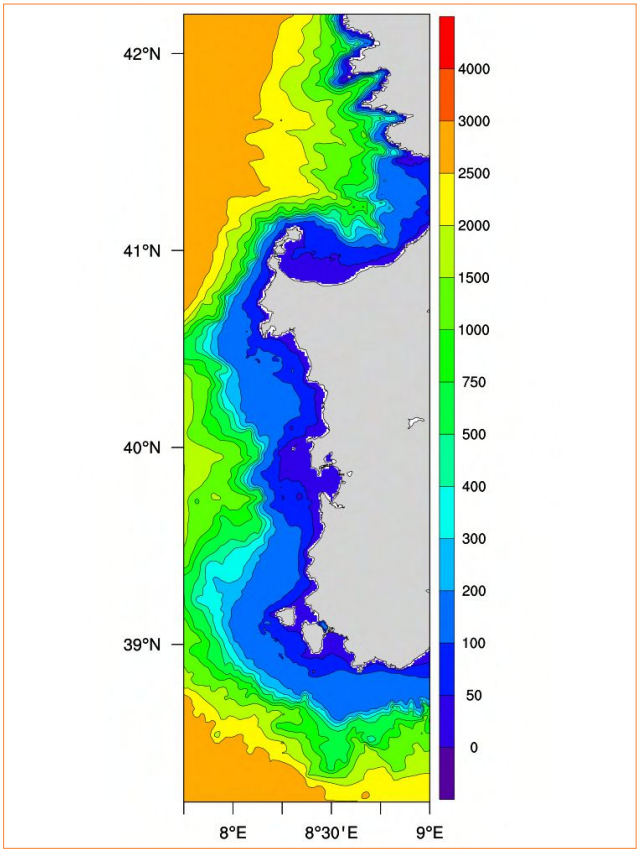

FIGURE 3 Model bathymetry for the western Sardinia sub-basin (in meters)

Higher resolution forecast simulations are computed over ten sub-basins around the Italian coasts. In order to take into account both waves generated locally by winds and waves propagating from distant areas, a nesting procedure has been applied. Spectral wave data derived from the WAM model are used as boundary conditions for the higher resolution models. The domains, shown in Figure 2, have been selected looking at the wave energy production. The most extended areas include the entire western coast of Sardinia (Fig. 3) and the westernmost part of Sicily, that are the most energetic in the Central Mediterranean, being reached by the strong north-westerly winds from the Gulf of Lions. Other areas have been defined around some minor Italian islands, where wave energy production can contribute significantly to the energy independence. All these models have a spatial resolution of 1/128°, the boundary conditions are applied hourly.

These simulations are carried out using SWAN model (Simulating WAves Nearshore) [5]. SWAN is specifically built to be used in shallow water and includes depth-induced wave breaking and triad wave-wave interactions, which are important for near-shore wave prediction. SWAN is a third-generation wave model integrating the action density spectrum, without any assumption on the spectral shape. The equation is solved using an implicit propagation scheme based on finite differences. Here the same discretization in frequency and direction has been used as that defined for the WAM model.

The entire forecast system composed by WAM and SWAN models is forced with hourly wind fields obtained from the meteorological operational system SKIRON, developed by the Atmospheric Modeling and Weather Forecasting Group of the University of Athens [6]. The atmospheric model is based on the limited area model Eta/NCEP and is run daily over the Mediterranean basin at the horizontal resolution of 0.05° × 0.05°. The forecast spans over a period of five days.

Wave forecast for the entire Mediterranean basin and the ten sub-basins are performed daily for the following five days. The main wave variables are stored at each grid point every hour, in particular: the wave significant height, mean wave period and mean direction of propagation, and the same parameters for the swell and sea components separately. Moreover, the wave power flux per unit crest, defined by the expression:

$$J = \frac{\rho g^2}{64\pi} T_e H_s^2$$

where J is in Watt per meter of wave crest, g is the gravity acceleration, r the sea water density assumed to be $r = 1025$ kg m^{-3}, H_s the significant wave height, and T_e the significant wave period. A web page is daily updated with images of the hourly forecast of the main integrated wave parameters.

Model validation

The forecast system has been operatively running since June 2013. A validation of the wave forecasts has been performed by comparison with satellite data from radar altimeters that provide significant wave heights (Hs) measurements. In this work data from two satellites, Jason-2 and Saral/Altika, in service over the last year and downloaded from the AVISO web site [7], have been used. In Figure 4 satellite tracks are shown, over which measures are periodically performed. Jason-2 repeats its cycle every 10 days and the tracks are spaced 315 kilometers at the equator; the Saral satellite, instead, repeats its cycle every 35 days but the separation between tracks is only 75 kilometers at the equator.

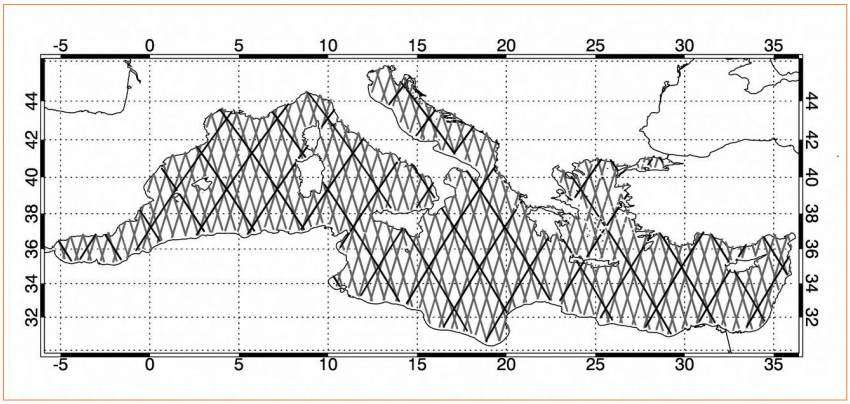

FIGURE 4 Satellite ground tracks used for model validation. Black lines identify Jason-2 and gray lines Saral/Altika

Satellite	forecast	samples	Bias (m)	Rmse (m)	si	slope	d
Jason-2	Day 1	100,399	0.20	0.40	0.34	0.83	0.93
	Day 2	101,036	0.22	0.44	0.37	0.81	0.92
	Day 3	99,386	0.24	0.50	0.42	0.78	0.89
Saral/ Altika	Day 1	74,709	0.19	0.38	0.36	0.82	0.93
	Day 2	74,896	0.20	0.42	0.39	0.80	0.91
	Day 3	74,691	0.21	0.46	0.44	0.78	0.89

TABLE 1 Satellite statistics and model significant wave-height comparison for the entire Mediterranean basin

The comparison with these data can be used to evaluate the overall behavior of the model over the entire Mediterranean Sea.
Data have been processed following the procedure described by Queffeulou and Bentany [8] to remove outliers. This procedure is based on the statistical analysis of the difference between consecutive points along the track. Tracks represented by less than three points are not considered, and points where the depths derived by the satellite and the model depth differ of more than 50% are also removed. Satellite data have been directly compared with the nearest model point, without any interpolation in space nor in time.
Significant wave heights derived by the WAM model for the entire Mediterranean basin have been validated using data obtained for the first, second and third day of the simulation.
Table 1 reports, for each satellite, the values of the statistical indices used to evaluate the model performance. In our analysis we included the bias between model and measures (*bias*), the root mean square error (*rmse*), the scatter index (*si*) and the slope of the best fit line passing through the origin (*slope*). Considering the series of n measures x_i and the corresponding model values y_i, these indices are calculated as follows:

$$bias = \frac{1}{n}\sum_{i=1}^{n}(y_i - x_i)$$

$$rmse = \sqrt{\frac{1}{n-1}\sum_{i=1}^{n}(y_i - x_i)^2}$$

$$si = \frac{rmse}{\frac{1}{n}\sum_{i=1}^{n} y_i}$$

$$slope = \frac{\sum_{i=1}^{n} x_i y_i}{\sum_{i=1}^{n} x_i x_i}$$

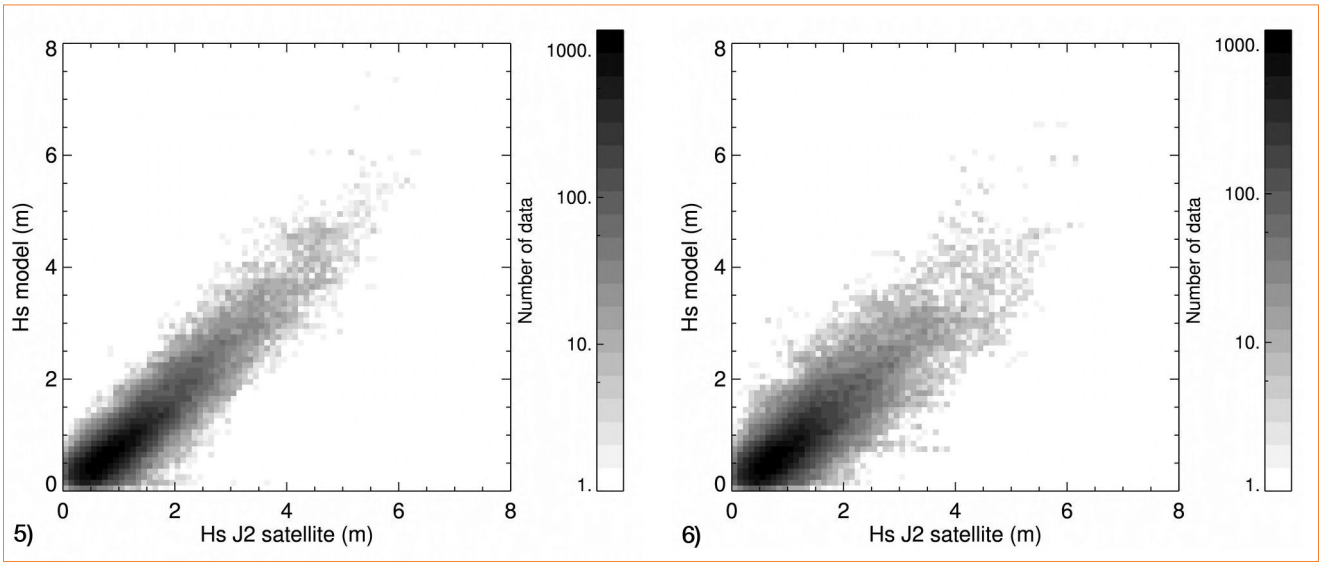

FIGURES 5-6 Scatter plot of model vs. Jason-2 satellite Hs for the entire Mediterranean basin. Values are grouped in 0.2 m wide bins. Model data are taken from the first day of forecast

The last index shown in the table is represented by the Willmott index (d), defined as:

$$d = 1 - \left[\sum_{i=1}^{n} (y_i - x_i)^2 \Big/ \sum_{i=1}^{n} (|y'_i| - |x_i'|)^2 \right]$$

where y_i' and x_i' are the deviations with respect to the average. This index assumes a value of 1 when the match between the two series of data is perfect. For each satellite the comparison has been performed using model outputs derived separately from the first three days of the forecast. All the statistical parameters do not change significantly from the first to the third day of the simulation; statistical parameters regularly get lightly worse with the number of the forecasted day. However the Willmott index always remains close to 0.9 and the bias near 0.2 m. A systematic underestimation is always present with values of the slope around 0.8. Scatter plots computed using all the available Jason-2 satellite data and WAM significant wave heights, respectively from the first and the third day of the forecast, are shown in Figures 5 and 6. A logarithmic scale has been used to represent the number of data in each bin. Values are grouped in bins of 0.2 m. The increase in the spreading of data in the third day of forecast with respect to the first can be observed.

Satellite	model	samples	Bias (m)	Rmse (m)	si	slope	d
Jason-2	WAM	1,421	0.33	0.60	0.40	0.82	0.93
	SWAN	1,421	0.32	0.51	0.34	0.83	0.95
Saral/ Altika	WAM	860	0.26	0.50	0.38	0.78	0.91
	SWAN	860	0.24	0.40	0.30	0.81	0.94

TABLE 2 Satellite statistics and model significant wave height comparison for the first day of the simulation in the sub-basin C01, corresponding to western Sardinia

In order to compare the results obtained by the WAM model with those of the higher resolution SWAN model, the procedure of validation has been performed using the first forecast day, also using only data from the domain of Sardinia's sub-basin. In

Table 2 are reported the statistical parameters computed using significant wave heights in this domain from the two simulations. Even if only few tracks are included in the area, the number of samples is sufficient for the comparison. Statistical results obtained in this region for the WAM model present higher values of bias and rmse with respect to those computed for the entire Mediterranean basin. This can be explained with the better representation of waves in the open ocean than those near-shore. All the statistical values obtained using the SWAN model show a clear improvement for both satellites.

Conclusions

A wave forecast system for the Mediterranean basin is currently running at ENEA. It provides output data for the following five days at the temporal resolution of an hour. The system consists in a simulation performed with the WAM model at the spatial resolution of 1/32° and ten nested simulations performed using the SWAN model at a resolution of 1/128°. A validation of the significant wave heights against the data measured by two satellites (Jason-2 and Saral/Altika) has been achieved using the data produced over the period between June 2013 and November 2014, both for the entire Mediterranean basin and the largest sub-domain considered, corresponding to the western coasts of Sardinia. The comparison executed separately over the first three days of the forecast has shown a reasonable agreement; in particular, the Willmott index and the slope do not vary significantly in the different days. The statistics of the significant wave height computed using only data in the sub-domain corresponding to western Sardinia show a slight improvement of the higher resolution simulation performed using SWAN model against the results obtained using the global simulation.

Adriana Carillo, Gianmaria Sannino, Emanuele Lombardi
ENEA, Technical Unit for Energy and Environmental Modelling, Rome, Italy

references & notes

[1] L. Liberti, A. Carillo, G. Sannino, WAM energy assessment in the Mediterranean, the Italian perspective, in *Renewable Energy 50*, 938-949, 2013.

[2] WAMDI-group: S. Hasselmann, K. Hasselmann, E. Bauer, P.A.E.M. Janssen, G.J. Komen, L. Bertotti, P. Lionello, A. Guillaume, V.C. Cardone, J.A. Greenwood, M. Reistad, L. Zambresky, J.A. Ewing, The WAM model - a third generation ocean wave prediction model, in *J. Phys. Ocean*, 18, 1775-1810, 1988.

[3] H. Günther, A. Behrens, The WAM model validation document version 4.5.3, Tech. Rep. Institute of Coastal Research Helmholtz-Zentrum Geesthacht (HZG), 2011.

[4] GEBCO.http://www.gebco.net/data and products/gridded bathymetry data/.

[5] N. Booij, R.C. Ris, L.H. Holthuijsen, A third-generation wave model for coastal regions: 1. Model description and validation, in *J. Geophys. Res*, vol. 104, C4, 7649-7666, 1999.

[6] G. Kallos, The regional weather forecasting system SKIRON, in *Proceedings, symposium on regional weather prediction on parallel computer environments, 15-17 October 1997*, Athens p. 9, 1997.

[7] The altimeter products were produced and distributed by *Aviso* (http://www.aviso.altimetry.fr/), as part of the Ssalto ground processing segment.

[8] P. Queffeulou, A. Bentamy, Analysis of wave height variability using altimeter measurements: application to the Mediterranean sea, in *Journal of Atmospheric and Oceanic Technology*, 24(12), 2078-2092, 2007.

Marine Waves Energy: A spatio-temporal DSS-WebGIS to support the wave-energy potential assessment in the Mediterranean Sea

GIS technologies are able to provide a useful tool for estimating the energy resource from the sea waves, assessing whether this energy flux is exploitable and evaluating the social and environmental impacts in deep water and/or in the seaboard. The DDS-WebGIS "Energy Waves" represents a tool for displaying and sharing geospatial data and maps, as well as a valuable support for new installations planning, forecasting system and existing infrastructure management.

DOI: 10.12910/EAI2015-048

M. Pollino, L. La Porta, E. Caiaffa

Introduction

As part of the activities related to the project "Ricerca di Sistema Elettrico" (Electric System Research), in the framework of an agreement between the Ministry of Economic Development and ENEA, a Web-based GIS (WebGIS) application, called Waves Energy, has been implemented and developed. Designed for sharing and exploiting geographic data and information about the marine and coastal environment, the application has been primarily set up as a tool for estimating the energy resource from the sea waves. The WebGIS can be reached at the following URL: http://utmea.enea.it/energiadalmare/.

The application was realized using Free/Open Source Software (FOSS), including a set of applicative solutions suitable for the above mentioned purposes and implemented in the context of a well-integrated platform and easy-to-use interface. This solution has allowed to publish, via the Web, a comprehensive data-set of geospatial information (thematic maps, marine phenomena trends, coastal environment information, etc.), according to the standards required by the Open Geospatial Consortium (OGC), using a set of specific features for viewing and consulting the maps in a framework, tailored for the Waves Energy application.

Objectives of the work

The WebGIS Waves Energy was designed and implemented in order to store and manage geographic and spatial data concerning marine and coastal areas of interest and, therefore, to provide support in the estimation of energy resources from the sea, by assessing whether this energy flux is exploitable and the impacts on social and environmental realities located in deep water and/or along the seaboard. The basic geospatial data and

Corresponding Author: Maurizio Pollino
maurizio.pollino@enea.it

the maps produced have been stored and managed in a repository, *ad hoc* structured. In such a way, the WebGIS represents the natural geographic interface of the Decision Support System (DSS) envisaged in the project: basic local information and maps can be visualized and queried via the Web, by means of a standard Web browser or mobile devices (e.g., tablet) and, consequently, the main results are open and accessible online.

The specific objectives of the DSS-WebGIS Waves Energy are to:

- define and characterise the marine and coastal areas investigated;
- support the integrated analysis of the study-areas, along with the identification of specific environmental indicators (e.g., during the phases related to the design of new facilities);
- provide support to monitoring and forecasting activities;
- share data, maps and information via the Web.

Implementing these features has required an advanced and integrated management of:

- basic geo-spatial data, necessary for marine and coastal areas characterisation (e.g., various natural components and infrastructures);
- new geo-spatial data, produced to support management and planning activities (e.g., weather and marine forecasts, etc.).

Among the advantages of using the WebGIS technology, it is possible to include:

- global sharing of geographic information and geospatial data;
- usability (the WebGIS application is exploitable by any common internet browser);
- widespread availability and capability to reach a broader audience of users.

System design and logical architecture

A fundamental, preliminary phase has concerned the implementation and use of spatial analyses and procedures (via GIS algorithms, the so-called *geoprocessing*): the aim was to develop, standardize and organise the available database, as well as to define the geo-statistics processing of data itself.

In this context, a key role was played by the data resulting from the simulations carried-out by the numerical oceanographic model used (WAM, model over the entire Mediterranean basin): these data-sets are produced in NetCDF files format (Network Common Data Form); then, through appropriate processing, they are transformed into a GIS-compatible format (ESRI shapefile, .shp) and made available for subsequent processing steps.

Concerning the implementation of the WebGIS application, a client-server architecture was adopted, using FOSS packages. Such architecture has been properly conceived to allow the interchange of geospatial data over the Web and to provide the system with characteristics of originality and applicative versatility.

The WebGIS architecture is shown in Figure 1 and can be outlined by the following logical chain:

Data Repository -> Web Server (GeoServer) -> Library (OpenLayers) -> Map Viewer (WebGIS)

The Data Repository identifies the storage area containing the data-set used (in GIS format). The access is allowed only to devices physically defined at the level of the Storage Area Network, in order to ensure the absolute integrity and consistency of the data themselves.

The Web Server represents the hardware/software environment that allows to organize information and make it accessible from the network. In the present case, it was decided to use the *GeoServer* suite. It is a largely used open-source application server, which plays a key role within the Spatial Data Infrastructure (SDI) implemented. It allows to share and manage (using different access privileges) information layers stored in the repository; it also supports interoperability (it reads and manages several formats of raster and vector data).

In the framework of the research activities just described, thanks to the above mentioned characteristics, Geoserver has been chosen to manage the layers (thematic maps, basic information and data, etc.) stored in the geospatial database and to accomplish their publication via the Web within the WebGIS application, according to the standards

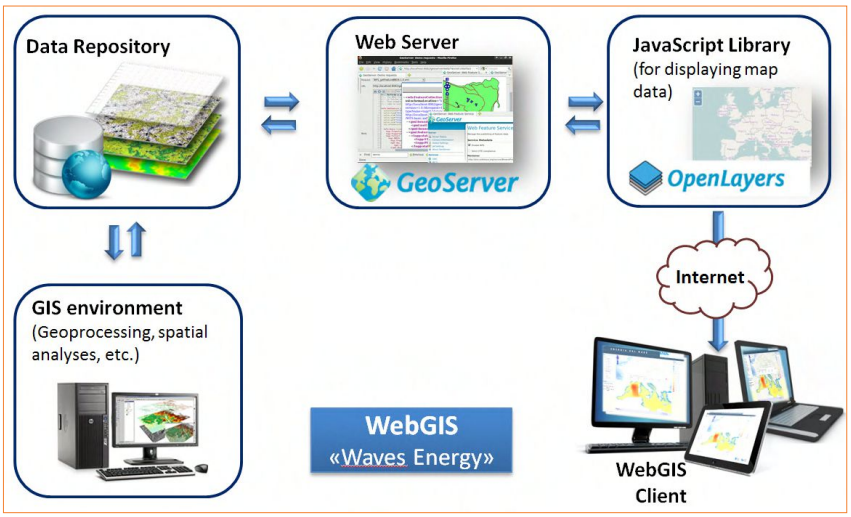

FIGURE 1 WebGIS architecture
(ENEA elaboration)

defined by the Open Geospatial Consortium (OGC), such as, for example, the Web Map Service (WMS). OpenLayers is an open-source JavaScript library, used to visualize interactive maps in web browsers. OpenLayers provides a so-called Application Programming Interface (API) allowing access to various sources of cartographic information on the Internet, such as WMS and WFS (Web Feature Service) protocols, commercial maps (Google Maps, Bing, etc.), different GIS formats, maps from the OpenStreetMap project, etc.
Thanks to the WebGIS interface the user (not necessarily with GIS-specific skills), through his own web browser, can view maps representing the results produced within the project activities. In particular, to visualize the data available, the WMS standard is exploited, by means of a *map-server* approach that allows to produce thematic maps of geo-referenced data and respond to queries about the content of the maps themselves.

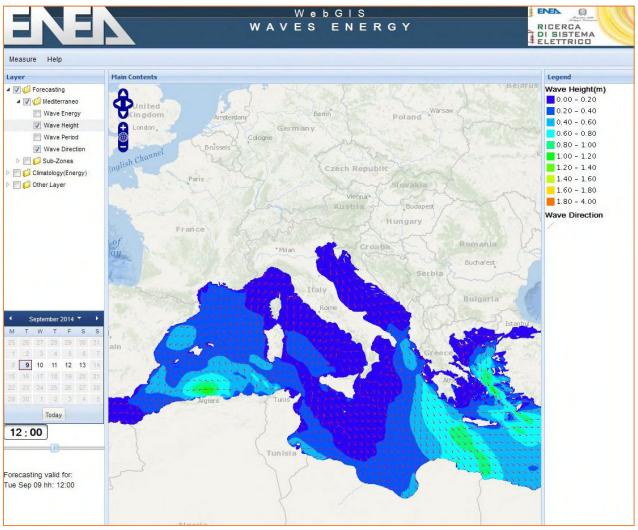

FIGURE 2 WebGIS Waves Energy interface, accessible at http://utmea.enea.it/energiadalmare/
(ENEA elaboration)

"Waves Energy" Application: Features and functions

The "Waves Energy" Application makes various basic features available , which are typical of a WebGIS such as, for example, zoom, pan, transparency, linear and areal measurements, etc. (Fig. 2). In addition, by clicking anywhere on the selected layer, the relevant information is displayed (qualitative or quantitative attributes, the so-called *inquiry* function).
The data-set provided by WebGIS has been grouped, according to its characteristics and specifications, into three distinct typologies:
a) Forecasting (Prediction models outcomes);
b) Climatology (Time series);
c) Other Layers (Basic geographic information).
The first set of data, produced for the entire Mediterranean Sea (with spatial resolution of about 3 km, 1/32 degree), provides 5-day forecasts, at hourly intervals, of the following physical quantities: wave energy flux, wave height, wave direction and wave period. In particular, by clicking a point of interest on the sea map, it is possible to obtain a specific graph,

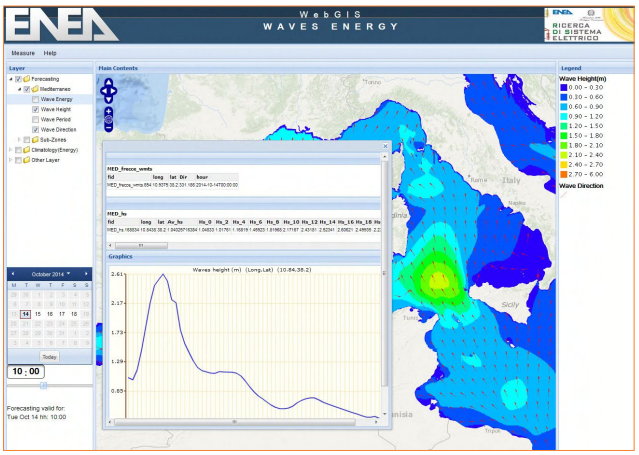

FIGURE 3 Forecasting: thematic maps related to height and direction of waves (GIS overlay), with the relative daily trend chart
(ENEA elaboration)

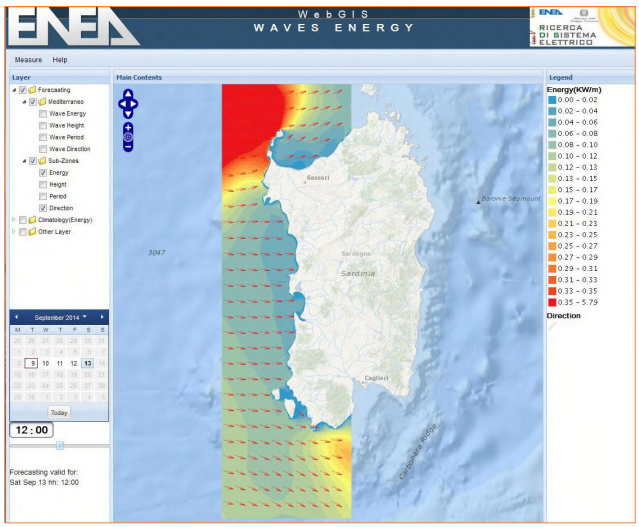

FIGURE 4 Forecasting: subset map of the Sardinian western coast
(ENEA elaboration)

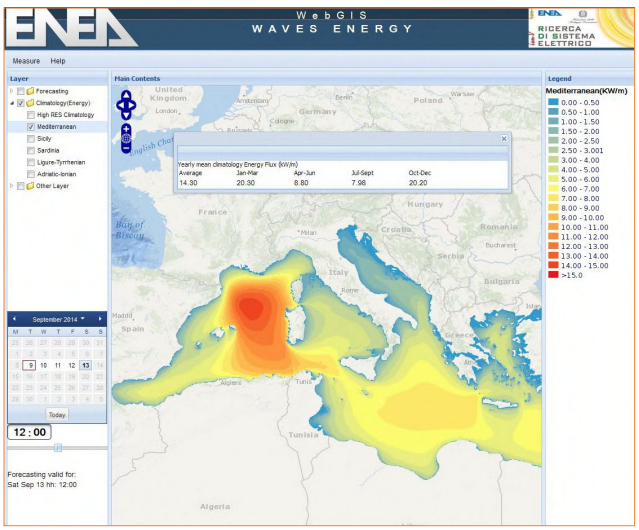

FIGURE 5 Thematic map of potential waves energy flux, derived from climatological data (2001-2010)
(ENEA elaboration)

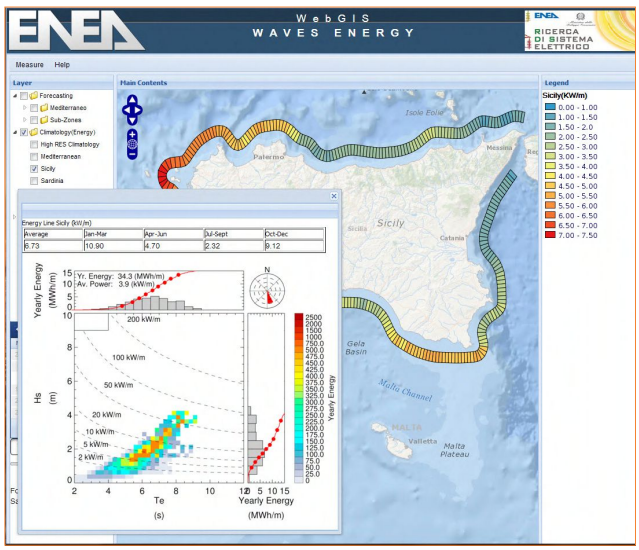

FIGURE 6 Average energy flux values observed during the considered period (2001-2010) and related graphs for the Sicilian coast
(ENEA elaboration)

showing the temporal trend of a selected variable (height, direction, etc.) for the following five days, at hourly intervals (Fig. 3). Furthermore, these same data are available and queryable at a greater detail for some specific sub-areas of interest (Fig. 4).

The Climatology data (listed at point b) are derived from time series and related to the potential energy flux from waves; they contain the average values of energy flux in kW m^{-1} for the time-span 2001-

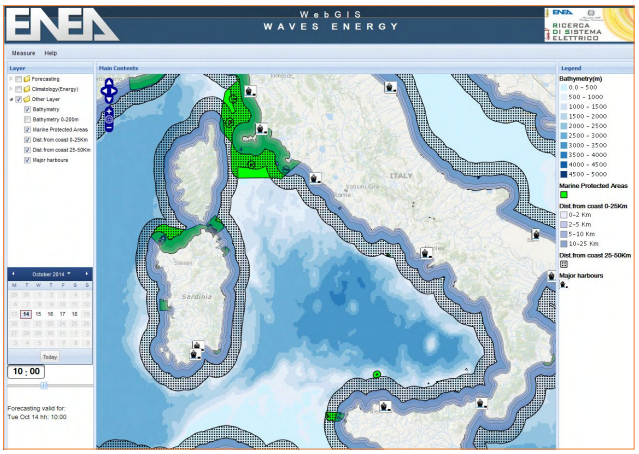

FIGURE 7 Italian Marine Protected Areas and major Italian harbours. GIS overlay with distance from the coast and bathymetry
(Source: SINANET, GEBCO and ENEA elaboration)

2010, subdivided into quarterly periods (Fig. 5). In particular, in the WebGIS data for the entire Mediterranean Sea are included, as well as additional layers representing a specific focus along the Italian coast in a range of 12 km from the shoreline (Fig. 6). The third category (Other Layers, point *c* of the list) includes a series of basic geospatial data and environmental information. Such ancillary layers, in addition to those previously described, allow to provide a better geographic and thematic characterisation of the Mediterranean area considered for the application purposes (Fig. 7). The most significant are: the bathymetry of the Mediterranean Sea (source: GEBCO, General Bathymetric Chart of the Oceans); a bathymetry subset, with depth values ranging from 0 to 200 m (layer specifically derived from GEBCO data); Distance from the coast, articulated in two zones: 0-25 km and 25-50 km; Major harbours; Italian Marine Protected Areas (source: SINANET, Italian Ministry of the Environment and Protection of Land and Sea of Italy).

Conclusions

The capability of digital maps in providing a comprehensive overview of environmental phenomena is universally recognized. Through appropriate descriptions and thematic maps, it is easier to understand environmental features and characteristics, as well to point out patterns and interactions.
The activities described in this paper were aimed at developing a specific spatial DSS, based on a WebGIS application, which served as a means for the publication of the data used as input and produced as results: thematic maps, forecasting data and climate time series. Data and thematic maps were properly structured within the WebGIS application, not only to show a range of information about the areas of interest, but also to support management and monitoring policies related to the exploitation of energy flux from the sea.

Maurizio Pollino, Luigi La Porta, Emanuela Caiaffa
ENEA, Technical Unit for Energy and Environmental Modelling, Rome, Italy

further readings

- A. Bargagli, E. Caiaffa, A. Carillo, L. Liberti, G. Sannino, Energia dal mare: modelli numerici e GIS per la valutazione del potenziale energetico, in *GEOmedia*, 15(6), 2012.
- A. Bargagli, A. Carillo, V. Ruggiero, P. Lanucara, G. Sannino, Modello di onde per l'area mediterranea, http://www.enea.it/it/Ricerca_sviluppo/documenti/ricerca-di-sistema-elettrico/correnti-marine/rds-26.pdf, 2011.
- E. Caiaffa, F. Borfecchia, A. Carillo, L. La Porta, M. Pollino, L. Liberti, G. Sannino, Tecnologie GIS per la valutazione della risorsa energia dal mare, Atti della 17.ma Conferenza Nazionale ASITA, Riva del Garda, 5-7 Novembre 2013.
- P. Janssen, J.R. Bidlot, ECMWF Wave Model Operational - Implementation 9 April 2002, IFS Documentation Cy25R1.
- L. Zambresky, J.A. Ewing, The WAM model - a third generation ocean wave prediction model, in *J. Phys. Ocean*, 18, 1775-1810, 1988.

Evaluation of wave power by integrating numerical models and measures at the Port of Civitavecchia

An assessment of the available wave power at regional and local scale was carried out. Two hot spots of higher wave power level were identified and characterized along the coastline of northern Latium Region, near the Torre Valdaliga power plant and in proximity of Civitavecchia's breakwater, where the presence of a harbour and an electric power plant allows wave energy exploitation. The evaluation process was implemented through measurements, and numerical model assessment and validation. The integration of wave gauges measurements with numerical simulations made it possible to estimate the wave power on the extended area nearshore. A downscaling process allowed to proceed from regional to local scale providing increased resolution thanks to highly detailed bathymetry.

DOI: 10.12910/EAI2015-040

F. Paladini de Mendoza, S. Bonamano, F.M. Carli, A. Danelli, C. Burgio, M.A. Peviani, M. Marcelli

Introduction

The Mediterranean Sea is a semi-enclosed basin with a highly variable climate. Its central area, where Italy is located, is subject to a temperate climate with seasonal variation of weather conditions. In particular, at the Tyrrhenian Sea the most relevant wave conditions are from the third quadrant, due to the larger fetch length [1]. Wave propagation to the nearshore depends on several factors, such as coastal morphology and orientation related to wave direction, bathymetry and shape of the submerged beach. In particular, the northern Latium coast is characterized by the presence of Capo Linaro, which determines a change in both coastline orientation and morphology of the submerged beach. As for other renewable sources, a thorough resource assessment is a prerequisite for the successful exploitation of wave energy [2]. The object of this work is the assessment of wave energy potential from regional to local scale, detecting hot spot wave energy. The study was performed at Civitavecchia, taking advantage of the wave buoys that allow to evaluate wave power and wave propagation from deep to shallow water trough numerical model simulations. The proximity of a power plant, the presence of industrial activities and a large port infrastructure makes this area attractive for wave energy exploitation. Moreover, the deployment of coastal wave buoys allows to compare numerical results with data measured at the nearshore zone. The available wave energy is investigated in detail, characterising each sea stage that provides the energy resource in terms of intensity and direction. In order to assess the nearshore wave energy distribution, it is important to evaluate the propagation of waves, from deep to shallow waters, taking into account the modifications of their characteristics due to refraction, shoaling, diffraction (in some cases) and related physical processes [3]. To this concern, nearshore wave power patterns are investigated applying the CMS-Wave coastal wave

Contact person: Francesco Paladini de Mendoza
f_paladini@unitus.it

model [4]. It is found that the irregular bathymetry of the northern Latium region leads to the concentration of wave energy in certain nearshore areas, while others are left with a relatively low resource. The knowledge of these patterns is a fundamental to selecting the optimum site for wave energy exploitation. This study drives the installation of a new experimental device for wave energy exploitation designed by RSE, in support of the port authority to achieve a more sustainable development.

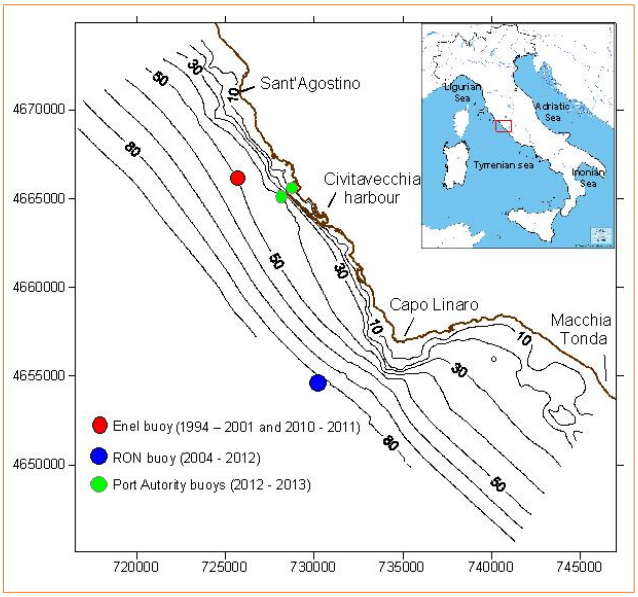

FIGURE 1 Study area (coordinates in UTM zone 32)

Methodology

The proposed methodology to assess the wave energy potential in the study area is composed of different main phases.

Wave data

The wave dataset is provided by different sources: National Wave Monitoring Network (RON) (www.idromare.it), National Authority for Electric Energy (ENEL) and Port Authority (Fig. 1). Significant wave height, peak period and direction are used in this work with a double purpose: assessing wave power and providing boundary conditions in the numerical simulations of wave propagation. The ENEL and RON time series (located at a depth of 50 and 100 m, respectively) do not correspond except for a short time window (2010-2011). However, considering the geographical proximity of the sites it may be very useful to merge datasets into a unique one, in order to enhance time data availability from 1994 to 2012. This was pursued through the application of the Geographical transposition method [5]. Therefore, the ENEL time series (1994-2001 / 2010-2011) were geographically transposed to the site of the RON time series (2004-2012) and the overlapping period was used to verify the method obtaining a determination coefficient (R2) of 0.80 and a residual mean square of 0.044. The two Port Authority's wave buoys (Fig. 1), located near Civitavecchia's harbour, were installed at a depth of 10 meters (onshore point) and 30 meters (nearshore point), respectively.

Bathymetry

In the simulations of wave trains through transitional waters, the resolution of the bathymetric map plays a fundamental role. As wave propagation dynamics

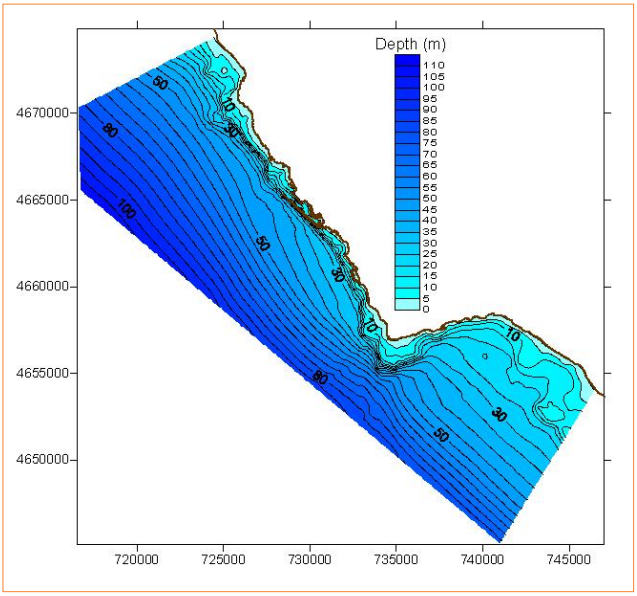

FIGURE 2 Bathymetric map of the regional domain

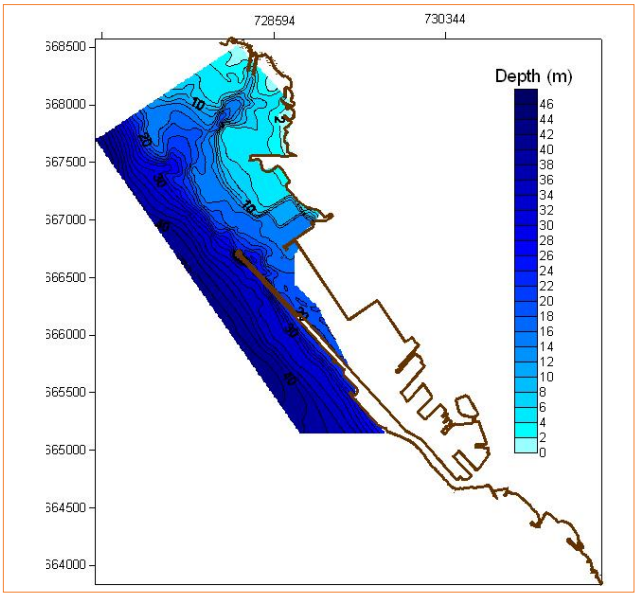

FIGURE 3 High resolution Bathymetric map of Civitavecchia harbour area

at regional and local scale are very much depending on the shape of the seabed, the accuracy of model results is deeply dependent on the accuracy of bathymetric information. Therefore, a bathymetric map with a resolution scale 1:30.000 is suitable for the regional study (Fig. 2). Instead, for the local scale analysis a finer resolution is needed. In the present study two surveys have been carried out, one with single bean till -30 m deep, another with multibeam in Civitavecchia's harbour area, as reported in Figure 3.

The Kriging gridding method [6] was used to build the 50 m resolution mesh for the regional study and the 10 m resolution mesh for the local analysis.

Wave power computation

In this work, wave power was computed in deep, transitional, and shallow waters.

For regular waves the sum of kinetics and potential energy density per unit area can be computed according to the linear wave theory.

According to Cornett [7] and Iglesias *et al.* [8] for irregular waves random in height, period and direction, the spectral parameters have to be used.

Significant wave height is based on the zero moment spectral function (m0) as:

$$Hs \equiv Hm0 = 4\sqrt{m_0} \qquad (1)$$

Where, m_n represents the spectral moment of order n,

$$m_n = \int_0^{2\pi}\int_0^{\infty} f^n S(f,\theta)\,df\,d\theta \qquad (2)$$

In this expression $S(f,\theta)$ denotes the directional spectral density function, which specifies how energy is distributed over frequencies (f) and directions (θ). As for the energy period, it is defined as:

$$T_e = \frac{m_{-1}}{m_0} \qquad (3)$$

After appropriate simplification and substituting Hm0 and Te into equations of wave power of regular waves, under a wave crest the equation is given by:

$$\overline{P} = \frac{\rho g^2 Hm0^2 T_e}{64\pi}\left[1 + \frac{4\pi d/L}{\sinh 4\pi d/L}\right]\tanh\frac{2\pi d}{L} \qquad (4)$$

Every wave power value, corresponding to a certain sea condition, has been multiplied for the corresponding frequency of the events that, subsequently summed up, gives the annual wave power potential.

$$P_{rel} = \sum_{i=1}^{n} \overline{P}_i f_i \qquad (5)$$

Wave model

The wave model used in the present study is the CMS-Wave, a steady-state, finite difference, two-dimensional spectral wave model formulated from a parabolic approximation equation [9] with energy dissipation and diffraction terms. The wave model is based on the wave-action balance equation[10], which determines the evolution of the action density in space and time. The main boundary input is the wave spectra, that is a statistical representation of the wave field and is calculated from wave direction, significant height and peak period.

The JONSWAP wave spectra parameters, used as model boundary conditions, were derived considering the Tyrrhenian wave characteristics. The nesting process allows to produce wave power distribution maps in local scale at a very high resolution. Such a process is performed with a linear interpolation of wave spectra from the coarse to the fine grid domain, as proposed by Smith *et al.* [11]. A hundred and ten wave scenarios have been simulated to compute wave height (Hs), Peak period (Tp) and wave direction (Dir) at each grid point. Furthermore, wave power computation has been carried out applying equations (4) and (5).

Results

Measurements

The annual wave climate of Capo Linaro's buoy (Fig. 4) shows the predominant directions in the third quadrant. The seasonal analysis indicates that wave height is maximum in fall and winter, as well as the most frequent directions spread between 135 °N and 315 °N. In particular, during the fall the south direction occurs more often than other directions, while in winter season the highest frequency is between SSW and WSW. In summer and spring, the highest wave height comes from narrow direction spectra, ranging from 200 °N to 247 °N.

Figure 5 shows wave power spectra of Capo Linaro's buoy, where contour lines indicate the wave power for each sea state, whereas contour colours indicate the wave power values, for each wave condition, weighted with frequency. The spectra show two peaks of energy, The first one encloses the events with wave height of about 2 m and energy period of 6 sec, while the second one represents those with wave height of about 3 m and energy period of 8 sec. The yearly average wave power value computed for this area is 3.1 kW m^{-1} that represents the offshore value at the boundary of the model domain. Figure 6 shows the wave power spectra of Port Authority's wave buoy located at a depth of 50 m, where a different wave energy distribution is detected. The most energetic wave conditions occur for the events with wave height between 1.5 and 3 m and energy period between 5 and 6 sec. The yearly average wave power value computed is 3 kW m^{-1}.

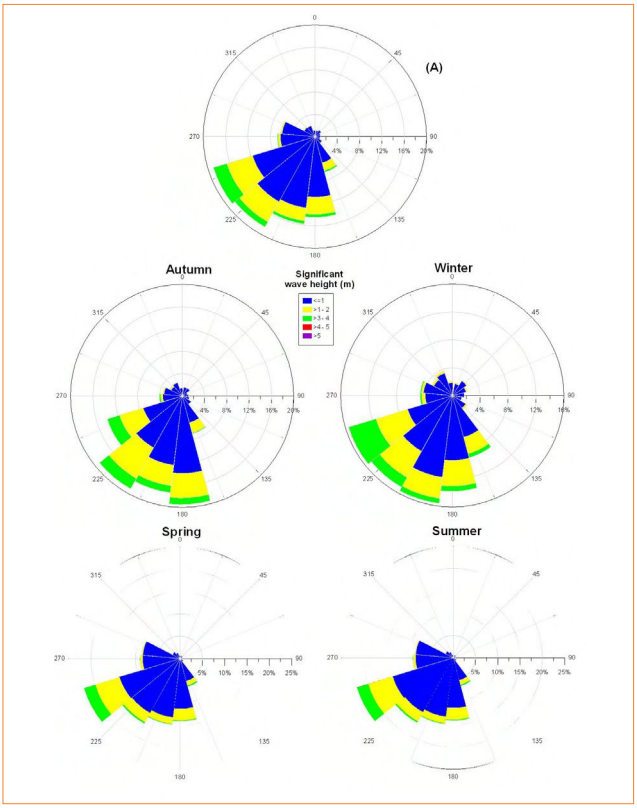

FIGURE 4 Seasonal and annual (A) wave rose based on data from Capo Linaro's buoy (RON) and transposed data from Torrevaldaliga's buoy (ENEL) between 1994-2012

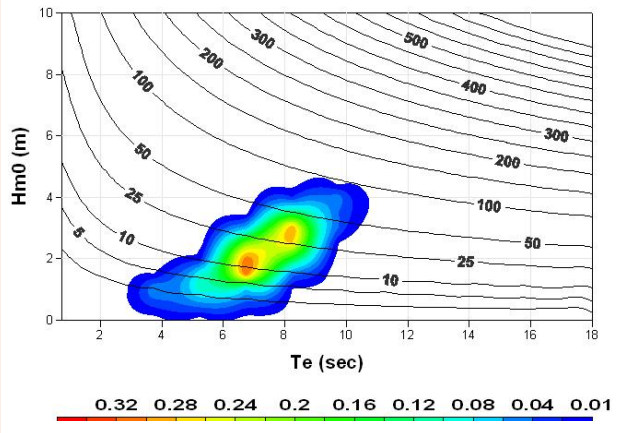

FIGURE 5 Combined map of relative wave power (kW/m) recorded at Capo Linaro. Contour lines indicate absolute wave power for each wave condition of Hs and Te

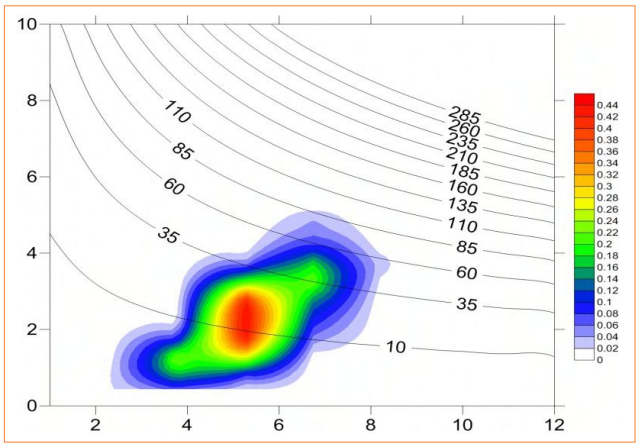

FIGURE 6 Combined map of relative wave power (kW m^{-1}) recorded at Port Authority's buoy. Contour lines indicate absolute wave power for each wave condition of Hs and Te

Regional model

At the regional scale, the nearshore energy distribution is influenced by two factors: morphology of the seabed and variation of coastal orientation. Figure 7 shows that the whole area is separated into two different energetic environments, north and south of Capo Linaro, respectively.

The northern area is more exposed to wave conditions and it shows higher values at short distance from the shoreline, in particular in proximity of the harbour breakwater where wave power reaches 2.6 kW m^{-1}. In the southern zone, high wave power is located far of the coast with two powerful spots, included between 2.6 and 2.8 kW m^{-1} in correspondence of Santa Severa and Ladispoli, respectively.

Local Model

In this chapter we discuss the results of wave energy propagation at local scale. In Figure 8, the yearly average wave power levels are presented in the highest resolution domain. The choice of the study domain corresponds to the area where the Port of Civitavecchia is placed, considering that a power device could be placed along the external breakwater with minimum costs and visual impact. As already stated above, for the local scale analysis, higher resolution bathymetry is fundamental. A 10-meter-detail bathymetric data from multi-beam survey is available for this area.

From Figure 8, it is possible to observe how wave power distribution strictly depends on the coastal morphological features and seabed shape.

The most suitable site is in front of the harbour breakwater, where wave power reaches 2.8 kW m^{-1}. Two additional high energetic hotspots are placed respectively at the north and south sides of the harbour, where wave power front gets closer to the coast.

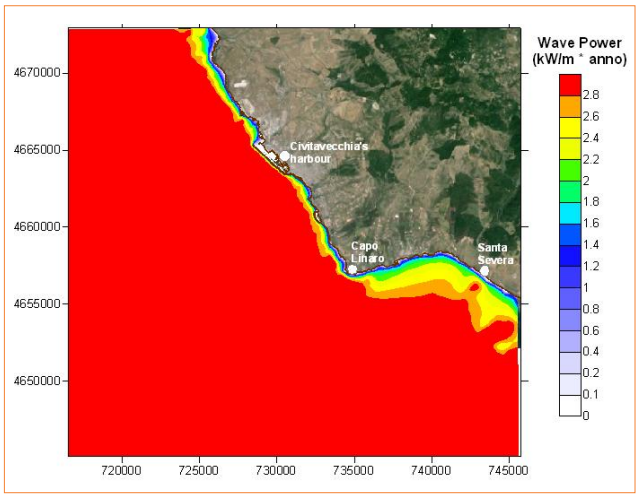

FIGURE 7 Numerically simulated wave power in the pilot area – Regional scale

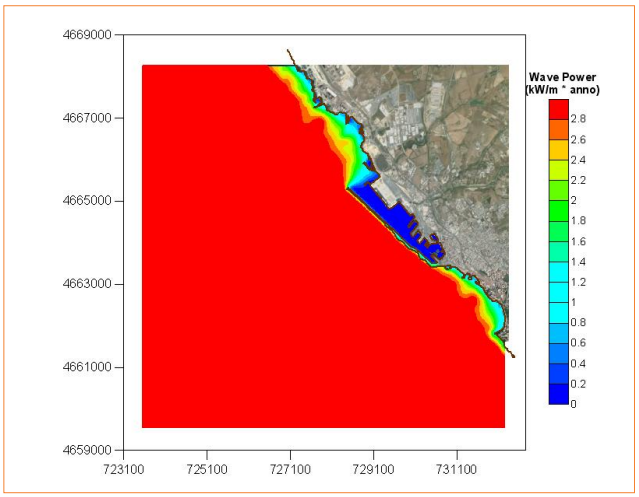

FIGURE 8 High resolution model result for wave power distribution in the pilot area

Nearshore point		Nearshore point	
Coefficient of determination (R^2)	Residual mean square	Coefficient of determination (R^2)	Residual mean square
0.912112	1.33674	0.879648	1.92103
Onshore point		**Onshore point**	
Coefficient of determination (R^2)	Residual mean square	Coefficient of determination (R^2)	Residual mean square
0.783192	0.0396924	0.831916	0.0850484

TABLE 1 Statistical results of computed wave power and measured wave power, for regional (left) and local (right) scale analysis

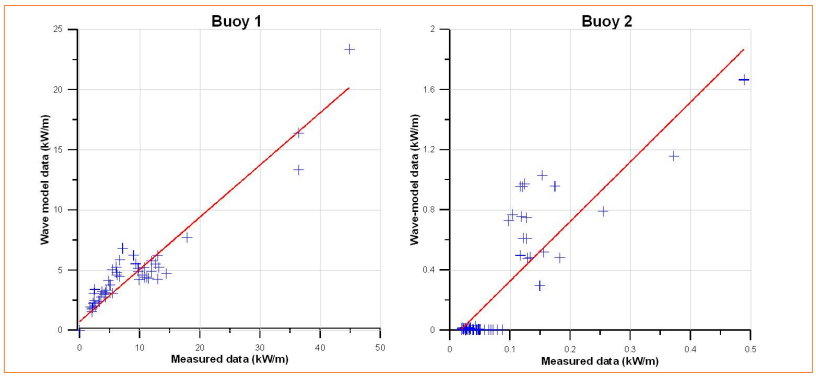

FIGURE 9 Regression analysis between wave buoy measure and regional model results nearshore (buoy 1) and onshore (buoy 2)

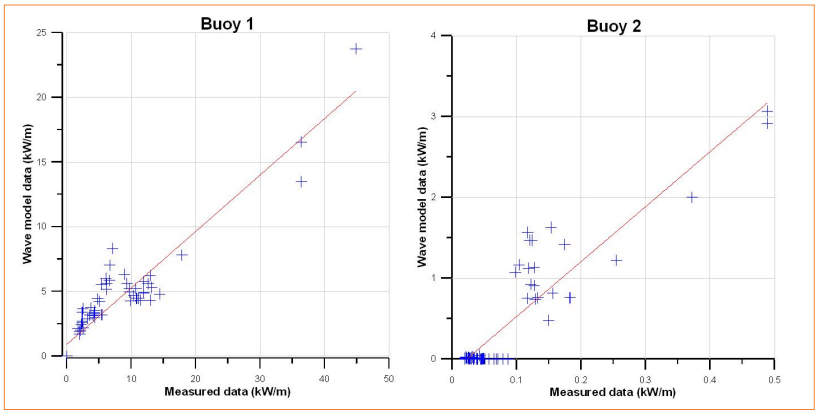

FIGURE 10 Regression analysis between wave buoy measure and local model results nearshore (buoy 1) and onshore (buoy 2)

Validation

We have evaluated the ability of CMS-Wave to simulate the propagation of the waves, as well as attenuation of wave energy in transitional and shallow waters.
The records of two wave Port Authority's buoys were used to compare *in situ* measurements with results from the numerical computation. Seventy wave events registered in both buoys have been chosen for the analysis, using the offshore wave data registered at Capo Linaro (RON).
Wave events with height from 0.8 to 3 m and direction range from 130° to 240°N were chosen.
Modelling validation has been carried out through wave power correlation, for both regional and local scale simulations. Linear regressions are shown in the Figure 9 and 10 and statistical values are summarized in the Table 1.

Present and future developments

The hotspot detection drives the implementation of measurements deploying the Mini-ADP Sontek 1.5MHz in order to verify the potential of the site. This device allows to measure the wave spectra through acoustic transducers and a strain gauge sensor. At present, the sensor was installed on 14/11/2014,in the hot spot in front of of Civitavecchia's harbour breakwater (Fig, 11).
Future development consists in the deployment of the experimental device WAVE SAX designed by RSE in the hot spot site. This modular system will be installed on the harbour breakwater, as reported in Figure 12, where the cross-section of breakwater and location can be observed.

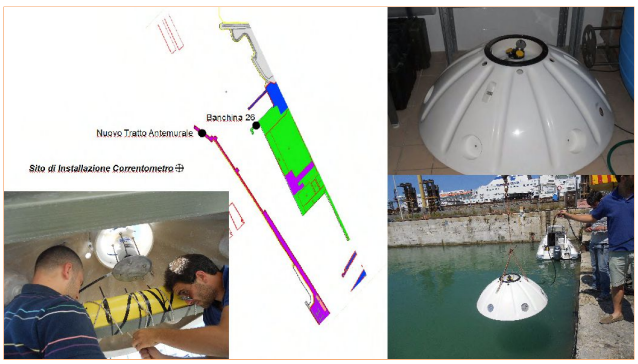

FIGURE 11 Map of location and operative phases of installation

divergence areas where wave energy is subject to concentration and dissipation. In the northern part of the regional domain the seabed is steeper, and higher values are present. In the southern part of the regional domain the seabed slope is smoother producing larger dissipation of energy. Two areas of shallower water are present that coincide with two hotspots of wave power, exactly at the Site of Community Importance (SCI) called Macchia Tonda. The nesting process with increased resolution allows a more accurate description of wave propagation in coastal areas and the wave power hotspots are clearly detected.

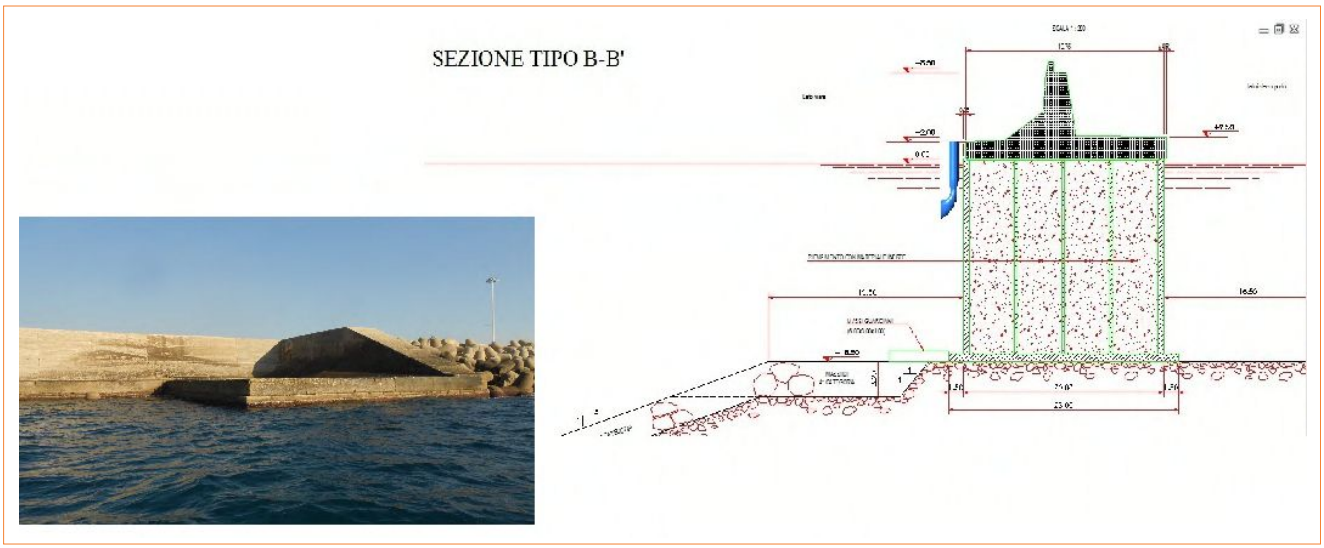

FIGURE 12 Location and cross-section of breakwater with experimental device

Conclusions

The methodology allows to assess the nearshore hotspots for wave energy exploitation and the downscaling process has proven to be very suitable to describe the dynamics at local scale.
At regional scale large variations in nearshore wave power distribution were identified. According to wave model results, wave propagation is strongly dependent on the effect of the morphology of the seabed, which generates convergence and

At local scale resolution the model allowed to account for a more accurate description of wave propagation in coastal areas and the wave power hotspots are clearly detected. In particular, in front of the harbour breakwater higher depth occurs and it results in lower energy attenuation.
In addition, modelling results are confirmed by in situ wave measures and the downscaling process, which has proven to be a useful tool for the detection of wave distribution in transitional and shallow water areas. The methodology allows to

assess the nearshore hotspots where the presence of infrastructures (power plant, harbour, etc.) easily accessible ensures lower costs of installation, operation and maintenance for wave energy converters. Future developments, including the record of data at the hotspot, the installation of the experimental converter and the measure of energy production, will help to achieve more accurate methods and prediction of energy availability.

Francesco Paladini de Mendoza, Simone Bonamano, Filippo Maria Carli, Marco Marcelli
University of Tuscia, Department of Environmental and Biological Sciences (DEB) - Laboratory of Experimental Oceanology and Marine Ecology, Civitavecchia, Italy

Andrea Danelli, Maximo Aurelio Peviani
Electric Research System (RSE), Sustainable Development Department, Milano, Italy

Calogero Burgio
Port Authority of Rome, Italy

references

[1] M.A. Peviani, F.M. Carli, S. Bonamano, European Wave Energy and Studies for Italy's Potential, in *International Journal of Hydropower & Dams*, Issue 5, pp. 98-102, 2011.

[2] European Ocean Energy Association (EU-OEA), Oceans of Energy – European Ocean Energy Roadmap 2010-2050, 2010.

[3] R.G. Dean, R.A. Dalrymple, Water wave mechanics for engineers and scientists, in *World Scientific*, 1991.

[4] L. Lin, Z. Demirbilek, H. Mase, J. Zheng, F. Yamada, CMS-Wave: A Nearshore Spectral Wave Processes Model for Coastal Inlets and Navigation Projects, ERDC/CHL TR-08-13 US Army Corps of Engineers, 2008.

[5] A. Noli, P. De Girolamo, Caratterizzazione Climatica e Modellistica Litoranea delle Coste Laziali, Regione Lazio and University of Rome "La Sapienza", 2001, http://www.osservatoriomare.lazio.it/.

[6] G. Matheron, Principles of geostatistics, in *Economic Geology*, 58, pp. 1246-1266, 1963.

[7] A.M. Cornett, A global wave energy resource assessment, in *Proceedings of the 18th ISOPE Conference*, Vancouver, Canada, 2008.

[8] G. Iglesias, R. Carballo, Wave energy resource in the Estaca de Bares area (Spain), in *Renewale Energy*, 35, pp. 1574-1584, 2010.

[9] H. Mase. H. Amamori, T. Takayama, Wave prediction model in wave-current coexisting field, in *Proceedings 12th Canadian Coastal Conference*, 2005.

[10] H. Mase, Multidirectional random wave transformation model based on energy balance equation, in *Coastal Engineering Journal*, 43(4):317-337 JSCE, 2001.

[11] J.M. Smith., S.J. Smith. Grid Nesting with STWAVE. ERDC/CHL CHETN I-66, U.S. Army Engineer Research and Development Center, Vicksburg, MS, 2002.

Website library: www.idromare.it

Recent developments at CNR-INSEAN on testing and modelling marine renewable energy systems for waves and currents

Hydrodynamic testing centers are nowadays challenged by a continuously increasing demand for studies aimed at the development, verification and assessment of marine renewable energy capturing systems. This paper describes the experience matured over the last years at CNR-INSEAN, the marine technology research Institute of the Italian National Research Council. Originally designed for hydrodynamics testing of marine vehicles, the Institute's experimental facilities like wave and calm water tanks, circulating water channel, now host testing programs on wave energy converters, marine current turbines and hybrid systems, combining devices to extract energy from different marine sources like waves and winds. Selected case studies are described and main findings are discussed in the paper.

DOI: 10.12910/EAI2015-043

F. Salvatore, F. Di Felice, L. Fabbri

Introduction

The next one-two decades will be crucial to the assessment of marine renewable energy as a primary alternative to conventional, environmentally non-sustainable energy sources.
The enormous potential of the energy stored in the oceans is nowadays fully recognised. Nevertheless, in spite of the plenty of concepts, patents, promising prototypes materialised over the last two-three decades, the real possibility to achieve a massive exploitation of marine renewable energy in the short term is still under debate.
The main factors hindering the final affirmation of marine renewables are related to persisting uncertainties about the real cost-effectiveness of energy-generating plants over their whole life-cycle from deployment to final decommissioning. Existing knowledge from few full-scale prototypes deployed at sea highlights contradictory results and, in many cases, unsatisfactory performance in real operating scenarios.
A huge R&D effort is then underway to develop and demonstrate new energy harvesting concepts with enhanced productivity, safety and reliability also in harsh operating conditions, at reduced maintenance and operational costs.
To achieve such challenging objectives, careful studies are necessary from the early stages of the design process. Most of this work is carried out in hydrodynamics testing facilities, where small-scale model devices are analysed, improved and assessed before deploying larger-scale prototypes at sea.
The experience on marine renewable energy technologies matured at CNR-INSEAN, the marine technology research Institute of the Italian National Research Council, is the subject of the present paper. The Institute has an international recognition for fundamental and applied research on marine vehicles and structures. Research and technology

Contact person: Francesco Salvatore
francesco.salvatore@cnr.it

FIGURE 1 CNR-INSEAN facilities for hydrodynamic testing of marine renewable energy systems. From left to right: wave tank, calm-water tank and circulating water channel

support activities take advantage of a network of world-class hydrodynamics testing infrastructures and of theoretical/computational modelling laboratories, where in-house solvers for analysis and design applications are developed.

During the last few years, an increasing amount of R&D work has been dedicated to studies on marine renewable energy systems. Experimental and computational studies address wave energy converters, marine current turbines and hybrid systems, where devices to extract energy from different marine sources like waves and winds are integrated.

Activities are partly funded under national and international research programs, and partly carried out as technology support to private companies and other entities.

Recently, a boost to the involvement of CNR-INSEAN on marine renewables has come from the participation in the collaborative R&D project MARINET (www.fp7-marinet.eu), co-funded by the EU under the Seventh Framework Programme (EU-FP7). In this context, CNR-INSEAN has hosted many experimental programs for the development of marine energy systems and has collaborated to important joint research activities.

An overview of selected activities performed at CNR-INSEAN on testing and modelling marine renewable energy systems is presented in the following pages. The main findings from accomplished work and future research perspectives are also discussed.

Marine energy systems testing facilities at CNR-INSEAN

The experimental facilities at CNR-INSEAN provide a world-class, multi-purpose platform of infrastructures for hydrodynamic testing. A description of these plants, the equipment available and the type of tests that can be conducted therein can be found at www.insean.cnr.it.

Originally designed for hydrodynamics testing of marine vehicles, facilities have demonstrated to be perfectly suited for the analysis of marine renewable energy devices.

In particular, the following three infrastructures:

- Wave towing tank
- Calm water towing tank
- Circulating water channel (or, flume tank)

are utilised for applications to marine renewables technologies (Fig. 1).

These three infrastructures are ranked among the largest hydrodynamics facilities in the world currently available for testing marine energy systems. This makes it possible to use large-size scaled models and perform tests that are fully representative of device operation at full-scale.

Marine current devices

Two main natural mechanisms originate currents in oceans and seas. One is related to the Moon's

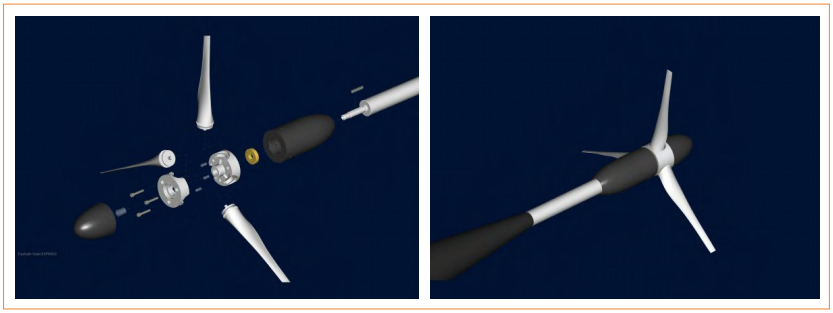

FIGURE 2 CAD model of a three-bladed model turbine built for tests in the flume tank

gravitational effect, which determines a periodic variation of the sea free surface level (tidal range) and yields water flowing from high- to low-tide regions. These currents are referred to as tidal currents and are characterised by a periodic inversion of the direction of the flow. Tidal currents mostly occur close to the coast, with intensity, direction and velocity profile that depend on a combination of local factors.

In other cases, marine currents are generated by gradients of water density due to different temperature or salinity of water masses. Gradient-driven currents typically develop offshore in the oceans (ocean currents) and are uni-directional. A classic example of ocean current is the Gulfstream, where warm waters from the Gulf of Mexico flow up to Polar latitudes along the west coasts of Northern Europe. Both tidal and ocean currents are predictable on a long timeframe with large accuracy.

Marine current energy-capturing devices are classified as "turbine systems," where rotating blades are used to convert water kinetic energy into mechanical energy, and "non-turbine systems", with moving parts consisting of oscillating lifting surfaces (foils, sails or kites) or vibrating cylinders. For details, see e.g. the final report of the 27th ITTC Specialist Committee on the Hydrodynamic Modelling of Marine Renewable Energy Devices [1].

Turbine-like systems represent the most popular technology for marine current energy harvesting. Devices are referred to as Horizontal Axis Current Turbines (HACT) when the rotor axis is aligned to the incoming flow, and cross-flow turbines when the axis is orthogonal to the current direction. Vertical-Axis Current Turbines (VACT) represent a particular case of this type of devices. Both HACT and VACT can be fixed to the sea bottom or floating by surface platforms or submerged structures.

Experience on testing and modelling both horizontal- and vertical-axis current turbines has been matured at CNR-INSEAN over the last few years, in the framework of national research programs as well as under industrial R&D programs funded by private companies. One of the first examples of studies of vertical-axis turbines was performed in 2005-2006, in collaboration with the Italian company developer of the "Kobold" turbine concept [2].

The activity on marine current devices has experienced a dramatic increase during the EU-FP7 MARINET Project (2011-2015), with testing programs on both HACT and VACT, fundamental research and validation of in-house-developed computational models to predict turbine performance.

In support to testing activities, specific know-how has been developed for the design and manufacturing of components of model turbines being tested. Figure 2 shows details of a three-bladed turbine model commissioned by a research team from the Universities of A Coruña and Santiago de Compostela under the MARINET project.

Model turbines tested in both flume and towing tanks have typically diameters of 400-500 mm. Reynolds numbers characterizing the flow around the model rotor are in a critical range (approximately, Re = 10^5), characterized by a laminar flow on blades, that may be not representative of real operating conditions for a rotor with 10-15 m diameter in full-scale, where the Reynolds number is 1-2 orders of magnitude higher and a fully-developed turbulent flow occurs around the rotor blades.

To overcome scaling problems, unconventionally large models should be tested. Such a challenging experiment has been performed in fall 2014 at CNR-INSEAN. A 1.5 m diatemer rotor, designed at Queen's

FIGURE 3 The 1.5 m model of a horizontal-axis marine current turbine (INI-TTT project) during set-up and tests in the calm water towing tank at CNR-INSEAN

University of Belfast (INI-TTT Project) for lake and sea trials in Nothern Ireland's tidal sites, has been tested in the large calm water tank. This 460 × 13.5 × 6.5 m facility offers width and depth dimensions suitable for hosting such an exceptionally large device, see Figure 3.

The rotor was tested at variable onset flow speed and immersion depths for different system layouts. Device performance results were determined as delivered thrust, torque and power over a full range of variation of the rotor tip-speed ratio, TSR = $\omega R/V$, where ω and R denote, respectively, rotor angular velocity and radius, whereas V is the inflow speed.

Results from towing tank tests were compared to those collected after years of trials in real tidal flows. Results are of extraordinary importance because the 1.5 m model operated in the towing tank in a Reynolds number range that is fully representative of full-scale operations. Moreover, the comparative analysis made it possible to investigate the effect on the device operation performance in a real tidal environment against the idealised, uniform speed, calm-water, zero inflow turbulence conditions that may be established in a towing tank. Data analysis results are given in [3].

If wind-energy inspired marine turbines like those described in figures 2-3 may represent a conservative design strategy, nonetheless many efforts are devoted to develop concepts that are more tailored to the peculiarities of marine currents. A main challenge is to ensure an adequate power output regardless of the periodic inversion of the flow direction in a tidal environment.

A classic approach is to use vertical-axis current turbines (VACT). Darreius-type turbines, like those in Figure 4, are insensitive to the direction of the inflow. This represents a clear advantage for tidal currents, in that complex and costly systems to adjust rotor blades to the incoming flow directions are made unnecessary. The trade-off is a generally lower power efficiency of VACTs versus HACTs.

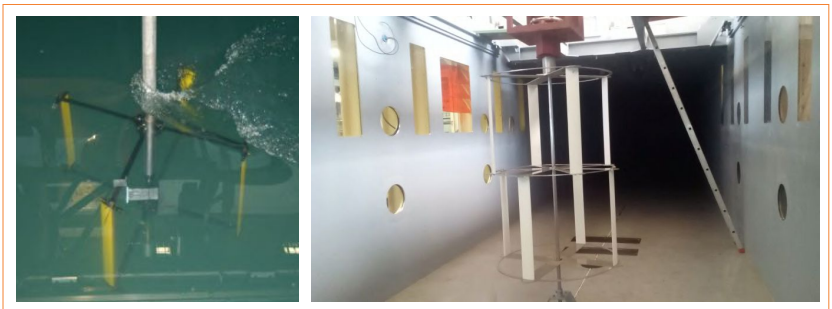

FIGURE 4 Examples of vertical-axis marine current turbines (VACT) models tested in the CNR-INSEAN towing tank (Kobold turbine, left), and flume tank (ABENGOA project, right)

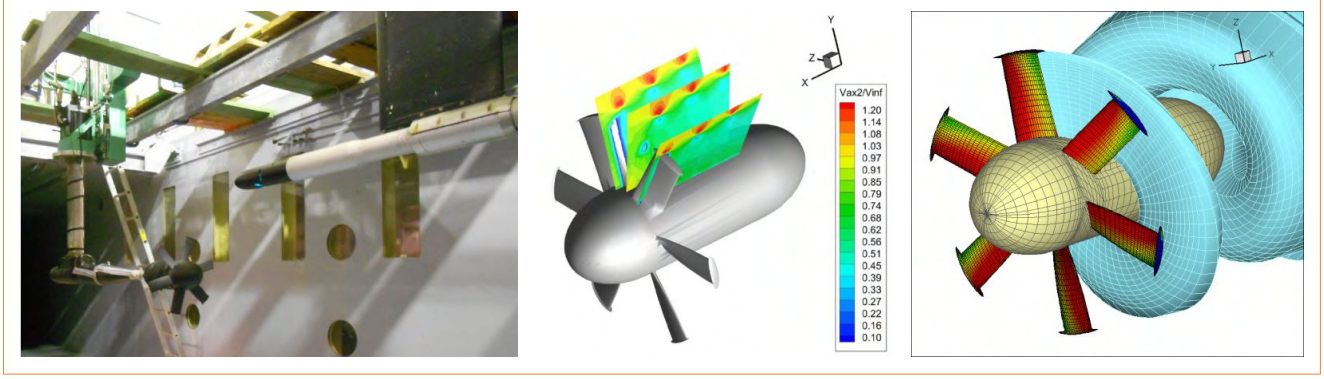

FIGURE 5 SABELLA horizonthal-axis turbine: set-up in the CNR-INSEAN water flume (left), results of wake flow measurements by Laser-Doppler velocimetry (center) and results of CFD simulations (right)

An attempt to realise an unconventional horizontal-axis rotor that can operate in both ebb and flow tidal phases without the need to change the device orientation is the concept developed by the French company SABELLA SAS. The device consists of a conventional HACT (Fig. 5) with blades having bi-directional sectional profiles, that is leading and trailing edges have the same shape. Model tests carried out at the CNR-INSEAN water flume have demonstrated that such a design can operate with power efficiencies of about 40%, that is fully comparable to conventional HACT devices.

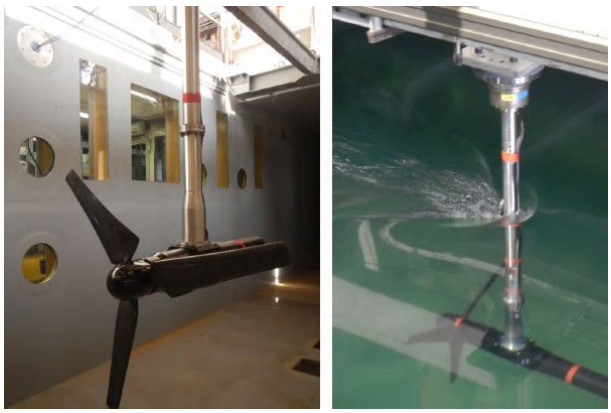

FIGURE 6 The horizontal-axis, 3-bladed rotor designed at IFREMER (France) used in the Round-Robin tests. Pictures show trials at CNR-INSEAN water flume (left) and towing tank (right)

Tests allowed to compare hydrodynamic performance of four alternative rotor designs over a range of operating conditions (TSR and *yaw* angle between shaftline and inflow) and for different device installations (bottom-fixed or floating). In addition to this, a complete rotor wake flow characterization was accomplished using advanced Laser-Doppler Velocimetry (LDV) and Particle-Image Velocimetry (PIV) techniques [4].
The performance/velocimetry dataset collected for the SABELLA rotors is unique for the completeness of information given and represents a fundamental resource for the enhancement of design techniques and tools. The dataset is currently used to perform validation studies of CFD models developed at CNR-INSEAN to predict the hydrodynamic performance of marine current turbines. Preliminary results of this study are presented in [5].
Another aspect worth the effort of dedicated studies is the impact of testing environment on turbine performance estimations. Considering the turbine tests described above, it should be noted that the same type of device, horizontal- or vertical-axis, can be tried in a towing tank as well as in a circulating water channel (or, flume tank). The choice of the type of facility is usually related to practical issues like availability of the infrastructure, dimensions of the model to test, easy installation of the set-up, and so on. Nevertheless, towing or flume tanks may imply different inflow speed ranges and, above all, different inflow turbulence levels.

In this context, in 2014 CNR-INSEAN and other partners of the EU-FP7 MARINET Project have shared the first systematic attempt to address the problem. Specifically, a notional horizontal-axis rotor (design by IFREMER, Fig. 6) was tested across four infrastructures, two towing tanks and two flume tanks. CNR-INSEAN contributed with tests in both types of facilities. Preliminary results of this Round-Robin test presented in [6] document the influence of onset flow turbulence and of other testing conditions on the measured performance of model turbines.

Wave energy conversion

Waves are maybe the most tangible representation of the energy stored inside seas and oceans. As opposed to marine currents, waves are present everywhere but with characteristics like period and elevation that are predictable only with approximations in the short term. As a general rule, ocean waves have a much higher energy potential than that in confined seas like, e.g., the Mediterranean.

The variability of energy resource characteristics explains the great variety of existing energy capturing concepts. The following broad classes can be used to group most technologies, see e.g. [1] for details:

a) *oscillating bodies/point absorbers*: waves induce oscillating motions of floating or submerged bodies, and linear/rotational generators are used to convert motions into electrical power. This type of devices is preferably deployed offshore;
b) *oscillating water columns*: incident waves penetrate a chamber and determine an alternative rise and fall of the free surface therein; this yields reciprocal pumping in/out air from the chamber top and the resulting flux is used to drive Wells turbines connected to generators. This type of devices are suited for onshore installations;
c) *overtopping devices*: floating dam structures are deployed in deep sea areas to focus waves in a restricted area and determine an artificial water rise, whose head is used to move low head turbines.

The hydrodynamic testing of small-scale WEC models in wave basins presents specific challenges. In particular, WECs are characterised by a typically complex interplay between station-keeping properties of the energy capturing system and the dynamics of the power take-off system (PTO). The accurate modelling of the PTO in small-scale devices is difficult as mitigation of passive loads like friction among moving parts is typically hard to be correctly scaled, as described by ITTC [1].

A recent demonstration of WEC testing possibilities at CNR-INSEAN is related to tests of the ISWEC (Inertial Sea Wave Energy Converter) concept developed by a research team from the Technical University of Turin, Italy [7]. This technology is characterised by a wave energy capturing system, based on the gyroscopic effect of oscillating masses. Wave tank tests of a 1:8 scaled model were performed at CNR-INSEAN in 2012, in the framework of a national funding program, see Figure 7 left, and new tests are planned to be carried out in mid-2015.

Test data collected so far have been used to validate a RANSE-based Computational Fluid Dynamics (CFD) model to predict device response to incoming wave patterns, see Figure 7 right.

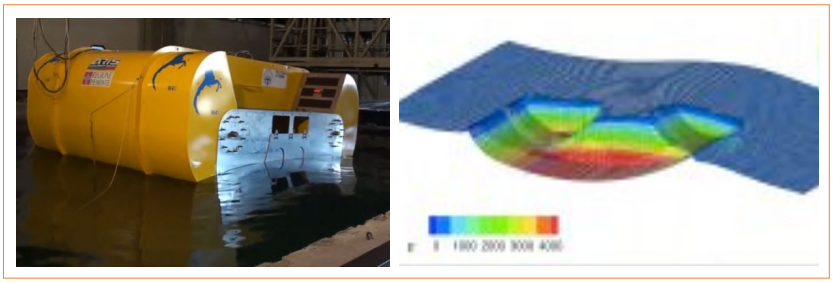

FIGURE 7 The ISWEC wave energy converter: model tests in the CNR-INSEAN wave tank (left) and simulation of station-keeping response by CFD (right)

A recent trend: Hybrid systems

The idea of combining different energy capturing systems into a single device deployed offshore

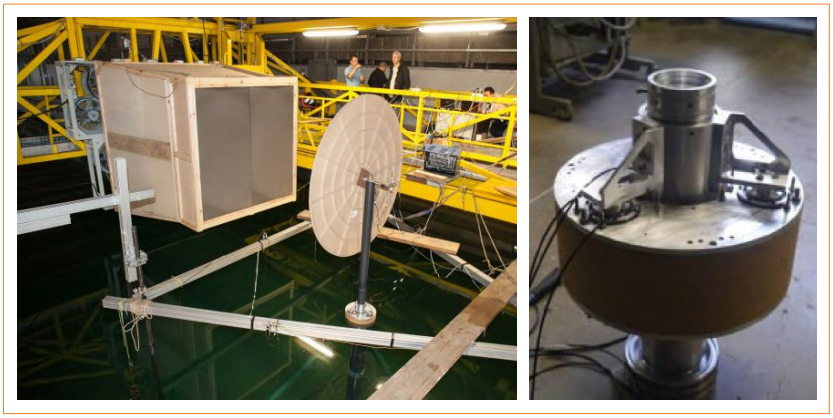

FIGURE 8 Wave tank tests at CNR-INSEAN of the STC system, a hybrid wave/wind energy device. Overview of the set-up with wind generators and nozzle (left) and close-up of the WEC (right)

is considered as a potentially effective strategy to maximise power output capabilities by limiting the investment costs related to the various phases of the device life-cycle.

Systems of this type are usually referred to as "hybrid" systems. The advantages of this solution stem from the possibility to share most of the infrastructure components like platforms, moorings, grid-connection cabling, that support any energy conversion mechanism.

Synergy between wave energy and wind energy systems characterizes the concept developed by a team of Norwegian researchers from CESOS and NTNU. This is the Spar-Torus Combination (STC), which consists of a Spar floating offshore-wind turbine with a torus-shaped heaving body wave-energy converter that can oscillate along the turbine spar.

Numerical simulations of the combined systems showed [8] that the resulting assembly may have a better performance of two separate devices for wave and wind energy harvesting. In particular, the wave absorber has the double effect of producing power and mitigating the intensity of waves impinging at the wind rotor tower. Nevertheless, the combined system is inherently more complex and, hence, it may have a potentially critical behaviour in harsh conditions.

The assessment of structural integrity under extreme operating conditions was the main purpose of a first experimental program on the STC device, conducted at CNR-INSEAN in 2013. A scaled model was manufactured and tested in the wave tank. Wind forcing on the rotor was simulated by using an array of 12 fans inducing a flow with given intensity at the rotor disk through a specifically-designed nozzle. To limit the complexity of the set-up, the wind rotor was simulated by a dummy disk realised with a special porous material. An overview of the set-up during wave tank tests is shown in Figure 8.

System survival tests were performed with a wave-energy device locked in non-operative mode. Alternative survival modes were analysed and compared. Further tests in 2014 were carried out in order to characterise the wave-energy converter power output under a variety of sea- and wind-states. The system PTO was simulated by a sophisticated miniaturised system scaled to the dimensions of the model used in tank tests. Results of tests [9] allowed to determine the power generated for different operating conditions as well as the response amplitude operator (RAO) of the system in station-keeping conditions under waves and wind forcing. Both test programs in 2013 and in 2014 were partly funded under the EU-FP/ MARINET Project.

Concluding remarks and future work

An overview of recent studies on marine renewable energy systems at CNR-INSEAN has been presented. Experimental techniques and computational modelling tools have been developed and are extensively applied for the analysis of the hydrodynamic performance of devices for energy harvesting from waves, winds and marine currents.

Experimental work takes benefit out of a network of testing facilities that are among the largest

worldwide and have a rich equipment with the most advanced measuring systems. In parallel to that, in-house computational models to predict device performance and response to operations at sea are developed and validated through comparisons with results of model tests.
Since 2012, a large part of work in this area has been performed in the framework of the project MARINET, co-funded by the EU under the Seventh Framework Programme (EU-FP7).
Results of experimental studies allowed to achieve a better understanding of the mechanisms of marine energy conversion and gave valuable information to designers as to enhancing systems power generation capabilities.
Experience during model tests also provided new knowledge to improve testing protocols and quantify the effect of different testing environments (towing or flume tanks versus sea trails) on the results of system performance measurements.
The application of non-intrusive measuring techniques, like LDV and PIV to characterise velocity fields around marine turbines as well as in-house developed sensors to render the wave pattern around wave energy converters, gave a comprehensive description of device operation and provided valuable data for the spatial planning of devices in farms or arrays.
Not least, the collection of experimental data into datasets is a fundamental tool for the validation of computational models to predict device performance at the design stage.
In the next years, R&D work on marine renewables is expected to further increase in hydrodynamics testing facilities. CNR-INSEAN aims to face this challenge by pursuing the enhancement of in-house know-how and tools to support the development and assessment of energy-capturing technologies. Collaboration with leading institutes at international level will be hopefully fostered through the participation in joint research projects and international networks.

Francesco Salvatore, Fabio Di Felice, Luigi Fabbri
CNR-INSEAN, Italian Maritime Technology Research Center

references

[1] A.H. Day, I. Penesis, A. Babarit, A. Fontaine, Y. He,M. Kraskowski, M. Murai, F. Salvatore, H.K. Shin, Final Report of the 27th ITTC Specialist Committee on Hydrodynamics Testing of Marine Renewable Energy Devices and Recommended Guideline 7.5-02-07-03.9: Model Tests for Current Turbines, Twenty-seventh ITTC Conference, Copenhagen, Denmark, September 2014.

[2] G. Calcagno, F. Salvatore, L. Greco, A. Moroso, H. Eriksson, Experimental and Numerical Investigation of an Innovative Technology for Marine Current Exploitation: the Kobold Turbine, ISOPE 2006 - Sixteenth International Offshore and Polar Engineering Conference, San Francisco, California, USA, May 28-June 2, 2006.

[3] P.Jeffcoate, B. Elsaesser, C. Boake, F. Salvatore, Effect of submergence on tidal turbine performance, 11th EWTEC Conference, Nantes, France, September 2015.

[4] B. Morandi, G.P. Romano, D. Dhomé, J.C. Allo, F. Di Felice, M. Costanzo, Experimental investigation of the wake of an horizontal-axis tidal current turbine, First Int. Conference on Renewable Energies Offshore (ReNew 2014), Lisbon, Portugal, October 2014.

[5] F. Salvatore, F. Di Felice, D. Dhomé, J.C. Allo, Validation of a computational hydrodynamics model for horizontal-axis marine current turbines, 11th EWTEC Conference, Nantes, France, September 2015.

[6] B. Gaurier, G. Germain, J.V. Facq, C.M. Johnstone, A.D. Grant, A.H. Day, E. Nixon, F. Di Felice, M. Costanzo, Tidal Energy Round Robin Tests: comparisons between towing tank and circulating tank results, Manuscript submitted to *Int. Journal of Marine Energy*, September 2014.

[7] G. Bracco,E. Giorcelli, G. Mattiazzo, E. Tedeschi, M. Molinas , Control Strategies for the ISWEC Wave Energy System, 9th EWTEC Conference, Southampton, U.K., 2011.

[8] M.J. Muliawan, M. Karimirad, T. Moan, Z. Gao, Extreme responses of a combined spar-type floating wind turbine and floating wave energy converter (STC) system with survival modes, in *Ocean Engineering*, vol. 65, pp. 71-82, 2013.

[9] L. Wan, Z. Gao, T. Moan, C. Lugni, Numerical and experimental comparisons of two model tests in different testing facilities of a combined wind and wave concept, Manuscript submitted to *Coastal Engineering Journal*, 2015.

Marine renewables: Exploring the opportunity for combining wind and wave energy

Resource diversity is considered the key to manage the intrinsic variability of renewable energy sources and to lower their system integration costs. The expected development of Marine Renewable Energy Installations is likely to result in further transformation of coastal sea areas, already heavily impacted. In this perspective, the combination of different renewables and their potential impact on the environment must be evaluated in the context of the existing pressures. In this study the opportunity of co-locating offshore wind turbines and wave energy converters and their environmental sustainability is evaluated through a quantitative Marine Spatial Planning (MSP) approach.

DOI: 10.12910/EAI2015-042

A. Azzellino, L. Riefolo, C. Lanfredi, D. Vicinanza

Introduction

Marine Renewable Energy Installations (MREIs) are likely to become a large part of the future energy mix worldwide. Some authors [1, 2] have recently suggested that resource diversity may be used to manage the variability of renewable energy sources and lower the system integration costs of renewables. The key benefit, deriving from the diversification of the mix of renewable technologies, lies in the possibility of reducing the variability of the produced power. When adopting a single variable source (for example wind) the only way to reduce variability is by geographical diversity and displacement of the farms. When considering different variable sources, if they are uncorrelated their combination is a powerful alternative in order to obtain a reduction of the overall variability of the produced power. On the other hand, the increasing awareness of the cumulative effects of human activities on the marine ecosystem and the rapid development of the offshore renewable energy sector has led to an increased requirement for Marine Spatial Planning (MSP) to fulfill the need of a holistic and integrated approach to management [3, 4]. The expected development of MREIs is likely to result in further transformation of our coastal sea areas, already heavily impacted by anthropic activities. In this perspective, both the possible combination of different renewable technologies, and their potential impact on the environment should be considered in the context of the existing pressures. Spatial planning approaches to marine areas are increasingly required and a distinct field of study and practice is emerging as the result of this new awareness [5, 6, 7]. The spatial conflicts of sea uses and the demand for sea space are in fact increasingly growing. The development of the MRE sector in such a complex framework of existing uses, pressures and expected developments, makes the

Contact person: Arianna Azzellino
arianna.azzellino@polimi.it

need for MSP even more urgent. Spatial decision support systems, through the efficient exchange of information between experts, stakeholders and decision makers offer the opportunity to guide the transition from the single sector management toward the integrated management of sea uses. The early prediction of the areas of potential conflicts creates the ground for mitigation actions or early negotiations between stakeholders. In this study the opportunity of co-locating offshore wind turbines and wave energy converters in the Italian seas is analyzed. The fact that waves are more constant than winds and the delay between both resources provide the background of the investigation. Although wind [8] and wave energy assessment off the Italian coasts have been recently developed [9, 10, 11, 12], this is the first time that the opportunity for combining wind and wave energy is investigated.

Materials and methods

Study area

The Mediterranean sea is known to be one of the most impacted marine environments [13] and, the Italian seas, according to the same study [13], are among the highest impacted waters, being about 80% of the Italian territorial waters subject to mid to high impacts. The development of the offshore renewable energy sector is likely to result in further transformation of our seas, already affected by significant pressures. Figure 1 shows the study area and the used ECMWF (European Center Medium Weather Forecast) data points.

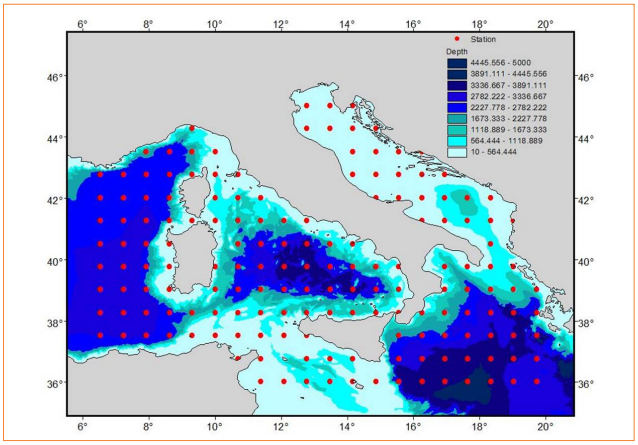

FIGURE 1 Study area

Used data

We used the ECMWF ERA-Interim Data Set (http://www.ecmwf.int/en/research/climate-reanalysis/era-interim). The fields used from this dataset were: horizontal and vertical components of wind speed at 10 m, mean wave direction, mean wave period, significant wave height. We used the ECMWF stations available at all the stations encompassed in the geographical range 36-46 degree of latitude and 6–20 degree of longitude. The data covered a 10-year period from 2005 to 2014. Moreover, a grid was created for the study area for the purpose of the spatial analysis, dividing the area into cells of 60 × 50 kilometers of grid size. As indicators of human pressure the ship traffic and the relevance of the area for the fisheries were taken into account considering their highest impact. Data on naval traffic was derived from the results of PASTA-MARE project which processed AIS (Automatic Identification of Ships) data into estimates of maritime traffic density, whereas the fishery productivity of the different areas were evaluated based on the statistics available from *Osservatorio Nazionale Pesca* (2011). Bathymetry data were obtained through the GEBCO (General Bathymetric Chart of the Oceans) One minute Digital Atlas.

Statistical methods

The potential delay between wind and wave resources provides the background of this study.

Wind and wave conditions

The correlation between wind and wave parameters at the different locations were quantified through the Pearson's correlation coefficient:

$$r = \frac{1}{N}\sum_{k=1}^{N}\frac{[x(k)-\mu_x][y(k)-\mu_y]}{\sigma_x\sigma_y}$$

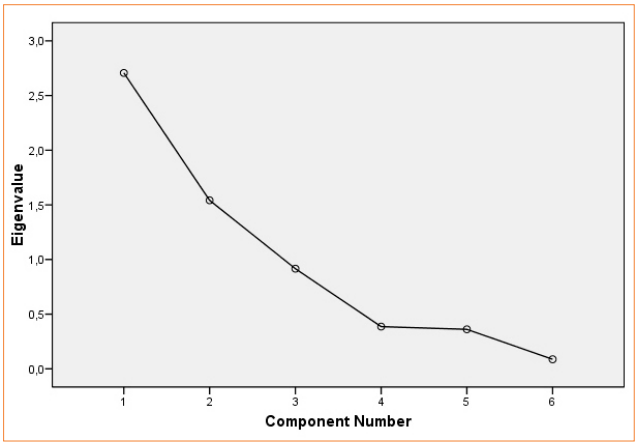

FIGURE 2 Scree plot showing the eigenvalues extracted from the covariance matrix of the original variances

Where μ_x, μ_y, σ_x, σ_y are the mean and the standard deviation of the variables *x* and *y*, of k observations and *N* is the total sample size.

Classification of the meteo-climatic conditions

Two different multivariate techniques were used to analyze wind and wave energy data and the final multicriteria matrix: Principal Component Analysis and Cluster Analysis [14]:

1) **Principal Component Analysis**
   Principal Component Analysis (PCA) was chosen to reduce the dimensionality of the wind and wave statistics. PCA extracted the eigenvalues and eigenvectors from the covariance matrix of the original variances. The number of factors to retain was chosen on the basis of the scree plot (see Fig. 2). That allowed to select few components to describe the whole data set with minimum loss of original information.
2) **Cluster Analysis**
   Cluster Analysis (CA), both hierarchical (HCA) and non-hierarchical K-means [14] were used to analyze the similarities of data groups. As distance measure, the Euclidean Distance was chosen:

$$d_2(x_i, x_j) = \sqrt[2]{\sum_{k=1}^{q} (x_{ik} - x_{jk})^2}$$

K-means was used when the data set was constituted by several thousands of records whereas HCA was preferred when the data set accounted only some hundreds of records. When the hierarchical procedure was run, the Ward linkage method was selected as agglomeration criterion. K-means CA, on the other hand, was run twice: the final cluster centroids of the solution obtained after the first run were in fact used as initial centers in the second run. Only the second run results are showed here.

Spatial interpolation

AIS data on ship traffic were interpolated using an Inverse Weighted Distance interpolator (IWD).

		Wind speed ($m \cdot s^{-1}$)	Mean Wave Direction	Mean Wave Period (s)	Significant Wave Height (m asl)
N	Valid	332804	522612	522612	522612
Mean		5.0235	215.4373	4.8533	0.8701
Median		4.4740	236.3722	4.7288	0.6724
Std. Deviation		2.63165	95.77630	1.31472	0.67705
Minimum		0.35	0.39	1.66	0.06
Maximum		19.41	359.51	11.39	6.39
Percentiles	25	3.0076	141.6582	3.9487	0.4032
	50	4.4740	236.3722	4.7288	0.6724
	75	6.5166	298.3866	5.6686	1.1354

TABLE 1 Main Statistics of the wind and wave parameters

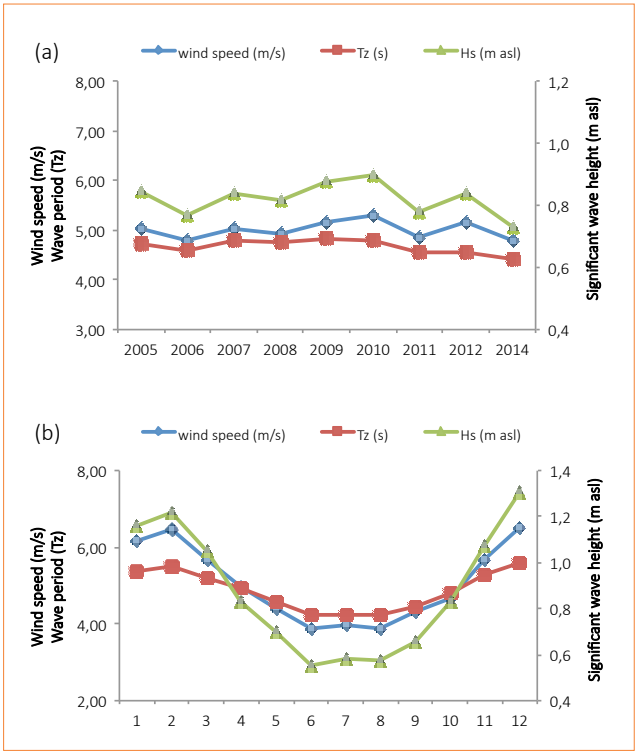

FIGURE 3 Interannual variability (a) and monthly variability (b) in wind and wave patterns

Results and discussion

Wind and wave conditions

Table 1 presents the main statistics of the wind and wave parameters throughout the study period (2005-2014).

As can be observed in Figure 3, the area is characterized by a certain degree of inter-annual and seasonal variability. Table 2 shows the correlations between the wind and wave parameters and their correlation with time.

Although wind and waves temporal patterns (i.e. annual and monthly) are generally well correlated, there might be conditions when the two are less correlated and these conditions are the most interesting in the perspective of reducing the overall variability of the produced power. So, in order to identify those patterns, the different meteo-climatic conditions were classified by means of the k-mean CA algorithm.

Classification of the meteo-climatic conditions

PCA was applied to the wind and wave data (i.e. U and V wind components, the resulting wind speed, the wave direction, period and significant height).

		Correlations wind speed (m/s)	MEAN WAVE DIRECTION	Tz (m asl)	Hs (m asl)	year
wind speed (m/s)	Pearson Correlation Sig. (2-tailed) N					
MEAN WAVE DIRECTION	Pearson Correlation Sig. (2-tailed) N	,058** .000 283239				
Tz (m asl)	Pearson Correlation Sig. (2-tailed) N	,634** .000 283239	,180** .000 522612			
Hs (m asl)	Pearson Correlation Sig. (2-tailed) N	,861** .000 283239	,157** .000 522612	,815** .000 522612		
year	Pearson Correlation Sig. (2-tailed) N	,008** .000 332804	,033** .000 319374	-,066** .000 319374	-,020** .000 319374	
month	Pearson Correlation Sig. (2-tailed) N	-,064** .000 331876	-,006** .000 522612	-,059** .000 522612	,065** .000 522612	-,006** .000 374216

**. Correlation is significant at the 0.01 level (2-tailed).

TABLE 2 Wind and wave correlations

	Components 1	2	3
Wind Vertical component at 10 m (V, m·s^{-1})	-0.106	-0.449	**0.885**
Wind Horizontal component at 10 m (U, m·s^{-1})	0.499	**0.693**	0.271
Wind speed (m·s^{-1})	**0.872**	-0.225	-0.101
Mean wave direction	0.283	**0.832**	0.220
Mean wave period (Tz)	**0.850**	-0.240	0.008
Significant wave height (Hz, m asl)	**0.940**	-0.244	-0.024
Extraction Method: Principal Component Analysis			

TABLE 3 Factor loadings of the PCA solutions

Three components were extracted explaining 86.1% of the original variance, the first component explaining 45.1%, the second 25.7%, and the third 15.3% of the whole variance. Table 3 shows the factor loadings of the PCA solutions.

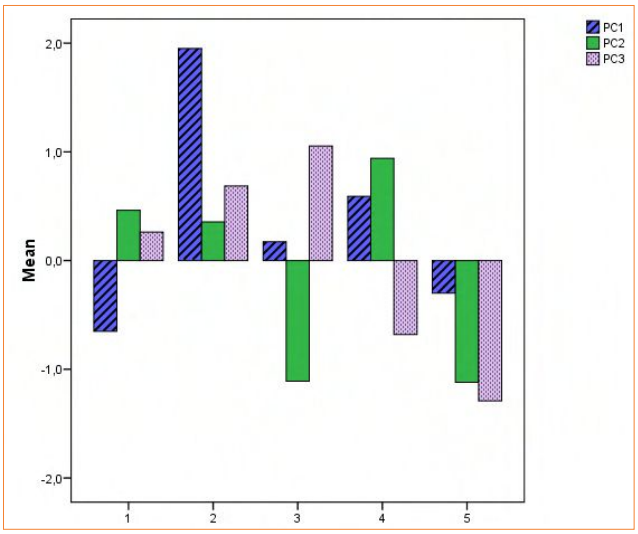

FIGURE 4 Standardised characteristics of the five clusters: *Cluster 1* wind and wave characteristics below the average, horizontal and vertical wind component and wave direction above the average; *Cluster 2* all wind and wave characteristics highly above the average; *Cluster 3* wind and wave characteristics slightly above the average, wave direction and horizontal wind component highly below the average, and vertical wind component well above the average; *Cluster 4* wind and wave characteristics, wave direction and horizontal wind component above the average, vertical wind component below the average; *Cluster 5* all wind and wave characteristics below the average

As can be observed, the first component accounts for wind speed, significant wave height and wave period and, for this reason, it is the component that should be minimized to find wind and wave patterns uncorrelated, whereas the second (accounting for wave direction and wind horizontal component) and the third component (accounting for the only wind vertical component) represent the uncorrelated variability of both wind and wave energy sources.

A K-means Cluster Analysis was then applied to the component scores obtained by the principal component extraction. And a five-cluster solution was chosen. Figure 4 shows the characteristics of the five clusters in terms of principal component scores, and Table 4 summarises the different meteo-climatic characteristics of the five clusters.

Figure 4 shows the characteristics of the five clusters and particularly the following:

- *K-means Cluster 1* wind and wave characteristics below the average, horizontal and vertical wind component and wave direction above the average;
- *K-means Cluster 2* all wind and wave characteristics highly above the average;
- *K-means Cluster 3* wind and wave characteristics slightly above the average, wave direction and horizontal wind component highly below the average, and vertical wind component well above the average;
- *K-means Cluster 4* wind and wave characteristics, wave direction and horizontal wind component above the average, vertical wind component below the average;

Cluster Number		wind speed (m·s¯¹)	mean wave direction	Tz (s)	Hs (m asl)
1	Mean	3.07	242.55	3.92	.40
	Median	2.98	256.22	3.91	.37
	Std. Deviation	1.10	69.59	.95	.21
	Minimum	.35	4.47	1.66	.06
	Maximum	8.97	359.30	8.93	1.74
	N	110626	110626	110626	110626
2	Mean	9.22	269.32	6.44	1.94
	Median	9.04	271.08	6.36	1.80
	Std. Deviation	2.32	27.04	.91	.69
	Minimum	1.12	78.20	4.15	.58
	Maximum	18.20	353.27	10.36	6.07
	N	24492	24492	24492	24492
3	Mean	6.30	172.70	5.15	1.06
	Median	5.99	169.39	5.06	.95
	Std. Deviation	2.17	38.36	.99	.52
	Minimum	.75	4.18	2.66	.14
	Maximum	16.34	327.98	10.19	5.20
	N	48673	48673	48673	48673
4	Mean	6.42	308.80	5.04	1.01
	Median	6.04	315.78	4.98	.90
	Std. Deviation	1.86	35.04	.91	.47
	Minimum	1.82	84.38	2.54	.15
	Maximum	18.37	359.36	10.02	4.49
	N	51240	51240	51240	51240
5	Mean	5.40	72.09	4.69	.82
	Median	4.87	64.25	4.56	.67
	Std. Deviation	2.53	46.47	1.12	.57
	Minimum	.62	0.57	1.76	.06
	Maximum	19.41	308.37	9.39	4.71
	N	48208	48208	48208	48208
Total	Mean	5.16	215.83	4.68	0.83
	Median	4.62	234.98	4.59	0.65
	Std. Deviation	2.67	93.40	1.23	0.63
	Minimum	0.35	0.57	1.66	0.06
	Maximum	19.41	359.36	10.36	6.07
	N	283239	283239	283239	283239

TABLE 4 Summary statistics of the five meteo-climatic clusters

- *K-means Cluster 5* all wind and wave characteristics below the average.

It is interesting to compare the correlations between the wind and wave parameters obtained pooling all the data set (Tab. 2) with the ones obtained by splitting the data set into the described meteo-climatic clusters (Tab. 5). As expected, the cluster showing the lowest correlation between wind speed, wave period and significant wave heights is the first, which refers the meteo-climatic conditions that should be dominant to maximize the advantage to combine wind and wave.

In order to highlight the areas where the most favorable meteo-climatic conditions are dominant a new cluster analysis was performed, aggregating the data by station. This aggregation shrinked the data set from several thousands of records to a hundred. This allowed to use a hierarchical approach (HCA) when running this second cluster analysis. Figure 5 shows the characteristics of this new solution of five clusters: the clusters of highest interest in this case are clusters 4 and 5 which include the stations where the favorable meteo-climatic conditions (i.e. K-means Cluster 1) are dominant.

Cluster Number	wind speed (m·s^{-1})	mean wave direction	Tz (s)	Hs (m asl)	Year
1 Wind speed (m·s^{-1})					
Mean wave direction	0.238(**)				
Tz (s)	0.139(**)	0.112(**)			
Hs (m asl)	0.570(**)	0.144(**)	0.646(**)		
Year	0.045(**)	-0.002	-0.111(**)	-0.034(**)	
Month	-0.015(**)	0.018(**)	-0.061(**)	-0.050(**)	-0.021(**)
2 Wind speed (m/s)					
Mean wave direction	0.207(**)				
Tz (s)	0.531(**)	0.131(**)			
Hs (m asl)	0.766(**)	0.202(**)	0.785(**)		
Year	0.048(**)	0.040(**)	0.037(**)	0.049(**)	
Month	-0.090(**)	0.026(**)	-0.028(**)	-0.088(**)	-0.035(**)
3 Wind speed (m/s)					
Mean wave direction	0.041(**)				
Tz (s)	0.382(**)	0.098(**)			
Hs (m asl)	0.723(**)	0.037(**)	0.726(**)		
Year	0.063(**)	0.055(**)	-0.022(**)	0.041(**)	
Month	-0.039(**)	-0.064(**)	-0.030(**)	-0.041(**)	-0.043(**)
4 Wind speed (m/s)					
Mean wave direction	0.085(**)				
Tz (s)	0.474(**)	-0.159(**)			
Hs (m asl)	0.776(**)	-0.025(**)	0.763(**)		
Year	0.029(**)	0.018(**)	-0.050(**)	-0.019(**)	
Month	-0.059(**)	0.005	-0.102(**)	-0.111(**)	0.024(**)
5 Wind speed (m/s)					
Mean wave direction	0.038(**)				
Tz (s)	0.471(**)	0.223(**)			
Hs (m asl)	0.794(**)	0.109(**)	0.778(**)		
Year	-0.012(*)	-0.016(**)	-0.083(**)	-0.054(**)	
Month	-0.023(**)	-0.027(**)	-0.042(**)	-0.038(**)	0.031(**)

* Correlation is significant at the 0.05 level (2-tailed).
** Correlation is significant at the 0.01 level (2-tailed).

TABLE 5 Correlation analysis between wind and wave. Data splitted into the five meteo-climatic clusters

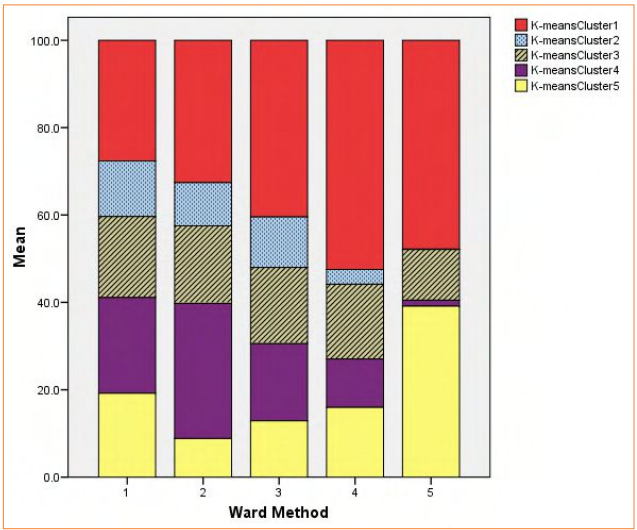

FIGURE 5 Bar charts show the characteristics of the five clusters obtained from performing the hierarchical CA based on the data aggregated by stations: the clusters of highest interest in this case are clusters 4 and 5 which include the stations where the favourable meteo-climatic conditions (i.e. K-means Cluster 1, see Fig. 4) are dominant

It must be observed that Cluster 4 should be preferred to Cluster 5 since it presents also a higher frequency of the K-means Cluster 5 conditions which are less favorable in terms of net potential energy (see Tab. 4 and Fig. 4).

Spatial Analysis

At this point the spatial position of the most favorable meteo-climatic conditions for combining wind and wave are analyzed and overlaid with the most significant anthropic pressures (i.e. naval traffic and fishery). Figure 6 shows the position of the HCA Cluster 4 and the situation in terms of naval traffic density and the relevance of the different areas for fishery.

It can be observed that the most interesting areas for combining wind and wave are the southern Adriatic sea, the coastal areas of the central and southern Tyrrhenian sea, and some spot coastal areas in the Ionian sea. As shown in Figure 6, these areas are also relevant for fishery (e.g., the Adriatic sea) and naval traffic (e.g., central Tyrrhenian sea and the coastal areas surrounding the Strait of Messina). This highlights the potential conflictual use of the marine space by these different human activities. It is also worthwhile to remind that the Italian seas are among the most impacted marine environments [13] and, particularly, the areas outlined in this study as of potential interest for the MREI area, characterized by mid to high cumulative impacts (Fig. 7).

In these situations quantitative criteria are needed to implement Marine Spatial Planning (MSP) to better coordinate the different uses of space, and to address the need for protecting the common interests from the unsustainable exploitation of finite spatial resources.

The spatial conflicts of sea uses and the demand for sea space are in fact increasingly growing. The development of the MRE sector in such a complex framework of existing uses, pressures and foresees developments, makes the need for quantitative MSP even more urgent.

In this study examples are given on how spatial planning methods should support the optimal siting of new marine infrastructures in the perspective of the mitigation of conflicts between competitive uses and their environmental sustainability.

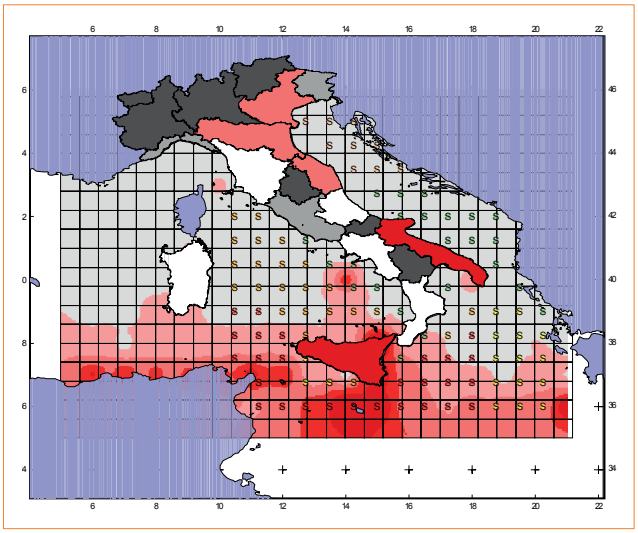

FIGURE 6 Map of the meteo-climatic clusters overlaid with naval traffic and fishery pressure

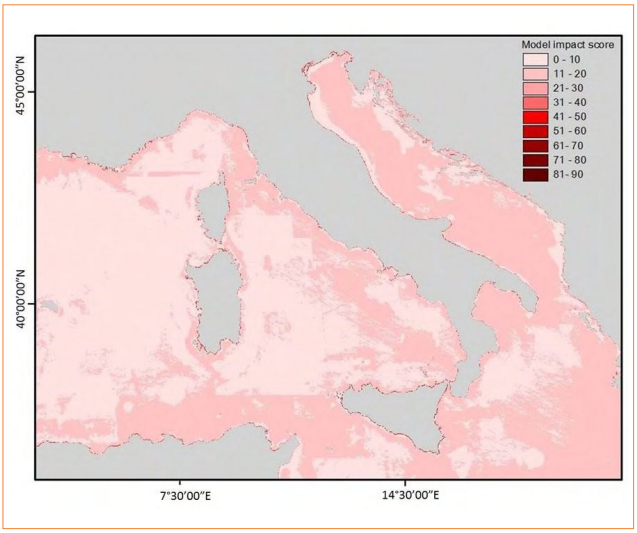

FIGURE 7 Map of the cumulative anthropic impact of the Italian seas
Source: [13]

Conclusions

This study highlights the potential benefits of combining wave and wind power in the Italian seas. The hypothesis of the diversification of renewable energies is grounded on two key benefits: 1) the variability of the produced power can be decreased; 2) power availability can be increased. These benefits are greater when un-correlated resources are combined. This study showed that, although waves and winds are strongly correlated, in some conditions their correlation may be lower. In these situations the combined production would be less variable and more available.

This pattern in the Italian portion of the Mediterranean Sea occurs more frequently in the southern Adriatic Sea closer to the Tyrrhenian and Ionian Sea coasts. Moreover, this study demonstrates how quantitative spatial planning methods may support the selection of the sites of potential interest in the perspective of co-locating wind and wave energy installations, allowing an early identification of the potentially conflictual uses (i.e., ship traffic and fisheries) and providing support for the optimal siting of the wind-wave parks in the light of the environmental sustainability.

Acknowledgment

The work described in this paper was partially supported by the EC FP7 Marie Curie Actions People, Contract PIRSES-GA-2011-295162 – ENVICOP project (Environmentally Friendly Coastal Protection in a Changing Climate).

Arianna Azzellino, Luigia Riefolo, Caterina Lanfredi
Politecnico di Milano, Department of Civil and Environmental Engineering (DICA), Italy

Diego Vicinanza
Second University of Naples, Department of Civil Engineering, Design, Building and Environment (DICDEA), Italy

references

[1] F. Fusco, G. Nolan, J.V. Ringwood, Variability reduction through optimal combination of wind/wave resources – An Irish case study, in *Energy*, 35: 314–325, 2010.

[2] E.D. Stoutenburg, N. Jenkins, M.Z. Jacobson, Power output variations of co-located offshore wind turbines and wave energy converters in California, in *Renewable Energy*, 35: 2781-2791, 2010.

[3] H. Backer, Transboundary maritime spatial planning: a Baltic Sea Perspective, in *J Coast Conserv*., 15: 279–289, 2011.

[4] A. Azzellino, D. Conley, D. Vicinanza, J.P. Kofoed, Marine renewable energies: Perspectives and implications for marine ecosystems, in *The Scientific World Journal*, art. no. 547563, 2013.

[5] F. Douvere, C. Ehler, Introduction, in *Mar Policy* 32:759–761, 2008.

[6] C Ehler, F. Douvere, Marine Spatial Planning: a step-by-step approach toward ecosystem-based management, *Intergovernmental oceanographic Commission* and *Man and the Biosphere programme*, IOC Manuals and Guides 53 ICAM Dossier 6, UNESCO, Paris, 2009.

[7] S. Jay, Built at sea: marine management and the construction of marine spatial planning, in *Town Plan Rev* 81(2):173–191, 2010.

[8] C. Accadia, S. Zecchetto, A. Lavagnini, A. Speranza, Comparison of 10-m wind forecasts from a regional area model and quikscat scatterometer wind observations over the Mediterranean sea, in *Mon. Wea. Rev*., 135, 1945–1960, 2007.

[9] D. Vicinanza, L. Cappietti, P. Contestabile, Assessment of wave energy around Italy, in *Proceedings of the 8th European wave and tidal energy conference*, Uppsala, Sweden, 2009.

[10] D. Vicinanza, L. Cappietti, V. Ferrante, P. Contestabile, Estimation of the wave energy in the Italian offshore, in *Journal of Coastal Research*, 64(12):613-7, 2011.

[11] D. Vicinanza, P. Contestabile, V. Ferrante, Wave energy potential in the north-west of Sardinia (Italy), in *Renewable Energy*, 50, 506-521, 2013.

[12] L. Liberti, A. Carillo, G. Sannino, (2013). Wave energy resource assessment in the Mediterranean, the Italian perspective. R*enewable Energy* 50 (2013) 938-949.

[13] F. Micheli, B.S. Halpern, S. Walbridge, S. Ciriaco, F. Ferretti, S. Fraschetti, R. Lewison, L. Nykjaer, A.A. Rosenberg, Cumulative Human Impacts on Mediterranean and Black Sea Marine Ecosystems: Assessing Current Pressures and Opportunities, in *Plos One*, 8(12), Article Number: e79889, 2013.

[14] A. Afifi, V. Clark, Computer-Aided Multivariate Analysis. Texts in Statistical Science, fourth ed. Chapman & Hall/CRC Press, 1996.

Resonant Wave Energy Converters: Concept development

The Resonant Wave Energy Converter (REWEC) is a device for converting sea wave energy to electrical energy. It belongs to the family of Oscillating Water Columns and is composed by an absorbing chamber connected to the open sea via a vertical duct. The paper gives a holistic view on the concept development of the device, starting from its implementation in the context of submerged breakwaters to the recently developed vertical breakwaters.

DOI: 10.12910/EAI2015-045

F. Arena, G. Barbaro, V. Fiamma, V. Laface, G. Malara, A. Romolo, F.M. Strati

Introduction

Nowadays, the wave energy resource is accepted for being a remarkable source of energy. In this regard, recent global estimates show that the theoretical potential for ocean energy technologies is between 20,000 and 90,000 TWh/yr (consider that in 2004 world's electricity consumption was less than 20,000 TWh/yr) [1]. In this context, the energy from sea waves is the most conspicuous form of ocean energy. The total theoretical wave energy potential is approximately 32,000 TWh/yr [2]. In the last decades, the wave energy resource was mapped in several areas. For instance, Liberti *et al.* [3] and Arena *et al.* [4] investigated the wave energy potential in the Mediterranean Sea with an emphasis on the Italian coasts. They showed that the most energetic area of the Mediterranean Sea is Alghero (Sardinia, Italy).

Contact person: Felice Arena
arena@unirc.it

A large number of concepts defining different Wave Energy Converters (WEC) were developed to harvest the energy from ocean waves. More than 1000 wave energy devices were patented all around the world. One of the fundamental aspects that need to be taken into account in the development of the conversion technology is linked with the remarkable variability of energy and of time scales. The conversion is established through the so-called power take-off (PTO) system. Commonly, turbines or hydraulic motors provide the mechanical component, which converts the alternate motion of the waves into a continuous one-directional motion. The PTO mechanism is usually coupled with a control system in order to optimize the performance of the device under a range of operating conditions. Then, cables and an electrical infrastructure connect the power output from the device to the electric grid.
Several methods were proposed to classify the WECs [5-8]. Specifically, a classification based upon the operating principle of the device distinguishes among: Overtopping devices; Oscillating Bodies; and Oscillating Water Column (OWC).

- ***Overtopping.*** An overtopping device is wave terminator that converts wave energy into potential energy by collecting surging waves into a water reservoir above the mean water level. This device can be either floating or fixed to the shore. The PTO component usually is an axial turbine. See e.g. Margheritini *et al.* [9].
- ***Oscillating bodies.*** Oscillating bodies can be classified with respect to the motion in: heaving, pitching, surging and rotating mass.

Heaving oscillating devices are characterized by a linear oscillatory motion of the immersed, or floating body. These mechanical and/or hydraulic devices convert the vertical motion due to the waves into linear or rotational motion to drive an electrical generators. See, e.g., Archimede Wave S. [10].

Pitching devices oscillate around the horizontal axis in the direction perpendicular to the incident wave. These devices usually consist of a number of floating bodies hinged together across their beams. The relative motions between the floating bodies are used to pump high pressure oil through hydraulic motors, which drive the electrical generators. These devices can be ether: submerged or semi-surface type. See, e.g., Aquamarine Power Oyster, Wave Roller.

Surging devices are characterized by the horizontal motion of an immersed body in the direction of its longer extension. If the body, such as an axisymmetric body, has predominant direction, the direction for surge motion may be specified as the direction of wave incidence. See, e.g., Pelamis [10].

Rotating mass devices drive an eccentric weight or a gyroscope thanks to the heaving and swaying motion of the incoming wave. See, e.g., ISWEC [11]

- ***Oscillating Water Column (OWC).*** OWCs are the most popular wave energy devices. They are composed by a structure with an upper air chamber, which is exposed to the action of the sea waves. The water column inside the chamber oscillates because of the incident wave action. The air into the upper chamber flows through an air turbine coupled to an electrical generator, which converts the kinetic energy into electricity. The air turbine rotates in the same direction, regardless of the flow. A scheme is shown in Figure 1.

Heath [12] defines the major advantages of OWCs, with respect to others WECs:

- There are few moving parts;
- There are no moving parts in the water;
- The use of an air turbine removes the need for gearboxes;
- It is reliable;
- It is easy to maintain;
- It uses sea space efficiently.

Among this, the possibility of being embodied into a conventional breakwater must be mentioned. Indeed, such a solution has several advantages: the construction costs of a breakwater are only slightly increased, and the access for construction, operation and maintenance of the wave energy plant become much easier [6].

The eigenperiod of oscillations inside OWCs is typically smaller than the period of the incident waves; with conventional OWC is not possible to modify this eigenperiod, therefore some complex devices where proposed for phase control in order to reach the resonance condition (latching control) [13].

Starting from the '90s, several full-size OWC prototypes were built all around the world. Examples are [10]: the installation of Pico (1999) in the Azores (Portugal), equipped

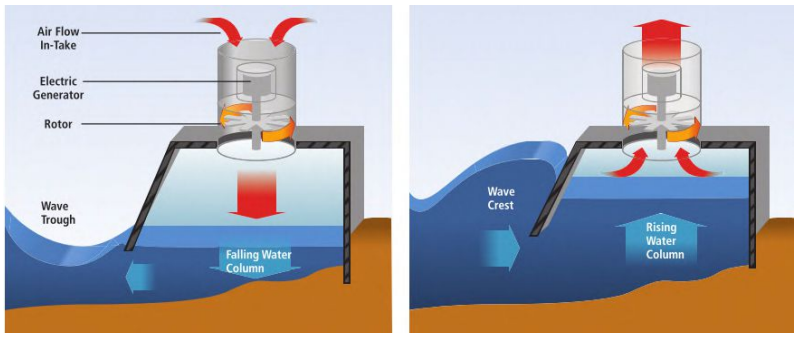

FIGURE 1 Scheme of an OWC during the crossing of a wave through (left) and of a wave crest (right)
Source: Lewis et al. [8]

with a Wells turbine whose capacity is of 400 kW; the installation of LIMPET (Land Installed Marine Power Energy Transformer) (2000) in Islay Island, Scotland (UK), containing three water columns, with an installed capacity of 250 kW. The integration of an OWC wave energy converter into a conventional vertical breakwater was made for the first time in the harbor of Sakata, Japan (1988), whose installed power was of 60 kW. The first prototype of a "multi-chamber OWC breakwater" was made in the port of Mutriku (Spain) (2009) [14]. The installed power is of 296 kW, with 16 Wells turbines of 18.5 kW each, spread over 16 distinct rooms.
Boccotti [15-21] has recently proposed a new kind of OWC, called U-OWC or REWEC. REWEC is the acronym of "Resonant Wave Energy Converters". This device removes some limitations of classical OWCs, such as the small eigenperiod of the water column oscillations, or the low connecting point to the open wave field. In the next sections, the features of this device are discussed by disseminating the experiences conducted at the Mediterranea University of Reggio Calabria in the last 10 years.

Development of the REsonant Wave Energy Converters (REWEC)

The REWEC has been conceived as a way for connecting the traditional need of protecting a certain area to the opportunity of harvesting energy from sea waves. In this regard, it is worth mentioning that the traditional approach of marine engineering is to utilize massive structures at the borderlines of the area. Structures like vertical breakwaters and submerged barriers are all devoted to this task. Considering the fact that they are expected to withstand the continuous action of sea waves, the idea of incorporating wave energy converters is not surprising. In this context, the family of REWEC devices is an example of successful application of the principle of reaching two objectives by one unique structure. Boccotti and his research group at the Mediterranea University developed it in the past 10 years from both a theoretical and an experimental perspective. The development stages and the related major findings are disseminated by reference to the evolution of the REWEC system.

REWEC: An invisible barrier for protecting a coastal area

The first model of REWEC was conceived as a modification of a classical submerged breakwater (Fig. 2). Such a structure is composed by 3 elements: an air pocket, a vertical duct and an air feed. In this system, the water waves are partially reflected by the structure and partially transmitted, while the opening at the top of the vertical duct allows the system interacting with the environment. Specifically, the interaction involves the absorption of sea wave energy.
The REWEC dynamics was investigated by Boccotti [15]. He verified via a small-scale field experiment that the device has the unique feature of being able to reach the resonance condition with the incident waves. Such a possibility relates to the fact that the eigenperiod of the system can be tuned by changing the volume of the air pocket. By doing so, the device is able to absorb a remarkable quantity of wave energy. Thus, reducing the transmission of incident waves.
The experimental activity has also assessed the reliability of the mathematical model used for describing the REWEC dynamics. Indeed, the fluctuations of the inner water surface can be predicted quite well from a time history of the pressure fluctuation at the top of the vertical duct. In this regard, the formulation of the proposed equation of motion is the following:

$$\frac{c-\xi}{g}\frac{d^2\xi}{dt^2}+\frac{l}{g}\frac{du}{dt}=h_1-h_2-h_f \qquad (1)$$

where the symbols are shown in Figure 2, u is the water particle velocity in the vertical duct, g is the acceleration due to gravity, h_1 is the total head at point 1, h_2 is the total head at point 2 and h_f are head losses. Thus, Eq. (1) is a nonlinear second order differential equation, where the nonlinearity is due mainly to the head losses, which are of a drag type.
Based on the small-scale field experiment, the performance of the REWEC at full-scale can be predicted. By assuming a REWEC exposed to wind-generated waves with a JONSWAP [22], it is seen that the plant can absorb up to 45% of the incident waves.

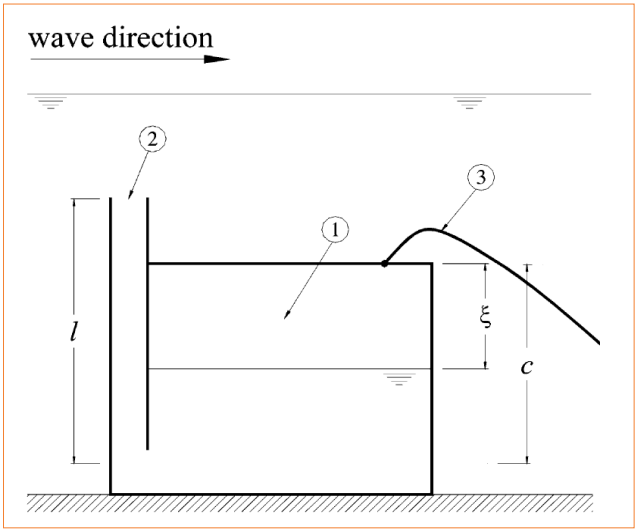

FIGURE 2 Scheme of a REWEC including an air pocket (1), a vertical duct (2) and an air feed (3)
Source: Boccotti [15]

REWEC2/3: A vertical breakwater incorporating a wave energy converter

In parallel to the REWEC system, a second wave energy converted (REWEC2) was proposed by incorporating the vertical duct-air, pocket-air feed system into a vertical breakwater (Fig. 3). This second system was proposed as an alternative to the classical vertical breakwaters employed for creating a safe basin.
Obviously, in this condition the open wave field has only a reflected wave field, which is modified by the absorption of wave energy. The mathematical description of the REWEC2 dynamics is quite similar to the REWEC1. In this situation, the relevant difference relates to the possibility of employing a bidirectional turbine for converting the absorbed wave energy to electrical power.
The working principle of the device is analogous to the one of the REWEC. Indeed, by controlling the air pocket volume the eigenperiod of the system is appropriately tuned. It is worth mentioning that this feature allows implementing a real time control strategy for optimizing the performance of the plant in variable climatic conditions. Indeed, sea waves are expected to have a time-varying peak spectral period. Therefore, resonance can be reached by adjusting the air pocket volume. Predictions based on a Froude similarity have shown that this plant can absorb 40-55% of the incident wave energy. Further, by equipping the air duct with a monoplane Wells turbine, such a plant can produce an average electrical power up to 500 kW.
In addition to that, the plant has some good features from a global stability perspective. Indeed, the safety factors against sliding and overturning are slightly larger (nevertheless, quite close to) than the ones of a classical vertical breakwater.
It may be recognized that optimizing the performance of the REWEC2 requires a sophisticated real time system. Therefore, to remove this critical requirement of the device, a simplified version of the device has been proposed: the REWEC3 [16]. This system is shown in Figure 4. In this system, the air pocket is below the mean water level and the air pressure in still conditions is the atmospheric pressure. Resonance is still reached by the system, but the eigenperiod must be selected a priori during the design stage. Specifically, starting from the identification for the most relevant sea states from an energetic perspective, the eigenperiod is matched to a related peak spectral period. In this situation, the system is tuned by changing the length and the width of the vertical duct.
In 2005 a REWEC3 was installed at the natural laboratory of the Mediterranea University of Reggio Calabria. That experimentation has been pursued with the objective of validating the available hydrodynamic model and of monitoring the performance of the system in random sea waves [17, 18]. The key results of the experimentation relates to the definition of reliable tools for designing a REWEC3 plant, and also to the observation that waves in front of the structure can be amplified remarkably in case of swells. The experimentation emphasized also the capability of the plant in absorbing wave energy. Indeed, measurements to showed that the plant is able to absorb even 90% of the incident wave energy, resulting in a beneficial action from the perspective of wave energy conversion, as well as on improving vessel navigation.
The theoretical development around the device is interesting, as well. Indeed, starting from the model described via Eq. (1), the REWEC3 description is obtained by coupling the equation of motion to the air pocket dynamics. In this regard, a common

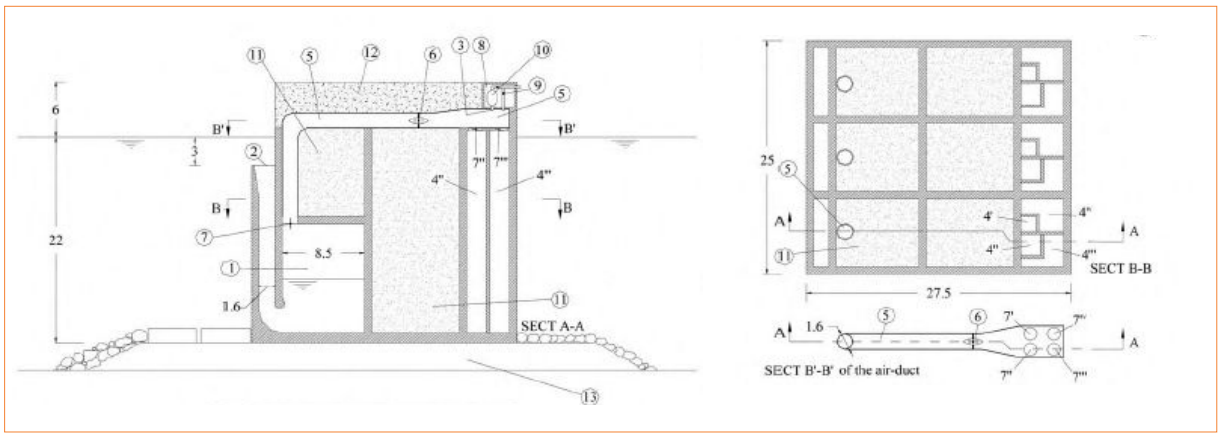

FIGURE 3 Example of REWEC2. 1 air pocket; 2 outer opening; 3 air feed; 4 air reservoir; 5 air duct; 6 Wells turbine; 7 butterfly valve; 8 service room; 9 exhaust valve; 10 compressor; 11 sand filling; 12 superstructure cast in concrete; 13 rubble mound foundation; volumes of reservoirs: 4I, 55 m³; 4II, 110 m³; 4III, 220 m³; 4IV, 275 m³
Source: Boccotti [15]

assumption is to consider the underlying thermodynamic process as isentropic. In parallel, the description of the modification of the surrounding wave field is pursued by an iterative approach based on the maximization of the ratio between the energy per unit width and the wave power. The relevant aspect is that the procedure can be implemented for designing the device based on a single parameter: the resonance index. It is calculated by the equation,

$$R = \frac{4\,T^*}{T_P} \qquad (2)$$

where T_p is the peak period of the spectrum of the wave pressure at the upper opening of the vertical duct (Δp) and T^* is the abscissa of the first maximum of the following cross-correlation function:

$$\psi(T) = <\Delta p(t)\cdot\xi(t+T)> \qquad (3)$$

Such an index is 1 close to resonance. Therefore, at the design stage, the plant is designed to reach resonance (that is, to have R = 1) at the desired sea state.

Conclusions

The paper has disseminated the main characteristics of the Resonant Wave Energy converter (REWEC). It has shown the historical development of the device considering the various concepts proposed by Boccotti in the past decade, starting from a device incorporated into a submerged breakwater to the case in which it is incorporated into a vertical breakwater.
The past small-scale field experiments pursued at the NOEL laboratory of the Mediterranea University

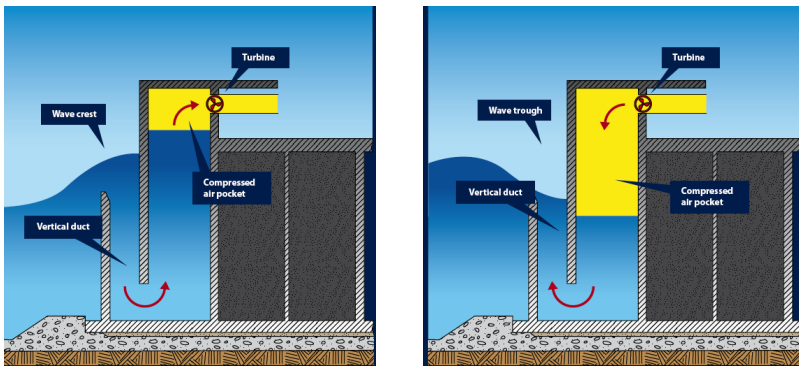

FIGURE 4 Scheme of a REWEC3 plant. Left panel: plant behaviour during a wave crest; right panel: plant behaviour during a wave trough

of Reggio Calabria has shown that the device has some peculiarities providing better performances in comparison with other devices belonging to the Oscillating Water Column family. Specifically, the REWEC is able to naturally reach the resonance condition with the wave pressure exciting the system for the desired sea state. Hence maximizing the absorption of the wave energy.
The future development of the device relates to the investigation of a REWEC3 small-scale model equipped with a turbine and to full-scale prototype. These future works are discussed in the second part of the paper, which reports the recent experiences in the context of the POSEIDONE project and of a modular REWEC3 developed in collaboration with ENEA. The REWEC3, under construction at the Civitavecchia port, will be described.

Felice Arena, Giuseppe Barbaro, Vincenzo Fiamma, Valentina Laface, Giovanni Malara, Alessandra Romolo, Federica Maria Strati
University of Reggio Calabria "Mediterranea", Italy

references

[1] IEA, http://www.iea.org/techinitiatives/renewableenergy/oceanenergysystems/.

[2] G. Mørk, S. Barstow, A. Kabuth, M.T. Pontes, Assessing the global wave energy potential, in *Proceedings of the 29th international conference on Ocean, Offshore and Arctic Engineering*, Shanghai, China, 2010.

[3] L. Liberti, A. Carillo, G. Sannino, Wave energy resource assessment in the Mediterranean, the Italian perspective, in *Renewable Energy*, 50, 938-949, 2013.

[4] F. Arena, V. Laface, G. Malara, A. Romolo, A. Viviano, V. Fiamma, G. Sannino, A. Carillo, Wave climate analysis for the design of wave energy harvesters in the Mediterranean Sea, in *Renewable Energy*, 77, 125-141, 2015.

[5] J. Falnes, A review of wave-energy extraction, in *Marine Structures*, 20, 4, 185-201, 2007.

[6] A.F.d.O. Falcão, Wave energy utilization: A review of the technologies, in *Renewable and Sustainable Energy Reviews*, 14, 3, 899-918, 2010.

[7] B. Drew, A.R. Plummer, M.N. Sahinkaya, A review of wave energy converter technology, in *Proceedings of the Institution of Mechanical Engineers, Part A: Journal of Power and Energy*, 223, 8, 887-902, 2009.

[8] A. Lewis, S. Estefen, J. Huckerby, W. Musial, T. Pontes, J. Torres-Martinez, Ocean Energy, in *O. Edenhofer, R. Pichs-Madruga, Y. Sokona, K. Seyboth, P. Matschoss, S. Kadner, T. Zwickel, P. Eickemeier, G. Hansen, S. Schlömer, C. von Stechow (Eds.) IPCC Special Report on Renewable Energy Sources and Climate Change Mitigation*, Cambridge, United Kingdom and New York, NY, USA: Cambridge University Press, 2011.

[9] L. Margheritini, D. Vicinanza, P. Frigaard, SSG wave energy converter: Design, reliability and hydraulic performance of an innovative overtopping device, in *Renewable Energy*, 34, 5, 1371-1380, 2009.

[10] J. Cruz, Ocean wave energy: current status and future perspectives, Springer, 2008.

[11] G. Bracco, E. Giorcelli, G. Mattiazzo, ISWEC: A gyroscopic mechanism for wave power exploitation, in *Mechanism and Machine Theory*, 46, 10, 1411-1424, 2011.

[12] T.V. Heath, A review of oscillating water columns, in *Philosophical Transactions of the Royal Society of London A: Mathematical, Physical and Engineering Sciences*, 370, 1959, 235-245, 2011.

[13] A.F.d.O. Falcão, P.A.P. Justino, OWC wave energy devices with air flow control, in *Ocean Engineering*, 26, 12, 1275-1295, 1999.

[14] Y. Torre-Enciso, I. Ortubia, L.I. Lopez de Aguileta, J. Marquéz, Mutriku wave power plant: from the thinking out to the reality, in *Proceedings of the 8th European Wave and Tidal Enegy Conference*, Uppsala, Sweden, 2009.

[15] P. Boccotti, On a new wave energy absorber, in *Ocean Engineering*, 30, 9, 1191-1200, 2003.

[16] P. Boccotti, Comparison between a U-OWC and a conventional OWC, in *Ocean Engineering*, 34, 5-6, 799-805, 2007.

[17] P. Boccotti, Caisson breakwaters embodying an OWC with a small opening –Part I: Theory, in *Ocean Engineering*, 34, 5-6, 806-819, 2007.

[18] P. Boccotti, P. Filianoti, V. Fiamma, F. Arena, Caisson breakwaters embodying an OWC with a small opening-Part II: A small-scale field experiment, in *Ocean Engineering*, 34, 5-6, 820-841, 2007.

[19] P. Boccotti, Design of breakwater for conversion of wave energy into electrical energy, in *Ocean Engineering*, 51, 106-118, 2012.

[20] F. Arena, P. Filianoti, Small-Scale Field Experiment on a Submerged Breakwater for Absorbing Wave Energy, in *Journal of Waterway, Port, Coastal, and Ocean Engineering*, 133, 2, 161-167, 2007.

[21] G. Malara, F. Arena, Analytical modelling of an U-Oscillating Water Column and performance in random waves, in *Renewable Energy*, 60, 116-126, 2013.

[22] K. Hasselmann, T.P. Barnett, E. Bouws, H. Carlson, D.E. Cartwright, K. Eake, J.A. Euring, A. Gicnapp, D.E. Hasselmann, P. Kruseman, A. Meerburg, P. Mullen, D.J. Olbers, K. Richren, W. Sell, H. Walden, Measurements of wind-wave growth and swell decay during the joint North Sea wave project (JONSWAP), in *Ergänzungsheft zur Deutschen Hydrographischen Zeitschrift*, A8, 1-95, 1973.

Resonant Wave Energy Converters: Small-scale field experiments and first full-scale prototype

The Resonant Wave Energy Converter 3 (REWEC3) is a device belonging to the family of Oscillating Water Columns (OWCs), that can convert the energy of incident waves into electrical energy via turbines. In contrast to classical OWCs, it incorporates a small vertical U-shaped duct to connect the water column to the open wave field. This article shows the results of a small-scale field experiment involving a REWEC3 designed for working with a 2 kW turbine. Then, the next experimental activity on a REWEC3 installed in the NOEL laboratory with the collaboration of ENEA is presented. Finally, the first prototype of ReWEC3 under construction in Civitavecchia (Rome, Italy) is shown. The crucial features of the construction stage are discussed and some initial performances are provided.

DOI: 10.12910/EAI2015-046

F. Arena, V. Fiamma, R. Iannolo, V. Laface, G. Malara, A. Romolo, F.M. Strati

Introduction

The Resonant Wave Energy Converter 3 (REWEC3) is an Oscillating Water Column (OWC) device, already described in Part I. The modeling of the REWEC3 is different from that of OWCs, as the equation of motion of the water column includes non-linear terms associated to the head losses in the vertical duct. A holistic view on the design process has been given by Boccotti [1], while the modeling and the experimental validation have been discussed by Boccotti [2], Boccotti *et al.* [3], and Arena *et al.* [4].
In 2013 a novel U-OWC was installed at the Natural Ocean Engineering Laboratory (NOEL) of the Mediterranea University of Reggio Calabria. Such a plant is equipped with a 2 kW turbine (Figs. 1-2). The best conditions for conducting the experiments occurred on September 1st, 2014, when a storm allowed to record optimal sea state conditions for the plant, for testing the power converted by the device (Fig. 3). The preliminary results of this activity are shown in Arena *et al.* [5].
On the basis of the existing experiences, a new small-scale filed experiment is planned to be carried out on a REWEC3 devices installed in the NOEL laboratory with the collaboration of ENEA (Fig. 4 shows a 3D view of the ENEA caisson; Fig. 5 shows the actual ENEA caisson). Some specific aspects related to the optimization of the device and on hydrodynamics inside the plant will be investigated.
Finally, the first prototype of REWEC3 is under construction in Civitavecchia (Rome, Italy). The device is embodied in a vertical breakwater, so that the plant can be employed both for protection purposes and for energy harvesting. The crucial features of the construction stage are discussed and some initial performances of the plant are provided.

Contact person: Felice Arena
arena@unirc.it

FIGURE 1 The REWEC3 plant installed in the breakwater in reinforce concrete at NOEL laboratory

FIGURE 2 Wells turbine installed at the REWEC3 breakwater at NOEL laboratory. The turbine has been designed within the POSEIDONE project by the team of the University of Rome La Sapienza and manufactured by Faggiolati Pumps SpA. Experimental activities are managed by Mediterranea University and Wavenergy.it

Recent experiences on fully equipped REWEC3 plant and future development stages

One of the main research activities on the REWEC3 plants are related to small-scale experiments carried out in the field. Indeed, the possibility of implementing a fully equipped plant requires specific investigations on the joint turbine-REWEC3 dynamics.

FIGURE 3 The Wells turbine installed at the REWEC3 breakwater at NOEL laboratory, during the storm of September 1st, 2014

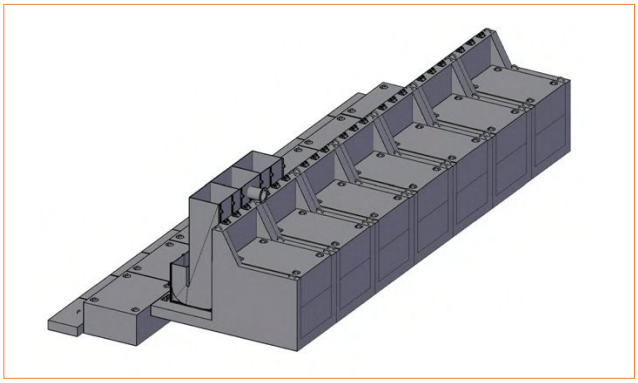

FIGURE 4 The 3D view of the REWEC3 caisson at NOEL laboratory realized in collaboration with ENEA

FIGURE 5 The REWEC3 caisson realized in collaboration with ENEA, during the installation stage at NOEL laboratory

The POSEIDONE project, funded by the Italian Ministry of Environment (G.U. – Serie V n. 150 del 21/12/2009), has involved the installation of a REWEC3 plant with a 2 kW turbine. The experimental activity has been pursued at the NOEL laboratory of the Mediterranea University. The novelty of this experiment relates to the installation of a turbine with such a remarkable power (consider that the experimentation is conducted at a laboratory with sea states having significant wave height of no more than 1.2 m). The project was proposed and conducted jointly by the Mediterranea University, the University of Rome La Sapienza, Faggiolati Pumps S.p.A. and Wavenergy.it S.r.l. (the licence of the REWEC3 patent by Professor Paolo Boccotti). The data of the experimentation are still under investigation. Therefore, the results will be disseminated at a later stage. However, here a confirmation about the favourable performance of the device can be given. Specifically, during the occurrence of sea states with significant wave height of 1m, the average converted power of about 500 W and peaks of 1.5 kW were recorded. This result has confirmed previous theoretical estimates and, to our knowledge, similar (scale-wise) experimentations were not able to reach these values of electrical power.

The next experimentation was conducted in collaboration with ENEA, which contributed to the installation of a new caisson that is going to be used for investigating problems on the optimization of the REWEC3 device. It is composed by one REWEC3 structure, equipped with 2 inner partition walls. The walls can be removed, so that different configurations of the inner part of the plant can be investigated. In this experimentation, the objective is to identify an optimal configuration of the REWEC3 and define criteria useful at the design stage, when the width of each REWEC3 cell must be designed. In addition, this experimentation is expected to provide a better insight into the REWEC3 dynamics. The mathematical models used for describing the REWEC3 dynamics will be reviewed and possibly improved, in order to define design tools even better.

In parallel to these activities, the problem of forcing an optimal turbine behaviour is faced. If the REWEC3 is exposed to the desired sea states, then resonance occurs. But, in other situations, the coupled REWEC3 – turbine behaviour must be improved by implementing adequate control strategies. The objective of a control strategy is to maximize the performance of the system in a variety of wave conditions. This is a crucial element of a full-scale prototype. It is worth noting that, at a fixed rotational speed, turbines such as Wells turbine are able to operate with good efficiency values only within a limited range of flow conditions around the peak efficiency point [6]. In this context, the choice of the optimal rotational speed of the turbine for a given sea state and a given turbine, as well as the determination of an effective control algorithm, are the key issues. This problem was investigated by Falcão and Justino [7] and Falcão [8] for a conventional OWC in random sea waves. Regarding the U-OWC, specific investigations on the PTO performance coupled to the active part are at their first stage of development.

The first approach to this problem was performed within the context of a MARINET project (Marine Renewable Infrastructure Network for emerging Energy Technologies) [9], which has allowed to access the test facilities of Tecnalia R&I, in Bilbao (Spain), providing an effective instrumentation for coupling the available numerical codes to the test-bench required for pursuing pertinent experimental measurements. A number of experiments have been carried out for a given geometric configuration and turbine characteristics. The determination of an optimal reference rotational speed for a fixed sea state and the differentiation of the system behavior in case of wind-generated waves and swells were the key findings of the project. Numerical models have been implemented to simulate the physical behavior of the designed plant. This process required the modelling of the hydrodynamic system, the PTO components, the electrical system and the control strategy. The electrical testing included two systems: a real part and a simulated part. The former is composed by both the emulated and the real component, meaning the numerical model featuring the behavior of the device (from the wave energy resource to the generator shaft)

and the physical equipment of the test bench. The latter represents the behavior of the whole device used for validations and comparisons of the experimental testing. Results pointed out that there is a relevant connection between the spectral shape of the incident wave field and the optimal working conditions of a REWEC3. In this context, the activity performed at MARINET was crucial as it led to the determination of the future steps for developing a fully optimized REWEC3 plant. Actually, a Maximum Power Point Tracking (MPPT) method is under development for optimizing the performance of the plant in a variety of sea states. Considering the relevance of the sea state parameters, the proposed strategy relates to the identification of an optimal rotational speed given the significant wave height of the sea state.

FIGURE 6 Layout of the new structures in the Port of Civitavecchia

The first prototype of REWEC3 caisson under realization in the Port of Civitavecchia

The small-scale experimentation in the field on REWEC3 plants proceeds parallel to the activities of implementation of the new device at full-scale. The Port of Civitavecchia (Rome, Italy) will host the first full-scale prototype of the REWEC3 device incorporated in a caisson breakwater, within the works planned for improving the services of the port and the quality of the infrastructure. Specifically, the construction of two new basins of about 50 ha, devoted to ferries and cruises (extension of quays of about 1.4 km) and to naval services (extension of quays of about 1.7 km), and the extension of the breakwater "C. Colombo" (the main breakwater of the port) to a total length of 400 m are mentioned. The new structures will be built by utilizing reinforced concrete cellular caissons (over 120 reinforced concrete caissons of different sizes). An overall view is given in Figure 6, which shows the layout of the port. In the outlined context, the embodiment of 17 REWEC caissons was proposed by the Constructor for reducing the reflection coefficient in front of the structure. Indeed, in a first instance, the caissons were designed for absorbing wave energy, without employing devices for exploiting wave energy. Then, the use of the REWEC3 technology was conducted by Wavenergy.it (www.wavenergy.it).

The contract on the extension of the Port of Civitavecchia was awarded in spring 2012. The time schedule has been planned for completing the works about at the end of 2015. The construction started in July 2012.

Obviously, the novel configuration of the REWEC3 breakwater has been designed for harvesting as much energy as possible (Figs. 7 and 8). In this context, the crucial change pertains to the inclusion of the pneumatic chamber, which has been utilized into all the REWEC3 caissons, for a total length of 510 m, at a water depth of 15 m.

Each REWEC3 caisson is 33.94 m long and includes 8 independent absorbing cells (vertical duct and pneumatic chamber) 3.87 m wide. The vertical duct is 1.60 m wide and the U-duct opening is located at -2.00 m below MWL, so that the opening is not always below the free surface, while the pneumatic chamber is 3.20 m wide. The external walls of the absorbing part of the REWEC3 are 0.50-0.60 m thick while the inner walls are 0.35 m thick.

Some cells of the caissons are filled with concrete in order to ensure both the global stability and a monolithic behavior of the structure. The remaining

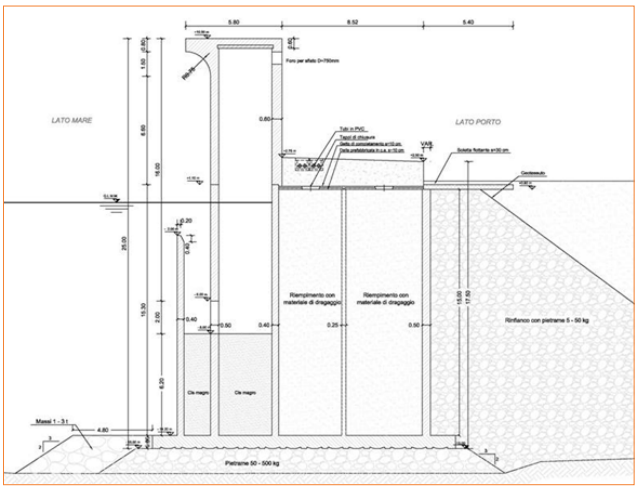

FIGURE 7 Cross-section of the REWEC3 wave energy converter in the Port of Civitavecchia

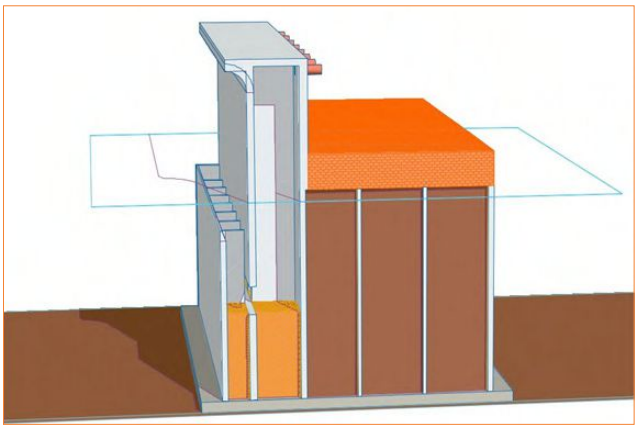

FIGURE 8 Perspective views of a single REWEC3 caisson, with independent cells, employed in the works of the Port of Civitavecchia

part is filled by using dredged materials. Some results have been shown on Arena *et al.* [10].
At present, 4 REWEC3 caissons have been completed up to 10 m above M.W.L. at the Port of Civitavecchia (Rome, Italy) (Figs. 9 and 10).

The caissons casting

The construction of the reinforced concrete REWEC caissons consists of the following main steps:

FIGURE 9 Progress of the construction of the REWEC3 caissons at the Port of Civitavecchia

FIGURE 10 4 REWEC3 caissons completed up to 10m above M.W.L. at the Port of Civitavecchia (Rome, Italy)

- rubble layer foundation placement;
- casting up to 0,80 m SWL on a floating plant and launching;
- towing to preliminary site and sinking with water;
- towing to final site;
- filling with concrete and dredged material;
- backfilling;
- completion up to 10,00 m SWL on site.

The rubble mound foundation consists of a quarry rock layer of 50-500 kg and about 1 m thick, placed on the seabed and topped with a final levelling/

blinding layer of finer aggregate. The quarry material is placed and levelled by means of a crane pontoon, which discharges by means of a hydraulic grab on site.
Owing to its dimensions and weight, the caissons are cast in two different main phases. The first one considers the construction of the REWEC caissons for a total height of 15,80 m (down to +0.80 m under MSL) on a floating casting plant.
The bottom slab (0,80 m thickness) is cast in one single operation; during this phase the sliding formwork is hung up from the floating plant. Once the base slab is completed, the sliding formwork is lowered to start with the caisson body casting.
The concrete is cast in layers and in the meantime the horizontal reinforcement is positioned. Concrete is carried to the upper frame and distributed by means of a pump. The self-climbing formwork is raised by hydraulic jacks acting simultaneously on steel vertical bars, which stand on the caisson base slab and cause the formwork to rise slowly until the final level is achieved.
A series of mix designs were set at the beginning of the work, so the caissons are made with concrete, respecting the following requirements:
- cubic compressive strength 45 MPa;
- exposure class XS3;
- workability S4/S5;
- cement CEM III or CEMIV;
- w/cm 0.40-0.44;
- maximum diameter of aggregates 25-32 mm;
- concrete cover thickness value of 5 cm.

When the caisson body casting and concrete ballasting needed to ensure the caisson nautical stability are completed, the mobile upper frame with the formwork hung up is raised to allow the caisson launch. At the same time, the plant is brought down to the depth necessary for allowing the caisson floatation. Once floating, the caisson is moved out of the plant and towed, waiting for the final positioning.
The placing phase consists in towing the caisson, by means a tugboat, to the placing site, where it is maintained in the right position by means of winches connected with some eyebolts on the caisson top at one end, and with other eyebolts on a crane pontoon or on the nearest caisson already sunk at the other end. Pumps are put on the caisson top slab and the seawater is pumped into the cells.
The caisson position is constantly kept under observation by a topographic surveyor during the final step of the operation. A final check of the rubble mound levelling is made by divers, just before a complete sinking is reached. If it is acceptable, the caisson is completely sunk and filled with seawater to ensure it is stable until filling is complete.
The caisson filling is made of concrete and dredged material. The filling material will be unloaded on the caissons directly by lorries and then pushed into the cells by an excavator (from the placing of the first caisson a terrestrial connection has been realized).
Backfilling operation (when necessary) is started behind the caisson once it has been filled. The backfill material placed just behind the caisson consists of selected quarry material (5-50 kg).
The second phase of REWEC3 caisson casting considers the completion of the caissons with the construction of the upper part of the pneumatic chamber (“the seawall”) by using a sliding formwork *in situ* in order to align the pneumatic chamber from the +0,80 m SWL up to +10,00 m SWL.
The final step of the construction involves the concrete demolition of the upper part of the vertical duct from -+2,00 m SWL up to +0,80 m SWL (the sea side row of cells) by cutting.
Behind the active part of the REWEC3, a superstructure of reinforced concrete will be built *in situ* including configurations for water, electricity and telecommunications services (see Fig. 8). The current design does not include the mechanical and the electrical parts to transmit energy into the port grid.

Wave climate description via available data (project TEN-T, annual programme 2013 - action 2013-IT-92050-S)

The performances of the Civitavecchia plant took place by considering the wave data recorded since November 2012 by two buoys located in front of the breakwater. The monitoring system of the two buoys provides the statistical information on the sea states interacting with the structure. Specifically, the quantities of interest are: significant wave height; mean spectral period; and dominant direction. The

data are representative of 30-minute sea states and were recorded from November 16th 2012 to November 31st 2013. Totally, the available records are 17,218. Then, the mean wave power available per unit width at Civitavecchia is calculated as,

$$\overline{\Phi} = \int_0^{\infty} \Phi(h) \left| \frac{dP(H_s > h)}{dh} \right| dh \qquad (2)$$

where the probability of exceedance of the significant wave height at a certain location $P(H_s>h)$ is given by Eq. (1). Then, the power per unit width associated with a certain sea state (Φ) is estimated by the equation

$$\Phi = \rho g \int_0^{\infty} \int_0^{2\pi} c_g(\omega) S(\omega,\theta) d\theta \, d\omega \qquad (3)$$

where ρ denotes the water density, g is the acceleration due to gravity, $S(\omega,\theta)$ is the directional wave spectrum of the incoming waves and c_g is the group celerity.

From the available data, the mean wave power per unit length $\overline{\Phi}$ in Civitavecchia has been estimated about 2.80 kW m^{-1}.

The results obtained have been compared to those achieved by the third order generation WAM model provided by ENEA [11, 12], showing a good agreement (see Tab. 1 and Fig. 11). In detail, Figure 11 shows the average wave power associated with

Data	Φ(Kw/m)
WAM data	2,37
TEN-T buoy	2,80

TABLE 1 Mean wave power per unit length $\overline{\Phi}$

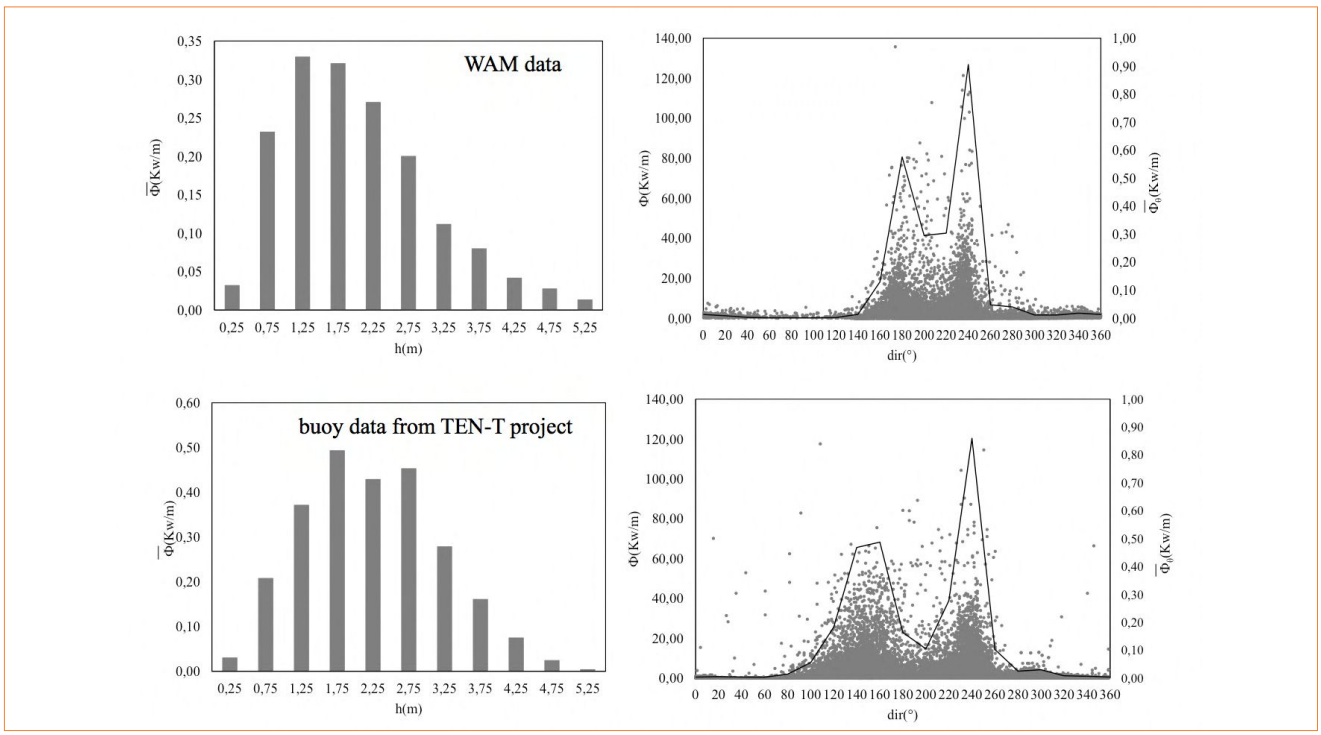

FIGURE 11 Left panels: average wave power associated with certain significant wave height intervals; right panels: wave power calculated for each sea state with the related wave direction (dots) and mean wave power calculated for a certain directional sector (continuous line). The left vertical axis pertains to the wave power; the right vertical axis pertains to the mean wave power; the horizontal axis shows the wave direction

certain significant wave height intervals (left panels). It is seen that the largest amount of incident wave power is related to sea states with significant wave height belonging to the interval (1.25 m, 2.75 m), both with the WAM model and the measurements of buoys. Obviously, such a consideration is crucial for characterizing the performance of the plant. Indeed, the plant has to be designed to maximize the energy absorption for sea states with the occurrence of the largest incident wave energy. Then, in the right panels of Figure 11 the wave power calculated for each sea state with the related wave direction (dots) and mean wave power calculated for a certain directional sector (continuous line) are shown; the left vertical axis pertains to the wave power; the right vertical axis pertains to the mean wave power; the horizontal axis shows the wave direction.

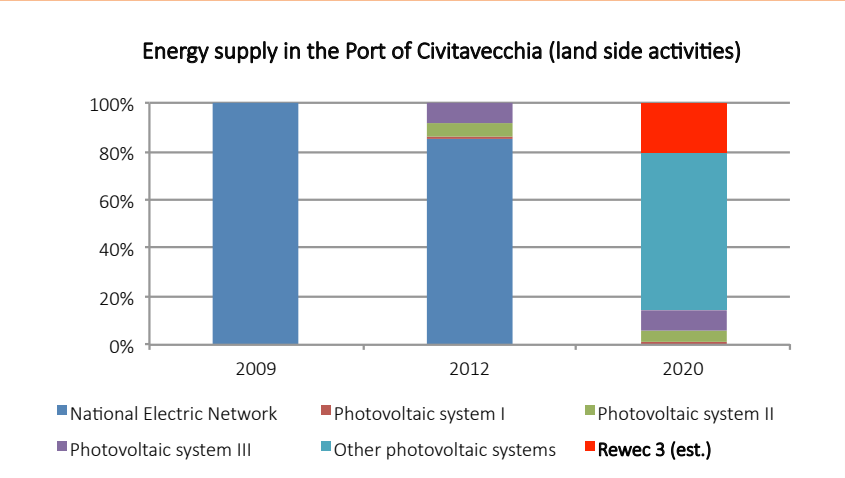

FIGURE 12 Electrical needs in the Port of Civitavecchia: the perspective of electricity supply from renewable sources up to 2020
Source: TEN-T ANNUAL PROGRAMME 2013 - ACTION 2013-IT-92050-S

Expected performances of the REWEC3 device in Civitavecchia

The average wave energy absorbed by the REWEC3 in Civitavecchia is evaluated from the mean power of incoming waves estimated in the previous section. In this regard, the hydrodynamics of the REWEC3 is described via the theoretical model proposed by Boccotti [2] and [1], described in Arena *et al.* [10], and developed with a different approach by Malara & Arena [13].

Initial estimates of the wave energy absorbed by the REWEC3 in Civitavecchia have been shown in Arena *et al.* [5]. It is seen that the plant absorbs the largest amount of wave energy in the most significant sea states. Specifically, the absorbed mean wave power is 1,281 MWh/yr/km for sea states with H_s ranging in the interval (2.5-3] m and T_m in (5.5-6]s (H_s being the significant wave height and T_m the mean wave period). Whereas it absorbs 1163 MWh/yr/km with H_s (2-2.5] m and T_m in (5-5.5] s, for which the absorbed mean wave power is more than 80% the incident one. The REWEC3 plant in Civitavecchia is able to absorb about 12.1 GWh/yr/km.

Initial estimations of the electrical power given by the REWEC3 plant are provided by considering a monoplane Wells turbine. By considering classical laboratory studies for the estimation of head losses and the efficiency of a Wells turbine (Curran and Gato, [14]), a production of electricity of 20 MWh/yr for each cell of the REWEC3 device in Civitavecchia has been estimated.

Better energy efficiency is expected to be reached with turbines optimized for the working condition of the REWEC3 in Civitavecchia for different wave conditions, for which the system REWEC3+turbine could be suitably regulated to maximizing the production of electricity from the turbine.

The installation and the complete exploitation of the systems REWEC3 for the absorption of the energy produced by the waves will contribute for almost 20% of the total needs of the port (2,510,000 kWh per year), see Figure 12.

Conclusions

The paper, in the first part, has shown the preliminary results of a field experiment on a REWEC3 model installed at the NOEL laboratory. The REWEC3 is a wave energy harvester belonging to the family of oscillating water columns. The key feature of the device is the ability of naturally reaching the resonance condition with the incident waves without the need of any phase control devices. This experimental activity has been pursued for testing in a relevant environment a REWEC3 equipped with a 2kW turbine. The best conditions for conducting the experiments occurred on September 1st, 2014, when a storm allowed to record optimal sea-state conditions for the plant. The first results of the research are: a U-OWC plant equipped with a turbine is able to reach the resonance condition with the incident waves; the turbine utilized at the NOEL is capable of producing an average power close to 500 W, with power peaks close to 1 kW. The results shown in this paper are preliminary and will be the basis for the next field experimental activity that will be executed on a new REWEC3 device installed at the NOEL laboratory with the collaboration of ENEA, for the investigation of some specific aspects related to the hydrodynamics onside the plant.
In the second part, the present work has dealt with the first caisson breakwater plant embodying a U-OWC device: the REWEC3. The plant is located in Civitavecchia (Rome, Italy). The construction stage of the REWEC has been described. Different phases have been described for highlighting the crucial steps involved in the construction of the structure. The details of the layout and of the cross-section of the plant have been shown, as well. Finally, the paper has dealt with the performances of the REWEC3 plant under construction in the port of Civitavecchia.

Acknowledgements
The authors express their gratitude to Impresa Pietro Cidonio S.p.a. and to DNC scarl for providing the images and the pictures relating to the REWEC3 caissons under construction in the Port of Civitavecchia, utilized in the paper.
Moreover, the authors are grateful, for funding part of the presented research, to:

- The Project: "POSEIDONE - U-OWC plant and air turbine for the production of electrical power from sea waves", funded by the Ministry of Environment (GU- SerieV n . 150 of 21/12/2009) - Partners: Mediterranea University, University of Rome La Sapienza; FaggiolatiPumps SpA.
- The POLONET, grant n. 13938 del 8/11/2011, Public Notice for the establishment of Regional Pole for the Innovation, POR FESR Calabria 2007/2013 Axis I - Lines 1.1.1.1 and 1.1.2.2, ordinance n. 14225, 14/10/2010.
- The EU FP7 project "REWEC3-Electrical PTO system Optimization", Project proposal number 236, 4th call for free-of-charge access to 17 specific MARINET infrastructures "MARINET - Marine Renewables Infrastructure Network for Emerging Energy Technologies" Seventh Framework Programme of the European Union. Host research infrastructure and project partner: TECNALIA (Spain).
- ENEA for financing the research "Experimental activity on Oscillating Water Column (OWCs) devices" within the agreement MSE-ENEA on the Research on the Electricity System 2012, Project B.1.4 "Studi e valutazioni sulla produzione di energia elettrica dalle correnti marine e dal moto ondoso".
- The project "Study for the development of the green mobility in the port of Civitavecchia through the implementation of the pilot technology REWEC 3" funded by the European Commission. TEN-T ANNUAL PROGRAMME 2013 - ACTION 2013-IT-92050-S.

Felice Arena, Vincenzo Fiamma, Roberta Iannolo, Valentina Laface, Giovanni Malara, Alessandra Romolo, Federica Maria Strati
University of Reggio Calabria "Mediterranea", Italy

references

[1] P. Boccotti, Design of breakwater for conversion of wave energy into electrical energy, in *Ocean Engineering*, 51, 106-118, 2012.

[2] P. Boccotti, Caisson breakwaters embodying an OWC with a small opening – Part I: Theory, in *Ocean Engineering*, 34, 806-819, 2007.

[3] P. Boccotti, P. Filianoti, V. Fiamma, F. Arena, Caisson breakwaters embodying an OWC with a small opening – Part II: A small-scale field experiment, in *Ocean Engineering*, 34, 820-841, 2007.

[4] F. Arena, P. Filianoti, Small-Scale Field Experiment on a Submerged Breakwater for Absorbing Wave Energy, in *Journal of Waterway, Port, Coastal, and Ocean Engineering*, 133(2): 161-167, 2007.

[5] F. Arena, G. Malara, A. Romolo, V. Fiamma, Field experiment on a U-OWC wave energy converter in confused sea waves. Computational Stochastic Mechanics, in *Proc. of the 7th International Conference (CSM-7)*, G. Deodatis and P.D. Spanos (eds.), Santorini, Greece, June 15-18, 2014.

[6] A. Brito-Melo, L.M.C. Gato, A.J.N.A. Sarmento, Analysis of Wells turbine design parameters by numerical simulation of the OWC performance, in *Ocean Engineering*, 29, 12, 1463-1477, 2002.

[7] A.F.d.O. Falcão, P.A.P. Justino, OWC wave energy devices with air flow control, in *Ocean Engineering*, 26, 12, 1275-1295, 1999.

[8] A.F.d.O. Falcão, Control of an oscillating-water-column wave power plant for maximum energy production, in *Applied Ocean Research*, 24, 2, 73-82, 2002.

[9] F. Arena, A. Romolo, G. Malara, V. Laface, F.M. Strati, REWEC3-Electrical PTO system Optimization, MARINET Report of the 2014, (Activity at TECNALIA).

[10] F. Arena, A. Romolo, G. Malara, A. Ascanelli, On design and building of a U-OWC wave energy converter in the Mediterranean Sea: a case study, in *Proceedings of the 32nd International Conference on Ocean, Offshore and Arctic Engineering OMAE2013*, Nantes, France, 2013.

[11] L. Liberti, A. Carillo, G. Sannino, Wave energy resource assessment in the Mediterranean, the Italian perspective, in *Renewable Energy*, 50, 0, 938-949, 2013.

[12] F. Arena, V. Laface, G. Malara, A. Romolo, A. Viviano, V. Fiamma, G. Sannino, A. Carillo, Wave climate analysis for the design of wave energy harvesters in the Mediterranean Sea, in *Renewable Energy*, 77, 0, 125-141, 2015.

[13] G. Malara, F. Arena, Analytical modelling of an U-Oscillating Water Column and performance in random waves, in *Renewable Energy*, 60, 116-126, 2013.

[14] R. Curran, L.M.C. Gato, The energy conversion performance of several types of Wells turbine designs, in *Proceedings of the Institution of Mechanical Engineers, Part A: Journal of Power and Energy*, 211: 133-145, 1997.

Double system wave energy converter for the breaker zone

In this paper a particular type of wave energy converter, namely EDS (Energy Double System) is presented. It is a two-body point absorber composed by a heaving float and a surging paddle, mounted on the same structure and aligned along the wave propagation direction. The system is designed for working in the breaker zone, where waves close to breaking can generate a considerable surging force on the paddle.
A scale EDS model has been built and tested in the wave flume of the Hydraulics Laboratory of the Politecnico di Milano. The power absorbed by the system, varying its configuration, distance from the shoreline and wave, has been measured, and interesting efficiencies have been found.

DOI: 10.12910/EAI2015-047

S. Malavasi, M. Negri

Introduction

After more than forty years since its beginning, scientific research in wave energy harnessing still continues nowadays: the great availability of wave energy on the coasts of the world is continuously pushing scientists and the engineering community to study new methods and invent new machines for wave energy harvesting, with the hope to establish one or more technologies that are economically feasible. Unlike wind energy, where the technology of wind turbines is well established, for wave energy no system has reached the commercial state, despite the fact that several different prototypes have been placed in the sea: just to mention a few, Wavestar, Oyster, Pelamis, Limpet, AquaBuOY, Wave Dragon and many others. In the reference literature, this great variety of technologies are classified according to the type of operation of the WECs (point absorber, attenuator, terminator, oscillating water columns, overtopping) and their positioning (offshore, nearshore, shoreline); reviews of wave energy technology can be found in the works of Falnes [1], Falcao [2], López *et al*. [3].
Research on wave energy has been developed mainly in northern Europe, also owing to the highly energetic seas that characterize this zone. Lately, also less energetic seas are being considered for wave energy harvesting, like the Italian coasts, which are characterized by power ranging from 2 to 10 kW m^{-1} (Vicinanza *et al.* [4]); in Bozzi *et al*. [5] a simulation of wave energy production in various Italian sites is made, and it is shown that fairly good results are obtainable if ocean WEC are downscaled according to the wave climate.
Recently, researchers have paid some attention on the nearshore region, because it seems to be a good compromise between structure costs and energy availability, which can be a large part of the correspondent offshore one (Folley and Whittaker

Contact: Marco Negri
marco.negri@polimi.it

[6]); furthermore, the nearshore region has the advantage of natural concentration of wave direction and storm filtering.
In this work, we present the experimental analysis of the behavior of a particular wave energy converter designed for the breaker zone. The tests we present were performed in the wave flume of the Hydraulics Laboratory of Politecnico di Milano.
The peculiarity of this WEC, called EDS (Energy Double System), is to harness wave energy in the breaker zone, shortly before waves break. This position allows the energy harvesting before the dissipation due to the wave breaking, moreover it reduces the cost of installation and maintenance of the device. An optimal solution could be installing the EDS on existing structures like piers and breakwaters. The use of a nearshore WEC agrees with what discussed in [6], where it is shown how energy dissipation by bottom friction can be small if bottom slope is some high, and so a relevant part of offshore wave energy can reach shallow waters (5-10 m, depending on the wave dimension). Furthermore, in [7] it is shown that the surge force is considerably higher in the nearshore region than offshore.
The possibility of harnessing both the high surge wave force that characterizes the nearshore zone and the still present heave wave force led to the design of a wave energy converter with two different oscillating bodies, a surging paddle and a heaving float, held by the same arm, which is pivoted over the free surface (Fig. 1). The EDS system draws inspiration from the Wavestar machine (Hansen *et al.* [8], www.wavestarenergy.com), and it mainly differs for the presence of the paddle, and in that the arm holding the float is aligned along the wave direction propagation, instead of perpendicular to it.

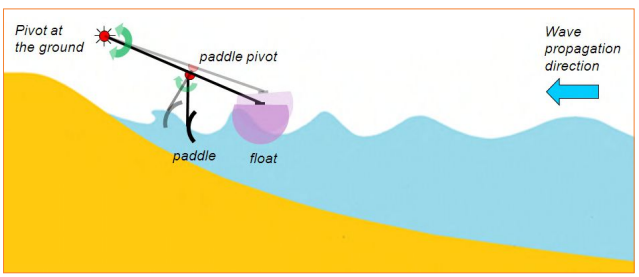

FIGURE 1 Scheme of the EDS wave energy converter

Experimental setup

The EDS lab model was realized at 1:25 scale (see scheme in Fig. 2). The main arm $\overline{AB}$, pivoted over the free surface in point O, supports the float and the paddle on the right side. The A point of fastening between the float and the main arm is rigid. The float PTO, a heaving disc immersed in oil, is connected through a leverage in point B.
The arm $\overline{CE}$, pivoted on the main arm in point C, holds the paddle. The paddle PTO, again a heaving disc immersed in oil, reacts against the paddle arm in D and the main arm in F.
The system has two degrees of freedom, which we indicate as x_1 and x_2, position of heaving disc with respect to their position at rest.
The float is hemispherical at the bottom and cylindrical in its upper part. The radius of the float is 0.2 m, and total height is 0.140 m.
The paddle has cylindrical shape, a chord of 0.12 m and a width of 0.2 m. The principal characteristics of the model are reported in Table 1. The moment of inertia of EDS was calculated considering the second degree of freedom x_2 as blocked.

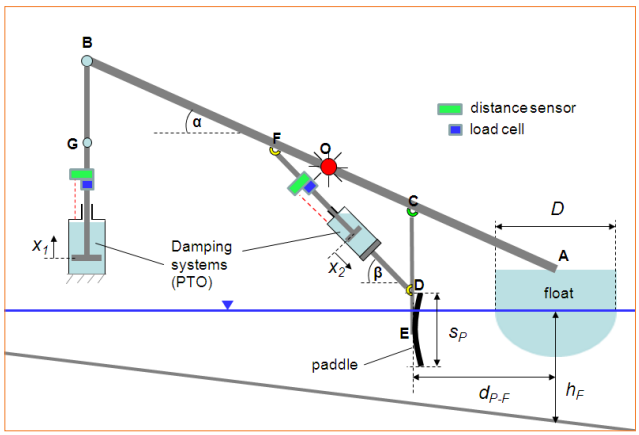

FIGURE 2 Scheme of the EDS lab model

Float arm length	*OA* [m]	0.4
Damper arm length	*OB* [m]	0.45
Diameter of the float	*D* [m]	0.2
Float static draft	d_F [m]	0.055-0.060
Moment of inertia	*I* [kg·m²]	0.30
Main arm inclination	α [°]	24°-26°
Paddle chord	s_P [m]	0.12
Paddle draft	d_P [m]	0.09
Inclination of paddle PTO	β [°]	35-45°

TABLE 1 Some characteristics of the EDS scale model

In Figure 3 the front part of the EDS is reported. The paddle PTO is visible. As mentioned before, the PTOs of paddle and float are heaving discs immersed in oil. In Figure 4 the scheme of the PTO systems of float and paddle are reported. Each PTO was equipped with a load cell and a sensor distance, in order to measure the position of the disc and the force exerted on it. The float damper (Fig. 4a) is a single disc, held by a stem that can slide through bearings fixed to the cylinder top, the cylinder being in turn fixed to the ground. To obtain a different amount of damping, different sizes of the disc have been used. The paddle damper is similar, except for two characteristics. Firstly, the stem supports two discs, a porous one which is fixed on the stem, and one that can slide along the stem for a short distance (Fig. 4b). This solution allows to have different damping levels along the two directions of the stem movement: as the paddle receives the positive force from the wave, the stem is pushed into the cylinder and the two discs quickly approach, closing the holes of the fixed porous disc. The two discs remain attached until the motion is reversed, that is when the paddle gets back to its position. In that phase, the discs are detached, so the holes of the fixed disc are freed. In this way, during the wave push a major damping is generated on the paddle with respect to the return phase. However, it was also possible to generate a similar damping in the two directions of movement by tightening the two discs together. The other difference between float and paddle PTOs is that the latter reacts against the main arm in point F and not against the ground.

The amount of energy dissipated by the disc during an oscillation period T was calculated as:

$$E = \int_T F_D \dot{x}\, dt$$

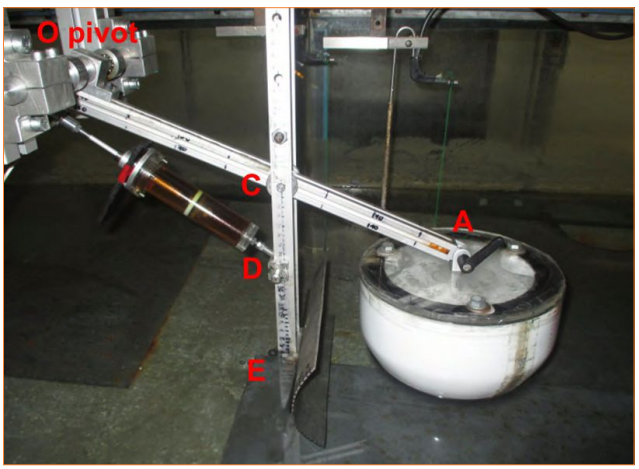

FIGURE 3 Front part of EDS lab model

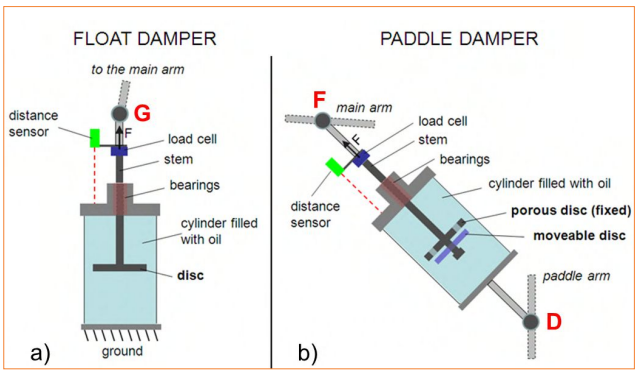

FIGURE 4 PTOs of float (a) and paddle (b)

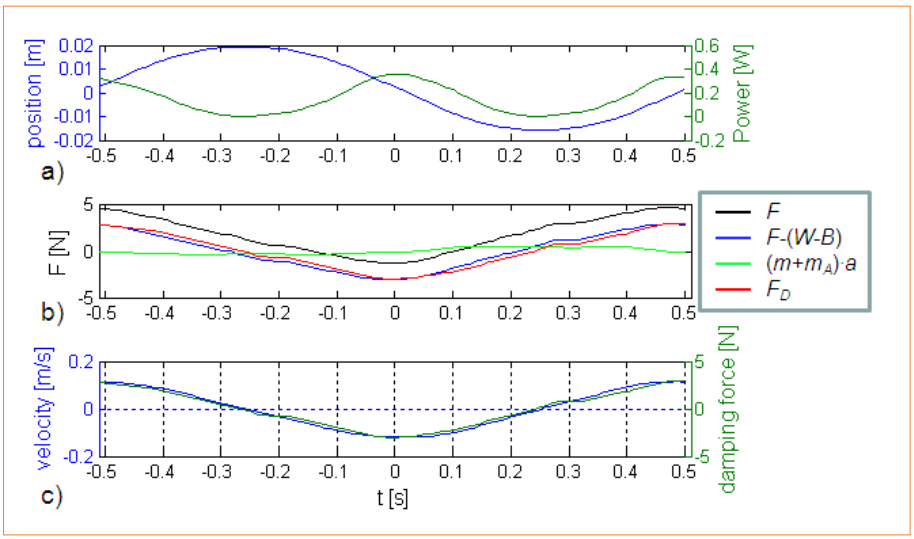

FIGURE 5 Float PTO dynamics during a cycle of oscillation: a) disc position and dissipated power; b) forces on the disc; c) disc velocity and damping force

Where F_D is the damping force of the disc and v is the relative velocity between the disc and the cylinder that contains the oil. The damping force F_D was calculated from the total force F recorded by each load cell, by subtracting the inertial and gravitational contributions:

$$F_D(t) = F(t) - (m + m_A)\ddot{x}(t) - \left[W - B(x(t))\right]$$

Where m is the mass of the objects attached below the load cell, m_A is the disc added mass, W is the weight of the objects attached below the load cell, B is the buoyancy of the immersed objects in oil. As an example, in Figure 5 the dynamic parameters of the float PTO during an oscillation cycle is reported. Fig. 5a reports the relative disc position x and the power dissipated by the disc, Figure 5b reports the total force F measured by the load cell and its contributions, Figure 5c reports disc velocity and damping force F_D.

The average power absorbed by the EDS was calculated as the ratio between the total energy absorbed by the system in one period and the period duration.

$$P_{out} = \frac{E_1 + E_2}{T}$$

Where E_1 is the energy absorbed by the float and E_2 is the energy absorbed by the paddle. In Figure 6 an example of the instantaneous power absorbed in an oscillation cycle of the EDS is reported. The colors represent the different motion phases of float and paddle. The absorbed energy is also reported.

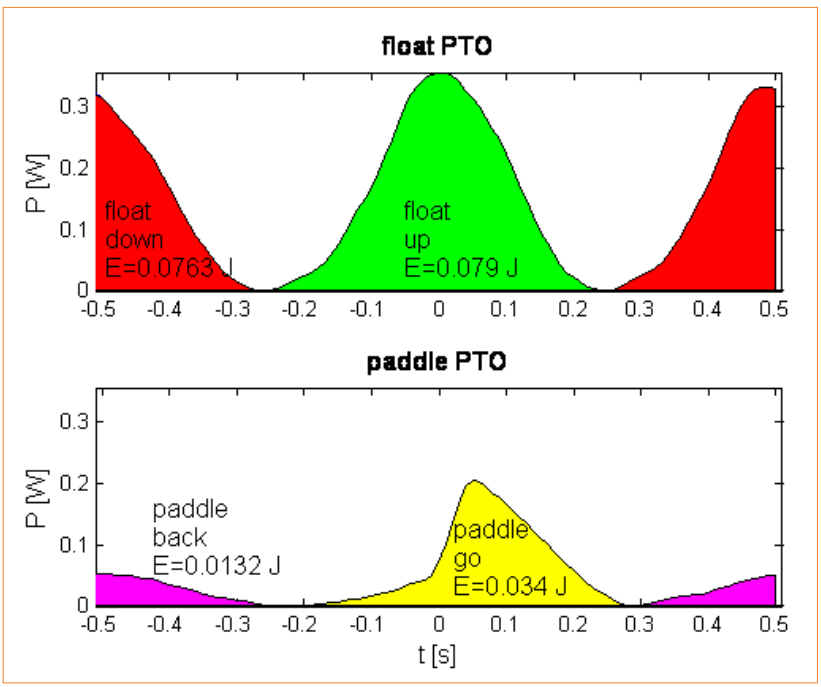

FIGURE 6 Instantaneous power dissipated by float and paddle PTOs

The damping generated by the PTO systems was not linear, and equivalent linear damping was calculated. With the approximation of considering the float motion vertical and the paddle motion horizontal, we calculated an equivalent vertical linear damping in point A for the float, and an equivalent horizontal linear damping in point E for the paddle. Furthermore, two values of equivalent linear damping were calculated for the paddle, one for the go-motion and the other for the back-motion. Expressions are reported below.

$$b_{1eq} = \frac{E_1}{\frac{T}{2}\omega^2 A_{x1}^2}\frac{\overline{OB}}{\overline{OA}}$$

$$b_{2eq-go} = \frac{E_{2-go}}{\frac{T}{4}\omega^2 A_{x2}^2}\frac{\overline{CD}}{\overline{CE}}\cos\beta$$

$$b_{2eq-back} = \frac{E_{2-back}}{\frac{T}{4}\omega^2 A_{x2}^2}\frac{\overline{CD}}{\overline{CE}}\cos\beta$$

Where A_{x1} and A_{x2} are the oscillation amplitudes of the heaving discs and

$$\omega = \frac{2\pi}{T}$$

The EDS was tested in a 30 m long and 1 m wide wave flume, equipped with a piston wave maker. The water depth inside the flume was 0.4 m. At the end of the flume a constant slope beach was installed. The slope of the beach was 1:8.25.

Three monochromatic waves were used to test the model; their properties were measured by two capacitive wave gauges, without the EDS model in the channel. Waves were measured on the beach and in the middle part of the channel with water depth h=0.4 m. Wave measurements in the middle part of the channel were analyzed by separating the incident and reflected waves according to the method of Goda and Suzuki [9]. We found a nearly constant reflection coefficient for the three waves considered. In Table 2 wave properties in water height h = 0.4 m are reported.

Wave power per unit width crest was calculated from linear theory, considering $H = 2a_I$ the reference wave height:

$$P_I = \frac{1}{8}\rho g H^2 c_g$$

Group celerity c_g was calculated as:

$$c_g = \frac{c}{2}\left(1 + \frac{2kh}{\sinh(2kh)}\right)$$

With $c = L/T$ being wave celerity, k the wave number and h the water depth.

The efficiency of the system CWR (capture width ratio) was calculated as:

$$CWR = \frac{P_{out}}{P_I D}$$

The efficiency is referred to the incident wave power P_I and not to the actual wave power, which may be minor and change along the beach. It follows that the EDS efficiency is calculated on the basis of a somehow "offshore wave energy" (more correctly, wave energy in a non-dissipative zone, since water depth in the channel is not deeper).

The wave height measured on the beach is reported in Figure 7 for the three waves. For wave B and wave C, a steep rise of height can be seen for h/D = 0.4, that is a sign of incipient breaking. Wave height relative maxima can be seen at h/D = 0.8, 1.3, 1.8 for wave A, h/D = 1.5 for wave B, at h/D = 1.5 and 1.9 for wave C.

The experiments were conducted in stationary condition, that means that only the part of the signals where waves and oscillations of the EDS were stabilized were considered for the subsequent analysis. All the acquired signals, *i.e.* positions of the

Wave id	a_I [mm]	a_R [mm]	T [s]	L [m]	P_I [W/m]	r [%]
Wave A	24.4	1.6	1.02	1.52	2.70	6.4
Wave B	25.4	1.6	1.36	2.29	3.97	6.2
Wave C	31.7	2.1	1.20	1.92	5.45	6.8

TABLE 2 Wave properties in water height h=0.4 m

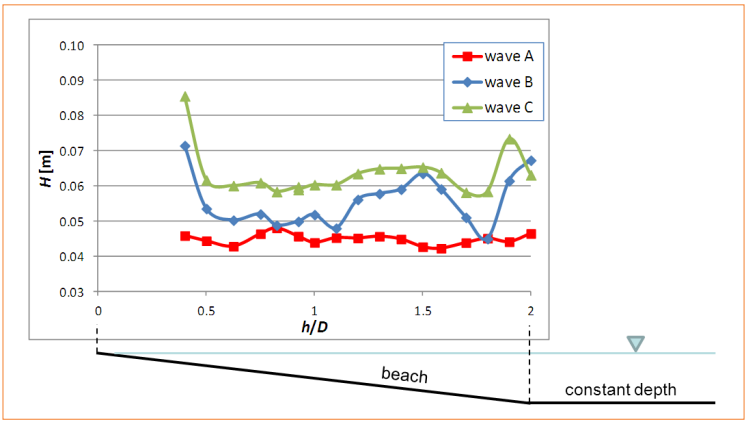

FIGURE 7 Wave height along the beach

heaving discs, force exerted on heaving discs, and water elevation were phase averaged on the basis of the wave period.

Results

Many geometrical and mechanical parameters characterize the EDS. In this work, we considered the influence of some of them, keeping the others constant. The parameters that varied through the tests were: distance between paddle and float, float external damping and water depth at the float. The fixed parameters were the moment of inertia of the structure, paddle damping in the two directions, paddle immersion at rest. The moment of inertia of the EDS was set as small as possible, given the physical limitation of the model scale. Paddle damping was set to a reasonable value. The paddle immersion at rest d_P was 0.09 m. This value was found to be the optimal one in the previous work of Negri *et al.* [10]. Paddle damping was set to about 15 Nsm^{-1} in the shoreward motion and about 5 Nsm^{-1} in the seaward motion.

In Figure 8 efficiency of the EDS system is reported as a function of water depth at the float, float external damping (circle dimension), distance between paddle and float (line color). Wave height is also reported as a function of water depth. The efficiency of the EDS for wave A is quite influenced by the parameters that characterize the EDS, whereas for wave B and wave C the efficiency is less sensitive to these changes. This is due to the fact that wave A has the shortest period, and it should be the closest to natural periods of the EDS.

For all the three waves, it can be seen that CWR fairly follows the trend of H.

The best value of float-paddle distance was the smallest tested, that is $d_{P\text{-}F}/D$ = 0.8, for all the three waves. The

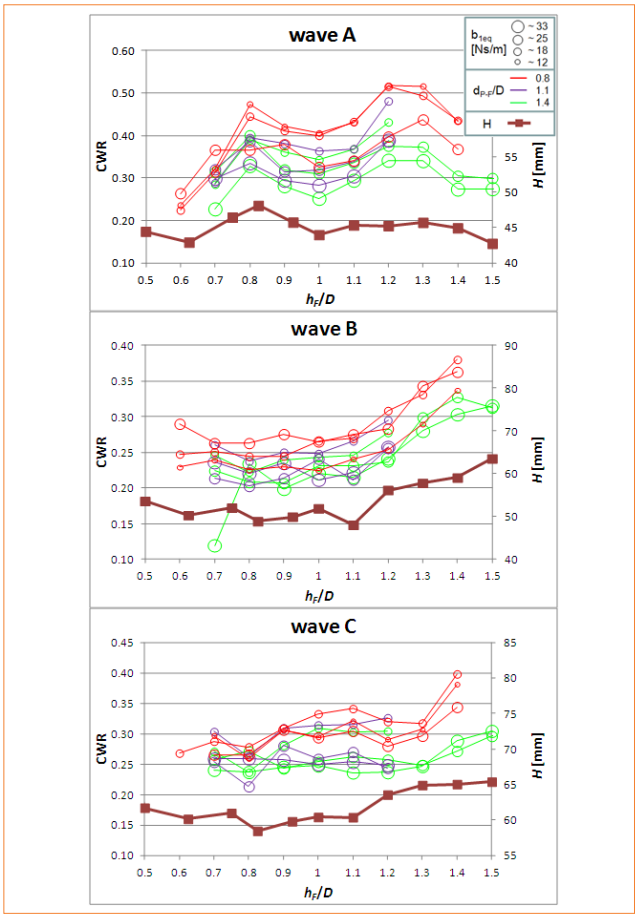

FIGURE 8 Efficiency of the EDS depending on float external damping, distance between paddle and float, and water depth at the float

worst configuration was $d_{P\text{-}F}/D$ = 1.1, even if there was not much difference with $d_{P\text{-}F}/D$ = 1.4.

For wave A, it can be seen that the effect of float damping on the efficiency is almost independent from the other two parameters: indeed, best damping is almost always the small value tested, regardless of paddle-float distance and water depth; only for h_F/D < 0.8, higher efficiency is obtained with a higher float external damping. For wave A, the highest efficiencies were obtained with the smallest float damping we tested $b_{1,eq}$ = 12 Nsm^{-1}; it was not possible to reach the optimal float damping, due to the physical limitation on the amplitude of motion of the heaving disc.

For wave B, optimal float damping changes with paddle-float distance: for $d_{P\text{-}F}/D$ = 0.8, optimal damping is 25 Nsm^{-1}, whereas for the other two distances the optimal damping is less, $b_{1,eq}$ = 18 Nsm^{-1}.

For wave C the optimal damping is almost always 18 Nsm^{-1}, regardless of the paddle-float distance.

It is interesting to see how the absorbed EDS power is subdivided between the float and the paddle. In Figure 9 the partial efficiency of the float, further divided into upward and downward motion, and the paddle, further divided into shoreward and seaward motion (go- and back-motion), are reported. For the three waves, configuration with $d_{P\text{-}F}/D$=0.8 and float external damping b_{1eq} = 12, 25, 18 Nsm^{-1}, respectively, are reported. They are the best configurations found for each wave, except from some isolated points discussed before.

Fig. 9 shows how float efficiency increases and paddle efficiency decreases as water depth increases.

For low depth (h_F/D = 0.6-0.7), paddle efficiency is about half the total efficiency, while it becomes a third or minus as depth increases. The reduction of paddle efficiency in deep water is due to the reduction of surge force and to the greater linearity of the waves: a light paddle, which is not resonant with the waves, works better with shallow-water waves, because they have shoreward transport mass. Float efficiency individually taken follows the trend of total efficiency. Float efficiency is quite evenly distributed between the upward and downward motion, however some differences can be noted;

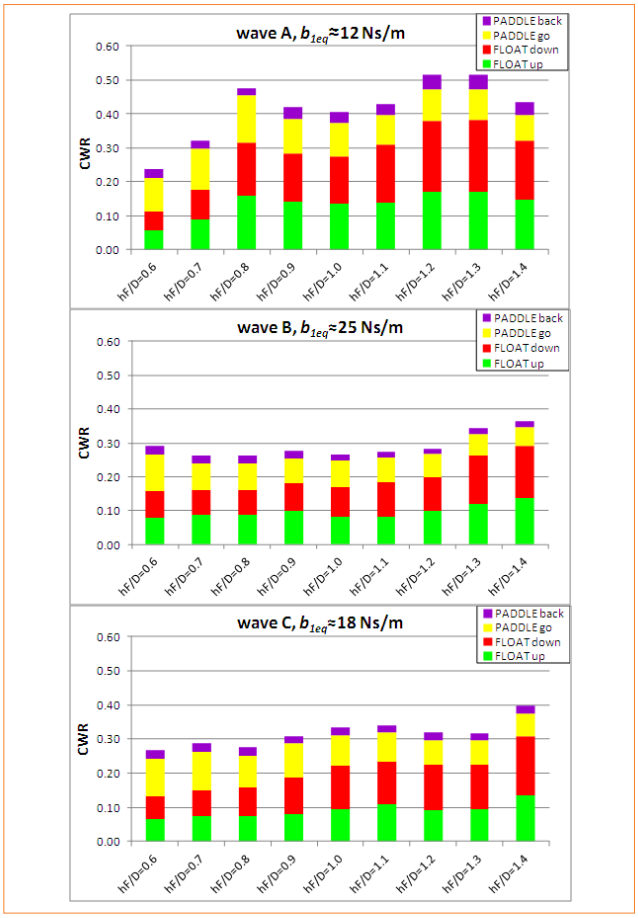

FIGURE 9 Subdivision of efficiency between float and paddle

they are generated by the non-linearity of both the external damping and the shallow water waves. The energy absorbed by the paddle in the go-phase is much higher than in the back-phase, because of the aforementioned mass transport of the waves.

Conclusions

The potential of the EDS, a multi-body WEC composed by a heaving float and a surging paddle, has been analyzed in this work. The EDS scale model has been tested in a wave flume, at

various depths along a constant slope beach and in various configurations, varying some of the main parameters that characterize the system. The system has been tested with three monochromatic waves. The efficiency of the system was calculated on the basis of the wave power off the beach, making the results comparable with the ones about exploiting offshore wave energy. We found that the system efficiency is dependent on the distance from the shoreline. This is due to two reasons, which are linked to one another: water depth and wave height, that punctually is established along the beach. Wave height variation is due to the wave reflection over the beach. Efficiency peaks of the EDS occur where wave height peaks occur, more markedly for the smallest wave tested.

Generally, the efficiency of the float increases as water depth increases, while paddle efficiency decreases. The highest EDS efficiencies were found with the paddle close to the float, $d_{P\text{-}F}/D = 0.8$.

We found that optimal external damping of the float is generally independent from water depth and float-paddle distance.

The optimal damping of the float is almost independent from the paddle-float distance and the water depth.

The experimental efficiency measured is about 30%, increasing on average from shallow to deep waters. For the smallest wave the efficiency reached values up to 50% in a water depth $h_F/D = 1.1$.

Although the main EDS parameters were analyzed in this work, the characteristics of the paddle have yet to be optimized, especially as regards damping and shape. We are therefore confident that EDS efficiency will further increase.

Stefano Malavasi, Marco Negri
Politecnico di Milano, Department of Civil and Environmental Engineering (DICA), Italy

references

[1] J. Falnes, A review of wave-energy extraction, in *Marine Structures*, 20, pp. 185-201, 2007.

[2] A.F. de O. Falcao, Wave energy utilization: A review of the technologies, in *Renewable and Sustainable Energy Reviews*, 14, pp. 899-918, 2010.

[3] I. López, J. Andreua, S. Ceballos, I. Martínez de Alegría, I. Kortabarria, A review of wave energy technologies and the necessary power-equipment, in *Renewable and Sustainable Energy Reviews*, 27, pp. 413-434, 2013.

[4] D. Vicinanza, P. Contestabile, V. Ferrante, Wave energy potential in the north-west of Sardinia (Italy), in *Renewable Energy*, 50, pp. 506-521, 2013.

[5] S. Bozzi, R. Archetti, G. Passoni, Wave electricity production in Italian offshore: A preliminary investigation, in *Renewable Energy*, 62, pp. 401-416, 2014.

[6] M. Folley, T.J.T. Whittaker, Analysis of the nearshore wave energy resource, in *Renewable Energy*, 34, pp. 1709-1715, 2009.

[7] M. Folley, T.J.T Whittaker, A. Henry, The effect of water depth on the performance of a small surging wave energy converter, in *Ocean Engineering*, 34, pp. 1265-1274, 2007.

[8] R. H. Hansen, M.M. Kramer, E. Vidal, Discrete displacement hydraulic power take-off system for the Wavestar Wave Energy Converter, in *Energies*, 6, pp. 4001-4044, 2013.

[9] Y. Goda, Y. Suzuki, Estimation of incident and reflected waves in random wave experiments, in *Marine Hydrodynamics Division Port and Harbour Research Institute*, Ministry of Transport Nagase, Yokosuka, Japan, 1976.

[10] M. Negri, F. Clerici, S. Malavasi, A breaker-zone wave energy converter, International Conference on Renewable Energies and Power Quality, ICREPQ'13, Bilbao, Spain, 2013.

Designing a point-absorber wave energy converter for the Mediterranean Sea

This work aims to assess the potential for wave energy production in the Italian seas by the deployment of arrays of heaving point absorbers, specifically optimized for mild climates. We model a single-body WEC, consisting of a cylindrical heaving buoy, attached to a linear electric generator placed on the seabed. The model includes both hydrodynamic and electromechanical forces. The results show that the best buoy-generator configuration at the selected sites (Alghero and Mazara del Vallo) is given by a 6 to 10 kW device and with a buoy with diameter between 4 and 5 m. This device can be brought to resonance, increasing the performances, by adding a submerged sphere. These results are encouraging and enlarge the perspective on wave energy production in the Italian seas.

DOI: 10.12910/EAI2015-052

R. Archetti, A. Moreno Miquel, A. Antonini, G. Passoni, S. Bozzi, G. Gruosso, F. Scarpa, F. Bizzozero, M. Giassi

Introduction

Among renewable energy resources, wave energy represents a large and viable source of power supply, which deserves serious attention [1]. Although it represents only a small portion of wind energy, which in turn is only a small fraction of solar energy, the energy of surface ocean waves is more predictable, persistent and spatially concentrated [2]. The enormous wave power potential, together with the technical advantages of wave energy conversion has stimulated the interest of governments and energy companies since the oil crisis of 1973. Nowadays, a number of full-scale wave energy devices have been deployed in real sea conditions and several others are at the end of their development phase [3]. Most of them have been installed off the western coasts of continents in moderate to high latitudes. At present only few attempts have been made to exploit wave energy in the Mediterranean Sea.

The aim of this paper is to present recent research on point-absorber wave energy converters (WEC) specifically designed for mild climates, such as the one of the Italian seas. The paper, which resumes the work of two research groups, is organized as follows: first, the wave resource along the Italian coasts is characterized. Then, we present a preliminary work on the downscaling of existing devices – designed for Atlantic conditions – to make them suitable for the Mediterranean wave climate. In the following section a point-absorber wave energy converter, directly driven by a linear generator, is modelled and optimized for the Mediterranean Sea conditions. Finally, the effect of WEC interactions on energy absorption is investigated and advice is provided for the design of small wave energy farms in the Italian offshore areas.

Contact person: Renata Archetti
renata.archetti@unibo.it

	Site	Depth (m)	Distance from shore (km)	Wave record length (y)	Missing data (%)	Average annual wave power (kW/m)	CV of average monthly wave power (%)	I	II	III	IV
1	Alghero	95	5.2	18.8	9%	9.1	48%	38%	25%	11%	26%
2	Mazara del Vallo	75	13	18.8	15%	4.7	59%	42%	27%	8%	23%
3	Ponza	100	1.44	17.7	10%	3.7	50%	37%	23%	11%	28%
4	La Spezia	92	15.6	18.8	13%	3.5	36%	33%	23%	14%	30%
5	Crotone	100	1.22	17.5	7%	2.9	56%	47%	23%	4%	26%
6	Monopoli	65	6.02	17.7	9%	2.1	55%	43%	24%	11%	22%
7	Catania	100	5.1	18.8	9%	1.9	63%	43%	28%	6%	24%
8	Ortona	60	10	17.7	12%	1.9	66%	46%	22%	9%	23%

Note: CV, coefficient of variation.

TABLE 1 Main features and statistics of the study sites. Columns I, II, III and IV represent the percentage of the annual wave energy in the months of December-February, March-May, June-August and September-November, respectively
Source: [4]

Wave resource characterization in the Italian seas

Wave energy exploitation starts with the characterization of the wave energy resource. Resource assessments allow to select the most promising locations for wave farms, design wave energy converters and estimate the production of energy and its possible costs. For these purposes it is crucial to know the amount of resource available, its monthly distribution and its composition in terms of sea states. In the present work, the wave energy resource of the most promising locations off the Italian coasts has been characterized. Table 1 reports the main features and wave energy statistics of these locations, sorted by decreasing wave power potential. More details are provided in Bozzi *et al.* [4].

The most energetic sites (1-4 in Tab. 1) are located in the Tyrrhenian Sea. Among them, we selected Alghero and Mazara del Vallo as possible deployment sites for wave energy farms, because they are the most productive of the whole Mediterranean Sea and the most favourable in terms of inter-annual variability of the energy resource [5]. At these locations, the prevalent sea states are characterized by relatively small and short waves, with peak periods around 6 s and significant wave height below 1 m.

Preliminary work: Downscaling of existing wave energy converters

In order to study the feasibility of wave energy exploitation off the Italian coasts, we start by estimating the energy production of three of the most promising and documented wave energy converters (AquaBuOY, Pelamis and Wave Dragon) at Alghero and Mazara del Vallo [6, 7]. As the selected devices were designed to maximize their electric production for Atlantic wave conditions, the estimated energy production and the capacity factors at the two Italian sites are very low (the capacity factor is around 8% at Alghero and 4% at Mazara del Vallo). This result indicates that, as expected, the WECs are oversized with respect to the Italian wave climate and that a more efficient energy conversion could be possibly obtained by downscaling the devices. Figure 1 shows the capacity factors as a function of scale for the hypothetical wave farms of AquaBuOY, Pelamis and Wave Dragon at Alghero and Mazara del Vallo. The geometric scales of the devices maximizing the capacity factors at the study sites range between 0.3 and 0.4 and the corresponding capacity factors between 16% and 21%. The main characteristics and performance indices of these smaller rated devices are summarized in Table 2. The results of this analysis suggest that deploying classic wave energy converters in the Italian seas would not be

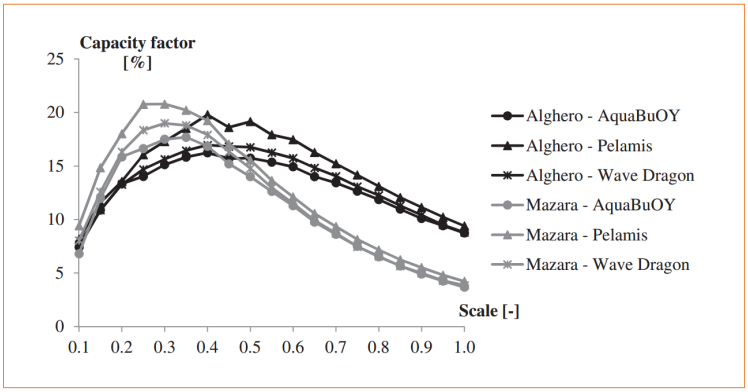

FIGURE 1 Capacity factors at Alghero and Mazara for different device dimensions
Source: [7]

cost-effective, but if the devices could accommodate a proper downscaling their performance in energy conversion would become economically attractive also for some Italian locations.

Modelling and optimization of a point absorber for the Mediterranean Sea

The results of the previous study claim for a wave energy converter specifically tailored for the Italian wave climate. Due to its reduced size and heterogeneous geography, the Mediterranean wave climate is quite singular and unique in the world. With respect to the ocean wave climate, characterized by long-period swells, the Mediterranean Sea presents wind seas, where waves of different heights, periods and directions merge and produce random conditions. For this wave climate, the most suitable technology is probably a WEC of the point-absorber type, which can harness energy from all the incoming directions and can be located in deep waters, where energy availability is higher. Between the existing heaving point-absorber devices, we selected the Sea-based device [8] because of its simple power take-off mechanism and for the similarity between the Italian and Swedish wave climates, for which it was developed. This device consists in a floating buoy, rope-connected to the piston of an electrical linear generator, placed on the seabed. The linear generator allows coupling directly the rotor to the vertical motion of the sea surface, eliminating the need of complex power take-off mechanism and gear-boxes.

Mathematical modeling

The behavior of the wave energy converter is simulated in regular waves of different heights and periods by a coupled hydrodynamic-electromagnetic model. The simulations are run in the time domain, due to the non-linearity of the

	Alghero AquaBuOY	Pelamis	Wave Dragon	Mazara AquaBuOY	Pelamis	Wave Dragon
Scale	0.4	0.4	0.4	0.35	0.3	0.3
Rated Power [kW]	10	30	283	6	11	104
Mean power output [kW]	1.6	6.0	48.1	1.1	2.3	19.9
Annual energy output [MWh]	14	53	421	10	20	175
Full load hours [h]	1423	1735	1486	1551	1837	1686
Capacity factor [%]	16	20	17	18	21	19
Coefficient of variation of monthly time series [%]	21	2	22	28	25	23
Correlation coefficient between energy input and output [-]	0.81	0.87	0.86	0.87	0.86	0.80

TABLE 1 Characteristics and performance of the downscaled devices at Alghero and Mazara del Vallo
Source: [7]

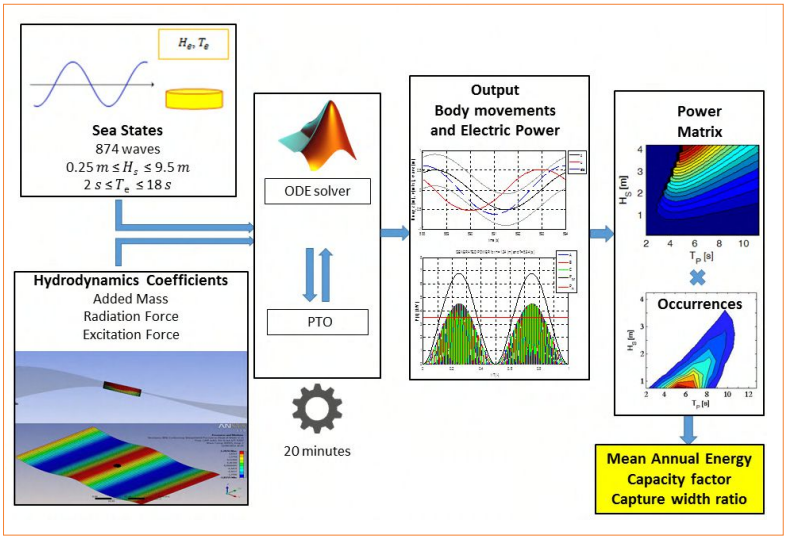

FIGURE 2 Sketch of the modelling procedure

PTO system. The power output of the device is calculated for each sea state to derive the so-called power matrix. This information is coupled with wave climate data to evaluate energy production and performance at each study site. The whole modelling procedure is summarized in Figure 2.

The floating body dynamics are determined by solving the following equation of motion, which combines the hydrodynamic forces $F_H(t)$ and the resistance forces $F_R(t)$ due to the PTO system:

$$mz(t) = F_H(t) + F_R(t) \qquad (1)$$

where m is the total mass of the system and $\ddot{z}(t)$ represents its vertical acceleration. The hydrodynamic forces on the heaving buoy are calculated by:

$$F_H(t) = -m_a z(t) - R_D z(t) - \frac{1}{2}\rho A C_D \left(z(t) - \eta(t)\right)\left|\left(z(t) - \eta(t)\right)\right| - \rho g A z(t) + F_e \frac{H}{2}\cos(\omega t + \alpha) \qquad (2)$$

where $z(t)$ is the vertical coordinate at time t, measuring deviation from the static equilibrium. The five terms on the right side of the equation represent the different forces acting on the buoy: (1) added inertial force, accounting for the fluid volume moving with the buoy, where m_a is the added mass; (2) radiation damping force, due to the waves created by buoy oscillations, where R_D is the radiation damping coefficient; (3) viscous damping force accounting for relative turbulent flow, where ρ is sea water density, A is the water-plane area, C_D is the viscous damping coefficient and $\dot{\eta}(t)$ is the vertical velocity of the free water surface; (4) hydrostatic restoring force, where g is gravity; and (5) vertical component of the excitation force, due to the incident waves on the assumedly fixed body, where F_e is force amplitude, H and ω are wave height and frequency, respectively, and ω is the phase angle between the wave and the wave-induced heaving force. The frequency-dependent coefficients of excitation and radiation force are estimated prior to model simulations by a boundary element code and given as inputs to the ODE solver (Fig. 2). More details on the numerical model can be found in Bozzi *et al.* [4]. The resistance force, $F_R(t)$, due to the PTO system, is modeled as:

$$F_R(t) = -F_M(t) - F_K(t) \qquad (3)$$

where $F_M(t)$ is the electromagnetic force, due to the electric linear generator, and $F_K(t)$ is the elastic force of the spring system attached to the translator, which is calculated by:

$$F_K(t) = K z(t) \qquad (4)$$

where K is the elastic constant of the spring. The electromagnetic force is obtained through Faraday's law and Maxwell equations that govern the magnetic induction in the stator-translator structure. The simplified analytical model presented by Thorburn and Leijon [9] is used to calculate the voltage generated in the stator with input parameters derived by finite element simulations of the electromagnetic

field [10, 11]. Finally the electricity production is estimated by multiplying the expected power output of each sea state (defined by H, T_e pairs) by its occurrence (in hours) and then by summing over all sea states (Fig. 2).

Optimization of buoy and generator parameters

Several buoys of different shapes, radii, heights and drafts are simulated to investigate the effect of floating body geometry on power absorption and to find the optimal buoy for the study locations. Conical, cylindrical and hemispherical buoy shapes are evaluated, both with a cylindrical upper part [12]. The sensitivity analysis shows that (*i*) for a given diameter of the upper part, the cylindrical shape is the most efficient in wave power absorption; (*ii*) the height of the floating body influences the hydrodynamics response only if it is associated with a change in draft; (*iii*) the effect of buoy draft is related to buoy mass: as the draft decreases the hydrodynamic coefficients increase; and (*iv*) the buoy diameter plays a key role in the process of wave energy absorption since it is directly proportional to the wave front width captured by the device. As a result, by increasing the diameter, the loads on the structure increase. This effect is much more significant for long periods, as the body can better follow the wave movement. Moreover, the added mass is higher for larger buoy diameters because the volume of the fluid moving with the buoy increases with its size. The results of the sensitivity analysis lead to identifying the cylindrical buoy with 5 m diameter and 0.8 m draft as the one with the highest capture width ratio, for a linear generator with nominal power of 10 kW (Fig. 3).

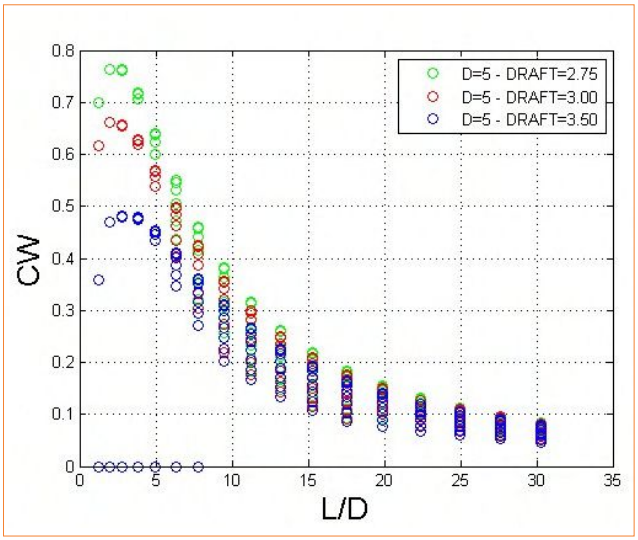

FIGURE 3 Capture width vs. L/D (L wave Length, D cylinder diameter) for the most efficient cylindrical buoy
Source: [12]

In order to better match the wave climate variability of the chosen locations, five linear generators of different nominal powers are designed (4, 6, 8, 10 and 12 kW, hereafter LG4, LG6, LG8, LG10 and LG12). Each electrical device is simulated with cylindrical buoys of different diameters to find the optimal buoy-generator configuration at each study site, using the maximum capacity factor criterion. Figure 4 shows that the capacity factor data plotted against the buoy diameter arranges itself in a concave curve, suggesting that for each generator there is a buoy diameter, which maximizes the energy production. If the buoy is too small, the excitation force is too low and the power absorption ability of the generator is limited by the available power. On the other hand, too large buoys have too much inertia to follow the sea motion and lower capture efficiency, due to larger diffraction effects. At the two study sites the maximum capacity factor (around 17%) is achieved by coupling a linear generator of 6 kW with a buoy of 5 m diameter. Although at Mazara del Vallo, the available wave power is almost half than Alghero's, the power output is almost the same, thanks to the lower intermittency in the wave climate. This fact makes it preferable than Alghero's, being a site with very energetic, albeit very rare, sea storms.

Resonant body

A resonant point absorber system has significantly higher power absorption, due to its enhanced amplitude and speed. However, for small point absorber devices, such as the one studied here, the resonant frequency tends to be much higher than the typical sea state frequency, so the resonant state is practically impossible to be achieved. One way to

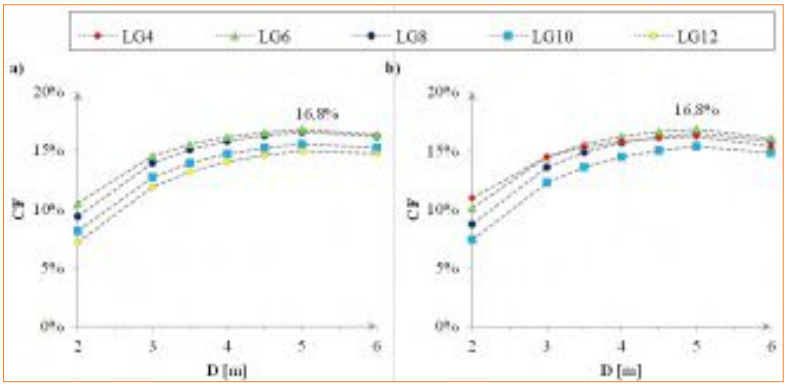

FIGURE 4 Capacity Factor (CF) as a function of buoy diameter (D) for different linear generators: (a) Alghero, (b) Mazara del Vallo

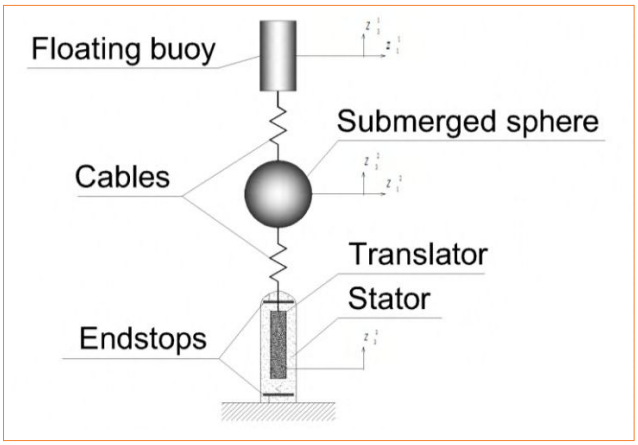

FIGURE 5 Sketch of the modelled device

increase the natural period of oscillation of a point absorber is by connecting a deeply submerged object with neutral buoyancy to the floating buoy [13, 14]. The additional inertia, due to both the submerged body mass and the added mass (Fig. 5), allows the decreasing of the natural frequency of the device, which is given by:

$$\omega = \sqrt{\frac{\rho g A + K}{m + m_a}} \qquad (5)$$

where m is the total mass of the WEC and m_a is the total added mass at the frequency of the incident wave. Depending on the submerged body mass, the system can be tuned to resonate with a different incident wave frequency. In this analysis, it is tuned to be in resonance with waves of peak periods of 5.5 s, which match quite well the wave climates of the study sites.

Figure 6 shows the hydrodynamic parameters of the 5 m-diameter buoy calculated by placing the submerged body at different depths, with respect to the ones of the single body system. It can be noticed that the distance

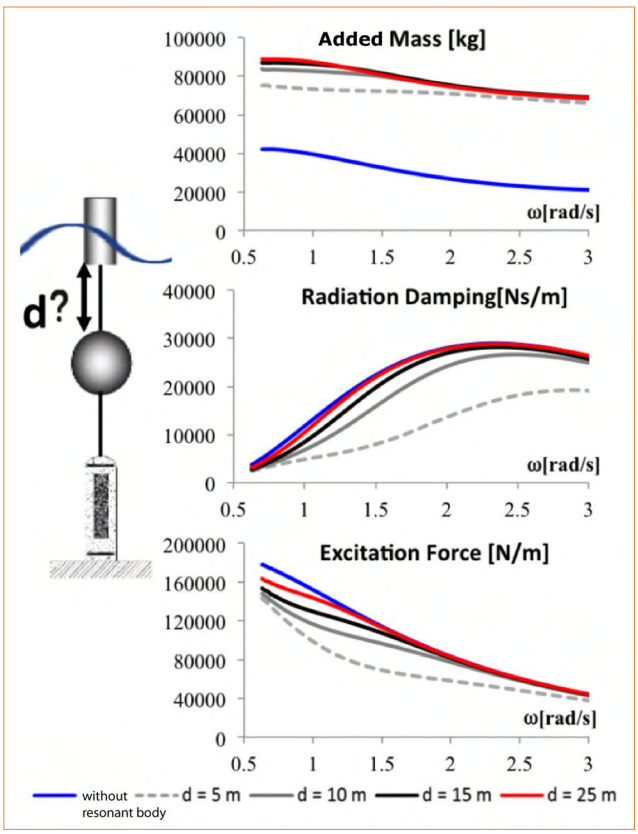

FIGURE 6 Hydrodynamic parameters of the buoy computed with the submerged body at different depths (d = 5, d = 10, d = 15 and d = 25) compared to the ones of the single-body device

between the floating and submerged body strongly affects the hydrodynamics of the buoy. In particular, if the sphere is placed too close to the free surface, it negatively affects the motion of the surface body, because it drives down excitation and radiation forces. On the other hand, when the submerged body is well below the motion of the waves, the radiation damping and excitation force coefficients of the single and two-body systems are practically coincident. In this case, the submerged body only contributes to add supplementary inertia to the system without destructively interfering with the floating body. As a result of this analysis the hydrodynamic parameters of the two body systems are calculated by placing the submerged body at a depth of 25 m (Fig. 6).

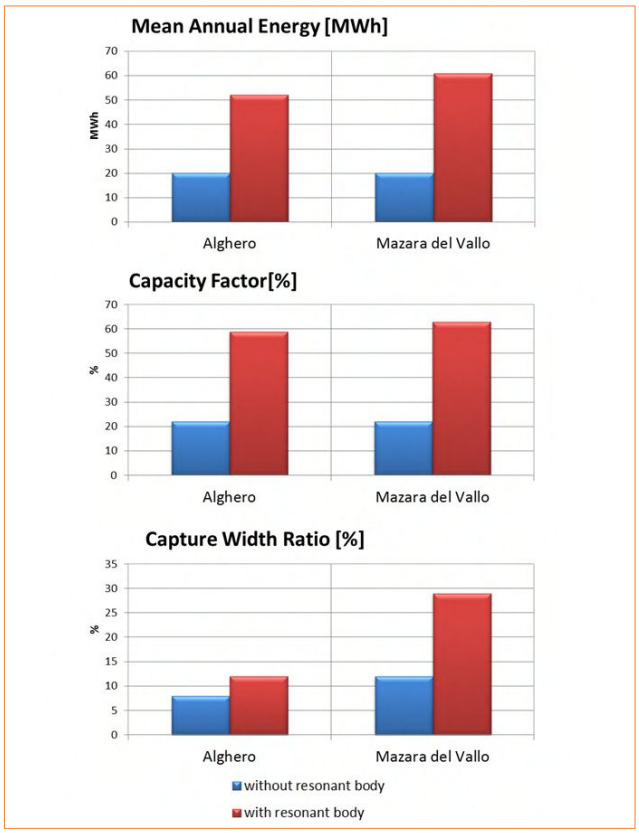

FIGURE 7 Mean annual energy, capacity factor and capture width ratio at Alghero and Mazara del Vallo without resonant body (Blue) and with resonant body (Red)

The simulation results show that the performance of the device substantially increases when the floating body is connected to a submerged sphere, thanks to the resonant behavior of the WEC. The capacity factor of the dual body device is higher than 40% at both locations and the capture width ratio doubles with respect to the single body system (Fig. 7).

Assessment of the surge effect

In this section, we investigate the effect of including more degrees of freedom (DoF) in the device model. In particular, the effect of the independence of the bodies and the contribution of the surge mode to wave energy absorption are assessed by implementing two more detailed modelling schemes. In the first scheme the two bodies are allowed to move independently but only along the vertical axis (3 DoF), while in the second one they can move independently both in heave and surge (5 DoF). The comparison with the results of the 1 DoF model shows that the energy production estimated by the simplified 1 DoF scheme is higher than the one predicted by the 3 DoF model. This is due to the fact that the 3 DoF model is less simplified and takes into account losses of energy which are neglected in the 1 DoF scheme [15]. On the contrary, passing from 3 DoF to 5 DoF does not imply significant changes in the energy production of the two sites. Regarding device efficiency, the capture width ratio decreases with the increase of the degrees of freedom: the reduction is about 20% from 1 DoF to 3 DoF and about 35% from 1 DoF to 5 DoF (Fig. 8). However, the value of wave height and energy period which maximizes the capture width is the same for the three models.

These results indicate that: (1) the modelling of the connections between the three bodies of the device (1 DoF versus 3 DoF) plays a considerable role in the prediction of energy production; (2) no significant changes in power output are induced by adding the surge motion of the floater and of the submerged body; (3) the device efficiency is more sensitive to the modelling approach and accuracy than power output; and (4) surge motion can be significant for the estimation of capture width ratio.

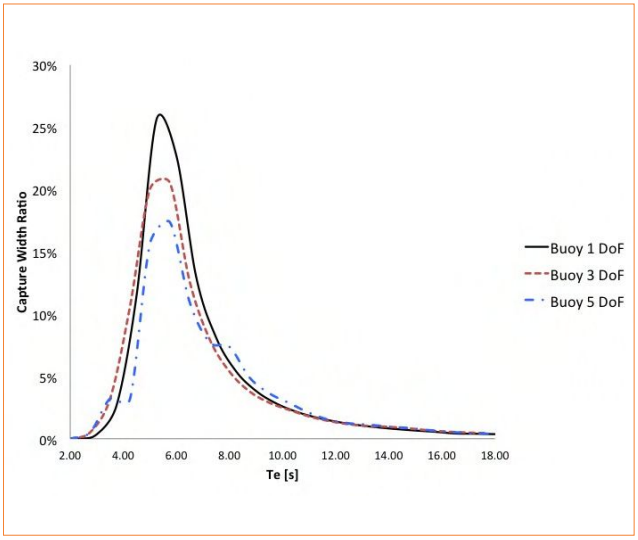

FIGURE 8 Capture Width Ratio of the modeled devices with 1, 3 and 5 DoFs vs. wave energy period

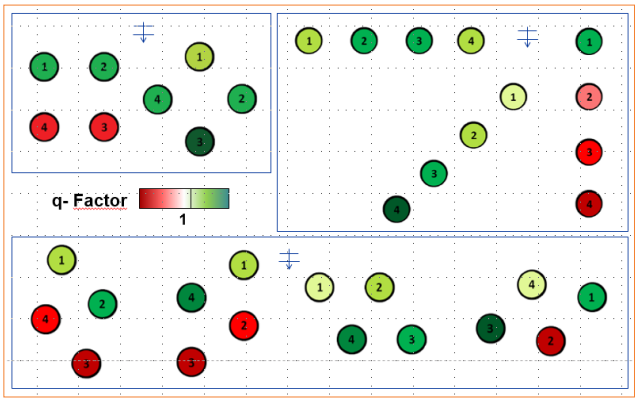

FIGURE 9 Interference factor of the park units for different array layouts, under unidirectional sea state

Array design

Point absorber WECs are designed to be deployed in large arrays, which allow increasing the power output and reducing the total cost. Within wave farms, each unit interacts with the others by absorbing, radiating and diffracting the incoming waves. The spatial distribution of the units plays a key role in their mutual interactions, which can be constructive, such as wave focusing or destructive, leading to the wave field attenuation. It is important to predict hydrodynamic interactions among wave energy converters in order to maximize the efficiency of the park.

In this section we present our recent research on this topic [16], aimed at providing advice for the design of small wave energy farms in the Italian offshore. A key strength of the work is the coupling between the hydrodynamic and electromagnetic model, which allows taking into account the effect of array interactions on the PTO system, instead of simply assuming a constant damping, as in many other works [17]. To evaluate the effect of WEC interactions on energy absorption and to identify the most important parameters affecting array production, we simulated small arrays of two and four devices, considering different layouts (linear, square-based and triangle-based), WEC separation distances (5, 10, 20 and 30 diameters) and incident wave directions (every 45°).

The results shows that: (*i*) assuming a unidirectional sea state and varying the distance between WECs, the energy production of the array varies up to 5%; (*ii*) the effect of the incident wave direction seems to be more important than the WEC separation distance, particularly for the linear and square-based layout; (*iii*) depending on the wave attack angle, the absorbed energy varies up to 14%, 13% and 5% for the linear, square-based and triangle-based layout, respectively; (*iv*) when the wave climate has a dominant wave direction, the best array configuration should be parallel to the wave front for the linear layout, at 45° with respect to wave direction for the square-based layout and with the line connecting the two leeward devices parallel to the wave front, for the triangle-based layout (Fig. 9).

At both the study sites, the linear layout is found to be the most favorable (Fig. 10). However, given the small differences with the other layouts in terms of energy production, we suggest that the design of small wave energy parks focuses also on other issues, such as the occupied sea area and the quality of the electric signal.

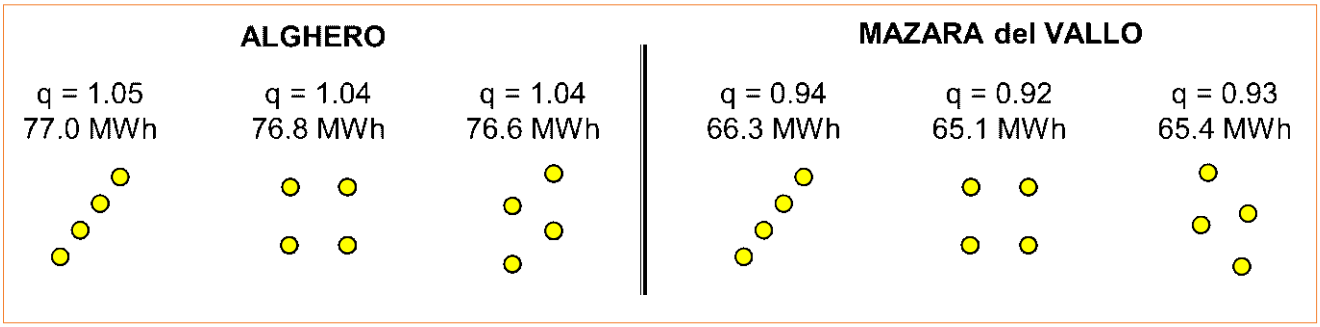

FIGURE 10 Optimal array configurations at the study sites

Discussion and conclusions

This paper presents a review of the recent research activities of the authors on the feasibility of wave energy conversion in the Italian seas. The work starts with the estimation of the energy production of two of the most promising wave energy converters, at two of the most energetic Italian sites: Alghero and Mazara del Vallo. The results of this study show that the considered WECs are oversized with respect to the local wave climate and suggest that they are resized according to the wave climate of the Mediterranean Sea. In this way, a more efficient energy conversion is obtained, and promising results are found in terms of energy production and degree of utilization of the available resource.

Following these conclusions, we investigated the feasibility of installing small-rated devices specifically designed for mild climates, such as the Seabased device. This simple point-absorber WEC consists in a floating body, capturing energy from incident waves, and a linear generator placed on the sea bottom and connected to the buoy via a rope. The device was simulated in the time domain by a hydrodynamic-electromagnetic model, coupled with a boundary element code for the estimation of the hydrodynamic parameters. To account for the different wave climates of the Italian coasts, five linear generators of different nominal powers were designed. Each of them was coupled with seven different buoys, which were designed after a sensitivity analysis of WEC hydrodynamics to buoy geometry (shape, radius, height and draft). The performance and the electricity production of each buoy-generator combination was calculated at Alghero and Mazara del Vallo, using 21 years of wave buoy records, covering the period from 1990 to 2011. The results showed that the best buoy-generator configuration at both sites is given by a device with nominal power between 6 and 10 kW and a buoy with diameter between 4 and 5 m. The selection criterion used in this work was based on the capacity factor, which enables to compare devices with different rated powers and to evaluate the economic feasibility of renewable energy technologies based on intermittent energy sources.

After the identification of the most suitable device configuration, we investigated the possibility of increasing the power output by adding a neutrally buoyant submerged sphere to the floating buoy, in order to bring the system into resonance with the typical wave frequency of the study sites. We showed that this solution allows to considerably increase the capacity factor of the device, from about 20% to more than 40%. Starting from this solution, we investigated the effect of including more degrees of freedom in the device model. In particular, we assessed the effect of the independence of the two bodies and the contribution of the surge mode to wave energy absorption. The results showed that the first contribution is important for energy production estimation, whereas including the surge mode in the hydrodynamic model does not provide significant improvements.

Finally, the work focused on the hydrodynamic interactions between the devices, deployed in small parks. Small arrays of two and four devices

were simulated considering different array layouts (linear, square- and triangle-based), WEC separation distances (5, 10, 20 and 30 diameters) and incident wave directions (every 45°). The results showed that: (*i*) assuming a unidirectional sea state and varying the distance between WECs, the energy production of the array varies up to 5%; (*ii*) the effect of the incident wave direction seems to be more important than the WEC separation distance, particularly for the linear and square-based layout; (*iii*) depending on the wave attack angle, the absorbed energy varies up to 14%, 13% and 5% for the linear, square-based and triangle-based layout, respectively; and (i*v*) at all the Italian study sites, the linear layout was found to be the most favourable.

The present work will be further improved, and other issues should be investigated before designing a wave energy farm off the Italian coasts. However, the work showed the feasibility of wave energy production in the Italian seas and provided advice on where and how to exploit the Italian wave energy potential.

Renata Archetti, Adria Moreno Miquel, Alessandro Antonini
University of Bologna, Department of Civil, Chemical, Environmental, and Materials Engineering (DICAM), Italy

Giuseppe Passoni, Silvia Bozzi, Giambattista Gruosso, Francesca Scarpa, Federica Bizzozero, Marianna Giassi
Politecnico di Milano, Italy

references

[1] J. Scruggs, P. Jacob, Harvesting ocean wave energy, in *Science*, 323, pp. 1176-1178, 2009.

[2] J. Falnes, A review of wave-energy extraction, in *Marine Structures*, 20, pp. 185-201, 2007.

[3] A. Clément, P. McCullen, A.F. de O. Falcão, A. Fiorentino, F. Gardner, K. Hammarlund, G. Lemonis, T. Lewis, K. Nielsen, S. Petroncini, M.T Pontes, P. Schild, B.O. Sjöström, H.C. Sørensen, T. Thorpe, Wave energy in Europe: current status and perspectives, in *Renewable and Sustainable Energy Reviews*, 6, pp. 405-431, 2002.

[4] S. Bozzi, A.M. Miquel, A. Antonini, G. Passoni, R. Archetti, Modeling of a point absorber for energy conversion in Italian seas, in *Energies*, 6, pp. 3033-3051, 2013.

[5] L. Liberti, A. Carillo, G. Sannino, Wave energy resource assessment in the Mediterranean, the Italian perspective, in *Renewable Energy*, 50, pp. 938-949, 2013.

[6] R. Archetti, S. Bozzi, G. Passoni, Feasibility study of a wave energy farm in the western Mediterranean sea: comparison among different technologies, OMAE, Rotterdam, The Netherlands, 2011.

[7] S. Bozzi, R. Archetti, G. Passoni, Wave Electricity Production in Italian Offshore: A Preliminary Investigation, in *Renewable Energy*, vol. 62, issue C, pp. 407-416, 2014.

[8] M. Leijon, C. Boström, O. Danielsson, S. Gustafsson, K. Haikonen, O. Langhamer, E. Strömstedt, M. Stålberg, J. Sundberg, O. Svensson, S. Tyrberg, R. Waters, Wave Energy from the North Sea: Experiences from the Lysekil Research Site, in *Surveys in Geophysics*, 29, (3), pp. 221-240, 2008.

[9] K. Thorburn, M. Leijon, Farm size comparison with analytical model of linear generator wave energy converters, in *Ocean Eng.*, 34, pp. 908–916, 2006.

[10] S. Bozzi, A.M. Miquel, F. Scarpa, A. Antonini, R. Archetti, G. Passoni, G. Gruosso, Wave Energy Production in Italian Offshore: Preliminary Design of a Point Absorber with Tubular Linear Generator, *4th International Conference on Clean Electrical Power 2013: Renewable Energy Resources Impact*, pp. 203-208, doi: 10.1109/ICCEP.2013.6586990, 2013.

[11] F. Bizzozero, M. Giassi, G. Gruosso, S. Bozzi, G. Passoni, Dyanimc Model, Parameter Extraction and Analysis of Two Topologies of a Tubular Linear Generator for Seawave Energy Production, *Internation Symposium on Power Electronics, Electrical Drives, Automation and Motion*, 2014.

[12] A. Antonini, A.M. Miquel, R. Archetti, S. Bozzi, G. Passoni, Preliminary design of a point absorber with linear generator designed for energy production off the Italian coast, EWTEC 2013.

[13] V. Ferdinande, M. Vantorre, Hydrodynamics of Ocean Wave-Energy Utilization, in *International Union of Theoretical and Applied Mechanics Symposium*, pp. 217–226, Springer, Berlin, Germany, 1985.

[14] J. Engström, V. Kurupath, J. Isberg, M. Leijon, A resonant two body system for a point absorbing wave energy converter with direct-driven linear generator, in *J. Appl. Phys.*, 110, 124904:1–124904:8, 2011.

[15] A.M. Miquel, A. Antonini, R. Archetti, S. Bozzi, G. Passoni, Assessment of the surge effects in a heaving point absorber in the Mediterranean Sea, in *Proceedings of the International Conference on Offshore Mechanics and Arctic Engineering (OMAE)*, Vol. 9A, 2014.

[16] S. Bozzi, M. Giassi, G. Gruosso, G. Passoni, Hydrodynamic interaction among heaving point absorbers: preliminary results for the Italian seas, in *Proceedings of the 11th European Wave and Tidal Energy Conference, EWTEC 2015*, September 6-11, Nantes France, 2015.

[17] A. Babarit, On the park effect in arrays of oscillating wave energy converters, in *Renewable Energy*, Vol. 58, pp. 68-78, 2013.

Innovative rubble mound breakwaters for wave energy conversion

This paper presents a new Wave Energy Converter named Overtopping BReakwater for Energy Conversion (OBREC) which consists of a rubble mound breakwater with a front reservoir designed with the aim of capturing the wave overtopping in order to produce electricity. The energy is extracted via low head turbines, using the difference in water levels between the reservoir and the mean sea water level. The new design should be capable of adding a revenue generation function to a breakwater while adding cost sharing benefits due to integration. The design can be applied to harbour expansions, existing breakwater maintenance or upgrades due to climate change for a relatively low cost, considering the breakwater would be built regardless of the inclusion of a WEC.

DOI: 10.12910/EAI2015-050

P. Contestabile, C. Iuppa, L. Cavallaro, E. Foti, D. Vicinanza

Introduction

The energy consumption is in constant growth and so is the impact on the environment determined by the systems used for the production of energy. Global energy demand is expected to increase around 35% from 2010 to 2040 [1]. As traditional energy sources are finite, Nations are mobilized by encouraging the implementation of systems based on renewable energy. For example, the European Community has established to achieve by 2020 a 20% share of energy produced from renewable sources (Renewable Energy Directive 2009/28/EC). In any case oil will remain the largest single source of energy until 2040 [2].
Nowadays new devices based on wave energy recourses are under development. However since wave energy is not going to be economically competitive, it will be very difficult to become a possible contender in the energy market. The main aim of the present study is to give a WEC design solution having a reliable technology and a positive payback period of the investment.
The only solution to reduce the device structure costs is to move from standalone device to hybrid systems embedded in other costal or offshore structure (offshore wind farms, offshore oil platforms, ports, costal defence). Integration and sharing costs will become a solution for WECs to be competitive with other renewable energy devices.
The ongoing research reported here gives information on an innovative coastal structure designed in terms of safe hydraulic performance and global stability but also able to produce electricity in a balanced cost-benefit frame. Overtopping BReakwater for Energy Conversion (OBREC) is a new rubble mound breakwaters with a front reservoir designed with the aim of capturing the incoming wave overtopping to produce electricity. The energy is extracted via low head turbines, using the difference in water levels between the reservoir and the average sea water level (Fig. 1).

Contact person: Pasquale Contestabile
pasquale.contestabile@unina2.it

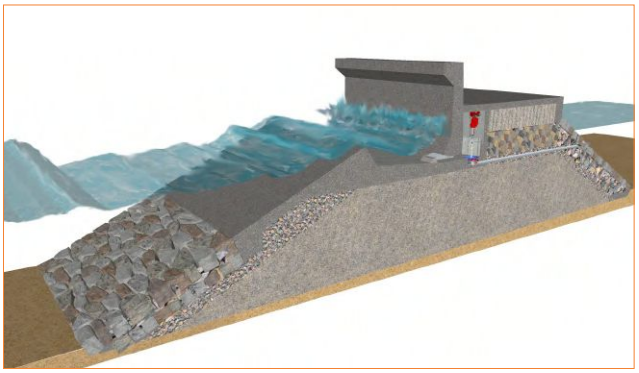

FIGURE 1 Innovative rubble mound breakwater with frontal reservoir for energy production

Laboratory experimental tests on OBREC have been carried out at Aalborg University (Denmark) in 2012 and 2014. The results of 2012 tests have been presented by [3, 4, 5]. The main aims were: (*i*) comparing OBREC with a traditional rubble mound breakwater in terms of hydraulic performances and loadings; (*ii*) validating the existing prediction methods to estimate structure reflection coefficient, overtopping and wave loadings; (*iii*) providing new formulae to design the first prototype.
The main aims of 2014 tests were to complete the analysis on OBREC geometric parameter variations. The paper is organized as follows: in the next paragraph a summary of 2012 tests is reported, then preliminary results of 2014 tests are presented. The paper ends with some conclusions and remarks for future works.

State of the art

OBREC is the outcome of composite seawalls evolution consisting of a frontal obstacle that dissipates the energy of the incoming wave reducing the wave loadings and related damage. These kinds of coastal projects have been constructed for many years in Japan and one example is the port of Mori [6], in which the Authors estimated a 30% reduction of the total cost. The contribute of wave overtopping reduction has been confirmed in [7]. The Authors demonstrated that a front reservoir solution is much more cost-effective than conventional cross section, such as beamed structures and mild slope structures. Another example is the composite seawalls proposed by [8], which represent an evolution with respect to the previous structures, for it is able to accumulate the wave. This new structure is composed by a reservoir realized in front of the seawall. The water is accumulated in the reservoir through the wave overtopping thus realizing a head difference between the water inside the reservoir and the mean sea water level. The head difference generates a flow which can be used to run a turbine and produce electricity.
In order to maximize the energy production, the WAVEnergy AS (Stavanger, Norway) have developed a device called Seawave Slot-cone Generator (or SSG) [9]. The SSG is an overtopping device that uses a number of reservoirs placed one on top of each other. The energy of incoming waves is stored as potential energy. Then, the captured water runs through turbines for electricity production. The peculiarities of SSG are: (*i*) its flexibility to work with a wide spectrum of different incident wave condition; (*ii*) availability of grid connection; (*iii*) the recirculation of water inside the harbour. This kind of structure should be constructed where wave energy is high because it has very high construction costs that may be compensated only by large electricity production.
OBREC is a solution to reduce installation and maintenance costs. In fact, it is a simpler structure than SSG and tends to be more economically viable than offshore floating as Wave Dragon [10] and WaveCat [11]. The device is still under development and physical model tests have been conducted to evaluate the hydraulic and structural performance.

Physical model AAU 2012

Prototypes in scale 1:1 are the most important development phase for WECs. However, a preliminary analysis in a smaller scale is necessary to understand the physical phenomena that characterise the device performance and its specific limits. For these reason, physical model tests on OBREC have been carried out at Aalborg University (Denmark) in 2012 in 1:30 length scale (Froude

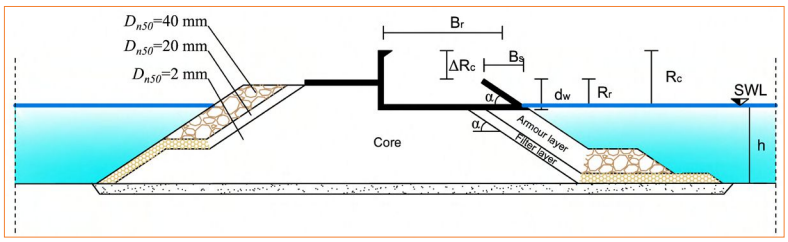

FIGURE 2 Model cross section in 2012 experimental campaign: definition of the principal geometrical parameters

scaling) [4]. The principal aim was to understand the different behaviour between OBREC and traditional rubble mound breakwaters. The main studied parameters were: reflection coefficient, overtopping at the rear side of the structure, overtopping in the front reservoir and the loading on the structure.

The wave flume has a length of 25 m and a width of 1.5 m. Moving from the paddle, a horizontal bottom characterized the initial 6.5 m, followed by a 1:98 slope that continues until just before the model. The rubble mound material characteristics were: D_{n50} 40 mm for the armour layer; D_{n50} 20 mm for the filter layer; D_{n50} 2 mm for core.

Figure 2 shows the section of the physical model. The principal geometrical parameters are: d_w height of sloping plate; R_r crest freeboard of front reservoir; R_c crest freeboard of crown wall; B_r reservoir width; α slope angle of the structure; h water depth at the toe of the structure.

A total of 48 tests were carried out under different wave condition. The parameter ranges for the OBREC structure are reported in Table 1.

The instrumental apparatus consists of: 28 pressure transducers for the estimation of the pressures/forces induced by the waves on the structure; 3 wave gauges for the estimation of the incident and reflected wave; 4 wave gauges installed in the boxes used to measure overtopping discharge at both the rear side of the model and in the frontreservoir. The incident and reflected spectra were determined using the approach of [12] and the positioning of the wave gauges was based on suggestions by [13].

The results below are expressed in terms of dimensionless parameters which are: break parameter $\xi_{m-1,0}$, relative reservoir crest freeboard R^*_r, relative crest freeboard of crown wall R^*_c, wave-structure steepness s^*_{Rr}, the parameter s^*_{Rc} and the non-dimensional average overtopping q^*. The parameters are defined as follow:

$$\xi_{m-1,0} = \frac{\tan(\alpha)}{\sqrt{\frac{H_{m0}}{L_{m-1,0}}}} \quad (1)$$

$$R^*_r = \frac{R_r}{H_{m0}}; R^*_c = \frac{R_c}{H_{m0}} \quad (2)$$

$$s^*_{Rr} = \frac{R_r}{H_{m0}}\frac{R_r}{L_{m-1,0}}; s^*_{Rc} = \frac{R_c}{H_{m0}}\frac{R_c}{L_{m-1,0}} \quad (3)$$

$$q^* = \frac{q}{\sqrt{gH^3_{m0}}} \quad (4)$$

Number of test	h [m]	H_{mo} [m]	$T_{m-1,0}$ [s]	R_c [m]	d_w [m]	R_r [m]	B_r [m]
48							
Extreme	0.30	0.141	1.68	0.20	0.075	0.075	0.415
(min-max)	0.34	0.177	2.26	0.24	0.125	0.125	0.488
Extreme with nose		0.145	1.66		0.075	0.035	0.415
(min-max)	0.34	0.161	2.28	0.20	0.125	0.085	0.488
Production		0.037	1.05		0.075	0.105	0.415
(min-max)	0.27	0.138	2.14	0.27	0.125	0.155	0.488

TABLE 1 Test 2012: Wave characteristic and reservoir geometrical parameters for the OBREC model (model scale)

Hydraulic performance

The principal results from the hydraulic point of view can be summarized from [5] as follow:

- the OBREC shows a similar or reduced average reflection coefficient with respect to traditional rubble mound breakwater;
- the overtopping at the rear side of the structure is greater than traditional rubble mound breakwater, but the use of a parapet wall with a protuberance reduces the average overtopping by 50-60%;
- the overtopping at the rear side of the crown wall is well fitted by Eq. 5 (range of application: $0.014 < \Delta Rc/L_{m-1,0} < 0.038$; $0.035 < s_{0m} < 0.058$; $1.24 < R_c^* < 1.38$);
- the overtopping in the front reservoir is well fitted by Eq. 6 (range of application: $0.45 < d_w/\Delta R_c < 1.08$; $0.0123 < s_{Rr} < 0.202$).

$$q^*_{rear} = 6.47 \cdot e^{-1.12 \cdot (s_{Rc})} \tag{5}$$

$$q^*_{reservoir} = \left(35.1 + 2.38 \frac{d_w}{R_c}\right) \cdot e^{\left(-58.99 + 17.7 \frac{d_w}{R_c}\right) s_{Rr}} \tag{6}$$

Reflection

The results showed that the presence of the reservoir does not determine increments of the reflection coefficient (K_r). Moreover, in some cases K_r is reduced. The comparison with various prediction methods has shown that the method of [14] may be used to estimate the values of K_r. In [14] the reflection coefficient can be expressed with the equation below:

$$K_r = \tanh\left(a\xi_0^b\right) \tag{7}$$

where a and b are two coefficients the value of which only depends on the roughness factor γ_f. The OBREC behaviour can be assumed as an impermeable rock with γ_f equal to 0.40 (a = 0.12 and b = 0.87). This method overestimates the values of K_r with apposite safety margin.

Overtopping discharge at the rear side of the structure

OBREC replaces the typical frontal rock area of traditional rubble mound breakwater with a concrete slope, significantly reducing the roughness of the structure. For this reason, with respect to a traditional rubble mound breakwater, OBREC slightly increases the overall wave overtopping. In order to reduce the overtopping without significantly raising the height of the wall, a parapet may be placed on the top of the crown wall. Indeed, test results have shown that the configuration with nose can reduce the overtopping of about 50-60%. In [5] a new prediction formula has been proposed to estimate the overtopping (see Eq. 5). This formula is a function of the significant wave height at the toe of structure, the wave length in deep water, the crest freeboard of the crown wall and the crest freeboard of the front reservoir.

Overtopping discharge in the front reservoir

Overtopping into the front reservoir has a high importance to understand the potential energy production of the device. In this phase it is important to understand how the overtopping is influenced by the geometrical characteristics of the reservoir. For this reason, different configurations have been tested under "production" wave conditions. The comparison with existing prediction methods showed a relatively good estimation from Van der Meer formula [15]. However, Eq. 6 has been proposed, which is a function of: height of sloping plate, crest freeboard of the crown wall, crest freeboard of the front reservoir, significant wave height at the toe of the structure and the wave length in deep water. The new method has shown a good agreement with the observed data.

Wave loading on the structure

The estimation of the wave loading and the structural response are important aspects to take into account for a consistent assessment on innovative devices. The analysis has been carried out by analysing the individual parts of the structure (see Fig. 3). The forms and magnitude of the wave pressures/forces acting upon the structures can be divided into impulsive, when they are rapidly varying and

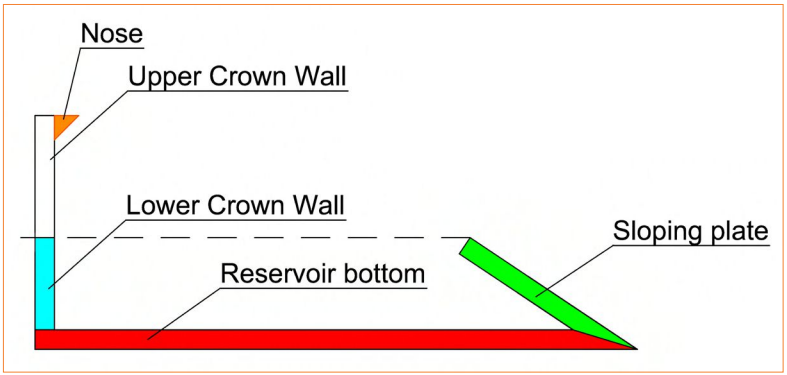

FIGURE 3 Overtopping device cross section

the pressure spatial gradient is extremely high, and non-impulsive, when they are slowly-varying in time and the pressure spatial gradient is relatively mild. The principal results of the tests can be summarized as follow:

- the wave loading on ramp may be evaluated averaging the non-impulsive and impulsive pressure distribution estimate with [16] using Goda's formula and [17] using Goda's formula modified by [18], respectively;
- the pressure distribution at the reservoir bottom may be assumed as triangular;
- the horizontal force on OBREC upper crown wall is well fitted by the modified formula proposed by [19], introducing a new empirical coefficient;
- the horizontal force on OBREC lower crown wall may be estimated with [20], introducing a correction parameter.

The measures of the wave loading on the ramp have been compared with the [16] using Goda's formula for non-impulsive conditions and with the [16] using Goda's formula modified by [18] for impulsive conditions. The comparison showed an over-prediction for the impulsive force and an under-prediction for the non-impulsive force. This behaviour is determined by the dynamics that occurs in the reservoir. Indeed, the backwash interacts with the uprush and generates a quasi-breaking wave conditions. Averaging the results for impulsive and non-impulsive conditions a good agreement is obtained.

The analysis of the wave loading in the reservoir bottom has shown that a triangular pressure distribution can be assumed based on [16]. Indeed, an error less than 20% has resulted from the comparison between observed and calculated data.

The behaviour of the wave loading on the crown wall is quite similar to the classical configuration of a berm in front of a crown wall. Two separate analyses have been performed for both the upper and the lower crown walls. For the upper crown wall the results have been compared with the formula proposed by [19]. The comparison has allowed the modification of the run-up formula by [5] in Eq. 5:

$$R_{u,0.1\%} = \gamma_{runup} \cdot c \cdot H_{0.1\%} \cdot \xi_m^{0.55} \qquad \xi_m > 3.5 \tag{8}$$

where $R_{u,0.1\%}$ is the wave run-up height exceeded 0.1% of the coming waves; γ_{runup} is a correction factor; c is the an empirical coefficient to take into account the change of the roughness factor from a traditional rouble mound breakwater; $H_{0.1\%}$ is the wave height exceeded 0.1% of the coming waves; ξ_m is breaker parameter. The empirical coefficient c is described as follow:

$$c = \frac{0.722 \cdot \gamma_{f,OBREC}}{\gamma_{f,trad}} \tag{9}$$

where $\gamma_{f,OBREC}$ is equal to 0.45 and $\gamma_{f,trad}$ is equal to 0.7.

For the lower crown wall the comparison with the formula of [20] has shown that the formula does not correctly interpret the measured loading. Even in this case, a modification factor has been introduced, which amplifies the force $F_{Takahashi}$ deriving from [20] and gives a better representation of the force $F_{H,Lcw}$ on the crown wall:

$$F_{H,Lcw} = \gamma_{falling} \cdot F_{Takahashi} \tag{10}$$

where $\gamma_{falling}$ is the amplification factor estimate with Eq. 11.

$$\gamma_{falling} = 2 \cdot \left(\frac{\gamma_{runup}}{R_r^*} \right)^{-1.3} \quad (11)$$

The analysis of the results has allowed to both understand the behaviour of the structure quite well and design prediction methods. However, new questions emerge about:

- the wave loading acting on the nose: the presence of the nose causes a reduction of the overtopping, but also an increase in the wave loading on the structure;
- how to increase the wave overtopping in front reservoir, without increasing, for example, the reflection coefficient and the overtopping rear the structure;
- how the geometrical parameters, e.g. the reservoir width and the length of the ramp, may be influenced by the performance of the device;
- how the uplift forces on the reservoir bottom can be reduced.

In such a framework, a second series of physical model tests were carried out in 2014. Different geometric configurations were investigated by varying the width of the reservoir and the slope profile of the ramp. Moreover, the behaviour of the device subject to still water level variations was simulated. Pressure transducers were placed on the nose.

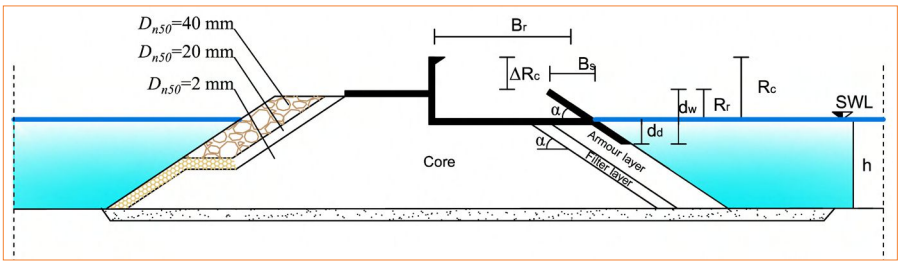

FIGURE 4 Model cross section in 2014 experimental campaign: definition of the principal geometrical parameters

Physical model AAU 2014

A second series of physical model tests on OBREC were carried out at Aalborg University (Denmark) in 2014 in 1:30 length scale (Froude scaling), compared to the prototype. Figure 4 shows the section of the physical model where d_d is the draft length.
Table 2 shows the wave characteristic and reservoir geometrical parameter for OBREC at model scale.
The principal parameters studied are: reflection coefficient, overtopping rear the crown wall of the structures, overtopping in the front reservoir and the loading of the wave motion.
Figure 5 shows the definition sketch for the overtopping Q_{in} and its three components (see Eq. 12), $Q_{reservoir}$ is the flow through section S_2, Q_{rear} is the flow through section S_3 and Q_{over} is the overflow. The water collected in the reservoir generates the $Q_{turbine}$.

$$Q_{in} = Q_{reservoir} + Q_{rear} + Q_{over} \quad (12)$$

The overtopping discharge in the front reservoir has gone into a box. A depth wave gauge was installed in the box to measure the $Q_{turbine}$ and to control the pump emptying the box when reaching a certain

Number of test	h [m]	H_{mo} [m]	$T_{m-1,0}$ [s]	R_c [m]	d_w [m]	R_r [m]	B_r [m]
200							
min	0.27	0.021	0.77	0.167	0.192	0.065	0.219
max	0.35	0.122	2.27	0.227		0.125	0.419

TABLE 2 Test 2014: Wave characteristic and reservoir geometrical parameters for the OBREC model (model scale)

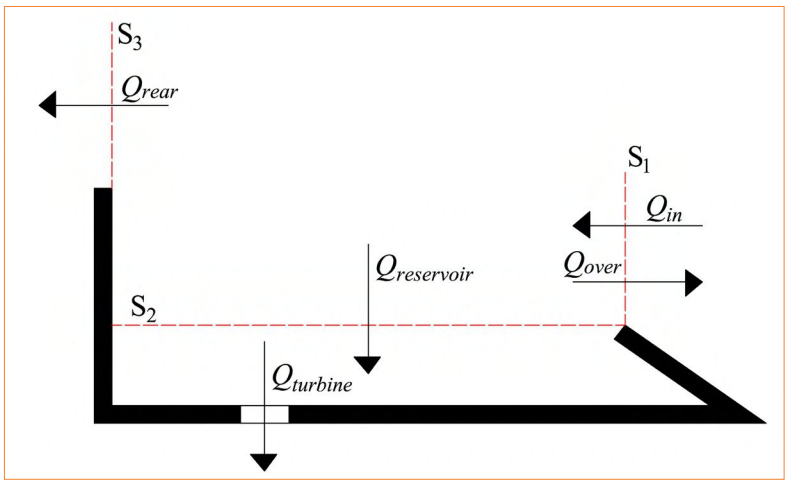

FIGURE 5 Definition of overtopping input, overtopping in front of the reservoir, in the rear side and the overflow

level. The hydraulic head has been measured with a pressure transducer installed in bottom of the reservoir. For all tests, overtopping discharge at the rear side of the model was determined using a ramp to guide the overtopping wave volumes into a box.

Figure 7 shows a comparison of the reflection coefficient measured in 2012 and 2014 tests, the isolines refer to the prediction formula of Zanutting and Van der Meer [14] with different value of the roughness factor γ_f. As indicated in [5]: the test results of 2012 show a similar behaviour of the traditional rubble mound breakwater, the reduction of the d_w causes a reduction of K_r and in a safe design the Zanutting and Van der Meer formula [14] for rock impermeable ($\gamma_f = 0.4$) may be used. In 2014 tests the effect of the increases in the draft length is evident in the reflection coefficient. The reduction of the roughness causes an increase in the value of K_r. This could represent problems for navigation and for the structure stability.

Figure 8 shows the comparison of the non-dimensional average wave overtopping rate of the rear crown wall model, measured in the tests performed in 2012 and 2014, respectively. The analysis shows that there is no change due to the increase in d_d, and the wave overtopping has similar trend and Eq. 5 may be also used for the some configurations analysed in 2014.

The non-dimensional average wave overtopping rates in the front reservoir from the experiments 2014 are compared in Figure 9 with both the measures of 2012 tests and the prediction formula of Kofoed [21], where the value of the parameter λ_{dr} has been estimated with the regression analysis. It is noted that in range $1.5<R^*_r<2$ the experimental curves show a different behaviour: this is due to the different length of the draft. In 2012 tests the d_d is equal to 0 m, whereas in 2014 tests it is equal to 0.067 m. It is apparent that the overtopping increases as the draft increases too. The prediction formula of Kofoed [21] has been designed for a structure with smooth impermeable slopes analogue to the configuration

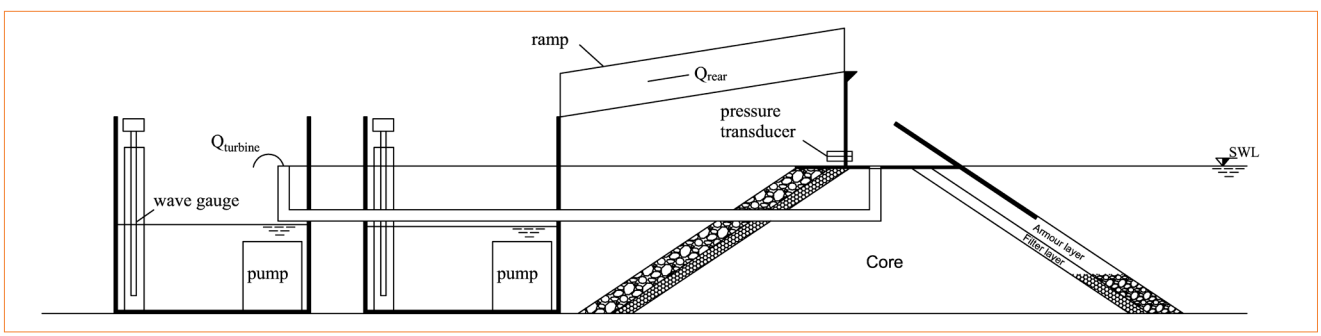

FIGURE 6 Wave-by-wave system for flow discharge measurement

of the model tested in 2014. Moreover, Kofoed [21] allows water to pass below the structure. Nevertheless, a good adaptation is noted. In the range $0.5<R^*_r<1.5$, the average wave overtopping rate in 2014 tests is constant: this is due the saturation of the reservoir. When the saturation level is reached, large quantities of water are lost, but in this case the $Q_{reservoir}$ is almost constant and there is a reduction of the variability of the energy production.

Figure 10 shows the non-dimensional average wave overtopping rate in the front reservoir with respect to the parameter s^*_{Rr}. Here the average wave overtopping is compared with Eq (6). The

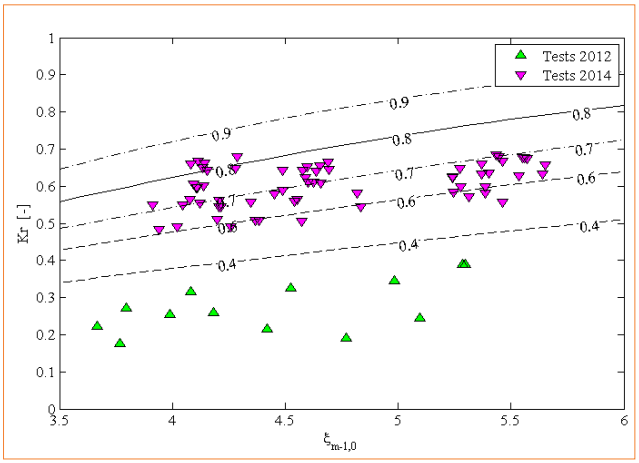

FIGURE 7 Comparison between the reflection coefficient of 2012 and 2014 tests results. The isolines refer to the prediction formula of Zanutting and Van der Meer [14] with different value of the roughness factor γf

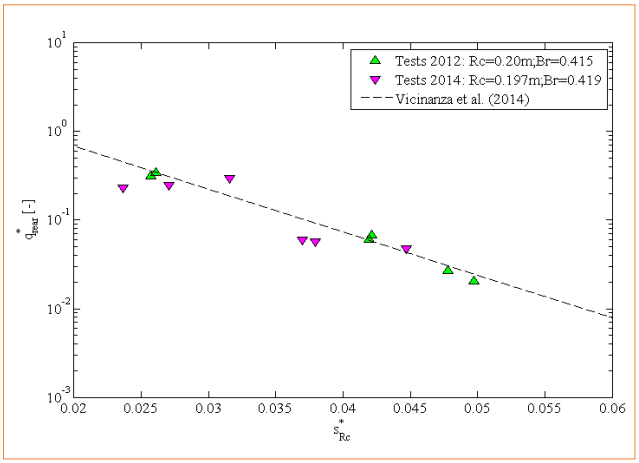

FIGURE 8 Comparison between non-dimensional average wave overtopping rate of the rear crown wall model resulting from 2012 and 2014 tests, and the prediction formula of [5]

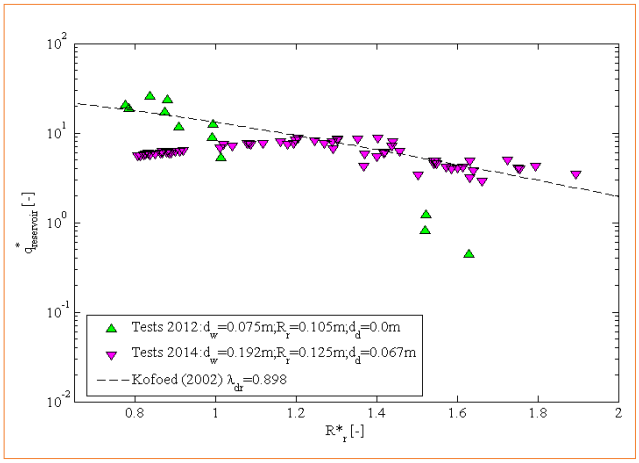

FIGURE 9 Comparison between non-dimensional average wave overtopping rate in the front reservoir resulting from 2012 and 2014 tests, and the prediction formula of Kofoed [21]

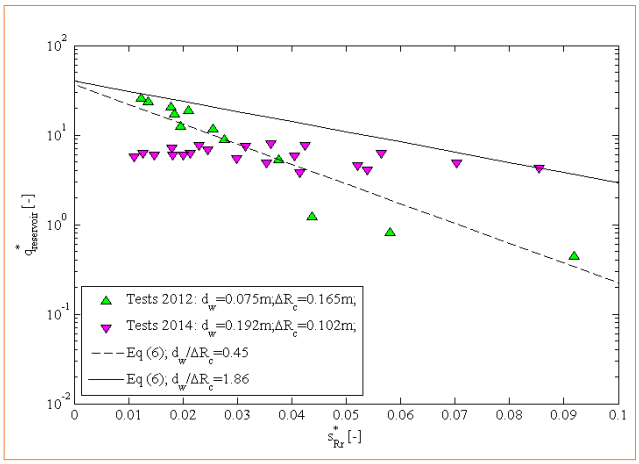

FIGURE 10 Comparison between non-dimensional average wave overtopping rate in the front reservoir resulting from the 2012 and 2014 tests and Eq. (6)

comparison shows an over-prediction of Eq. (6) for low values of s^*_{Rr}. The reason for such behavior is that, for the wave with low energy (higher values of s^*_{Rr}), the average Q_{in} is similar to the average $Q_{reservoir}$. When the wave energy grows, the reservoir is under saturated conditions for a larger percentage of the time. This causes an increase both in the average Q_{rear} and the average Q_{over}. In this case Q_{in} becomes greater than $Q_{reservoir}$.

Conclusions

WECs can be an opportunity to reduce the impact on the environment determined by the traditional systems used for the production of non-renewable energy. A new device called OBREC is presented. In particular, a summary of 2012 small-scale laboratory tests is reported, and preliminary results of 2014 tests are presented.

In 2012 model tests OBREC shows similar or reduced average reflection coefficient with respect to the traditional rubble mound breakwater. However, the ramp causes an increase in the overtopping rear the structure, which may be reduced by placing a parapet on the top of the crown wall. Indeed, the "nose" reduces the average overtopping by 50-60%. The analysis of the results has allowed the definition of formulas for the prediction of the overtopping rear the crown wall, in the front reservoir and the wave loading on the structure.

However, new questions come out about: (*i*) the wave loading at the nose: the presence of the nose causes a reduction of the overtopping, but also an increase in the wave loading on the structure; (*ii*) how to increase the wave overtopping in the front reservoir, without increasing, for example, the reflection coefficient and the overtopping rear the structure; (*iii*) how the geometrical parameters, e.g. the reservoir width and the length of the ramp, may be influenced the performance of the device; how the uplift forces on the reservoir bottom can be reduced.

For these reasons, a second series of physical model tests were carried out in 2014. Here only preliminary results on hydraulic aspects were reported. The principal difference between the 2012 and 2014 model tests are the length of the reservoir and the measurements of the wave overtopping in the front reservoir. In particular, the comparison has shown that: an increase in d_d determines an increase in the reflection coefficient; wave overtopping at the rear side of the crown wall does not increase compared to the configurations tested in 2012. The prediction formula provided in [5] shows a good adaptation with the test results of 2014. The prediction method of Kofoed [21] and Eq. 6 seem unable to predict the wave overtopping in the front reservoir under saturated conditions. For this reason it will be necessary to develop a new method that takes into account the saturation of the reservoir.

Pasquale Contestabile, Diego Vicinanza
Second University of Naples, Department of Civil Engineering, Design, Building and Environment, Italy

Claudio Iuppa, Luca Cavallaro, Enrico Foti
University of Catania, Department of Civil Engineering and Architecture, Italy

references

[1] A. Clément, P. McCullen, A. Falcão, A. Fiorentino, F. Gardner, K. Hammarlund, G. Lemonis, T. Lewis, K. Nielsen, S. Petroncini, M.T. Pontes, P. Schild, B.O. Sjostrom, H.C. Sørensen, T. Thorpe, Wave energy in Europe: current status and perspectives, in *Renewable and sustainable energy reviews*, 6(5), 405-431, 2002.

[2] ExxonMobil, The outlook for energy: A view to 2040, Technical Report, 2012.

[3] D. Vicinanza, D. Stagonas, G. Müller, J.Q.H. Nørgaard, T. L. Andersen, Innovative Breakwaters Design for Wave Energy Conversion, in *Proceedings of the 33rd International Conference on Coastal Engineering*, Santander, Spain, 2012.

[4] D. Vicinanza, J.Q.H. Nørgaard, P. Contestabile, T. L. Andersen, Wave loadings acting on Overtopping BReakwater for Energy Conversion, in *J. Coastal Res.*, SI 65, 1669-1674, 2013.

[5] D. Vicinanza, P. Contestabile, J.Q.H. Nørgaard, T. L. Andersen, Innovative rubble mound breakwaters for overtopping wave energy conversion, in *Coastal Engineering*, 88, 154-170, 2014.

[6] M Mori, Y. Yamamoto, K. Kimura, Construction and field observation of high mound composite seawall at Mori port, in *Coastal Structures*, 1480-1481, 2011.

[7] H.F. Burcharth, T. L. Andersen, Overtopping of rubble mound breakwaters with front reservoir, In *Coastal Engineering Conference*, vol. 30, No. 5, p. 4605, Asce American Society of Civil Engineers, 2006.

[8] D. Stagonas, G. Muller, N. Maravelakis, D. Magagna, D. Warbrick, Composite seawalls for wave energy conversion: 2D experimental results, 3rd International Conference on Ocean Energy, 2010.

[9] D. Vicinanza, L Margheritini, J.P. Kofoed, M. Buccino, The SSG Wave Energy Converter: Performance, Status and Recent Developments, in *Energies*, 5(2), pp. 193-226, 2012.

[10] J.P. Kofoed, P. Frigaard, E. Friis-Madsen, H.C. Sørensen, Prototype testing of the wave energy converter Wave Dragon, in *Renewable Energy*, 31, 181-189, 2006.

[11] H. Fernandez, G. Iglesias, R. Carballo, A. Castro, J.A. Fraguela, F. Taveira-Pinto, M. Sanchez, The new wave energy converter WaveCat: concept and laboratory tests, in *Mar. Struct.*, 29 (1), 58-70, 2012.

[12] E. Mansard, E. Funke, The Measurements of Incident and Reflected Spectra Using a Least Square Method, in *Proceedings of the 17th International Conference on Coastal Engineering*, Sydney, Australia, vol. 1, pp. 154-172, 1980.

[13] G. Klopman, J.W. Van der Meer, Random wave measurements in front of reflective structures, in *J. of Waterway, Port, Coastal and Ocean Eng.*,125 (1), 39-45, 1999.

[14] B. Zanuttigh, J.W. Van der Meer, Wave reflections from coastal structures, in *Proc. 30th International Conference on Coastal Engineering*, ASCE, World Scientific, Singapore, pp. 4337-4349. ISBN-13 978-981-270-636, 2006.

[15] J.W. Van der Meer, Wave run-up and overtopping, Chapter 8 In: Pilarczyk, K.W. (Ed.), Seawalls, Dikes and Revetments, Balkema, Rotterdam, 1998.

[16] K. Tanimoto, K. Kimura, A Hydraulic Experiment Study on Trapezoidal Caisson Breakwaters, Technical Note N.528Port and Harbour Research Institute, Yokosuka, Japan, 1985.

[17] Y. Goda, New Wave Pressure Formulae for Composite Breakwaters, in *Proceedings of the 14th International Conference on Coastal Engineering*, Copenhagen, Denmark, vol. 3, pp. 1702-1720, 1974.

[18] S., Takahashi, K. Tanimoto, K. Shimosako, A Proposal of Impulsive Pressure Coefficient for Design of Composite Breakwaters, in *Proceedings of the International Conference on Hydro-Technical Engineering for Port and Harbor Construction*, Yokosuka, Japan, pp. 489-504, 1994.

[19] J.Q.H. Nørgaard, T.L. Andersen, H.F. Burcharth, Wave loads on rubble mound breakwater crown walls in deep and shallow water wave conditions, in *Coastal Eng.*, 80, 137-147, 2013.

[20] S. Takahashi, K. Tanimoto, K. Shimosako, Wave Pressure on PerforatedWall Caissons, in *Proceeding of International Conference on Hydro-Technical Engineering for Port and Harbor Construction*, Yokosuka, Japan, pp. 747-764, 1994.

[21] J.P. Kofoed, Wave overtopping of marine structures: Utilization of wave energy, Hydraulics & Coastal Engineering Laboratory, Department of Civil Engineering, Aalborg University, 2002.

Development of analysis tools for self-rectifying impulse turbines for OWC systems

The paper presents the development of Performance Analysis Tools for Impulse-turbines for Oscillating water column wave energy converters, PATIOS. PATIOS applies the experimental correlations for axial turbomachines to self-rectifying impulse turbines and, with limited computational resources, provides prompt results as well as quantitative and qualitative analysis of the losses. Models and correlations for an OWC system with self-rectifying impulse turbines are presented and analyzed; the whole set was implemented in Matlab-Simulink environment. CFD simulations have been run to validate the results. PATIOS has been used for a wide-range sensitivity analysis, identifying the most relevant design variables and comparing the results with the experimental ones, available in the literature.

DOI: 10.12910/EAI2015-037

G. Cafaggi, G. Manfrida, L. Cappietti

Introduction

The harvesting of offshore renewable energies is an emerging topic in the scientific and technical field. Among other renewable energies, the conversion of wave energy [1, 2, 3] into a usable form has stimulated many researchers to develop Wave Energy Converters (WEC). At present there are thousands of patents in this sector. However, no one of these WECs has reached a commercial level and just few have reached a post-demonstration phase [4].

An Oscillating Water Column (OWC) is a WEC that comprises a partly submerged structure, open below the water surface, inside which a volume of air is trapped; the incident waves produce the oscillating motion of the internal free surface, making the air flow through a turbine that drives an electrical generator.

Contact person: Giovanni Cafaggi
giovanni.cafaggi@gmail.com

Some of the characteristics that make OWC systems promising WECs are their simplicity and absence of moving parts, except for the turbine. In the majority of works, the turbine is treated as a simplified linear system, and when this is not the case the design is mainly made by means of experimental campaigns or CFD simulations.

Recent development in the ongoing research on OWC systems [5, 6] seems to point out that the self-rectifying impulse turbine will be a better alternative to the traditionally used Wells turbine.

This paper presents the development of PATIOS (Performance Analysis Tools for Impulse-turbines for OWC Systems): a suite of tools meant to help and quicken the study of OWC systems using fixed-guide vane, self-rectifying impulse turbines (Fig. 1), intended for the preliminary analysis of OWC systems in different locations and sea climates.

PATIOS proposes to apply experimental correlations of turbomachines commonly used in other fields as the guidelines for system design and analysis. The main advantage of this approach

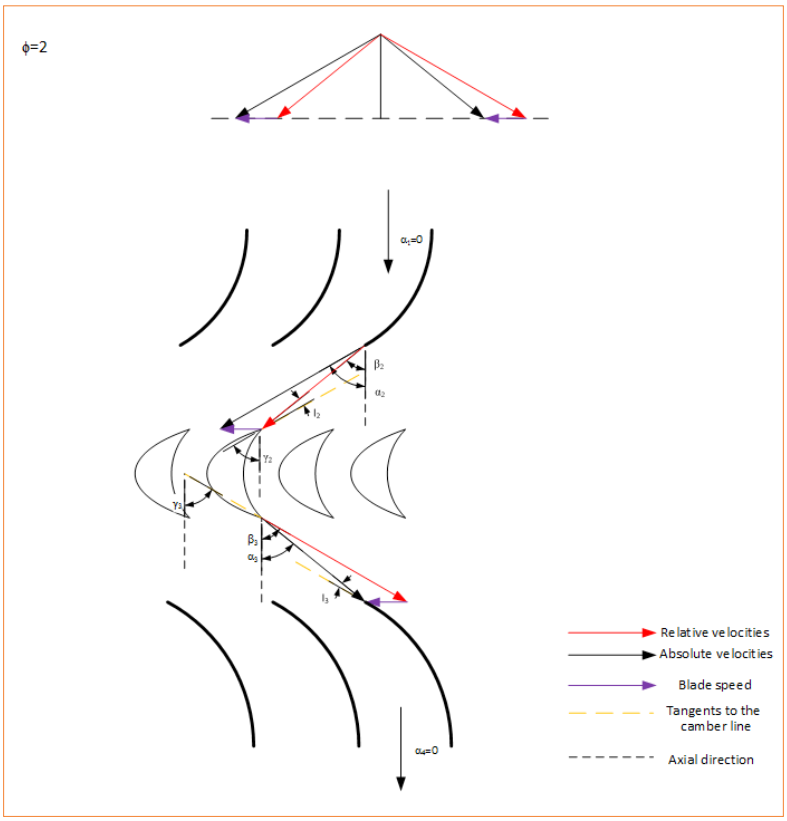

FIGURE 1 Fixed-guide vane, impulse turbine triangle of velocities and geometry at mean radius

is a major reduction of time and resources needed (either economical or computational), with the possibility of examining and comparing a large number of different options. Moreover, a second advantage is that the turbine losses analysis obtained is not only quantitative, but also qualitative, since the correlations divide the losses in each blade row into different categories. Lastly, it is possible to couple completely the simulation of the caisson and of the turbine. The drawback is that since the experimental correlations are designed for the gas turbines from other fields of energy conversion their validation for the present objective is needed, possibly by detailed experimental measurements; an alternative – presented in this work – is to apply CFD calculations to this purpose.

Turbine model

The examined system presents some peculiarities from a turbomachinery point of view: the fact that the turbine is operating with an alternating flow leads to the need for a symmetric geometry: thus, while the Inlet Guide Vane (IGV) is an accelerating row, the Outlet Guide Vane (OGV) is a diffusive one (Fig. 1). This also leads to the fact that the angles of incidence on the rotor and on the OGV blades are intrinsically remarkable. The non-dimensional variables used to characterize impulse turbines in OWC systems are the flow coefficient ϕ (Eq. 2), the torque coefficient C_T (Eq. 3), and the input coefficient C_A (Eq. 4). These coefficients represent the axial velocity, the shaft torque and the power available for the turbine, respectively.

$$\eta = \frac{T\omega}{\Delta p \dot{V}} = \frac{C_T}{C_A \phi} \quad (1)$$

$$\phi = \frac{c_x}{U_m} \quad (2)$$

$$C_T = \frac{2T}{\rho(c_x^2+U_m^2)Hl_r z r_m} \quad (3)$$

$$C_A = \frac{2\Delta p \dot{V}}{\rho(c_x^2+U_m^2)Hl_r z c_x} \quad (4)$$

$$P = L_{sp}\dot{m} = T\omega \quad (5)$$

These parameters are directly related to the efficiency η (Eq. 1), and through the rotational speed ω, the flow rate and the geometry of the turbine to the mechanical power available at the shaft P (Eq. 5) and to the total pressure drop across the turbine, Δp. The fundamental Euler equation for turbomachinery relates the specific work and thus the shaft power to the velocity triangles of the rotor stage. A number of experimental correlations to determine the

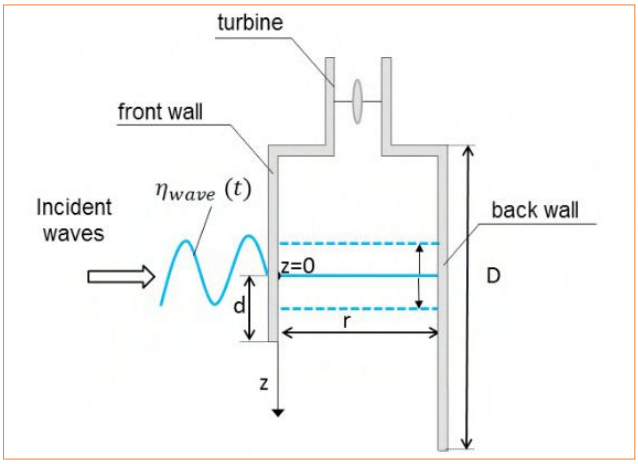

FIGURE 2 OWC system scheme

deviation of the flow, as well as the total pressure loss, can be found in the literature for turbine [14, 15, 16, 17] and compressor [13, 18] cascade rows. By applying the correlations, it is possible to calculate the loss coefficient and the resulting Δp; by removing the kinetic component, the static pressure drop Δp_s is obtained. This calculation can be repeated for different flow rates (covering the full off-design operating range, within the boundaries connected with the specific correlation used), determining the expected characteristic curve of the turbine, $\Delta p_s = f(\dot{m})$.

Simplified caisson model

While the rotational speed and the geometry can be chosen at will, the axial velocity is dependent on the caisson characteristics and on the features of the incoming wave, which is the real input for an OWC system. One of the possible methods to model the caisson is the weightless piston model (Fig. 2). Considering the mass of water adjacent to the free surface inside the caisson as a rigid body, and applying the Newton's second law, it is possible to obtain its equation of motion, thus giving the height of the water column (Eq. 6, 7, 8, 9 and 10).

$$m\ddot{z} = f_e + f_{rad} + f_{hstat} - f_p \quad (6)$$

$$f_e = A_c \rho g H cos(\omega t + \varphi) \frac{coshk(h-d)}{cosh(kh)} \quad (7)$$

$$f_{rad} = m_a \ddot{z} + B_r \dot{z} \quad (8)$$

$$f_{hstat} = A_c \rho g [d - (z - h_p)] - A_c \rho g h_p = A_c \rho g (d - z) \quad (9)$$

$$f_p = A_c \Delta p_s \quad (10)$$

The free surface motion is then linked to the mass flow through the turbine by the equation (Eq. 11):

$$\dot{m}_t = \frac{-d(\rho_{air} V)}{dt} = \rho_{air} A_c \frac{dz}{dt} - \frac{(V_0 - z A_c)}{c^2} \frac{dp}{dt} \quad (11)$$

Coupling caisson and turbine

Using the experimental correlation method mentioned above and fixing the rotational speed and geometry, it is possible to consider the $\Delta p_s = f(c_x)$ that together with equations 6 and 11 forms a system of differential equations, which can be solved by numerical methods once the geometry of the system and the fundamental features of the incoming wave are given.

In the turbine performance calculation, a dynamic stall model can also be implemented; in fact, it is well-known that airfoils can resist in dynamic conditions without profile stall to very large angles of attack. The dynamic stall model developed by Strickland *et al.* [7] (eq. 12, 13, 14) enables to calculate an equivalent angle of attack α_m for each row. This angle is then the one used to find the pressure losses.

$$\alpha_m = \alpha - \gamma K_1 S_{\dot{\alpha}} \sqrt{\left(\frac{C\dot{\alpha}}{2W}\right)} \quad (12)$$

$$K_1 = 0{,}75 + 0{,}25 S_{\dot{\alpha}} \quad (13)$$

$$\gamma = 1{,}4 - 6(0{,}06 - t/C) \quad (14)$$

Development of modeling tools and examples of results

The above theory and equations have been coded into Matlab language to provide an easy-to-modify, fast, and reliable system simulator. Two are the main tools developed in this way.
The first tool implements only the turbine performance calculation theory for stationary flow: given geometry and design axial velocity, it calculates the working curves of the turbine.
The second comprehends the caisson equations and performs a wave to shaft simulation, given system geometry, incoming wave shape and initial conditions.

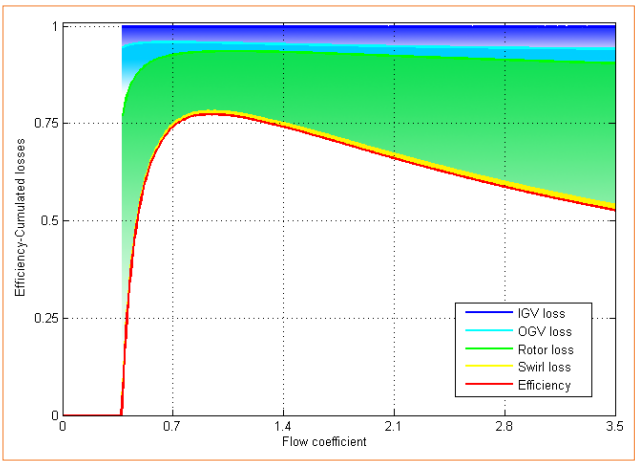

FIGURE 4 Efficiency and losses in each row

Turbine stationary simulator

After evaluating and testing the most popular correlations describing the performance of axial turbines, the set which has been found best suited and, consequently, implemented for simulations includes the modified Ainley-Mathieson and Carter-Hughes correlations for rotor and IGV rows, and Howell's correlation for the diffusive row [8].
A series of simulations has been carried out using this tool on turbines of different sizes (with blade angles suggested by Setoguchi *et al.* [9] and an outer radius of 0.15 m, 0.5 m and 1.3 m) for a wide range of flow rates. The typical trends of the non-dimensional coefficients C_T and C_A can be seen in Figure 3. The input coefficient C_A is artificially set to zero when the machine is not working properly, that is, when the power generated is negative (in this case, the experimental correlations are clearly not valid anymore).
One of the advantages of this approach is that the losses are found separately for each blade row (Fig.

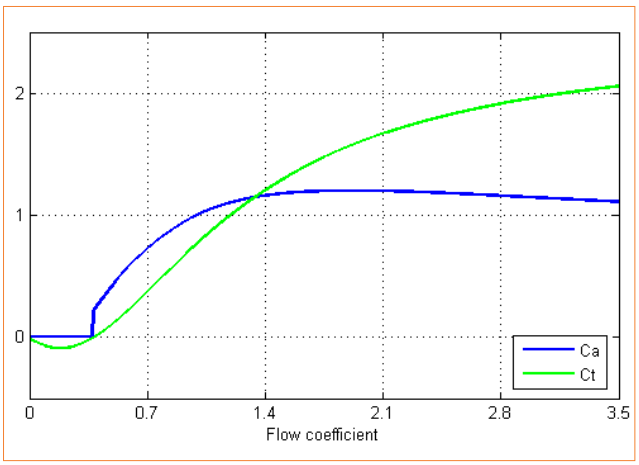

FIGURE 3 Input and torque coefficient for varying flow coefficients

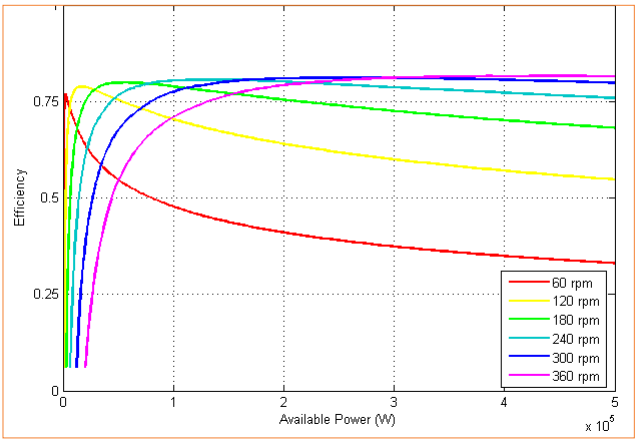

FIGURE 5 Turbine efficiency against available power for different rotational speeds

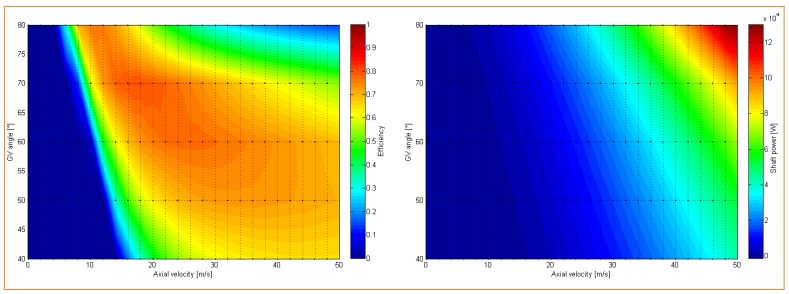

FIGURE 6 Efficiency and shaft power mapping for varying GV blade angles and axial velocity

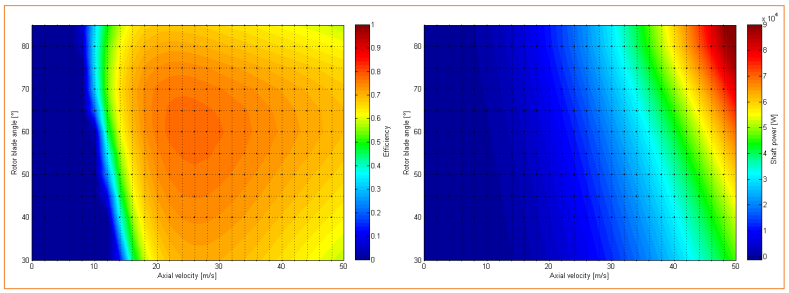

FIGURE 7 Efficiency and shaft power mapping for varying rotor blade angles and axial velocity

4); moreover, depending on the correlation used, in each blade row the losses are internally subdivided as profile, secondary, incidence and annulus losses. The trends for non-dimensional coefficients and efficiency are in line with experimental studies found in the literature.

Since the tool developed is of quick use (compared to CFD and experimental methods), during the simulation campaign it is convenient to run a sensitivity analysis on parameters like rotor speed, hub-to-tip ratio, stator and rotor blade angles. This analysis was mainly aimed at obtaining data to compare with the literature sources and not at optimizing a certain geometry.

The first sensitivity analysis was run varying the rotor speed of each turbine, but maintaining the geometry fixed: in Figure 5 one of the resulting graphs can be observed. The efficiency is given as a function of the available power, P_{av}, so that the graph can be compared with the one given by Thakker *et al.* [10], which reports different numerical values (also due to the dimensional nature of the available power variable) but identical trends.

In another set of simulations the effect of changing the outlet blade angle of the IGV (and the inlet blade angle of the OGV in order to keep the geometry symmetrical) was studied. As can be seen in Figure 6, the best efficiency on a wide range of axial velocities is obtained for 60° in accordance with the experimental studies found in the literature [9]. An interesting fact is that the shaft power is always higher for the 80° blade angle; this is explained observing both figures and remembering the efficiency and shaft power definitions (eq. 1 and 5): axial velocity and flow rate are proportional, since the inlet area is constant, therefore the pressure drop across the turbine results higher for lower efficiency and higher shaft power.

In Figure 7 the same kind of mapping can be observed changing the inlet and outlet (symmetrical) blade angles of the rotor. The variations of efficiency and shaft power are not as pronounced as in the case of the guide-vane angles, but present a clear optimum point at 60°, with highest efficiency on the widest range of axial velocity. The differences with the mapping obtained changing GV angles seem to point out that rotor angles could be tuned with some flexibility without compromising the performance of the system. To have a partial confirmation of the results obtained with this method, a series of CFD simulations on the rotor row have been carried out for different axial velocities at turbine inlet and a comparison of the losses has been made.

An example of the results is shown in Figure 8; the loss coefficients ξ calculated from the total pressure field are compared in Table 1 with the values calculated by the model; it can be seen that the model provides reasonable results, with better accuracy for higher flow coefficients.

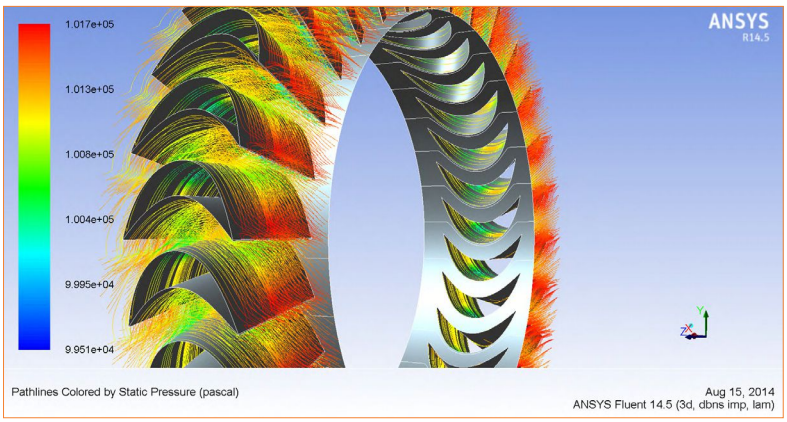

FIGURE 8 Streamlines through the rotor, depicting static pressure and flow direction

φ	ξ CFD	ξ Model
1,5	0,47	0,33
3,0	0,43	0,43
4,5	0,52	0,46
6,0	0,56	0,46
7,5	0,56	0,45

TABLE 1 Comparison of loss coefficient obtained using CFD and PATIOS (rotor)

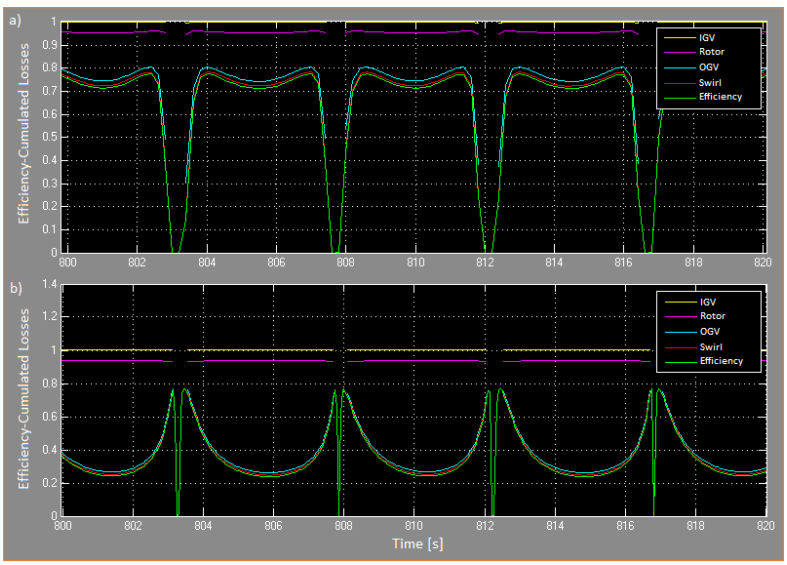

FIGURE 9 Efficiency and cumulative losses in each row for turbines with suitable (a) and not (b) geometries

Wave-to-shaft simulator

The wave-to-shaft simulator was developed in Simulink. It uses the numerical methods available in this environment for the solution in the time domain of the dynamic system differential equations coupled with the off-design turbine performance model. The caisson model implemented in the simulator is a modified weightless piston model [8]. The main inputs of the simulator are the geometry of the system, the incoming wave shape (as a sum of sinusoidal components) and the fixed rotational speed of the turbine. The main outputs are the instantaneous values of shaft power, pressure drop across the turbine and flow rate. Other variables extracted during the development process to observe the behavior of the system are the free surface level inside the caisson and its speed and acceleration, the pressure at the base of the caisson, and the axial velocity at the turbine inlet. A post-processing routine has been implemented to obtain efficiencies, losses, averaged values of all relevant parameters and graphs directly from the simulator. The efficiency and losses are calculated for the turbine in the same way as in the stationary code (efficiency of Eq. 1 and losses divided by row and cause). In Figure 9 two relevant cases are shown, depicting the efficiency and losses of two different turbines applied to the same caisson with the same incoming wave. The first turbine has values of rotational speed and stator blade angles optimized for the incoming wave. The second turbine reaches its peak efficiency just after the inversion of the flow, thus it would result better

Period [s]	Amplitude [m]	Average Shaft Power (kW)		Difference	
		with Dynamic stall	Simplified	Absolute	%
3	0,5	-0,07	-0,071	0,001	-1,43
4,5	0,75	0,188	0,187	0,001	0,53
5,5	1,1	19,16	19,18	-0,020	-0,10
6	1,5	54,6	54,5	0,100	0,18
7,5	2,25	77,2	76,9	0,300	0,39
9	3	85	85,1	-0,100	-0,12
Overall	-	236,08	235,80	0,282	0,12

TABLE 2 Comparison of shaft power obtained with and without the dynamic stall model

suited for lower axial velocities, that is, for incoming waves of smaller amplitude or longer period, but its performance deteriorates at higher flow rates where the energy that could be extracted is maximum.

A series of simulations have been carried out using sinusoidal waves with amplitude and length typical of the Tyrrhenian Sea [11]. The goal of the first set of simulation was to validate the relevance of the dynamic stall model. In practice, dynamic stall is proportional to the change in angle of attack, that is most evident for this highly unsteady flow application in proximity of the change of airflow direction. This zone is also the one in which the power available and, consequently, the shaft power are close to their minimum values, so it was reasonable to expect that the impact of the dynamic stall effect would be negligible. This was the case, in fact the simulations led to the results shown in Table 2, which presents the difference in the estimated shaft power for the two simulators. This conclusion however applies only to the sea conditions here considered (northern Tyrrhenian Sea), therefore for different locations the comparison should be made again, including the specific frequency and amplitude values.

The wave-to-shaft simulator has also been used to observe the effect of variation of coefficient B_r in the caisson model since, according to the studies from which the values used are taken [12], it is the one with the largest degree of uncertainty [8].

Lastly, the model has been used to map the average efficiency of the system for the range of incoming waves already described. Some of the results obtained from this campaign are visible in Figure 10. It can be observed that the efficiency of the turbine is relatively flat compared to the one of the caisson. It seems, in fact, that the performance of the latter is closely related to the frequency of the incoming wave and reaches its peak for a certain

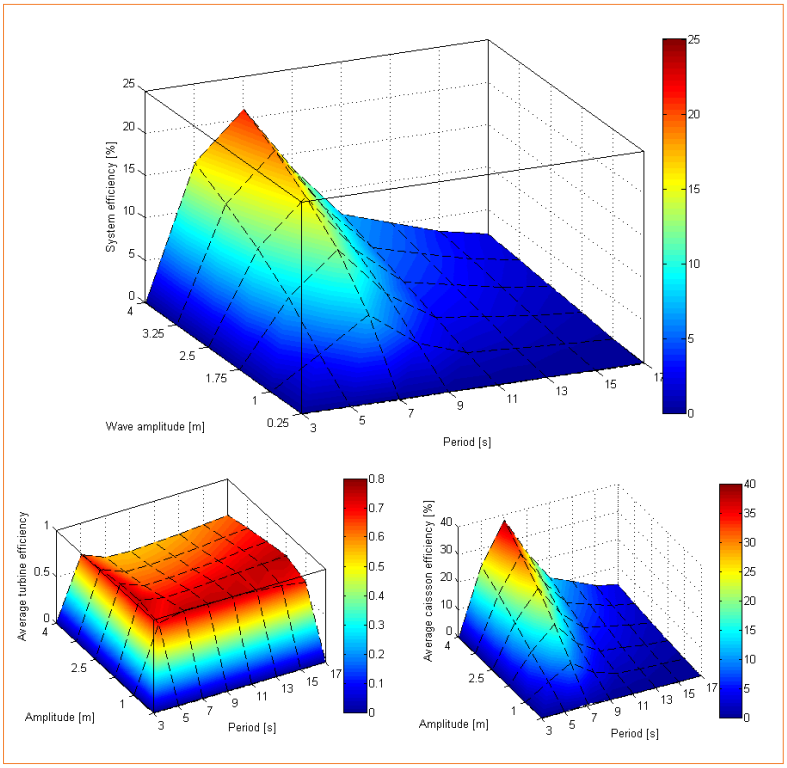

FIGURE 10 Average system, turbine and caisson efficiencies for varying incident waves

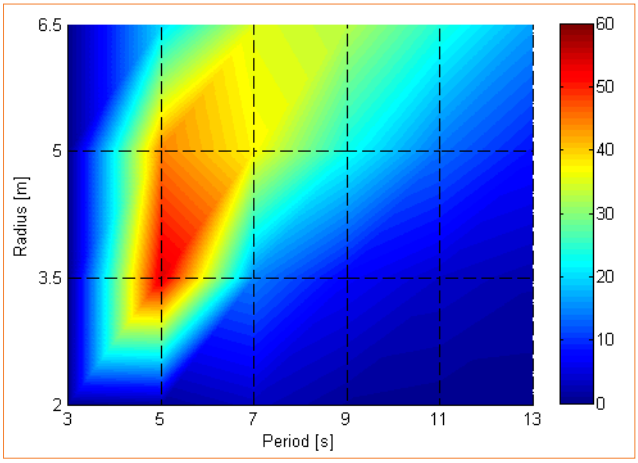

FIGURE 11 Average system efficiency mapping for varying incoming wave period and caisson geometry

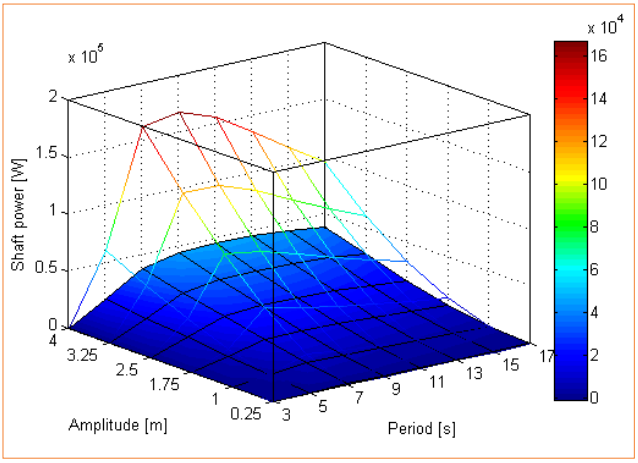

FIGURE 12 Comparison of shaft power of turbine with suitable geometry (netting) and not (surface)

frequency independently from the wave amplitude. A further study revealed that this frequency is closely related with the caisson dimensions (Fig. 11).
The same simulations have been run using turbines with different geometries and the results have been compared. The parameter used for this comparison was the shaft power, since from an economic point of view this is the parameter directly related with profit when considering null the marginal costs, and the O&M and capital costs independent from the turbine geometry. The example in Figure 12 shows a situation in which the device represented by the netting is clearly more suited than the one represented by the surface on the whole range of incoming waves.
Simulations have also been run with irregular waves (Fig. 13), but the results show that higher frequency components are subject to a high damping – at first through the coefficient Γ, which is calculated independently for each wave component, then both in the calculation of the free surface motion and of the turbine inlet velocity. This was confirmed by the negligible magnitude of higher frequency components in the efficiency and loss curves (Fig. 13).

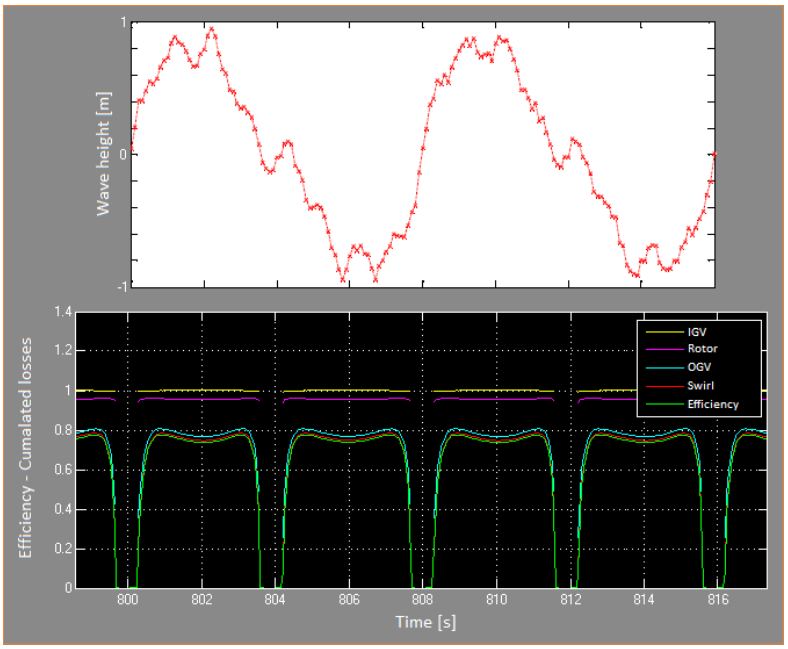

FIGURE 13 Irregular incoming wave shape (over) and resulting efficiency and losses (below)

Conclusions

In order to develop PATIOS (Performance Analysis Tools for Impulse-turbines for OWC Systems), a set of experimental correlations for axial turbines has been applied to self-rectifying impulse designs. The relevance of the effects of profile dynamic stall was assessed, a simple unsteady model for the caisson was coupled to the turbine correlations under off-design; the whole set was implemented in a Matlab-Simulink environment. A simulation campaign has been carried out using these tools to provide data comparable with the technical literature, and to perform a sensitivity analysis on the main design parameters. The comparison with the literature and with a set of CFD results for the rotor blade row shows an agreement in the trends for characteristic curves and efficiencies in all cases; however, the off-design performance of the simulated turbine results optimistic with respect to experiments or CFD. This could be due to several reasons: the experimental correlations were not originally intended for this kind of application, therefore it is possible that the blade profiles they refer to are more optimized than those actually used for OWC impulse turbines; moreover, the calculated losses are not influenced by the distance among the blade rows, while in the literature [9] this effect is considered relevant enough to be studied on its own. Direct or model testing is clearly needed to improve the accuracy of the correlations. The caisson model would also need more experimental data on different caisson sizes and shapes for the estimate of coefficients B_r and m_a. At the present stage, the tools developed seem well suited to conduct quick preliminary analyses and comparison of different OWC systems. Future development of this project includes the implementation of electrical components in the simulator and a study of the system inertia, in order to simulate also the starting characteristics of the system itself; after tuning the model, it should be possible to consider long-term simulations with real sea conditions, and to ascertain the possible benefits of operation with multiple, or variable rotational speeds and with a seasonal variable geometry of the caisson.

List of variables

A_c	horizontal caisson area
B_r	experimental radiation damping coefficient
C_A	Input coefficient
C_T	torque coefficient
c_x	axial velocity
d	OWC front wall draught
g	gravity acceleration
H_i	i^{th} incident wave component amplitude
h_p	height of the rigid water body considered
H_r	rotor blades height
l_r	chord length of rotor blade
m	mass of water considered as rigid body
m_a	experimental added mass coefficient
$\dot{m}_t$	air mass flow through the turbine
$S_{\dot{\alpha}}$	sign of $\dot{\alpha}$
t_r	maximum blade thickness
t	time
T	Torque
P	shaft power
U_m	ωr_m=circumferential velocity at r_m
$\dot{V}$	flow rate
V_c	air volume inside the caisson
V_0	air volume inside the caisson when z=0
w	relative velocity at rotor inlet
z	height of the free surface inside the caisson
z_r	number of rotor blades
α	angle of attack
α_m	equivalent angle of attack
Γ_i	i^{th} incident wave component depth damping factor
Δp	total pressure difference across the turbine
Δp_s	static pressure difference across the turbine
ξ	total pressure loss coefficient
ϕ_i	i^{th} incident wave component phase
Φ	flow coefficient
ρ	water density
ρ_a	air density
ω	rotational speed
ω_i	i^{th} incident wave component frequency

Giovanni Cafaggi, Giampaolo Manfrida, Lorenzo Cappietti
University of Florence, Italy

references

[1] A. Clement, P. McCullen, A. Falcão, A. Fiorentino, F. Gardner, K. Hammarlund, G. Lemonis, T. Lewis, K. Nielsen, S. Petroncini, M.T. Pontes, P. Schild, B.O. Sjöström, H.C. Sørensen, T. Thorpe, Wave energy in Europe: current status and perspectives, in *Renewable and sustainable energy reviews*, 6(5), pp. 405-431, 2002.

[2] D. Vicinanza, L. Cappietti, V. Ferrante, P. Contestabile, Estimation of the wave energy in the Italian shore, in *Journal of Coastal Research*, 64(12), pp. 613-617, 2011.

[3] V. Vannucchi, L. Cappietti, Wave Energy Estimation in Four Italian Nearshore Areas, from *ASME 2013 32nd International Conference on Ocean, Offshore and Arctic Engineering*, Volume 8: Ocean Renewable Energy Nantes, France, June 9–14, 2013, ISBN: 978-0-7918-5542-3, doi:10.1115/OMAE2013-10183.

[4] A.F.O. Falcão, Wave energy utilization: A review of the technologies, in *Renewable and Sustainable Energy Reviews*, 14(3), pp. 899-918, 2010.

[5] A.F.O. Falcão, L.M.C. Gato, E.P.A.S. Nunes , A novel radial self-rectifying air turbine for use in wave energy converters, in *Renewable Energy*, 53, pp.159-164, 2013.

[6] T. Setoguchi, M. Takao, Current status of self rectifying air turbines for wave energy conversion, in *Energy Conversion and Management*, 47, pp. 2382–2396, 2006.

[7] I. Paraschivoiu, Wind Turbine Design, Polythechnic International Press, Montreal, 2002.

[8] G. Cafaggi, Development of analysis tools for self-rectifying impulse turbines for OWC systems, Master Thesis, Università degli Studi di Firenze, 2014.

[9] T. Setoguchi, S. Santhakumar, H. Maeda, M. Takao, K. Kaneko, A review of impulse turbines for wave energy conversion, in *Renewable Energy*, 23, pp. 261–292, 2001.

[10] A. Thakker, F. Hourigan, Modeling and scaling of the impulse turbine for wave power applications, in *Renewable Energies*, 29, pp.305-317, 2004.

[11] V. Vannucchi, Wave Energy harvesting in the Mediterranean Sea, Tesi di dottorato, Università degli Studi di Firenze, Dottorato di ricerca in Ingegneria Civile e Ambientale, Ciclo XXV, 2013.

[12] I. Simonetti, L. Cappietti, G. Manfrida, H. Matthies, H. Oumeraci, State of the art review on analytical and numerical modelling for Oscillating Water Columns Wave Energy Converter Technology, internal report n° 2 (2013), Department of Civil and Environmental Engineering, Università degli Studi di Firenze, 2013.

[13] S.L. Dixon, Fluid Mechanics and Thermodynamics of Turbomachinery, Fifth edition. Elsevier (Ed.), ISBN 978-0-7506-7870-4, 1998.

[14] J.H. Horlock, Axial Flow Turbines, Butterworths (Ed.), London, 1966.

[15] J. Dunham, P. Came, Improvements to Ainley-Mathieson method of turbine performance prediction, in *Trans. Am. Soc. Mech. Engrs.*, Series A, 92, 1970.

[16] S.C. Kacker, U. Okapuu, A Mean Line Prediction Method for Axial Flow Turbine Efficiency, in *Journal of Engineering for Power*, vol. 104(1), pp. 111-119, 1982.

[17] S.H. Moustapha, S.C. Kacker, B. Tremblay, An Improved Incidence Losses Prediction Method for Turbine Airfoils, in *ASME J. Turbomach.*, 112, pp. 267–276, 1990.

[18] A.R. Howell, Design of axial compressors, in *Proc. Instn. Mech. Engrs.*, 153, 1945.

Development and field tests of GEM, the Ocean's Kite: A submersible floating device to tap tidal current energy

This paper presents the results of a series of test campaigns performed on an innovative system to harness clean energy from marine and river currents, developed in cooperation with the University of Naples "Federico II". It consists of an underwater vehicle linked to the seabed by means of a tether and supporting two hydro-turbines. Preliminary studies and experimental results of wind tunnel and towing tank tests on both single turbine and a complete scaled model will be illustrated. The behavior and performances of different configurations in both nominal and off-design conditions will be highlighted. Finally, experimental results on a full-scale prototype installed in the Venetian lagoon will be presented.

DOI: 10.12910/EAI2015-038

D.P. Coiro, G. Troise, F. Scherillo, N. Bizzarrini, G. Calise

Introduction

The exploitation of marine and river current power over the last few years has become one of the most promising fields in energy production from renewable sources, thanks to their low environmental impact and more stable and predictable behaviour with respect to other sources.

The ADAG (Aircraft Design & Aero Flight Dynamics) research group, in cooperation with Dr. Nicola Giorgio Morrone and Seapower Scarl, has developed since 2005 [1, 2] a system named GEM, The Ocean's Kite, specifically suited for this kind of energy sources. It is suitable for applications in both oceans and rivers. A CAD drawing of GEM is shown in Figure 1.

FIGURE 1 GEM, concept CAD drawing

It consists of a tethered system employing two shrouded, horizontal-axis turbines, mounted on both sides of two central floating bodies.

The upper body is designed to provide the necessary buoyancy force, while the lower one is used as dead weight. The upper body is

Contact person: Domenico P. Coiro
coiro@unina.it

also equipped with a "V-tail" to augment the longitudinal and lateral stability of the whole system and to allow the regulation of the pitching attitude into the stream by means of an adjustable flap. The tail also serves as damping device of lateral-directional oscillations. The two hydrokinetic turbines are counter-rotating and equipped with a diffuser (possibly with leading edge slats to enhance their aerodynamic role of accelerating the local velocity field toward the turbine rotor disks) to reduce the dimensions of actuator disks for a given rated power.
The system has a winch to allow the emersion of the system for control and maintenance purposes. A control system specifically designed avoids the rotation of GEM over 360 degrees and the twisting of the electrical cable.
The GEM has been designed to have specific advantages in terms of constructive simplicity and ease of operation, a relatively safe and easy self-orienting behaviour but, first of all, the possibility of avoiding the use of expensive submarine foundations, replaced by an anchorage to a single point on the seabed with a flexible tethering cable.
Two scaled models have been tested in the towing tank of the Department of Industrial Engineering (DII) at the University of Naples and a full-scale prototype has been tested in an open sea site, in order to characterize the static and dynamic behaviour of the system.
The present work will show a summary of the towing tank tests on a scaled model of the system and a brief report of the main results of the full-scale prototype testing in real sea conditions. Results of a simple numerical model of the GEM system equilibrium will also be discussed. The numerical model has been validated by comparing the results with experimental data.

Towing tank experimental tests

Characterization of the system and tests setup

The behaviour of the whole system was analysed under steady state and dynamic conditions in the DIN towing tank shown in Figure 2.

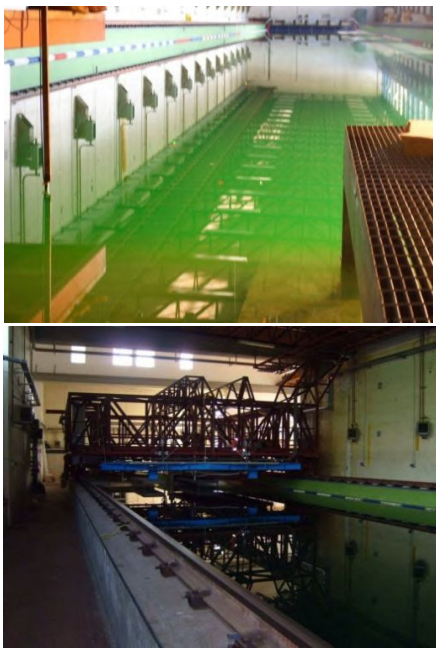

FIGURE 2 DII towing tank

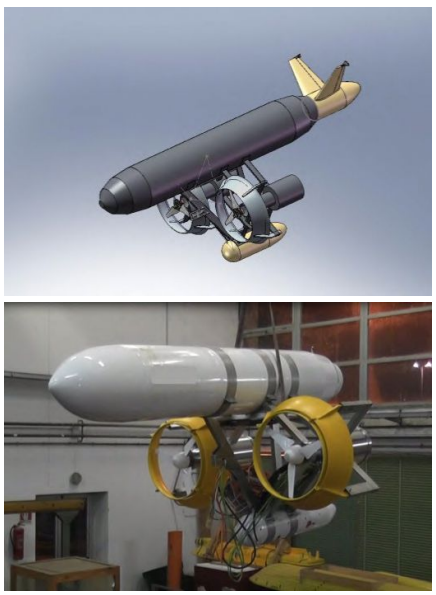

FIGURE 3 GEM prototype for towing tank tests. Scale 1:8

Turbine diameters	0.61 m
Distance between turbine axes	1.13 m
GEM overall length	3.55 m
GEM overall height	1.84 m

TABLE 1 GEM model. Main geometric data

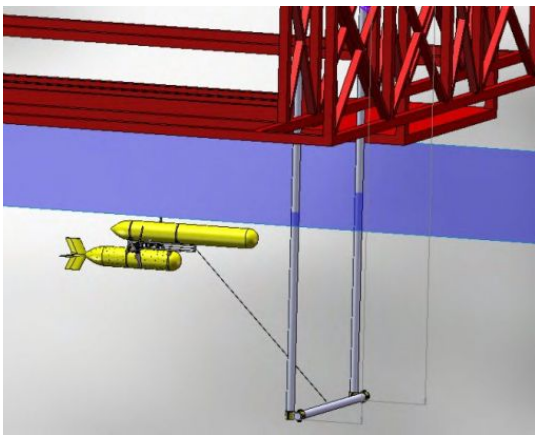

FIGURE 4 GEM model. Schematic of the testing support structure

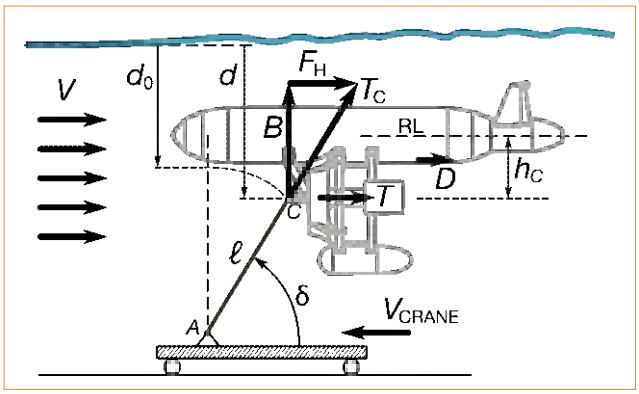

FIGURE 5 Schematic of the GEM system in a steady-state condition, immersed in a flow current

Initial depth d_0 of attachment point C	1.65 m
Depth d_A of towing attachment point A	3.27 m
Distance h_C of attachment point C from upper body reference line (RL)	0.75 m
Cable length, ℓ	1.62 m

TABLE 2 Geometric data of GEM model tethering system

Both nominal and off-design conditions were investigated by using differential braking of the two turbines. Off-design conditions may be caused in real conditions, for example, by an abnormal setback of one turbine.

The DII towing tank is 120 m long, 10 m wide and 5 m deep. A travelling crane carries the model at the desired velocity and a wave generator can simulate different operating conditions.

The actual shape of the model tested is shown in Figure 3, and the main dimensions are reported in Table 1.

Two electrical asynchronous motors (controlled by two inverters) acted on the turbine axes to control the rotational speed. Each of the two turbines was controlled separately.

The system was cable-connected to a steel frame structure attached to the travelling crane, as shown in Figure 4, and was then submerged in the tank at the desired depth by releasing, or tightening, the tether through a winch.

A schematic of the GEM system in a steady-state condition, immersed in a flow current, is shown in Figure 5. The equilibrium involves the cable tension force T_C, the buoyancy B, and the total horizontal force F_H. A list of geometric data of the GEM model tethering system is reported in Table 2.

The thrust T of the two ducted turbines (see Fig. 5) contributes to F_H as much as the hydrodynamic drag D of the submerged body. The combination of F_H and the buoyancy B is counter-balanced by the cable traction T_C.

The quantities observed and measured during the tests include:

- the attitude in terms of acceleration, velocity and angular displacement of the GEM by using an inertial platform located on board the floating body;
- the traction (Tc) on the tether cable by means of a dedicated load cell;
- torque and angular velocity of the left-hand-side turbine, from which the output power can be estimated (assuming symmetrical operating conditions) using a torquemeter;
- rotor and diffuser thrust with load cells.

The power is evaluated as $P=Q\Omega$, i.e. the torque times the angular speed.

Tests have been performed at various rotational speeds

and placing the model at various depths. In the following we consider the coefficient of power (or efficiency) defined as

$$C_P = \frac{P}{\frac{1}{2}\rho V^3 A} \qquad (1)$$

where P is the output measured power (left-hand-side turbine), V is the velocity of the current (i.e. the steady-state crane speed), A is the area of a reference surface (coincident with the turbine disk area), and ρ is the water density. Similarly, we define the torque coefficient as

$$C_Q = \frac{Q}{\frac{1}{2}\rho V^2 AR} \qquad (2)$$

where Q is the torque at the turbine hub and R is the nominal turbine disk radius. The thrust coefficient of the single turbine C_T is defined as

$$C_T = \frac{T}{\frac{1}{2}\rho V^2 A} \qquad (3)$$

where T is the thrust on turbine. The thrust (or drag) coefficient of the whole system is defined as

$$C_D = \frac{F_H}{\frac{1}{2}\rho V^2 S_{ref}} \qquad (4)$$

where F_H is the total drag (a horizontal force) developed by the system and S_{ref} is a reference area (not necessarily equal to A). Finally, the tip speed ratio is defined as

$$TSR = \frac{\Omega R}{V} \qquad (4a)$$

where Ω is the turbine angular speed. The TSR is a non-dimensional measure of the rotor tip speed.

Experimental results

Turbine efficiency

Two test campaigns have been carried out: the first related to a single turbine with and without the shroud, and the other related to the whole system-scaled prototype. The main result of the experimental tests is the comparison of C_P and C_Q versus TSR between GEM configurations with bare and shrouded turbines.

The main aim of using a shroud is to improve the turbine efficiency. Its function is to increase the mass flow rate through the turbine disc with a consequent power augmentation. The shroud had been previously optimised with a simple design method [3] and the experimental results have been confirmed by a CFD analysis.

As shown by [3,4,5], the power augmentation is proportional to the thrust exerted by the flow on the diffuser. The shroud design criteria were based on the maximization of this thrust, which is related to the chord, angle of attack, and lift coefficient of the diffuser airfoil section.

A high-lift airfoil has been opportunely chosen and a simple design method carried out [3] in order to define an optimum diffuser pitch angle and, consequently, its working angle of attack.

This simple design procedure is subject to several approximations: viscous effects are neglected, the induction factor is estimated to be constant along the turbine radius, the shroud equivalent diameter d is approximated to the turbine diameter. In order to

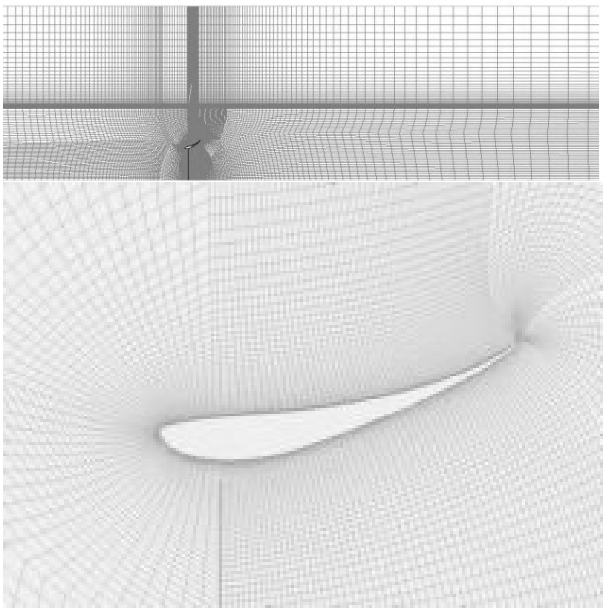

FIGURE 6 Mesh domain

evaluate the design diffuser angle more accurately, a numerical simulation has been carried out using FLUENT.

The turbine has been simulated as a constant pressure jump across the flow. The viscous effect has been included and the realizable k-ε turbulence model with enhanced wall treatment was used. Due to the axial symmetry of the system around the turbine axis, a two-dimensional mesh has been created applying the axisymmetric solution option, see Figure 6. The maximum C_P is reached for a pitch value (i.e., the angle that the diffuser airfoil section makes with axial direction) of ~ 26°.

Using the results obtained by the numerical simulation, experimental tests were carried out both in wind tunnel and in the towing tank on an isolated turbine in order to characterize its effective behaviour. Figure 7 reports the comparison of power coefficient for the bare turbine, a 23° shrouded turbine and a 26° shrouded turbine obtained during the wind tunnel tests.

The geometry with 26° section pitch has shown a better performance and has been chosen for further development. During towing tank tests different TSR values were obtained by using varying rotation speeds of the turbines and a fixed crane speed $V = 1.5\ m{\cdot}s^{-1}$. In Figure 8, a typical time history of the controlled angular speed of the turbines, crane speed V and torque Q measured at the turbine hub have been reported. This

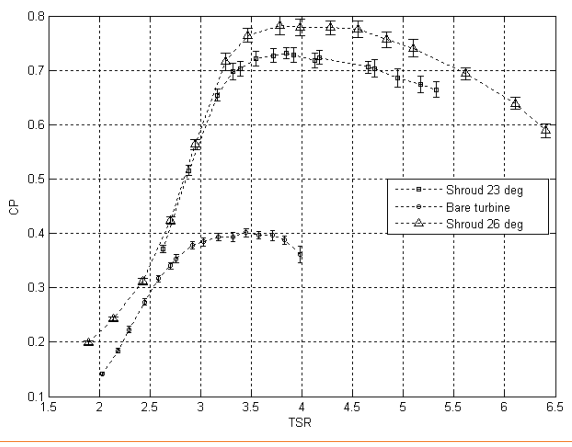

FIGURE 7 Comparison of C_P (*TSR*) for bare turbine, 23° shrouded turbine and 26° shrouded turbine. Wind tunnel tests

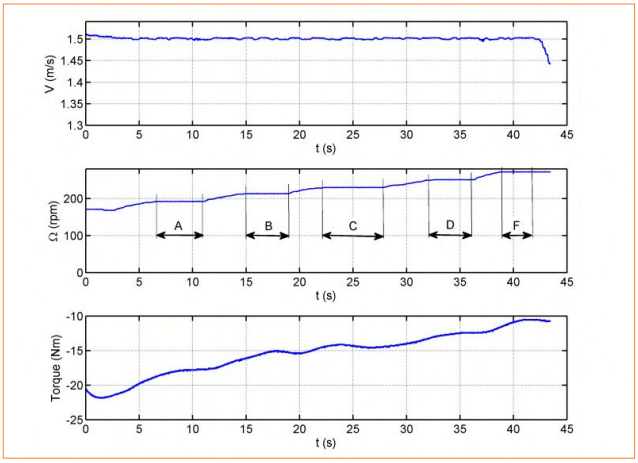

FIGURE 8 Time histories of crane advance speed, turbine controlled angular speed, and torque (turbines with diffusers, upright V-tail)

is the torque applied by the motor in order to obtain the desired TSR.

The time intervals named "A", "B", "C", "D", and "F" correspond to constant angular speed, that means constant TSR. Details of the testing structure and load cells are shown in figures 9, 10 and 11.

In Figure 12 we report the experimental power coefficient curves for an isolated turbine versus *TSR*, tested in water both with and without diffuser.

The curves confirm wind tunnel results and show the advantage of using ducted turbines, which results in almost a doubling of the maximum efficiency $C_{P,max}$.

It is worth noting that the power coefficient of the shrouded configuration is referred to the rotor disk surface area and that referring it to the overall frontal area (equal to the exit area of the shroud) the net increase is reduced at about 7%, as shown in Figure 13.

The yaw angle influence was also analyzed. Comparison between maximum *Cp* value versus yaw angle for ducted and non-ducted case is reported in Figure 14.

The maximum power coefficient of the bare turbine decreases linearly with the yaw angle, whereas the shrouded turbine seems to be not influenced by the yaw angle between 0 and 10 deg.

Experimental power coefficients for the turbines tested with the whole system confirm results for isolated turbines. The curves are reported in Figure

FIGURE 9 CAD view of the testing structure for an isolated turbine

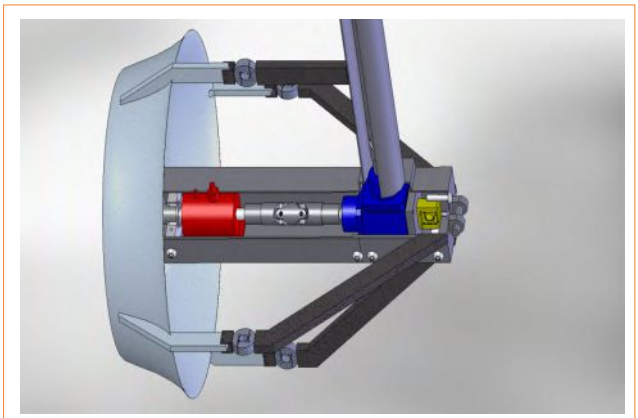

FIGURE 10 Detail of the diffuser on the support structure

FIGURE 11 Real testing structure

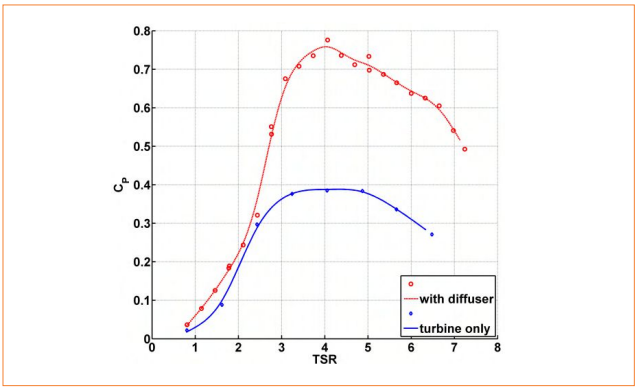

FIGURE 12 Comparison between bare and shrouded turbine. Single turbine test

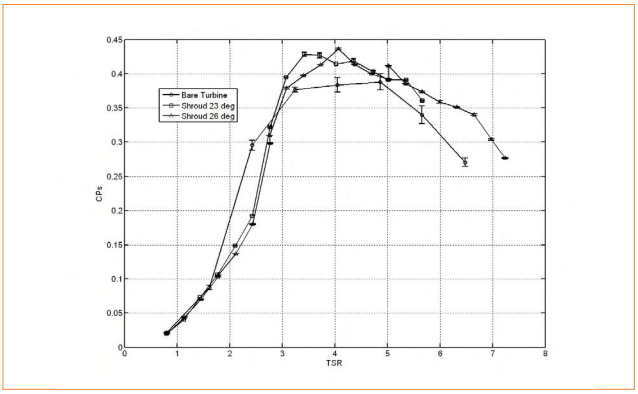

FIGURE 13 Towing tank tests: Comparison referring the coefficient to the diffusers exit areas

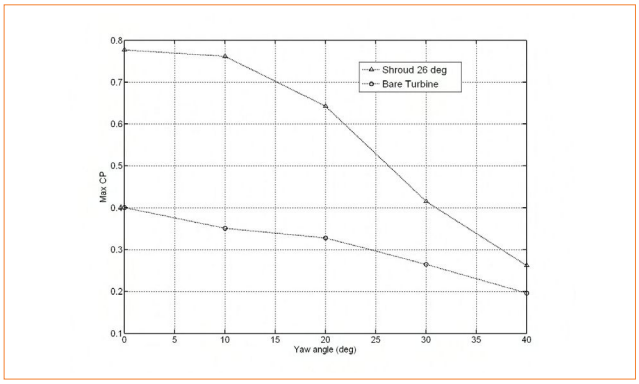

FIGURE 14 Maximum CP versus yaw angle comparison

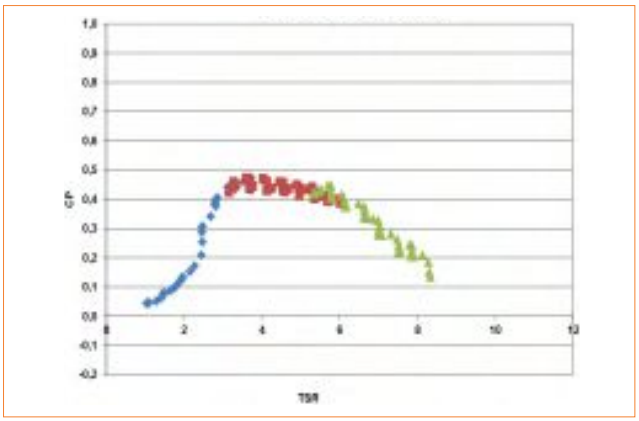

FIGURE 15 Experimental power coefficient values (turbines without diffusers, upright V-tail, V = 1.5 m·s-1)

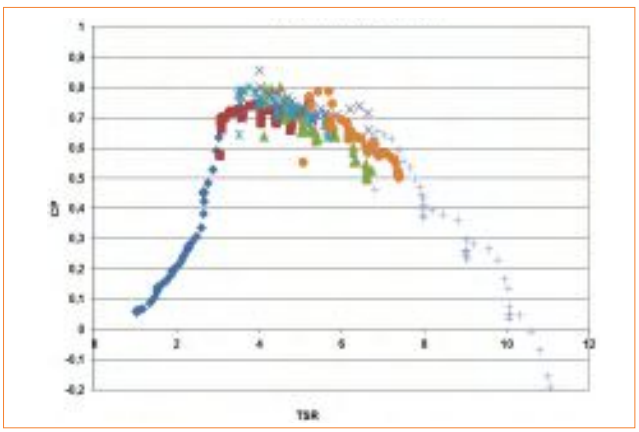

FIGURE 16 Experimental power coefficient values (turbines with diffusers, upright V-tail, V = 1.5 m·s⁻¹)

	CP,max	*TSR @ CP,max*
Ducted turbines	0.74	4.1
Turbines w/o diffusers	0.40	4.0

TABLE 3 GEM efficiencies with and without diffusers

15 and Figure 16 for both the ducted and bare turbines cases, and maximum *Cp* with relative *TSR* is reported in Table 3.
The fitting curve of power coefficient versus *TSR* is shown in Figure 17.

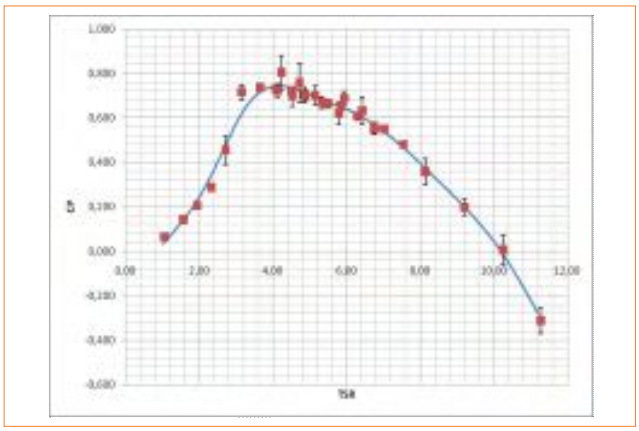

FIGURE 17 Power coefficient (turbines with diffusers, upright V-tail, V = 1.5 m·s-1)

Starting torque

The start-up torque Q_0 is the minimum torque needed to put the turbines in rotation in a current of given speed V. It is related to the minimum current speed above which the system is capable of generating power.
To assess Q_0 the turbine has been towed at different speeds keeping a zero angular speed by using a control motor. The measured torque acting in this case is identified with the required start-up torque Q_0 at the corresponding current speed V. The measured Q_0 and the corresponding torque coefficient C_{Q_0} at different current speeds are reported in Table 4 and Q_0 is shown in Figure 18. By averaging the values of Q_0 we have obtained the curve in Figure 19.

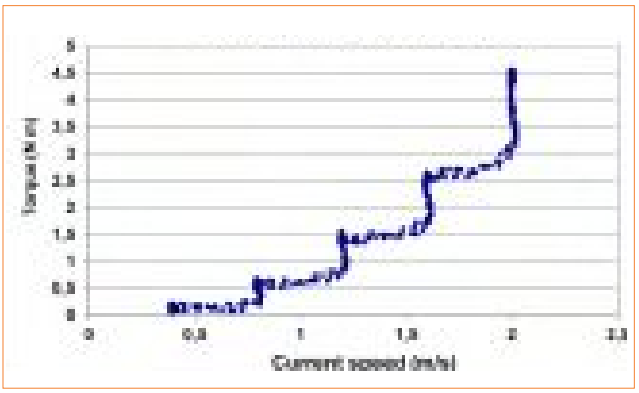

FIGURE 18 Measured start-up torque Q_0 at different current speeds (and zero angular speed)

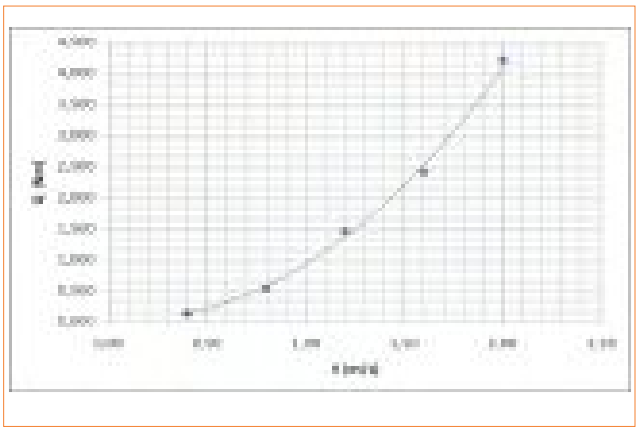

FIGURE 19 Variation of turbine start-up torque with current speed

V (m·s⁻¹)	C_{Q_0}	Q_0 (N·m)
0.40	0.0180	0.132
0.80	0.0181	0.528
1.20	0.0221	1.455
1.60	0.0205	2.403
2.00	0.0230	4.210

TABLE 4 GEM turbine measured start-up torques

Turbine thrust

In Figure 20 thrust coefficient C_T versus *TSR* is illustrated

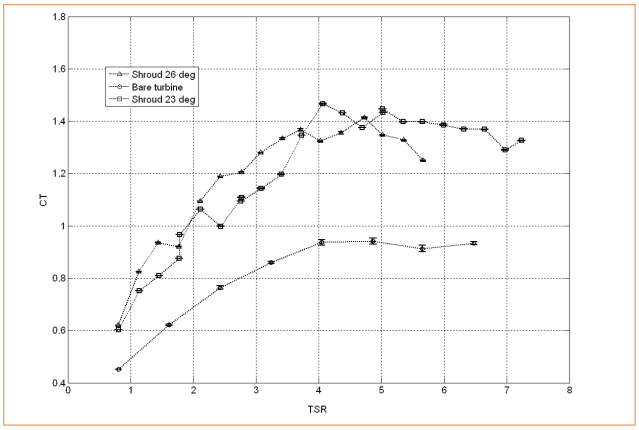

FIGURE 20 Turbine thrust coefficient comparison (coefficient referred to the turbine area)

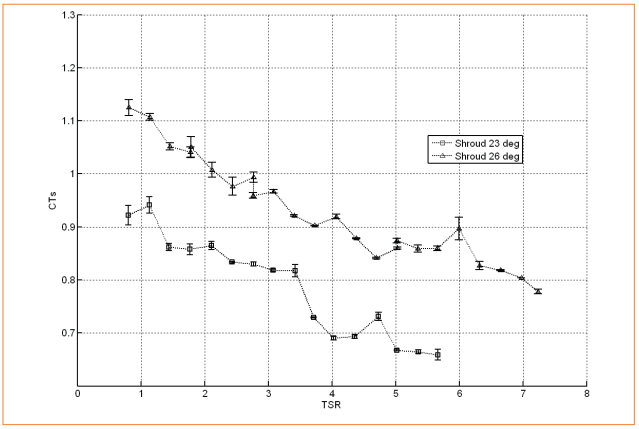

FIGURE 21 Shroud thrust coefficient comparison (coefficient referred to the turbine area)

for the bare turbine and for two diffusers with the same section but two different incidence angles (23° and 26°).
In discordance to some theories about the diffuser working principles, the diffuser causes a sensible increase in thrust coefficient on the rotor. Such results need further investigations and validations.
In Figure 21 shroud thrust coefficient C_T versus *TSR* is reported. The reduction with increasing *TSR* may be related to a reattachment of the flow over the diffuser inner side, due to the interaction with the turbine-induced flow.

Tether tension and inclination

Another important feature being investigated during the experimental tests is the amount of tension in the cable connecting the GEM to the crane. This gives an idea of the maximum stress to be accounted for when dimensioning the cable of the real system and enables the appropriate selection of the mooring and anchorage system. A load cell was used to observe the tether cable force T_C.
Considering the scheme of Figure 5, we derived two formulae for calculating the tether angle δ and the total horizontal force F_H. The amount of the buoyancy, i.e. the intensity of B, is observable in static conditions. Knowing B and by measuring T_c, we can calculate F_H and δ by the expressions:

$$\delta = \frac{\pi}{2} - \cos^{-1}\left(B / T_C\right) \qquad (5)$$

$$F_H = T_C \cos \delta \qquad (6)$$

Measures of δ and F_H versus the angular speed Ω, for a constant current speed V=1.5 m·s^{-1} are reported in Figure 23 and 24.

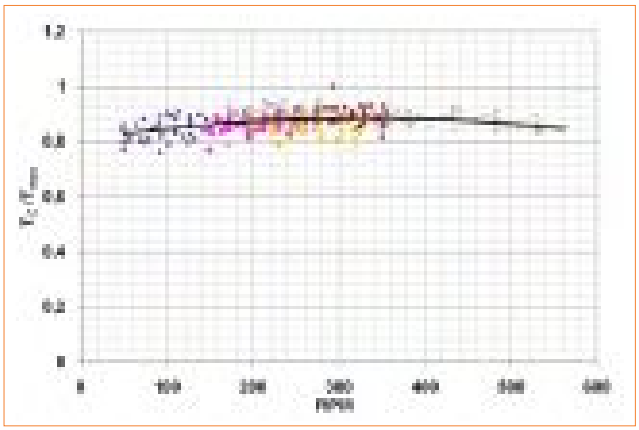

FIGURE 22 Tension force at the connection tether, referred to the maximum tension observed (turbines with diffusers, upright V-tail, V = 1.5 m·s-1)

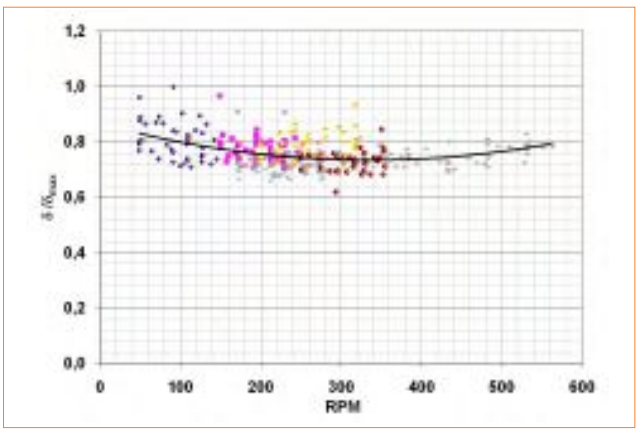

FIGURE 23 Measured tether angle with respect to the horizontal plane (turbines with diffusers, upright V-tail, V = 1.5 m·s-1)

Figure 25 shows the steady-state tether angle versus current speed V as calculated by observing the underwater vertical displacement d of the floating body during the tests. Knowing the cable length ℓ and the initial

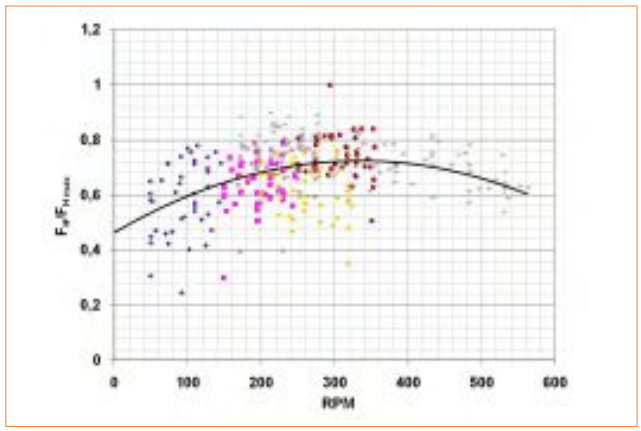

FIGURE 24 Resistance to the advancement motion opposed by the GEM, referred to the maximum value observed (turbines with diffusers, upright V-tail, V = 1.5 m·s-1)

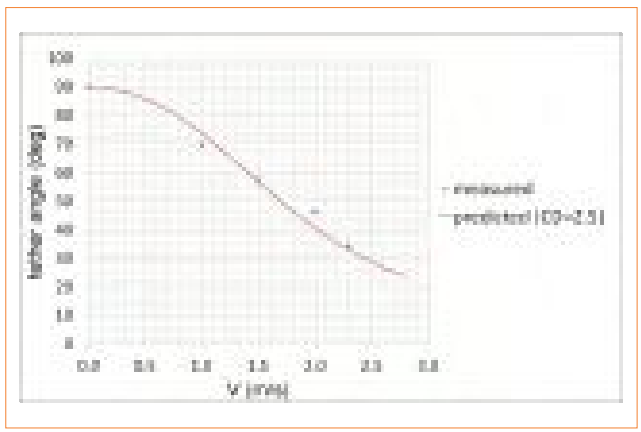

FIGURE 25 Steady-state tether angle (turbines with diffusers, upright V-tail). The solid line is predicted with a simplified model assuming a constant *CD*

static displacement d_0 (when V = 0), and observing the actual depth d, the angle δ may be calculated.
The solid line is predicted with a simplified model, assuming a constant total drag coefficient.

Full-scale prototype tests

Prototype general data

A full-scale prototype of a GEM system, shown in Figure

FIGURE 26 GEM full-scale prototype

Turbine diameter:	D_t=3.08 m
Diffuser throat diameter:	D_g=3.10 m
Diffuser exit area diameter:	D_e=4.08 m

TABLE 5 Turbine and diffuser dimensions

Overall length:	L=9.2 m
Overall height:	H=5.2 m
Overall width:	S=10.4 m

TABLE 6 Floating support structure dimensions

Overall weight:	W = 16100 kg
Net buoyancy force:	B = 51000 N
Horizontal thrust (on the overall system at 1.5 m·s^{-1}):	T = 45000 N
Rotational speed:	Ω = 38 RPM

TABLE 7 Weight, loads and operational characteristics

Depth (range): 15 m to 9.8 m (without current)
Nominal power 20 kW with a tidal current of 1.5 m·s^{-1}
Three-blades 3 m diameter rotor
Innovating blade section profiles
Carbon blades - Fiberglass diffuser
Rotor Efficiency: 0.8

TABLE 8 Technical and operational data

26, dimensioned to produce 20 kW at current speed of 1.5 m·s^{-1}, has been developed, built and installed in a test site. It has been partially sponsored by a consortium of companies operating in the Veneto region and partially by the Veneto Regional Authority.
The first prototype has been deployed in the Venice lagoon, near Forte Sant'Andrea, with a seabed depth of about 25 m. The system was operating at a depth of about 15 m.
In the Tables 5, 6, 7 and 8 overall dimensions of the prototype are reported.
On the basis of the preliminary development phase and the results of the towing tank tests, some of the operational and load data reported in Table 7 and Table 8 have been estimated for the prototype.

Measurement equipment

The following equipment has been installed on board the system:

- Inclinometer:
  - pitch angle,
  - roll angle;
- Pressure sensors:
  - depth;
  - Generators related data:
  - actual power,
  - actual torque,
  - actual number of revolutions of the engine,
  - torque and speed imposed by the controller;
- Wind vane on the floating body:
  - water current relative direction.

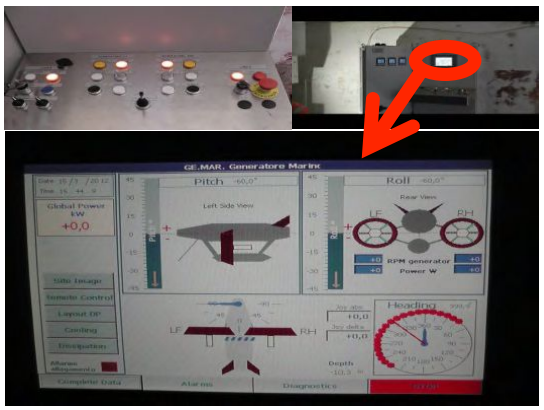

FIGURE 27 Data acquisition system software overview

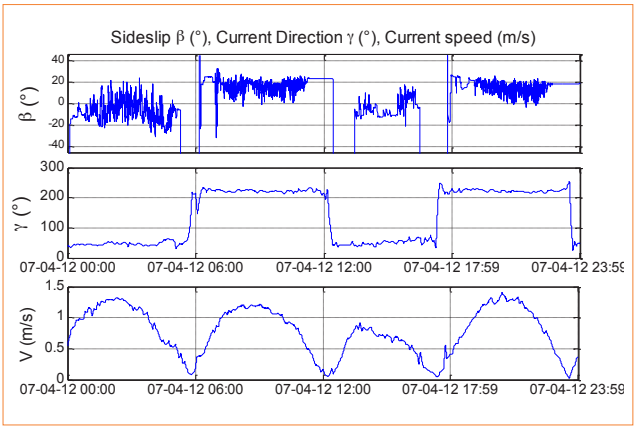

FIGURE 28 Typical time histories of current velocity direction (γ) and magnitude (*V*) during one-day observation. Current relative direction with respect to the system longitudinal axis is also reported (sideslip β). Current direction (γ) represents the direction of the flow velocity with respect to the north

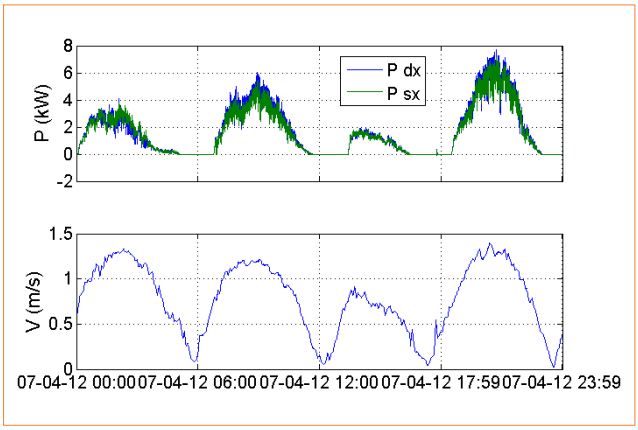

FIGURE 29 Generator power production of left and right turbines and current speed variation during the tide

The data have been recorded on board and radio-transmitted to a remote server. An acoustic speed sensor (ADCP) has been installed in proximity of the GEM to reconstruct the current velocity profile for the whole depth range. Typical measured data are reported in Figure 28.
Figure 28 shows a typical reversing pattern, characteristic of tidal current, whereas Figure 29 shows both produced electrical power and current speed during the day.

Experimental results

The power was measured for both the GEM turbines and is reported as a function of the measured speed in Figure 30. In order to better analyze the power performance, a binning procedure has been used (data are grouped in velocity bins over which an arithmetic mean is performed). The power curves for the right turbine after binning procedure and estimated shaft power are reported in Figure 31. As a reference, theoretical cubic power curves are also reported for a fixed power coefficient.

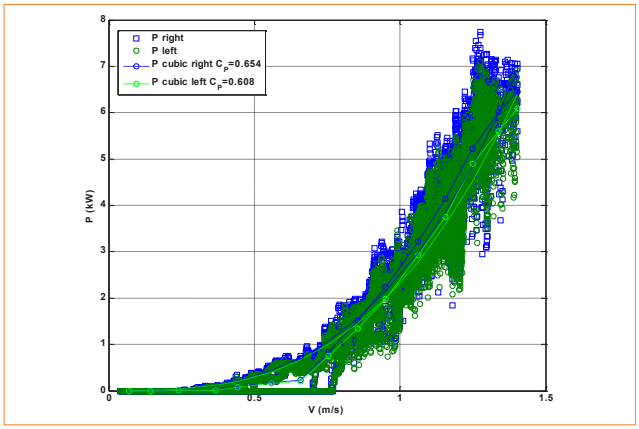

FIGURE 30 Left and right turbine power curve (best incoming direction)

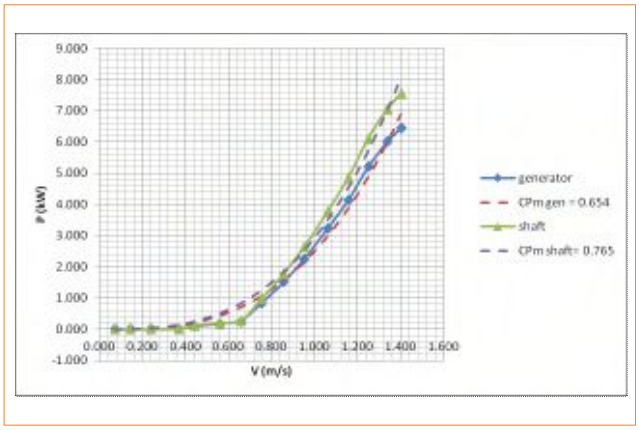

FIGURE 31 Power curve using binning technique. Right turbine. Electrical measured power compared to numerical estimated shaft power

Depth (range): 15 m to 9.8 m (without current)
Nominal power 100 kW with a tidal current of 2.6 m·s^{-1}
Three-blades 3 m diameter rotor
Innovating blade section profiles
Carbon blades - Fiberglass diffuser
Rated rotation speed: 65 rpm
Rotor Efficiency: 0.8
Expected average yearly production with 2.5 m·s^{-1} maximum
speed site: ~ 300 MWh

TABLE 9 Performance and technical data

The power coefficient may be estimated from the electrical measured power and has a value in the range $C_{P,max}$ = 0.6–0.65. Assuming an efficiency of the generator of 0.9 and a gearing efficiency of 0.9, a rough estimation of the shaft power coefficient may be obtained in the range $C_{P,max}$ = 0.75–0.8, which is in good agreement with previous model testing.
It has to be noted that the values of the power coefficient apparently exceed the Betz limit but this is obviously due to the presence of the diffuser. For details on Betz limit and diffuser augmented power coefficient, see, for example, [7]. To give an idea of the potential of a prototype of the same dimension deployed in a more energetic site, in Table 9 a list of characteristics for a prototype of a rated power of 100 kW at current speed of 2.6 m s^{-1} is reported.
Finally, inclinometers have been used to estimate the roll and pitch angle of the system that shows a relatively small oscillation around the levelled position, as expected for symmetry of the system.

Conclusions

Results of test campaigns of GEM model components in wind tunnel and towing tank, small-scale model in towing tank and full-scale prototype in a real sea site have been presented and discussed. The advantages of using shrouded turbines have been shown since the power coefficient doubles its value relative to bare turbine. Both model and full-scale prototypes have also shown static and dynamic stability and good performances, also under yawed flow condition.
The GEM system can represent a real breakthrough in the field of harnessing marine current energy thanks to its characteristics of easy deployment, no visual impact, reduced maintenance and operational costs as well as high performance, as proven in the present paper.

Acknowledgments
GEM has been patented by Dr. Nicola Giorgio Morrone and Prof. Domenico Coiro

Domenico P. Coiro, Nadia Bizzarrini, Giuseppe Calise
University of Naples "Federico II", Department of Industrial Engineering – Aerospace Division, Italy

Giancarlo Troise, Ferdinando Scherillo
SEAPOWER Scarl, consortium with University of Naples "Federico II", Italy

references

[1] D.P. Coiro, Development of Innovative Tidal Current Energy Converters: From Research to Deployment, Asian Wave and Tidal Energy Conference (AWTEC 2012), Jeju, South Corea, June 2012.

[2] D.P. Coiro, G. Troise, F.Scherillo, Design, towing tank test and deployment of full-scale GEM, a novel tethered system for harnessing tidal energy, Asian Wave and Tidal Energy Conference (AWTEC 2012), Jeju, South Corea, June 2012.

[3] F. Scherillo, U. Maisto, G. Troise, D.P. Coiro, S. Miranda, Numerical and Experimental Analysis of a Shrouded Hydroturbine, Clean Electrical Power International Conference (ICCEP), 14-16 June 2011.

[4] S. Mertens, Wind turbine in the built environment, in *Multi Science*, p. 99, Essex, 2006.

[5] O. De Vries, Fluid dynamic aspects of wind energy conversion AGARDograph No. 243 NLR.

[6] R. Tognaccini, Lezioni di Aerodinamica dell'ala rotante Lectures notes, Università degli studi di Napoli Federico II, 2008.

[7] G.J.W. van Bussel, The science of making more torque from wind: Diffuser experiments and theory revisited, in *Journal of Physics: Conference Series*, 75, 2007.

Numerical and tank tests of a pivoted floating device for wave energy

In this paper a system for extracting energy from waves is presented. The present work deals with numerical and experimental tests on a scaled model, performed in the DII towing tank facility. The device is made up of a floating body, which oscillates due to waves, and of a linear electromechanical generator. The electromechanical generator, based on ball-bearing screw, is linked both to the buoyant body and a fixed frame, converting relative movements of its anchor point in electrical power. Numerical analyses on such device have been performed in order to evaluate critical parameters for the system optimization, including analytical study of the system, potential flow and computational fluid dynamics (CFD) simulations, based on Reynolds Averaged Navier-Stokes (RANS), as well.

DOI: 10.12910/EAI2015-039

D.P. Coiro, G. Troise, G. Calise, N. Bizzarrini

Introduction

The new trends in the field of renewable energy are to enhance the extraction of energy from waves. This kind of renewable source represents an interesting field of investigation for its numerous recognized advantages: these are related to its relatively limited environmental impact and more predictable behavior with respect to other energy sources, making it a very attractive feature for energy systems design. In particular, ocean waves often show relatively repeatable amplitude and frequency characteristics, which depends on the specific installation site.

In the design of wave energy system, many configuration parameters are involved: buoyant body shape, overall system arrangement and conversion system device are some important key-features. This kind of system is mainly intended for installation in suitable sea coastal areas. Generally speaking, operating principle ensures ease of construction and operation; but, on the other hand, an adequate conversion system has to be developed for converting floating body movements into electrical power.

This work refers to an innovative configuration of such kind of devices, based on an available suitable body shape. The overall system arrangement effects are analyzed in order to optimize the power extraction from waves. In this work, a study of the power performance characteristic of a small-scale model of the system, under different operating conditions, will be presented.

As a starting point, an analytical study for extracting kinematic operating laws is carried out; then, computer-aided simulations are performed, both potential flow and Reynolds Averaged Navier-Stokes (RANS). At the end, several towing tank tests are performed to verify data from simulations, better tune-up the engineering process, and investigate other device arrangements as well.

Contact person: Domenico P. Coiro
coiro@unina.it

Wave energy conversion system

In this section, an overall description of the system operating principle will be developed. In Figure 1, the two main configurations investigated are presented: in rest condition, the horizontal arms configuration has the generator, here named PTO (Power Take-Off) device, perpendicular both to arms and free water surface; conversely, the inclined arms configuration, at rest, has the PTO approximately perpendicular only to arms. The rotation of the body is possible thanks to two hinges which are, respectively, above and below the water free surface. During the free motion of the body, the angle between arms and PTO direction changes with respect to perpendicular condition.

The dynamic behavior of the system may be described by the use of a 1 DOF equation, that is the equilibrium of moments around the hinge axis:

$$I\ddot{\theta} + B\dot{\theta} + K\theta = M_{ext} + M_{PTO} \quad (1)$$

where:

- I is the rotational inertia around the hinge axis, also accounting for the hydrodynamic added mass;
- B is a linear damping coefficient, accounting for part of the radiation force and which should also include the viscous contribution;
- K is a coefficient related to hydrostatic stiffness;
- M_{ext} is the external moment due to waves;
- M_{PTO} is the moment due to the point-pivoted PTO.

The PTO system was simulated during experiments by means of a controlled pneumatic actuator. The selected PTO system was controlled so as to produce a force response proportional to velocity variations (Eq. 2).

$$P_{inst} = \vec{F}\ \vec{V} = K\vec{V}\ \vec{V} \quad (2)$$

The coefficient K may influence the performance of the system in response to waves and it has become a key parameter for the choice of the electrical conversion system. This parameter may be set to a desired value through a controllable gain, via the actuator control software, in order to test different operating conditions and estimate the optimal condition for power production.

The system power production performances are also evaluated, measuring the PTO's anchor point displacements by means of a potentiometer, and PTO's axial force by means of a load cell: then, the power is indirectly estimated as product of force times velocity. Incident waves are measured by ultrasonic probes. Then, all these measurements are collected and compared with numerical results.

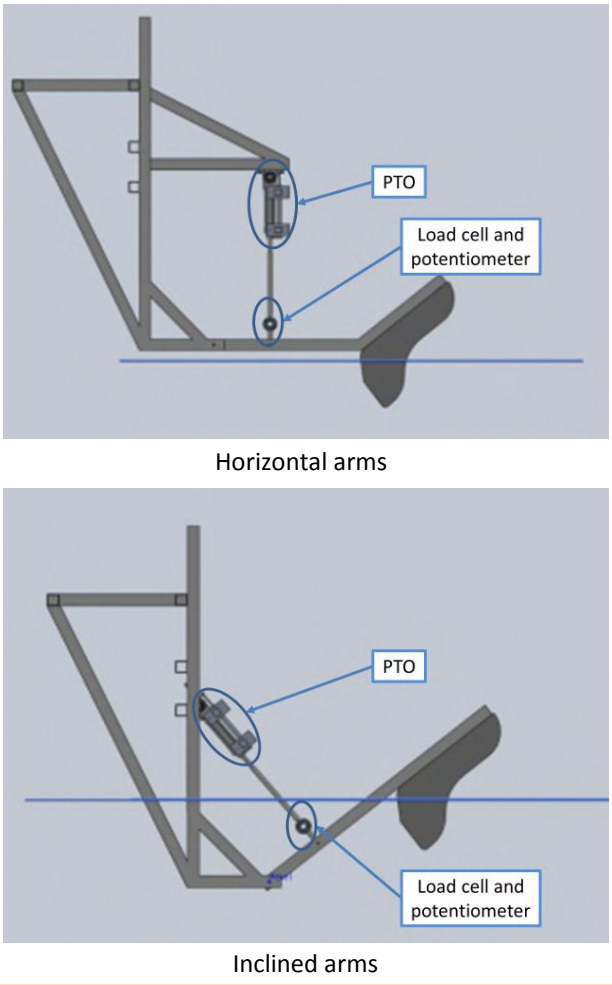

FIGURE 1 Two tested configurations

Towing tank experimental tests

Experimental towing tank tests were made in the facility available at the Department of Industrial Engineering – Naval Div. of the University of Naples. This facility has a wave generator capable of producing waves with variable frequency and amplitude. The wave tank has a length of 140 m, depth of 4.5 m and width of 9 m. For all tests performed, deep water assumption can be made. The main properties of the tested model (Fig. 2) are listed in Table 1.

Preliminary tests

Some preliminary verification tests were performed in order to determine the effective inertial characteristic of the body and to investigate the effect of hinge friction, which has been considered negligible. Hinge friction measurements have been performed using the buoy as a pendulum, suspended around its hinge axis. Buoyant movements around its equilibrium positions have been measured by a distance-laser measuring system and a typical linear decay in the amplitude oscillation has been observed.

Coulomb friction coefficient, from the observed decaying oscillations, has been evaluated even with different weights added to the buoy. The estimated hinge friction torque was is in the range 1.2-2.1 N m, acceptably small for the purposes of the tests even if not negligible.

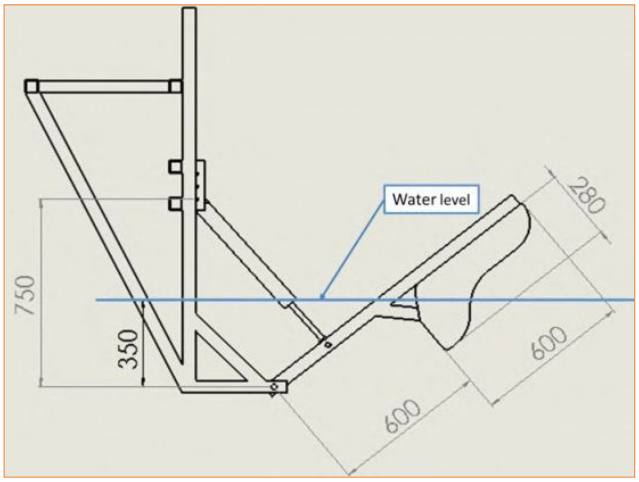

FIGURE 2 Tested model main properties

Scaled Model Properties		
Body height	0.60	m
Body width	1.00	m
Body weight	32.50	kg
Hinge moment (Body + arms)	21.65	Kg·m²
Draft	0.20	m
Body section@water level	0.210	m²
Immersed volume	0.0325	m³

TABLE 1 Scaled Model Properties

Free response from a non-equilibrium initial condition

In this kind of tests, the PTO is not yet installed and response of the system is measured by a potentiometer. The system has been slightly moved from its initial rest condition and kept free to move, for recording the damped response. From response data, in terms of angular displacement, the damping ratio and the damped oscillation period have been estimated, from the exponential decay of the damped free response and from the inertial properties of the body. These results were compared to a simple mass-damper model of similar characteristics (Fig. 3), as well.

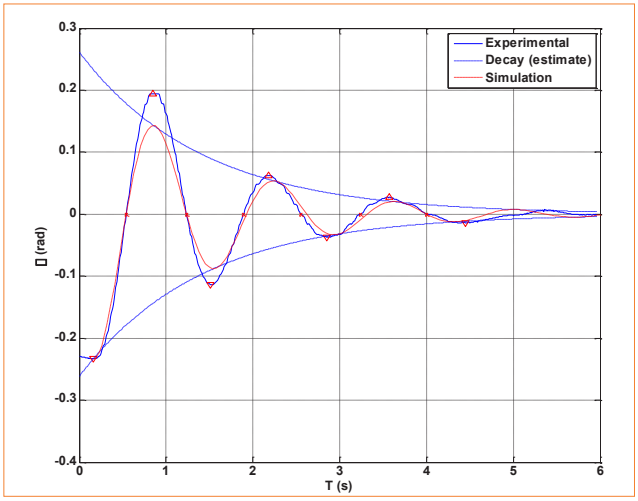

FIGURE 3 Free response test of the floating system (hinged buoy oscillation angle time history)

	Damping ratio	Natural frequency	Added inertia	Damping coefficient (around hinge axis)
	ζ (-)	f_n (Hz)	I_a (kg·m^2)	B (N·m·s·rad^{-1})
Mean	0.156	0.767	20.1	62.8
Std. dev.	0.012	0.020	2.146	5.267

TABLE 2 Damping response characteristics (mean values)

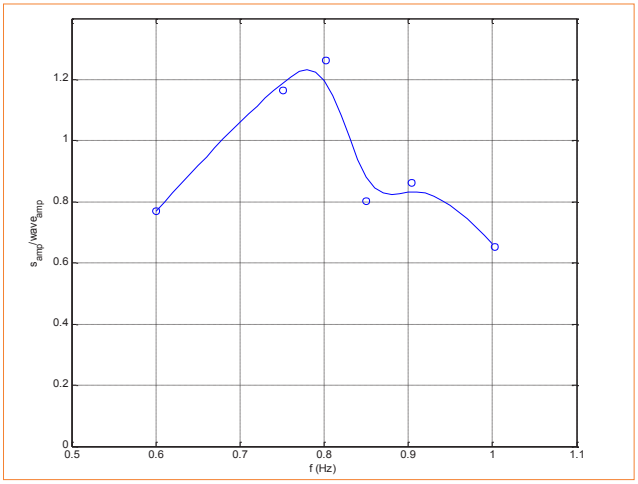

FIGURE 4 Response operator as piston displacement/wave amplitude ratio, as a function of wave frequency for 3 cm wave amplitude tests (Circles refer to direct experimental results, while the continuous line is a fitting curve)

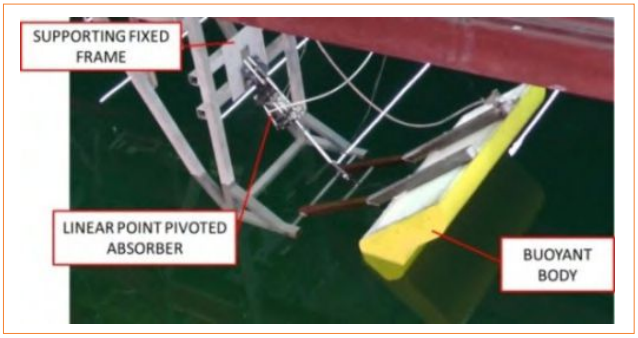

FIGURE 5 Scaled model for towing tank tests

From these data, other useful information was inferred such as the added inertia or the hydrodynamic damping. Some troubles have been observed in matching the simulated and observed response and these difference may be imputed to the lack of perfect control in the initial conditions imposed in each experimental test: indeed, the system was manually displaced from the equilibrium position and the effective starting conditions was not perfectly controlled, even if the overall behavior is correctly predicted. On the other hand, the oscillations are highly damped and the number of observed damped cycles is relatively small, reducing the number of data available for estimation. The mean value of the estimated parameters from all the performed tests is reported in Table 2.

System response to waves without PTO device

Under waves, the system has been tested under different wave amplitude and frequency conditions. The waves generated were sinusoidal.

A response amplitude operator (RAO) for the system has been experimentally estimated, dividing the linear displacement of the attachment point of the buoy (measured by the potentiometer) by the wave amplitude. These tests have also been performed only with the potentiometer (without PTO). Data collected, in terms of RAO (Fig. 4), show an amplitude peak in the range 0.75-0.8 Hz, in good agreement with free response test results.

Determination of PTO coefficient

In these tests, time histories of the instantaneous power were recorded under both different wave conditions (amplitude and frequency) and different values of the proportionality coefficient *K*. Both configurations in Figure 1 have been tested. The inclined arms model used during tests is shown in Figure 5. The two configurations allow to understand the effect of combined vertical and horizontal components of the forces from waves. The part of the body subject to hydrodynamic interaction is held approximately constant in both configurations. Two different types of actuators have been used during tests: a controlled pneumatic four-quadrant

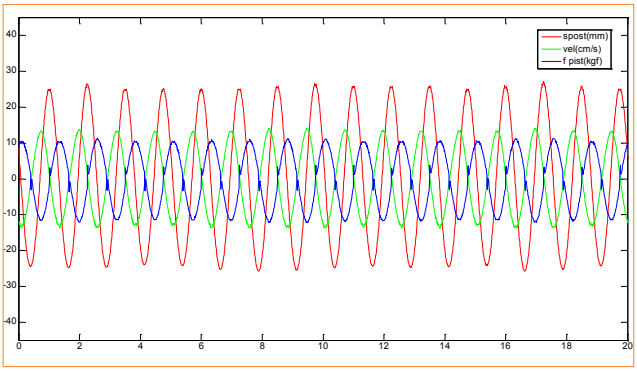

FIGURE 6 Time histories of measured quantities in a typical test: PTO piston displacement (red), piston force (blue), piston velocity (green). Amplitude A = 5 cm, Frequency f = 0.8 Hz, piston force-speed gain K = 800 N s m^{-1}

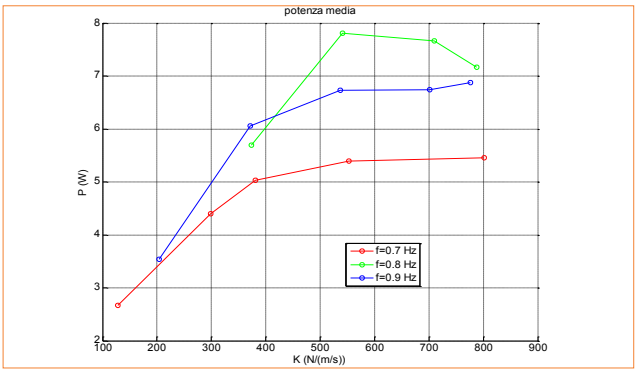

FIGURE 7 Experimental mean power as a function of piston force-speed gain for different incident wave frequency (5 cm wave amplitude). Inclined arms configuration (with better performance)

actuator, used as a damper, and a passive electric linear generator. A typical set of measured data is reported in Figure 6.

Different tests have been performed using different wave amplitude and frequency and varying the PTO gain *K*, in order to identify optimal conditions for energy conversion. The maximum allowable gain *K* was limited to about 800 N s m^{-1}. Results are shown in Figure 7 and Figure 8 in terms of mean power. Each point in the figure corresponds to a single test.

For the inclined arms configuration, power output

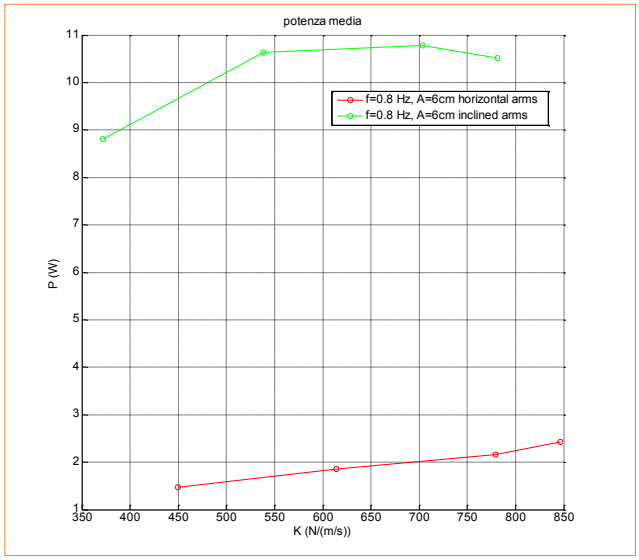

FIGURE 8 Experimental mean power as a function of piston force gain for fixed incident wave frequency (0.8 Hz) and wave amplitude (6 cm). Comparison of inclined arm configuration (green) with the horizontal one (red)

shows a peak for wave frequency in proximity to system natural frequency; max power output is at a value of the gain *K* of approximately 600 N s m^{-1}. For the scaled model, the power peak value is about 8 W for incident wave amplitude of 5 cm.

The two tested configurations have shown very different behaviors. The inclined arms configuration seems to be more effective in energy conversion. Probably this is due to the effect of the horizontal component of the hydrodynamic action which, in the inclined arms case, gives a favorable contribution to the moment around the hinge axis (the effective vertical distance between hinge axis and center of buoyancy is greater).

Wave breaker effect

A wave breaker behind the buoyant system was introduced to verify coastline effects. A small number of tests have been performed to investigate its effect and in only one configuration, with the wall mounted at a distance of about 2 m from the hinge axis. As inferred from results, it seems that the horizontal arm configuration was relatively more sensitive to the presence of the wall. The wave breaker influence

strongly depends on the wavelength of the incident wave: the augmented power output is a consequence of a stationary wave system which is established in front of the wall itself and, if the floating body is placed at a peak point in the stationary wave pattern, the power output may be significantly amplified. However, further investigations are needed.

Potential flow simulations

Potential flow simulations have been performed by the use of a boundary elements code. The dynamic response of the system due to waves is evaluated by estimating the hydrodynamic coefficients and solving the equation of motions. Physical constraints have been simulated as well. Both configurations have been tested and, for each wave frequency, added mass, radiative damping, diffractive and Froude-Krylov forces were recorded.
Numerical preliminary analyses, similar to experimental ones, were performed and free response of the system was evaluated to identify its natural frequency. At a second stage, the PTO effect, by means of its force on the anchor point, was introduced into numerical analyses. Then, other simulations were performed using wave conditions similar to tests for comparing the electrical power

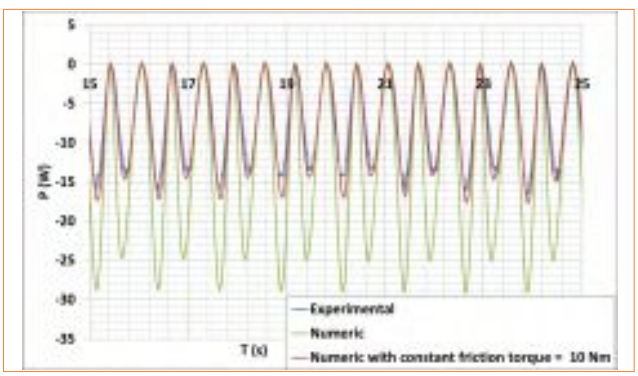

FIGURE 9 Numerical [potential theory] - experimental comparison. Instantaneous power time histories. [A = 0.05 m, f = 0.8 Hz, K =~570 N s m^{-1}]. In red the simulation with a fictitious constant friction torque of 10 N m added

output. The overall dynamic behavior of the numerical model resulted qualitatively similar to the tested ones, in terms of both motion and forces.
Numerical potential flow data have shown a good agreement with experimental tests, regarding the value of natural frequency and wave frequency for max power (both mean and instantaneous); but, absolute values of the electrical power output are almost twice those of the tests. This is probably due to an overestimation of the buoy velocity, since viscous effects were not accounted in this kind of simulations. Viscous actions may be accounted into the simulations, introducing a fictitious friction torque around the hinge axis: for some numerical analyses, a value of 10 N m has been used. Using such a constant friction action, the output power is reduced and the matching with experimental values is improved, as can be seen in Figure 9.

Performance optimization

For its quickness and suitability, the potential flow solver can be used for implementing an optimization procedure. Some geometrical parameters, identified as critical, mass and immersed volume were changed in order to increase the power extracted from waves. For optimization, each parameter can change in a preset range and a cost function is properly defined. Two different algorithms were used such as NSGA-II and SIMPLEX. Unfortunately, not all the optimization cases were successful, probably due to meshing problem; moreover, only a part of successful ones are feasible.
Optimizations were made on the full-scale model, by means of potential flow solver, and results are summarized in Table 3. In the first attempt, the buoy shape was modified changing only one geometric parameter, a frontal fillet radius of the buoy lateral profile, in addition to mass and PTO coefficient. Despite some fluctuations, results have shown a moderate increment of the average output power. The second attempt was made changing two fillet radiuses, mass and PTO coefficient. In this condition, only a small further increment of the average output is reached. Anyway, the most valuable contribution to power output enhancement seems to be related to the variation of the immersed volume and of the piston force gain. The

	Average Power P_{avg} (kW)	Mass M (kg)	Fillet Radius #1 R_1 (m)	Fillet Radius #2 R_2 (m)	PTO Coefficient K ($N \cdot s \cdot m^{-1}$)	Submerged Volume V_{sub} (m^3)
base	6.2	3780	1.00	0.800	$5.0 \cdot 10^5$	4.00
1	7.4	6940	1.70	-	$8.3 \cdot 10^5$	7.40
2	7.8	7275	1.92	1.433	$7.6 \cdot 10^5$	7.70
3	6.2	3365	1.00	0.810	$3.9 \cdot 10^5$	3.52

TABLE 3 Optimization results: best cases

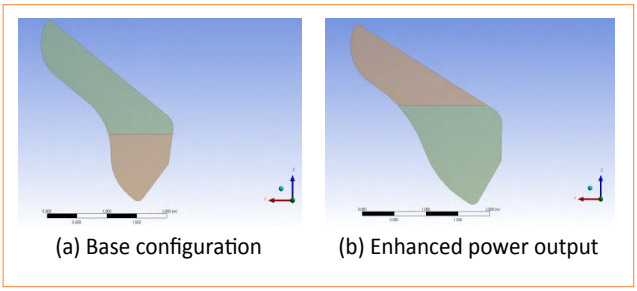

(a) Base configuration (b) Enhanced power output

FIGURE 10 Comparison of optimization results. (The final immersed volume is increased from 4 m^3 to 7.7 m^3)

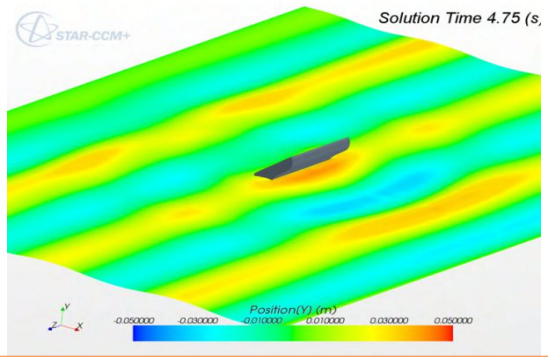

FIGURE 11 Typical RANS simulation screenshot

last try was made searching for the maximum specific power (P_{avg} divided by the submerged volume V_{sub}). In these first attempts, no effective increment in the power output is reached, even if the initial immersed volume is reduced, and the geometric parameters tend to remain very close to the base configuration (Fig. 10).

Reynold-Averaged Navier-Stokes simulations

Computational Fluid Dynamics (CFD) simulations, based on Reynolds-Averaged approach (RANS), were performed on the buoy, without considering supporting arms. CFD was used in the attempt of considering viscous effects as well. Only half of the real physical domain was considered, exploiting the symmetrical properties of the problem. A simulated towing tank was created, in which the buoy can rotate around a simulated hinge: the overlapping mesh approach was used to let the buoy rotate. Mesh sensitivity analysis was done, and a mesh of about 6 million cells, which ensures sufficient accuracy and less CPU time, was chosen. Despite this, each CFD simulation had required about two days on a 64 CPUs device, also for the use of computationally expensive physical models such as Volume-Of-Fluid (VOF) two-phases physics and turbulence model.
RANS simulations (Fig. 11) seemed to reproduce well the overall system dynamics as observed during tests. However, some data from CFD was not in agreement with experimental data. Results of free-response simulations had shown an underestimation of the natural frequency. Data from simulations under wave actions had revealed that maximum power values, both instantaneous and average ones, will occur at the natural frequency predicted by CFD, but it is quite different with respect to reality. Sensitivity of the model about inertia and boundary condition was also analyzed without significant effects. The introduction of other frame structural elements, such as supporting arms, did not produce relevant modifications to critical system parameters.

The PTO system was also accounted in simulations using the Eq. 2: velocity, normal to the supporting arms, is continuously updated during the simulation as the counteracting PTO's action. Then, sensitivity analyses about K were performed in order to determine its value for higher power extraction.
In the light of this, further investigation has to be made in order to understand how to tune-up and troubleshoot RANS simulation.

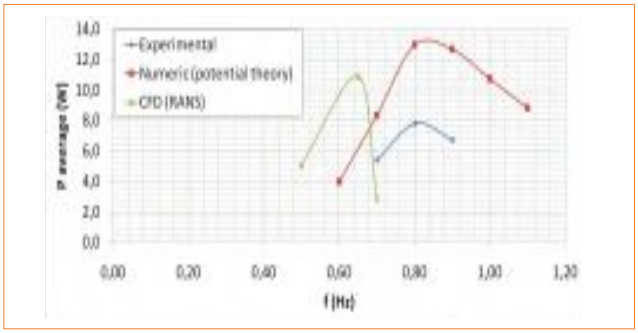

FIGURE 12 Experimental-numerical comparison (5 cm wave amplitude, K ≈ 600 N s m^{-1})

Final remarks

In [2] there are some insights about the definition of the capture width ratio (*CWR*) as:

$$CWR = P_{avg} / P_{wave}\, B \qquad (3)$$

where B is the width of the body, P_{avg} the cycle average power output and P_{wave} is the power amount enclosed in the wave. Based on *CWR*, the scaled model shows that for a maximum average power of about 7.8 W with at 5 cm wave amplitude, a *CWR* of about 0.65 is reached.
The results here presented, for both numerical analysis and experimental tests on a scale model, represent a suitable base for further investigation. Even if, comparing numerical data with experimental ones, some differences are present (Fig. 12), it can be stated that operating frequency of resonance is captured fairly well by potential flow simulations, but maximum power and average power are significantly overestimated. On the other hand, the peaks of power predicted by RANS simulations are slightly closer to experimental values.
Finally, a tentative optimization procedure has been developed in order to search for an enhanced geometric configuration, using the potential flow solver for its reduced computational cost. Therefore, with all the data and methods developed during this work, it is possible to define a reliable method for predicting performance and designing a wave generator full-scale system, or optimizing an existing device. Just to make an example, 5 m wide full-scale prototype with rated power of 60 kW, deployed on West coast of Sardinia in Italy, is capable of producing about 150 MWh of energy per year with an estimated average cost per kW installed of about 2500 Euro.

Acknowledgements
This work has been done in cooperation with Umbra Group company (www.umbragroup.it), which has sponsored the research.

Domenico P. Coiro, Giuseppe Calise, Nadia Bizzarrini
University of Naples "Federico II", Department of Industrial Engineering Aerospace Division, Italy

Giancarlo Troise
SEAPOWER Scarl, consortium with University of Naples "Federico II", Italy

references

[1] M. McCormick, Ocean Engineering Wave Mechanics, Wiley-Interscience, 1973.
[2] M. McCormick, Ocean Wave Energy Conversion, Dover Publications, 2007.
[3] G. De Backer, Hydrodynamic Design Optimization of Wave Energy Converters Consisting of Heaving Point Absorbers, Ghent University, 2009.
[4] H.O. Berteaux, Buoy Engineering, Wiley-Interscience, 1976.
[5] T. Matsuoka, K. Omata, H. Kanda, K. Tachi, A Study of Wave Energy Conversion Systems Using Ball Screws - Comparison of Output Characteristics of the Fixed Type and the Floating Type, Proceedings of The Twelfth International Offshore and Polar Engineering Conference, 2002.
[6] O.M. Faltinsen, Sea loads on ships and offshore structures, Cambridge University Press, 1990.
[7] G. Payne, Guidance for the experimental tank testing of wave energy converters, SuperGen Marine, 2008.
[8] CD-adapco, User Guide STAR-CCM+ version 7.06, 2012.

Stochastic control applied to the ISWEC Wave Energy System

ISWEC (Inertial Sea Wave Energy Converter) is a floating marine device able to harvest sea waves energy by the interaction between the pitching motion of a floater and a spinning flywheel which can drive an electric PTO. In the ISWEC the hull dynamics is governed and controlled by the gyroscopic torque. The optimal control logic results in tuning the floater dynamics to the incoming waves in order to maximize the power transfer from the waves to the floater. In this paper the control problems of the ISWEC are stated and a control scheme based on the sub-optimal stochastic control logic is presented. The control scheme here presented has been tested using real wave records acquired at the deployment location in Pantelleria Island, which is one of the most energetic sites of the Mediterranean Sea.

DOI: 10.12910/EAI2015-044

G. Bracco, M. Casassa, E. Giorcelli, M. Martini, G. Mattiazzo, B. Passione, M. Raffero, G. Vissio

Introduction

In the last two centuries many Wave Energy Converters (WECs) have been proposed to harvest the huge amount of power coming from sea waves. Nowadays, few of them are reaching a pre-commercial stage [1]. In fact, a number of problems must be solved in order to make this technology competitive [2]: the optimization of the control strategy is crucial to ensure efficient performance. The ISWEC belongs to the gyroscopic converters type, which owes its origins to Stephen Salter, who proposed the Duck device at the University of Edinburgh in the 1970s [3, 4]. Gyroscopes were initially used in marine applications for roll stabilization [5, 6]. In wave energy harvesting, the basic principle is the same, but the energy direction is opposite, as the gyroscopic torque is induced by the incoming waves and exploited by the electrical PTO. The gyroscopic technology is particularly suitable for closed seas, which are characterized by wave frequencies higher than the oceanic ones. From the viewpoint of the control, the ISWEC can exploit the gyroscope for two different control logics: the flywheel spinning velocity can be tuned to match the forecast sea state (mid-term control), while the PTO torque is controlled in real time to exploit the incoming wave. On the one hand, this may result in a more efficient energy extraction, but on the other hand the control strategy becomes more critical.
In this paper, after a brief presentation of the ISWEC working principle and its governing equations, a performance analysis is carried out based on the physical characteristics of the full-scale prototype. The stochastic control algorithm has been tested using real wave records representative of the installation site. The results are compared with a linear reactive controller, showing a 30% average increment in productivity. Finally, the influence of some parameters such as the hull mass constraint is evaluated.

Contact person: Giovanni Bracco
giovanni.bracco@polito.it

The ISWEC

The ISWEC [7,8] is a wave energy converter designed to exploit wave energy through the gyroscopic effect of a flywheel. The system is enclosed in a sealed hull retained by a slack mooring line. From the outside, it looks like a moored boat (Fig. 1). The core of the device is the gyroscopic system.
Figure 2 shows the three main components of the gyroscopic system: the flywheel (red), the gyro structure (blue), the PTO (green). To describe the system dynamics, two reference frames have to be introduced. The first, the green one, is fixed to the hull and its axes are x, y, z. The second, the blue one, is fixed to the gyro structure and its axes are x', y', z'.

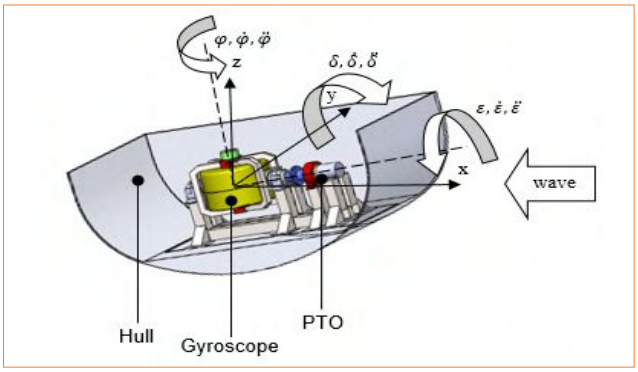

FIGURE 1 ISWEC scheme

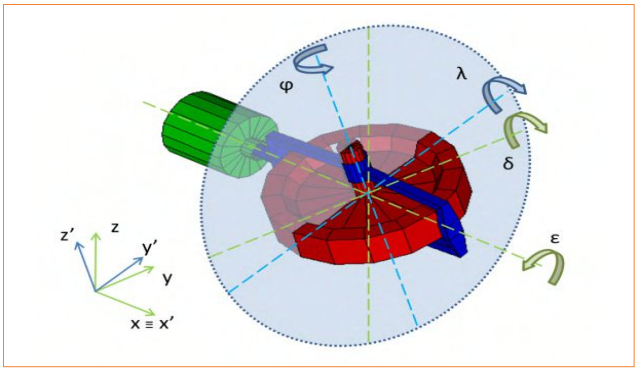

FIGURE 2 Gyroscopic system composed by the flywheel, structure and generator

Note that the origins of such reference systems are coincident with the flywheel center of gravity, so the gyro structure rotates around the PTO axis that matches the x axis. The x axis is oriented towards the bow, corresponding to the wave direction, while z is the vertical axis. The hull rotates around the y axis with the induced pitching motion δ due to the wave-floater-gyro interaction. As the flywheel rotates with angular speed $\dot{\varphi}$, its movement generates a gyroscopic torque around the x axis. The PTO exploits such torque to produce electrical power.
The ISWEC is characterized by several advantages. First, every mechanical moving part is enclosed into the sealed hull, so there is little risk of both environment contamination and components corrosion. This characteristic allows to achieve high reliability and reduced maintenance. From a technical point of view, the flywheel speed is a control parameter that can be exploited to optimize the coupling between the ISWEC and sea waves, and consequently broaden the power generation capability of the WEC.

System equations

The device involves two main phenomena: the hull hydrodynamics and the mechanics of the gyroscope. There is a significant coupling between them due to torques and energy interactions.

Gyroscope equation

From the derivation of the flywheel angular momentum, the equation of the motion around the x axis is:

$$I\ddot{\varepsilon} + (I - J)\dot{\delta}^2 \sin\varepsilon\cos\varepsilon + T_\varepsilon = J\dot{\varphi}\dot{\delta}\cos\varepsilon \qquad (1)$$

where T_ε is the generator torque and can be either braking or driving, depending on the control scheme. There are two more equations to describe the gyro effect: the equation of motion around the z' axis (2) and the one around the y' axis (3):

$$J\left(\ddot{\delta}\sin\varepsilon + \dot{\varepsilon}\dot{\delta}\cos\varepsilon + \ddot{\varphi}\right) = T_\varphi \qquad (2)$$

$$I\ddot{\delta}\cos\varepsilon + (J - 2I)\,\dot{\varepsilon}\dot{\delta}\sin\varepsilon + J\dot{\varepsilon}\dot{\varphi} = T_\lambda \qquad (3)$$

The T_φ torque acts on the flywheel, has a zero mean and a small value [8], so the system involves only a small

gyro speed oscillation. The T_λ torque has a key role in the system behavior: its projection on the vertical axis z is a yaw moment, while the projection on the horizontal axis y is the pitch moment T_δ. The latter can be written as:

$$(Jsin^2\varepsilon + Icos^2\varepsilon)\ddot{\delta} + J\ddot{\varphi}sin\varepsilon + \\ + J\dot{\varepsilon}\dot{\delta}\cos\varepsilon + 2(J-I)\dot{\varepsilon}\dot{\delta}\sin\varepsilon\cos\varepsilon = T_\delta \quad (4)$$

Hull equation

The hull hydrodynamics is described by six second-order linear differential equations, one for each degree of freedom [9]. They can be written in the following matrix equation, where the variable X groups the three positions and the three rotations of the rigid body expressed in the hull reference frame x, y, z:

$$\big(M + A(\omega)\big)\ddot{X} + B(\omega)\dot{X} + KX = F_W + F_G + F_M \quad (5)$$

The first term multiplies the acceleration vector and is composed by the mass matrix of the body M and the added mass $A(\omega)$ due to hydrodynamic forces. The second term $B(\omega)$ takes into account the hydrodynamic damping due to radiation forces. The last term in the left-hand side of the equation multiplies the position and is composed by the hydrostatic stiffness K. On the right-hand side of the equation the external forces acting on the rigid body are indicated: F_W due to waves excitation [9], gyroscopic forces F_G calculated with gyroscope dynamics (1), (3) and mooring forces F_M at this stage modeled simply as linear stiffness.

Control

WEC control

In this section, a review of the existing control algorithms for wave energy converters is given, so that the reader can have an overview of the state of the art in this field. In most cases, when analyzing the power extraction capabilities of a WEC, a one-degree-of-freedom system is analyzed. In the simplest case the hydrodynamic model of the device may be approximated by a second-order linear differential equation where coefficients are frequency dependent. Often, the first step is to develop a control strategy able to maximize the power output under plane (2D problem), monochromatic waves. Of course, this means that the wave profile is composed of a single frequency contribution and this is not what happens in the real sea state. Afterwards, the case of plane, polychromatic wave is analyzed, generating a wave time series based on the spectrum of a specific sea state, or using acquired wave data. In the most recent studies, a 3D sea state is analyzed taking into account wave contributions coming from different directions.

An emblematic example may be represented by the latching/declutching controller that has been firstly proposed for a heaving body by Falnes *et al.* [10]. This strategy is particularly suitable for waves longer than the WEC natural period; it basically consists in locking the floating body when its velocity approaches the zero value, by means of a clamping mechanism, and then releasing it at some point so that its velocity and the wave force will be at their highest point simultaneously; at this point the PTO force is set to its maximum value. The action on the system can thus be regarded as binary, that is either the body is locked, or moving under maximum PTO action - thus resulting in a highly non-linear control force. The declutching controller is similar to the previous one, but it is applied to waves shorter than the WEC natural period [11]. Differently from before, the floater is normally free to move and when its velocity reaches some desired value the maximum PTO force is applied.

The use of genetic algorithms indicated that, if applicable, the latching and declutching control is among the best control techniques for a wave energy converter, see Ringwood *et al.* [12]. A drawback of these strategies is that they need some kind of prediction of the incoming wave force, in order to actuate the device at the right time. Auto-regressive models and Kalman filters have been widely used in this context. However, these considerations apply to devices for which the control force is directly applied on the floater main degree of freedom, so that this could be locked or released at the desired time instant. The wave energy converter considered in this paper is not suitable for the implementation of this strategy, since in such a device it is not possible to lock/release the relative motion between floater and gyro at a desired time instant.

General considerations

In every energy converter the control strategy is of crucial importance in the whole system performance. The device needs to match the environmental conditions at best, in order to achieve the maximum power extraction taking into account the intrinsic physical constraints of the system. For the ISWEC, such constraints are represented by the torque and the power on the generator, and the flywheel speed specifications. The ISWEC control can be divided into two strategies characterized by different dynamics. The first one is a long-term control logic acting on the flywheel speed $\dot{\varphi}$, according to a rough forecast of the sea state. The second one is a short-term control logic consisting in tuning the PTO torque on the basis of a more precise evaluation of the incoming wave parameters. In both cases, a forecast algorithm is needed, and this topic has already been addressed by different authors (e.g. [13-15]). In this paper the study is carried out using acquired wave data.

Sub-optimal control

The control strategy here presented is based on the optimal control theory discussed in [16, 17] and its objective is to maximize the power transfer from waves to the floater in a wide range of sea states. The idea is to obtain a unidirectional power flow from the waves to the WEC. This goal is achieved by producing a control force able to compensate the floater dynamics and then damp its oscillations. It is possible to apply a linear hydrodynamic theory using the Cummins' decomposition [18] so, since the ISWEC is essentially a pitching device, equation (5) can be written for one DoF as:

$$\left(M_\delta + A_{\infty,\delta}\right)\ddot{X} + \int_0^t h_{r\dot{\delta}}(t-\tau)\dot{\delta}(\tau)d\tau + \\ + K_\delta \delta = F_{w,\delta}(t) - T_\delta(t) \tag{6}$$

From equation (6) it is clear that the gyroscopic reaction torque T_δ can be used as the control force, as it is the only variable that can be indirectly controlled. Assuming that all the state variables are deterministic quantities, it is possible to follow the analytical approach explained in [19], which leads to the optimal control torque that maximizes the mechanical energy absorbed from a given irregular sea state:

$$T_{\delta,opt}(t) = -\left(M_\delta + A_{\infty,\delta}\right)\ddot{\delta}(t) - \\ - K_\delta \delta(t) + \int_{-\infty}^{+\infty} h_{r\dot{\delta}}(t-\tau)\dot{\delta}(\tau)d\tau \tag{7}$$

This clearly results in a non-causal control law, depending on the future values of the velocity $\dot{\delta}$. Such problem can be tackled with two approaches. The first solution is to evaluate future $\dot{\delta}$ with a prediction algorithm of the incoming wave based on a stochastic autoregressive model [20] or on neural networks [21]. Another option is to replace the non-causal term with a closely related causal process, leading to a sub-optimal control.

$$\int_t^{+\infty} h_{r\dot{\delta}}(t-\tau)\dot{\delta}(\tau)d\tau \quad \rightarrow \quad 2b_c\dot{\delta}(t) \tag{8}$$

For the ISWEC, sub-optimal control has been chosen as a solution for the non-causality problem.

Since the irregular sea state is described by a spectrum, a stochastic approach is needed. It is legitimate to assume that the wave elevation can be regarded as a stationary zero-mean Gaussian process, and it is therefore possible to derive the optimal control law for known sea state conditions, using the linear stochastic dynamics theory [22, 23]. Under these assumptions, the pitching velocity and, in turn, the displacement and acceleration of the pitch DoF can be regarded as stationary zero-mean Gaussian, independent random processes.

For the sub-optimal control, assuming that all response processes are ergodic, the mean absorbed power becomes:

$$\bar{P}_a = E\left[T_\delta(t)\dot{\delta}(t)\right] = -(M + A_\infty)E\left[\dot{\delta}(t)\ddot{\delta}(t)\right] + \\ + 2b_c E\left[\dot{\delta}^2(t)\right] - E\left[K\dot{\delta}(t))\right] + \\ - \int_{-\infty}^{t} h_{r\dot{\delta}}(t-\tau)E\left[\dot{\delta}(t)\dot{\delta}(\tau)\right]d\tau \tag{9}$$

where the operator $E[\cdot]$ indicates the expected value. Applying the assumption of stationary process and the Wiener-Khinchin theorem, after some mathematical manipulation the equation for power becomes:

$$\bar{P}_a = \sigma_{F_e}^2\left(\frac{1}{2b_c} - \frac{1}{4b_c^2}\int_0^\infty h_{r\dot{\delta}}(u)\rho_{F_eF_e}(u)du\right) \tag{10}$$

where ρ_{FeFe} is the auto-correlation coefficient function of the wave excitation force process.

The maximum for the absorbed power function is finally found for a damping value of:

$$b_c = \int_0^\infty h_{r\dot{\delta}}(u)\rho_{F_eF_e}(u)du \qquad (11)$$

Therefore, once the sea-state and the hull hydrodynamic properties are known, it is possible to calculate the sub-optimal, unconstrained, stochastic value of the damping coefficient for the pitching DoF of the system.

Results and discussion

In the ISWEC device, one way to achieve the pitching torque for the sub-optimal control is by means of a velocity control on the PTO. As a matter of fact, there is a direct relationship between the gyroscopic reaction torque on the hull T_δ and the rolling speed $\dot{\varepsilon}$, so that a set value of the latter is defined for the linear gyroscope model:

$$\dot{\varepsilon}_{set} = \frac{T_{\delta,opt}}{J\dot{\varphi}} \qquad (12)$$

A closed-loop speed control is implemented acting on the PTO torque. Moreover, since the gyroscopic torque that acts as a disturbance on the PTO axis is known analytically, it is possible to add a feed-forward torque as:

$$T_{\varepsilon,ff} = -J\dot{\varphi}\dot{\delta} = -L\dot{\delta} \qquad (13)$$

The gyroscopic torque would force the PTO speed to deviate from its target value, and the feed-forward torque is used to cancel out this effect and improve the control. The resulting control system for the ISWEC device is shown in Figure 3, where k_P is the proportional gain of the closed-loop speed controller. It was necessary to introduce a relatively small stiffness k_R term in order to prevent position drifting in irregular wave conditions.

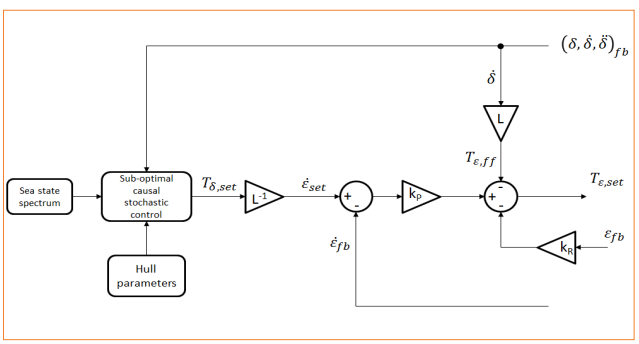

FIGURE 3 Closed loop optimal speed control for ISWEC

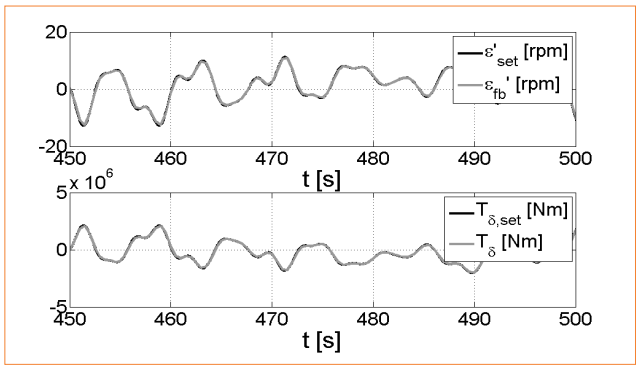

FIGURE 4 Set vs. feedback values for gyroscopic speed and torque

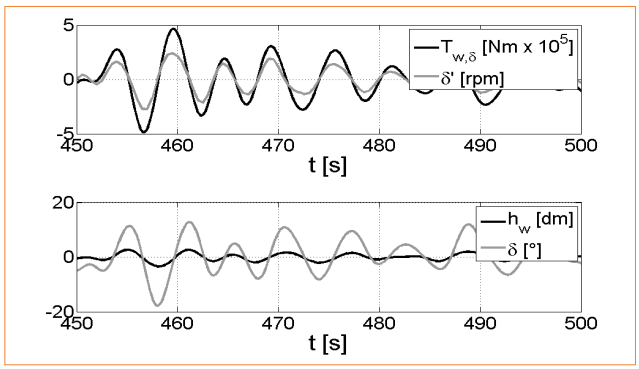

FIGURE 5 Wave force vs pitching velocity (upper plot); Wave elevation vs pitch angle (lower plot)

Notice that the hull parameters are known since they are characteristics of the device, while the sea-state spectrum is given by the weather forecast and by an on-board monitoring system that will be installed for the sea-state evaluation and prediction. Figure 4 attests the control loop efficacy, since the set and the actual values are perfectly overlapping.

The purpose of the sub-optimal control strategy was to force the response of the hull to be in phase with the excitation, meaning that their maxima occur at the same instants, as shown in Figure 5. Moreover, this implies that the power flux is always unidirectional from the gyroscope to the PTO, preventing the latter to act as a motor.

Conclusions

The discussion carried on so far in this paper highlights the main problems to face when a control strategy of a wave energy converter has to be designed. The first step is to define the level of approximation, hence the complexity, of the model, in particular dealing with the 2D or 3D sea state and regular or irregular waves. Among others, the latching and declutching control strategy gained reliability and nice performances, but it is not compatible with the ISWEC device, since it requires a direct control of the main degree of freedom. However, the same need of a prediction algorithm is present in the sub-optimal control used for the ISWEC. It is based on a stochastic description of the problem that leads to the definition of the stiffness and damping parameter of the control torque. The results show that the aim to put in phase the incoming wave with the gyroscope is perfectly accomplished. The accuracy and quality of this controller rely on the ability to forecast and predict the incoming wave in order to coherently tune the endogenous parameters to best match the exogenous ones.

Giovanni Bracco, Marta Casassa, Ermanno Giorcelli, Giuliana Mattiazzo, Biagio Passione, Mattia Raffero, Giacomo Vissio
Politecnico di Torino, Department of Mechanical and Aerospace Engineering, Italy

Michele Martini
Environmental Hydraulics Institute "IH Cantabria", Santander, Spain

references

[1] Electricity Innovation Institute 2004. Offshore Wave Energy Conversion Devices, E2I EPRI Assessment.

[2] M.J. French, On the difficulty of inventing an economical sea wave energy converter: A personal view, Proceedings of the Institution of Mechanical Engineers, Part M, in *Journal of Engineering for Maritime Environment*, 2006.

[3] S. Salter, Wave Power, in *Nature*, 1974.

[4] S. Salter, Recent Progress on Ducks, First Symposium on Wave Energy Utilization, Chalmers University of Technology, Gothenburg, Sweden, 30 Oct-1 Nov 1979, Proceedings, 1979.

[5] E. Sperry, The gyroscope for marine purposes, in *Trans. Soc. Naval Architects Mar. Eng.*, pp. 143-154, 1910.

[6] E. Schlick, The gyroscopic effect of flywheels on board ship, in *Trans. Inst. Naval Architects*, vol. 23, pp. 117-134, 1904.

[7] G. Bracco, ISWEC: a Gyroscopic Wave Energy Converter, LAP Lambert Academic Publishing, ISBN 9783848406524, 2012.

[8] M. Raffero, Design of a Wave Energy Converter-A case of application: ISWEC, PhD Thesis, Torino, 2014.

[9] J. Falnes, Ocean waves and oscillating systems, Cambridge University Press, Cambridge, 2002.

[10] J. Falnes, K. Budal, Wave-power conversion by point absorbers, in *Norwegian Maritime Research*, 6(4):2-11, 1978.

[11] P. A. P. Justino, A. F. De O. Falcao, Active relief valve for an OWC wave energy device, European wave energy conference, pp. 295-300, 2000.

[12] G.A. Nolan, J.V. Ringwood, W.E. Leithead, S. Butler, Optimal Damping Profiles for a Heaving Buoy Wave Energy Converter, Proc of the fifteenth International Offshore and Polar Engineering Conference, 2005.

[13] K. Fuat, Time domain prediction of power absorption from ocean waves with latching control, in *Renewable Energy*, 2010.

[14] M.P. Shoen, J. Hals, T. Moan, Wave prediction and robust control of heaving wave energy devices for irregular waves, in *IEEE Trans. Energy Convers.*, 2011.

[15] F. Fusco, J. Ringwood, A study on the Prediction Requirements in Real-Time Control of Wave Energy Converters, in *IEEE Transactions on Sustainable Energy*, 2012.

[16] R.E. Bellman, Dynamic Programming, Princeton University Press,1957.

[17] L.S. Pontryagin, The Mathematical Theory of Optimal Processes. New York: Pergamon Press, 1964.

[18] W.E. Cummins, The impulse response function and ship motions, David Taylor model basin, report 1661, Department of the Navy, Washington DC, 1962.

[19] S. Nielsen, Q. Zhou, M. Kramer, B. Basu, Z. Zhang, Optimal control of nonlinear wave energy point converters, in *Journal of Ocean Engineering*, 2013.

[20] F. Fusco, J. Ringwood, Short-Term Wave Forecasting for Real-Time control of Wave Energy Converters, in *IEEE Transactions on Sustainable Energy*, 2010.

[21] A.A.E. Price, A.R. Wallace, Non-linear methods for next wave estimation, Proceedings of the 7th European Wave and Tidal Energy Conference, Porto, Portugal, 2007.

[22] S. Nielsen, Linear Stochastic Dynamics, Structural Dynamics, vol. 3, Aalborg University, 2007.

[23] J. Li, Stochastic Dynamics of Structures, Wiley, 2009.

Wave Energy Converters based on Dielectric Elastomer generators: Status and perspectives

Dielectric Elastomers (DEs) are a very promising technology for the development of energy harvesting devices based on the variable-capacitance electrostatic generator principle. This paper discusses the potentialities of DE technology for advancing the ocean wave energy sector. In particular, three innovative concepts of wave energy converters with DE-based power take-off system are introduced and described.

DOI: 10.12910/EAI2015-049

M. Fontana, R. Vertechy

Introduction

Among the intermittent renewable resources, ocean-wave power is very persistent and highly spatially concentrated:

- The time-averaged wave-power intensity acting on an area placed just below the sea surface and lying perpendicular to the direction of wave propagation is typically between 2 and 3 kW m^{-2}; that is nearly four times larger than the average wind-power intensity acting on an area perpendicular to the wind direction and nearly ten times larger than the average solar-power intensity acting on a horizontal surface of the earth [1].
- Depending on the specific location, wave-power time-availability ranges between 35% and 70%; that is larger than the typical 30% of wind and 15% of solar resources [1, 2].
- Wave-energy predictability is very reliable within 2 or 3 days; whereas wind energy can be forecasted only within hours and solar-energy is almost unpredictable [2].

Similarly to off-shore wind, wave energy provides optimal matching between resource availability and electricity consumption (a large part of the population indeed lives within 90 km off a coastline), features a natural seasonal variability that follows electricity demand (especially in temperate climates alike in Europe), and brings limited environmental impacts with negligible necessity of land usage [2]. In addition, wave resources are usually complementary to wind ones [2], and their absorption and conversion may help the prevention of coastal erosion.

Off the Europe coastline, the average theoretical wave-power potential has been recently estimated in 360 GW (with roughly 75 GW within the Mediterranean regions and 10 GW in the Baltic sea) [3]. Although this is only a small portion of solar and

Contact person: Marco Fontana
m.fontana@sssup.it

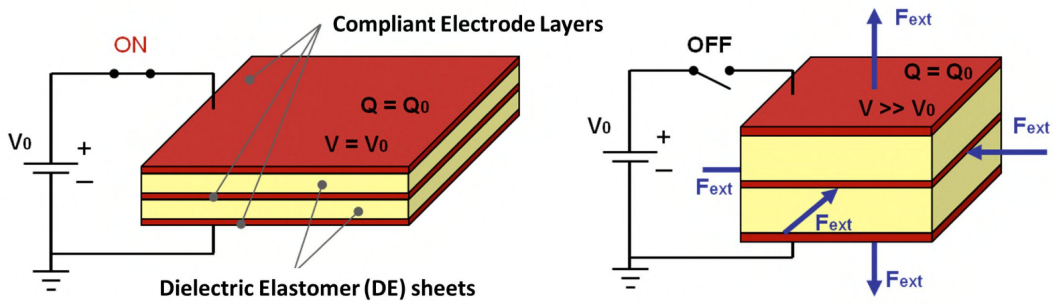

FIGURE 1 Schematic of a multi-layered DET: low electrical-energy and high elastic-energy state with no applied external force (left), high electrical-energy and low elastic-energy state with applied external force (right)

wind resources, for the reasons stated above, wave power can be a good candidate to cover between 15% and 35% of the intermittent renewable energy mix in the future [2, 4].

Harvesting energy from waves is very challenging:

- ocean wave power is available at high forces and slow speeds (which limits the usability of direct drive generators and requires the adoption of speed reducers);
- machines need to operate well out of their nominal rating conditions;
- machine members must resist to extremely high occasional mechanical loads (especially during storms);
- machine components must resist to a very hostile (in particular, corrosive) environment;
- machines are difficult to install, maintain and test in real operational conditions;
- machine development, construction and testing is very expensive.

As compared to wind and solar, Wave Energy Converter (WEC) technology is still immature, high-risk and cost-uncompetitive [2, 4, 5]. Since the forties in Japan and the seventies in Europe and the US, nearly a thousand of WEC concepts have been proposed, and nearly a hundred of reduced-scale physical devices have been constructed and tested both at University laboratories and at spin-off companies. Today, nearly fifteen pre-commercial WECs have been deployed in the ocean for short-duration testing programs, with only few of them having undertaken the first step towards commercialization.

The proposed WEC architectures are rather diverse, and optimal designs have yet to be converged upon [2, 4, 5]. Different systems have been developed for being deployed either off-shore, near-shore or on the shore-line, and which exploit very dissimilar working principles alike (point, multi-body, or large) wave-absorbers, wave-terminators, wave-attenuators, overtopping reservoirs and submerged seabed devices [6].

Irrespective of the architecture, the considered WECs have relied on traditional mechanical components (such as turbines, oscillating plates or heaving buoys), mechanical/hydraulic transmissions and electromagnetic generators (electric machines). Made by stiff, bulky, heavy and costly metallic materials (and rare-earth materials), these components did not succeed in making the proposed WEC designs to overcome all the challenges mentioned above.

To make ocean wave energy exploitable in an affordable manner, a major technological breakthrough is required.

In this context, this paper describes the Dielectric Elastomer Transducer (DET) technology and discusses its potentialities in the wave energy sector. In particular, three novel concepts of DET-based WEC are introduced: the Poly-Surge [12], the Poly-Buoy [13] and the Poly-OWC [14-16].

Dielectric Elastomer Generators

Dielectric Elastomers (DEs) are highly deformable rubber-like solids, which are mechanically incompressible and electrically non-conductive. The sequential stacking of multiple DE sheets separated by compliant electrode layers yields a deformable capacitive transducer (hereafter referred to as Dielectric Elastomer Transducer, or DET in short) that is capable of converting electricity into mechanical energy and vice-versa [9]. Typical materials used as DEs are natural rubbers, silicone elastomers, nitrile rubbers and polyacrylate elastomers (both in un-filled and filled form). Typical materials used for compliant electrodes are silicone compounds filled with conductive particles such as carbon black, carbon nanotubes, copper or silver.

DETs can be used as solid-state actuators, sensors and generators in any kind of machine featuring mechanical members with reciprocating motion [9]. In generator mode, DETs operate via the variable capacitance electrostatic generation principle, thereby increasing the voltage of the charges that lie on the electrodes as the DET capacitance decreases. A schematic of a simple DET generator made by three deformable electrode layers (in red) and two DE sheets (in yellow) is depicted in Fig. 1; the left figure shows the DET in its "low electrical-energy and high elastic-energy" state with no applied external force, whereas the right figure shows the DET in its "high electrical-energy and low elastic-energy" state with applied external force (figure on the right). In the schematic, V_0 indicates the battery voltage, V the DET voltage, Q the DET charge residing on each of its electrodes ($Q = Q_0$), and F_{ext} is an external force acting on the DET.

As shown, a possible operating sequence for a DET to convert mechanical energy into electricity is the following: 1) start from a configuration where DET capacitance is maximum and fully discharged (that is, with the DET having maximum area and minimum thickness, as shown in Figure 1 on the left); 2) with the DET locked in the same configuration, connect the electrodes to a battery (with electric potential equalling V_0) so as to place there an amount of charge equalling Q_0; 3) as the charging process is completed, disconnect the DET from the power supply; 4) with the supply disconnected, apply the external force F_{ext} to reduce the DET capacitance (which makes the electric potential difference between electrode layers to increase to the value V, with $V >> V_0$); 5) as the capacitance reaches its minimum value, connect the electrodes to an external electric circuit so as to withdraw the charge Q_0 that is at the electric potential V; 6) as the discharging process is completed, bring the DET back to the starting configuration.

During this cyclical process, the amount of mechanical energy that can be converted into electricity equals

$$U = 0.5 Q_0 (V \quad V_0) \tag{1}$$

In practice, this energy results from the mechanical work that is performed by F_{ext} in a cycle to win the internal forces of electrostatic attraction that exist between oppositely charged electrodes of the DET as the electrodes are being separated. The related energy gain reads as

$$G = \frac{U}{0.5 Q_0 V_0} = \frac{V}{V_0} \quad 1 \tag{2}$$

The energy conversion process described above is only one of the possible alternatives. In practice, different energy conversion cycles can be performed by controlling in a different manner the flow of charge that enters/exits the electrodes as a function of DET deformation, with the best controller being the one that enables the regulation of the electric field acting within the DE sheets as the DET deforms [10, 11].

Irrespective of the considered control law, the maximal energy that can be converted by a specific DET in a cycle depends on: 1) type of deformation state (for instance, uniform and equi-biaxial or non-uniform and mono-axial); 2) dielectric strength and permittivity of the employed DE material; 3) elongation at break and stiffness of the employed DE material and compliant electrodes. For practical DETs, which feature:

- deformations up to 700% and Young's modulus in the range 0.01-20 MPa;
- dielectric strength in the range 20-400 MV m^{-1} and permittivity in the range 1.8-7;

typical values for the energy gain range between

3 and 15, which are significantly larger than those achievable with piezoelectric ceramics.
Due to the low mass density of DE materials (nearly 1000 kg m^{-3}), values for the energy density of DETs (namely, the amount of energy converted in a cycle per kilogram of transducer) typically range between 0.1 and 2 kJ kg^{-1}, which, for generators operating at low frequencies (for instance, at less than 1 Hz), compare very well (and sometimes are even better, especially as the operating frequency is smaller) with that of traditional electric machines.
Beside good energy density, other advantageous properties of DETs that could make them the optimal choice for the development of machines that generate electricity from low-frequency reciprocating motions are:

- rather good electromechanical conversion efficiency (usually in the range 60-90%);
- moderate or low cost (100 €/kg for small batches and less than 10 €/kg for large batches);
- solid-state monolithic embodiment with no sliding parts and very low internal friction;
- easy manufacturability, assembling and recyclability;
- good chemical resistance to corrosive environments;
- silent operation and no need of lubrication.

Wave Energy Converters based on Dielectric Elastomers Transducers

In ocean waves, energy travels without any substantial overall motion of water. In fact, as a wave passes, water particles undergo orbital motions, with the energy of this movement being transmitted to succeeding water particles in a progressive manner. As such, ocean wave energy is available in both kinetic and potential forms; to be harvested, it requires machine elements undergoing slow reciprocating motions and capable to withstand large forces/torques. In addition to motion and force requirements, machines (and components) for the conversion of ocean wave energy into electricity should also feature: good electro-mechanical conversion efficiency (in both directions); high impact and corrosion resistance; lightness and compactness; easy manufacturability and low cost; silent operation.
As described in the previous section, all these application requirements are perfectly matched by the properties of DETs, which are now opening a new frontier for the ocean wave energy sector.
Three very promising concepts of DET-based WECs are the polymeric wave-surge (Poly-Surge), the polymeric buoy (Poly-Buoy) and the polymeric oscillating water column (Poly-OWC) systems. Their concepts, operating principles and peculiarities are described in the following.

Poly-Surge sea-Wave Energy Converter

A first WEC architecture that could be suited for sea-wave energy harvesting via DETs is the oscillating flap. This type of system consists of a buoyant flap

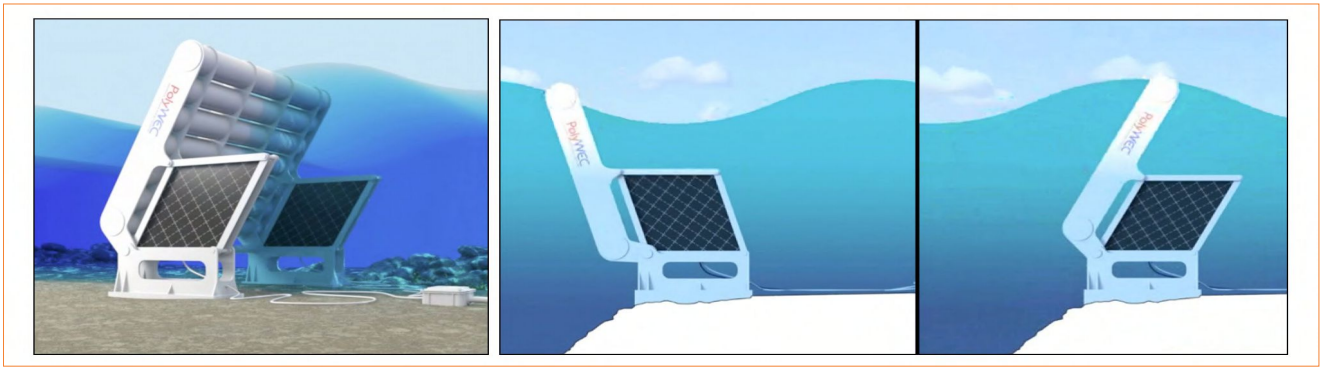

FIGURE 2 Poly-Surge – Oscillating Flap with a lozenge DET

hinged at the sea bottom and exploits the surging motion of waves. In traditional systems (such as the Oyster device by Aquamarine Power) the wave-induced oscillatory motion of the flap is used to pump water to the coast via hydraulic pistons and high-pressure flow lines. At the coast, the high-pressure water is then converted into electricity via a turbo-generator.
Replacement of the hydraulic power take-off system (and of the turbo-generator) with lozenge DETs [12, 13] could enable local conversion of wave energy into electricity without requiring any mechanical or hydraulic transmission. Besides simplifying the system and reducing part count, this replacement could improve system efficiency, simplify installation and reduce the noise pollution emitted at the coast by the turbo-generator.
An artistic drawing of a Poly-Surge WEC is reported in Figure 2.
Since they need to be attached to the seabed, Poly-Surge WECs are suited for near-shore installations at a nominal depth of nearly 10 m, possibly at locations where shoaling effects occur. At this depth, wave energy resource is still very significant, and usually characterized by limited maximum wave heights (due to wave breaking) and limited directional spread between longer and medium period waves.
As for the operating principle, Poly-Surge systems are excited by horizontal fluid accelerations mainly. Due to physical constraints in the oscillatory motion of the flap, Poly-Surge systems are likely to be not resonant in the working frequency range, and should be designed to maximize wave excitation force and to move at speeds that are adequate to limit vortex losses at the edges.
More details on Poly-Surge architecture, functioning principle, design issues and potential performances can be found in [12, 13].

Poly-Buoy sea-Wave Energy Converter

A second WEC architecture that could be suited for wave energy harvesting via DETs is the oscillating buoy. An oscillating buoy WEC consists of a floating body, either submerged or semi-submerged, that moves under the action of sea waves with respect to an appropriate number of submerged and nearly fixed reaction points.

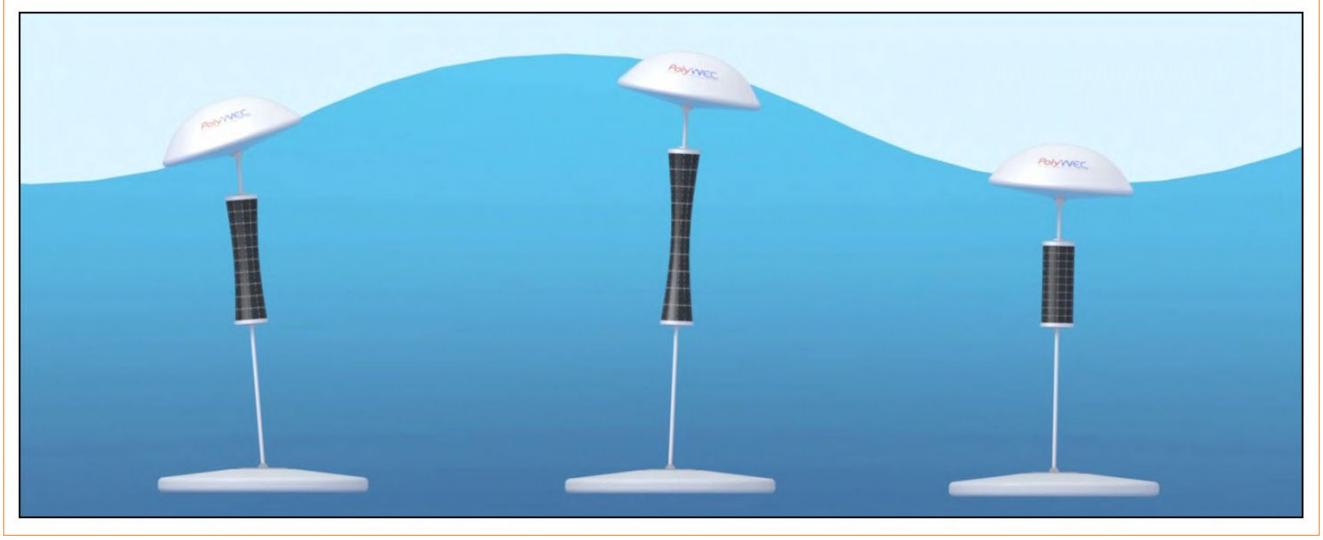

FIGURE 3 Poly-Buoy – Oscillating Buoy with a cylindrical DET

Depending on the water depth of installation, the reaction points can be located either on the seabed or on a floating body (namely a reaction body), that is submerged enough not to be excited by the wave field. Depending on the means of connection to the reaction points, the wave-induced oscillatory motion of the buoy can be in heave, surge or pitch (or a combination thereof).
During these oscillations, the distances between points of the buoy and those of reaction vary. These reciprocating changes in length can be used by power take-off systems with linear motions to extract energy from waves. As alternative to the traditional hydraulic rams or linear electrical generators, cylindrical DETs can be used for this purpose. Depending on the size of the device, the considered DET can be placed either inside the buoy, close to the reaction points (in particular on the seabed or inside the reaction body) or along the line connecting the reaction points and the buoy.
An artistic drawing of a Poly-Buoy WEC is reported in Figure 3.
In terms of hydrodynamic properties, Poly-Buoy systems are point absorbers that can be installed both on-shore and off-shore. For standard buoy shapes and aspect ratios, Poly-Buoys are likely to be designed so as to be resonant in the working frequency range, which makes their performances very sensitive to the intrinsic passive stiffness of the DET.
More details on Poly-Buoy architecture, functioning principle, design issues and potential performances can be found in [14].

Second-generation DET-based WECs

In this section, one concept of second-generation device is introduced and described.

Poly-OWC sea-Wave Energy Converter

Oscillating Water Column (OWC) wave energy converters are based on the reciprocating motion of a column of water enclosed in a chamber (tube or duct) that has at least one submerged opening. The water inside the closed chamber is moved by wave-induced oscillating pressures acting on this opening. In traditional OWC concepts, the movement of the oscillating water column induces a pressure variation inside a closed air chamber; such a pressure variation is used to drive a turbo-generator, which converts the stored pneumatic power into usable electricity. Due to reciprocating air-flow, energy harvesting from traditional OWC devices requires either a self-rectifying turbine or a complex system of non-return valves that makes it possible to rectify the flow passing through a conventional turbine.

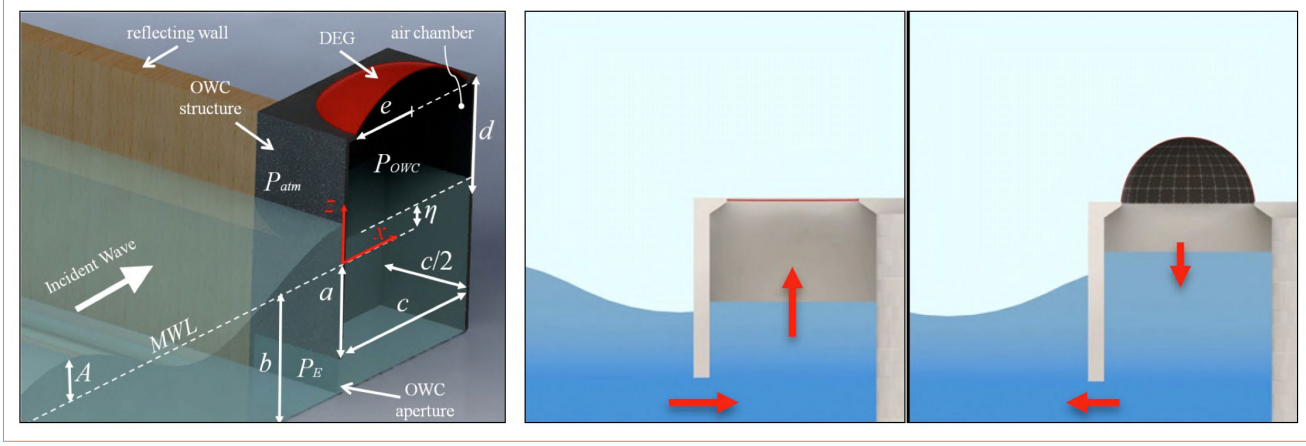

FIGURE 4 Poly-OWC – Osclillating Water Column with inflating circular diaphragm DET

In OWCs, replacement of the turbo generator by an inflating diaphragm DET could significantly simplify overall system architecture and installation, improve overall energetic efficiency and climate adaptability, and reduce operating noise.
An artistic drawing of a Poly-OWC WEC is reported in Figure 4.
In terms of hydrodynamic characteristics, Poly-OWCs can be installed both on the shore-line (with fixed structure) and off-shore (with floating structure); specifically, they are very suited for being integrated into breakwaters for harbour protection. For standard chamber shapes and aspect ratios, Poly-OWCs are likely to be designed so as to be resonant in the working frequency range, which makes their performances very sensitive to the intrinsic passive stiffness of the DET. Thanks to the presence of an air pocket, the dynamic response of a given Poly-OWC can be tuned to the prevalent frequency content of the incoming waves by simply acting on steady-state chamber pressurization.
More details on Poly-OWC architecture, functioning principle, design issues and potential performances can be found in [15-17].

Conclusions

This paper presented three different concepts of Wave Energy Converters (WECs) that employ Dielectric Elastomer Transducers (DETs) to convert ocean wave power into direct-current high-voltage electricity. As compared to traditional WECs with hydraulic or electromagnetic power take-off system, the presented machines offer the following potential features: reduced capital costs; easy installation and maintenance; good shock and corrosion resistance; good energy conversion efficiency; good climate adaptability; reduced noise during operation.
As of today, DET technology is however not yet ready to deliver fully-functional WEC systems that are capable to operate in real seas for sufficiently long periods of time. In this perspective, critical issues that need to be addressed are: assessing the long-term fatigue, ageing, degradation and reliability of the employed materials; conceiving better dielectric elastomers and conductive electrodes with improved electromechanical transduction properties and reduced dissipative effects; developing better design, optimization and control methodologies; conceiving alternative system architectures with reduced part counts and integrating multiple functionalities in single components.

Acknowledgements
The work presented in this paper is developed in the context of PolyWEC (www.polywec.org), an FP7 FET–Energy project. The research leading to these results has been funded from the European Union's Seventh Framework Programme [FP7/2007–2013] under grant agreement n° 309139.

Marco Fontana
Scuola Superiore Sant'Anna, Perceptual Robotics Laboratory (PERCRO), Pisa, Italy

Rocco Vertechy
University of Bologna, Department of Industrial Engineering, Italy

references

[1] M. Leijon, A. Skoglund, R. Waters, A. Rehn, M. Lindahl, 2010, On the physics of power, energy and economics of renewable electric energy sources, in Renewable Energy, 35, pp. 1729–1734.

[2] Oceans of Energy – European Ocean Energy Roadmap 2010-2050, European Ocean Energy Association, 2009.

[3] G. Mork, S. Barstow, A. Kabuth, M.T. Pontes, Assessing Global Wave Energy Potential, in Proc. of 29th International Conference on Ocean, Offshore Mechanics and Arctic Engineering, OMAE2010, China, 2010.

[4] Future Marine Energy: Cost Competitiveness and Growth of Wave and Tidal Stream Energy, Carbon Trust, 2006.

[5] Implementing Agreement on Ocean Energy Systems - Annual Report 2010 and 2011, International Energy Agency, 2010 and 2011.

[6] A.F.O. Falcao, Wave energy utilization: A review of the technologies, in Renewable and Sustainable Energy Reviews, 14, pp. 899–918, 2010.

[7] Annual Energy Outlook 2010 With Projections to 2035, Energy Information Administration, 2010.

[8] J. Huckerby, A. Brito Melo, International Vision on Ocean Energy Systems, WavEC Seminar 2011: Offshore Renewable Energy and its Potential for the Outermost Regions, Portugal, 2011.

[9] F. Carpi, D. De Rossi, R. Kornbluh, Dielectric elastomers as electromechanical transducers: Fundamentals, materials, devices, models and applications of an emerging electroactive polymer technology, Elsevier Science, 2008.

[10] R. Pelrine, R. Kornbluh, J. Eckerle, P. Jeuck, S. Oh, Q. Pei, S. Stanford, Dielectric elastomers: Generator mode fundamentals and applications, in Proc. SPIE, Vol. 4329, pp. 148-156, 2001.

[11] A. Koh, C. Keplinger, T. Li, S. Bauer, Z. Suo, Dielectric elastomer generators: How much energy can be converted?, in IEEE/ASME Transactions on Mechatronics, 16(1), pp. 33–41, 2011.

[12] G. Moretti, D. Forehand, R. Vertechy, M. Fontana, D. Ingram, Modeling of an oscillating wave surge converter with dielectric elastomer power take-off, in Proc. of ASME 33rd International Conference on Ocean, Offshore and Arctic Engineering, Paper No. OMAE2014-23559, San Francisco, CA, USA, 8-13 June, 2014.

[13] G. Moretti, M. Fontana, R. Vertechy, Parallelogram-shaped dielectric elastomer generators: Analytical model and experimental validation, in Journal of Intelligent Material Systems and Structures, first published on December 19, doi:10.1177/1045389X14563861, 2014.

[14] G. Moretti, R. Vertechy, M. Fontana, Modelling of a heaving buoy wave energy converter with stacked dielectric elastomer generator, in Proc. of ASME Conference on Smart Materials, Adaptive Structures and Intelligent Systems, Paper No. SMASIS2014-7565, Newport, Rhode Island, Sept. 8-10, 2014.

[15] R. Vertechy, M. Fontana, G.P. Rosati Papini, M. Bergamasco, Oscillating-water-column wave-energy-converter based on dielectric elastomer generator, in Proc. of SPIE, Vol. 8687, pp. 86870I-86870I, 2013.

[16] R. Vertechy, G.P. Papini Rosati, M. Fontana, Reduced Model and Application of Inflating Circular Diaphragm Dielectric Elastomer Generators for Wave Energy Harvesting, in ASME Journal of Vibration and Acoustics, 137(1), pp. 011004 (9 pages), doi:10.1115/1.4028508, 2015.

[17] R. Vertechy, M. Fontana, G.P. Rosati Papini, D. Forehand, In-tank tests of a dielectric elastomer generator for wave energy harvesting, in Proc. of SPIE, Vol. 9056, pp. 90561G, 2014.

INORE: The International Network on Offshore Renewable Energy

The International Network on Offshore Renewable Energy (INORE) is a non-profit organization run by volunteers. INORE was born to support early stage researchers in the offshore renewable energy field. Today, INORE has more than 1200 members from more than 70 different countries. The aim of this organization is to facilitate networking and information exchange between young researchers and professionals. This is achieved by arranging symposia, workshops, networking events and issuing scholarships. Three main knowledge areas are currently within INORE's dedication: sea wave energy, tidal current energy and offshore wind energy.

DOI: 10.12910/EAI2015-051

M. Martini, A. de Andrés

Introduction

INORE is a non-profit association of young researchers and professionals working in the area of marine renewable energy. Its dedication spans from offshore wind energy to sea wave energy and tidal current energy, and others. The activities of INORE are addressed to promoting education and knowledge sharing in the marine renewable energy field [1].

This organization was founded in Norway, in 2006, by a small group of Ph.D. students. Its initial purpose was to be a forum for exchanging experiences and ideas in the growing sector of marine renewable energy. Today, eight years later, INORE counts 1247 members from 73 countries, in its web page, and about 510 association members, or INOREans [2].

Contact person: Michele Martini
michele.martini@unican.es

INORE has been able to gather an international and multi-disciplinary group of people, and to strengthen the bonds between early stage researchers through giving them the chance to know each other and cooperate, independently of their experience or nationality.

To achieve its goals, INORE helps itself with several *knowledge sharing tools*: symposia, workshops, technological challenges, scholarships, networking events and its web page.

INORE's knowledge sharing tools

Symposium

The symposium is the major event organized by INORE. It is an international meeting where about 70 young professionals and researchers get together to present, discuss and analyze their works, in an informal atmosphere (Fig. 1). A Symposium includes presentations, group works, poster sessions, technological site visits and inspirational talks given by keynote speakers. To build bonds

FIGURE 1 Symposium participants doing group works

of collaboration, a symposium comprises also collaborative tasks: these are mini group-projects that participants work on for few days and report on at its end. They are usually designed with the help of INORE's partners (companies, research institutions, government agencies) and address real problems, providing a context for research and a broader understanding.
To make the difference, and to accelerate the *getting-to-know-you* process, a symposium includes also funny and entertaining social activities, which mark the event as more informal, compared to traditional scientific events.

FIGURE 2 Group picture at the 2014 European symposium

N°	Location	Year	Attendees
5°	Alcoutim, Portugal	2011	58
6°	Thisted, Denmark	2012	45
7°	Boston, USA	2012	26
8°	Pembrokeshire, Wales	2013	50
9 °	La Vega, Spain	2014	70

TABLE 1 Attendance data for the last five symposia

The symposium usually takes place in remote places, far from noisy cities with the aim of intensifying the experiences of its participants. Figure 2 shows a group picture taken at the last European symposium in the rural village of La Vega, in the region of Cantabria, Spain.
In Table 1 it is possible to find the most significant data about the last four INORE symposia. Recently, INORE managed to organize symposia also in North America and Canada. It is remarkable that these events are completely free for all attendees, since INORE provides food, accommodation and transportation over the entire event.
The 10th INORE symposium took place last May 2015, in Naples, Italy. Since all the previous events were held in North Atlantic regions, this as been a unique opportunity to put the lights on the activities carried on in the Mediterranean Sea, for which Italy may lead the way.

FIGURE 3 Participants at the workshop and discussion forum at OMAE, in San Francisco, USA (June 2014)

Workshops

INORE often arranges workshops and discussion forums, in parallel with other international events or conferences, such as AWTEC [3], ICOE [4], OMAE [5] or EWTEC [6]. These are informal talks that usually last a few hours and manage to gather a wide public attention, taking place jointly with important events in the field.

A panel of experienced and well-known people leads the discussions, interacting with the audience, in an active exchange of ideas and opinions. Figure 3 shows participants of the workshop that INORE organized at OMAE 2014, in San Francisco, USA.

FIGURE 4 Group picture at the 2015 INORE symposium, in Naples, Italy

Technological challenges

Lately, INORE has organized what they call *technological challenges*. These are competitions between small groups of researchers, which last one or two days, hosted by a well-known research institution. Groups of 4 to 6 people are supposed to propose innovative solutions to some real, technological problem. Each team is provided with basic materials that can be used to solve the proposed puzzle. Experts of the host institution then evaluate the solutions and give a symbolic prize to the winners. An example is the Floating Wind Turbine Challenge [7], which took place in September 2011 at the MARIN laboratories in the Netherlands.

Scholarships and travel grants

In the last few years, INORE has managed to collect funding to issue grants for its members. The ICIS (International Collaboration Incentive Scheme) scholarships are set up to allow young researchers to work with people of other institutions in collaborative, research projects. With a fixed budget, these are thought to facilitate the temporary relocation of the solicitants, allowing them to work *shoulder-to-shoulder* with their colleagues. To ensure that these grants are effective, the work resulting from this collaborations must be published in conferences, journals or freely distributed in the Internet, thus ensuring its maximum diffusion [8, 9].

Web page

The major web-based *communication channel* used by INORE is its web page (www.inore.org). This acts as a forum where members and other users can exchange experiences, news, job opportunities and be updated about future INORE events. The web page is managed by the members themselves, since they can upload attachments, events, and update their profiles. INORE aims at spreading its work and its activities worldwide, therefore anybody can register as a web member: today, 1247 members from 73 countries are networking on this virtual platform, which is still

expanding. At the moment, INORE has invested part of its time and funding to refurbish its web page, in order to make it more user-friendly and efficient. Moreover, another activity has started recently: OpenORE (www.openore.org), a virtual space in which people can exchange open-source software to better investigate marine renewable energies.

Sustainability and transparency

Since its very foundation, INORE managed to sustain economically all its activities thanks to its sponsors. Every year, companies, government agencies, research institutes and universities kindly help INORE to keep organizing all its activities, which are expanding and becoming bigger year by year. In turn, INORE guarantees a complete transparency of all its outgoings, and delivers detailed reports to the sponsors underlining the advancements made thanks to their donations.

Conclusions

INORE is a non-profit organization with the final purpose to foster collaboration and knowledge sharing between young researchers in offshore renewable energy. Since its very foundation in 2006, INORE has collected about 1200 members from more than 70 countries in the world. By means of an annual symposium, INORE facilitates the networking between researchers and professionals, increasing the opportunities of collaboration between different research centers. At the same time, through the ICIS grants, INORE promotes the cooperation between INOREans. INORE helps researchers and professionals to collaborate and cooperate with their colleagues in the field of offshore marine renewables, and thus contributes to move towards a sustainable energy world.

Acknowledgements

The activities of INORE would not be possible without the disinterested collaboration of its sponsors. In particular, our special thanks go to: Wave for Energy srl, Ocean Energy Systems, MARIN, WavEC, OceaNET, Sustainable Marine Energy, NOC, IH Cantabria, Dynamic Systems Analysis, Nova Scotia Department of Energy and Fundy Ocean Research Center for Energy.

Michele Martini
Environmental Hydraulics Institute «IH Cantabria», Santander, Spain

Adrián de Andrés
University of Edinburgh, Scotland

references

[1] K. Freeman, J. Davidson, An International Network on Offshore Renewable Energy, in *Proceedings of 1st Asian Wave and Tidal Conference Series*, Jeju Island, Korea, 2012.

[2] INORE, available at: www.inore.org, accessed on 12 December 2014.

[3] AWTEC, available at: www.awtec2014.org, accessed on 17 February 2014.

[4] ICOE, available at: www.icoe2014canada.org, accessed on 17 February 2014.

[5] OMAE, available at: www.asmeconferences.org/conference-home/OMAE, accessed on 12 December 2014.

[6] EWTEC. available at: www.ewtec.org, accessed on 17 February 2014.

[7] S. Geuydon, S. Harding, Floating Wind Turbine Challenge. EWEA - European Wind Energy Association Annual Event, Copenhagen, Denmark, 2012.

[8] G. Magagna, D. Carr, D. Stagonas, A. McNabola, L. Gill, G. Muller, Experimental Evaluation of the Performances of an Array of Multiple Oscillating Water Columns, in *Proceedings of European Wave and Tidal Energy Conference*, Southampton, UK, 2011.

[9] C. Perez Collazo, M.M. Jakobsen, H. Buckland, J. Fernandez Chozas. Synergies for a wave-wind energy concept. EWEA offshore - European Wind Energy Association Annual Event, Frankfurt, Germany, 2013.

Gli Speciali di Energia, Ambiente e Innovazione

La rivista, oltre ai fascicoli a cadenza bimestrale, realizza numeri "Speciali" monografici su tematiche tecnico-scientifiche di attualità.

Nove gli Speciali finora pubblicati:

- Le tecnologie di Carbon Capture and Storage
- Forests: a millenary heritage that guarantees us life
- Verso la green economy: strategie, approcci e opportunità tecnologiche
- Knowledge, Diagnostics and Preservation of Cultural Heritage
- Biotecnologie per lo sviluppo sostenibile
- ENEA Technologies for Security
- Idee per lo sviluppo sostenibile
- Transition and global challenges towards low carbon societies
- Ocean energy: Ongoing research in Italy

Tutti gli Speciali sono disponibili online.

energia ambiente e innovazione

speciale II - 2015

Bimestrale dell'ENEA
anno 61